POLITECNICO DI MILANO

DEPARTMENT OF ELECTRONICS, INFORMATION
AND BIOENGINEERING (DEIB)
Master of Science in Biomedical Engineering

PREDICTIVE MAINTENANCE FRAMEWORK FOR MEDICAL DEVICES

FROM DATA COLLECTION TO DATA ANALYSIS

Supervisor
Prof. Eng. Giambattista GRUOSSO

Co-Supervisor
Eng. Alberto SANCANDI

Candidate
Sara FUSE' – 905906

Academic Year 2019 – 2020

Sommario

L'ondata tecnologica degli ultimi anni sta vedendo dispositivi medici sempre più complessi, a cui si aggiunge un incremento della loro domanda sul mercato. Avere un dispositivo sicuro e pronto all'uso garantisce un elevato livello di assistenza e di qualità per la cura del paziente. Per soddisfare queste richieste ed evitare casi di malasanità, viene richiesto un corretto piano di manutenzione per ciascun dispositivo. Tuttavia, la gestione di un dispositivo medivo è più efficente se si conoscono le possibili cause di guasto. In questo contesto, la manutenzione predittiva può aiutare gli ingegneri biomedici a stilare un corretto piano manutentivo. Nonostante questo approccio non sia molto consolidato nell'industria medica, la manutenzione predittiva può migliorare l'efficienza delle attrezzature coinvolte in un osepdale andando a ridurne costi legati alla manutezione e tempi di inutilizzo.

Nel mio lavoro di tesi viene presentato lo studio delle vibrazioni come esempio di manutenzione predittiva, utilizzato per diagnosticare possibili cause di guasto in due componenti, un cuscinetto a sfere e una pompa peristaltica, dispositivo che rientra nelle applicazioni biomedicali. Per rilevare le vibrazioni dei componenti meccanici, un sistema di acquisizione è stato fatto su misura, scegliendo il tipo di accelerometro, collegandolo a un Raspberry Pi. I dati raccolti vengono poi importati in MATLAB. Tecniche di analisi dei segnali, precisamente la trasformata di Fourier, lo studio dell'inviluppo del segnale e della trasformata di Hilbert-Huang vengono prima discusse e

validate sul cuscinetto in quanto vi è un riscontro teorico in letteratura per poi essere riproposte per lo studio delle vibrazioni indotte da una pompa peristaltica. In questo caso l'obiettivo è quello di trovare dei pattern specifici con cui è possibile discriminare durante il normale funzionamento un particolare difetto. Questo lavoro è stato reso possibile grazie al supporto di ELETTROTECNICA ROLD S.R.L..

Abstract

Medical devices are becoming ever more complex due to technological advancements of last decades, and their demand is continuously growing in number. Having reliable and available equipment ensure high-quality patient care and high degree of patient safe. In order to satisfy these requests, a proper maintenance program is needed to avoid medical malpractise. However, knowing the characteristics of failure of a medical device is important to increase the efficiency of its management. In this framework, a Predictive Maintenance (PdM) application could assist biomedical engineers in planning maintenance activity. Although it is not so widely performed in healthcare industry, PdM could enhance the performance of the equipment within a hospital by reducing its downtime and decreasing its maintenance costs and effort.

In this thesis, a Predictive Maintenance approach is presented to help in failure diagnosis for two critical devices, a roller bearing and a roller pump by monitoring their vibration. An initial analysis on vibration monitoring of bearing was performed and based on it, a suitable data acquisition system is implemented, taking care of the every single electronic components. Signals are collected through an accelerometer wired to a Raspberry pi board and then imported in MATLAB. Every signal has been processed with advance signal processing techniques: both Fast Fourier transform, Envelope Spectrum and Hilbert Huang transform are first discussed and validated on

the bearing, for which theoretical references are affirmed, then repeated to the roller pump to find specific pattern that could discriminate healthy or faulty conditions. The whole set up was developed thanks to the support of ELETTROTECNICA ROLD S.R.L, where a I did my internship.

Contents

Acronyms

BPFI	Ballpass Frequency on Inner race
BPFO	Ballpass Frequency on Outer race
BSF	Ball Spin Frequency
CBM	Condition-Based Maintenance
D	Damaged
1D	One faced Damaged roller
2D	Double faced Damaged roller
DC	Circumferentially Damaged roller
DD	Holder contains both rollers that are damaged
EMD	Empirical Mode Decomposition
ENV	Envelope Spectrum
FFT	Fast Fourier Transform
FTF	Fundamental Train Frequency
GPIO	General Purpose Input-Output
H	Healhy

HHT	Hilbert-Huang Transform
I2C	Inter-Integrated Circuit
IMF	Intrinsic Mode Function
IE	Instantaneous Energy
IoT	Internet Of Things
MHS	Marginal Hilbert Spectrum
O	Obstruction
PdM	Predictive Maintenance
PM	Preventive Maintenance
+R	Roller out/consumption holder

List of Figures

List of Tables

Introduction

Overview

A medical device can be any instrument, apparatus, implement, machine, appliance, implant, reagent for in vitro use, software, material or other similar or related article, intended by the manufacturer to be used, alone or in combination for a medical purpose [1]. Due to the technological improvement over the last years, medical equipment is becoming more and more complex, e.g. medical ultrasound systems or other sophisticated imaging apparatus, ECGs, heart-lung machines, pumps for cardiac assistance. Medical equipment and devices must be regularly maintained to ensure proper functioning so that they are ready to be utilized without any complication by medical staff within hospitals or labs. Recording when such huge number of assets were last updated, inspected, replaced or fixed is important to improve maintenance workflow and minimize spare parts inventory holding costs [2, 3].

In this context, downtime is the most critical aspect to avoid: as a result, a proper maintenance policy should be developed. Maintenance policies have different shades: nowadays the coolest one concerns Predictive Maintenance (PdM). This newest concept has been launched hand in hand within the 4^{th} Industrial Revolution that pervades last decades. To better grasp the concept, PdM could be defined as the ability to keep something in a good con-

dition by understanding what happens in the future: in fact, this strategy relies on real-time data collected through sensors in order to identify, with provided tools, the types of failure of each component within the system. Based on them, prediction of possible failure helps technicians in drawing up precise maintenance program. If well planned, this method would ensure manufacturers to lower maintenance costs, extend equipment life and improve production quality, aiming to safety of patients and consumers.

Nowadays PdM is adopted in manufacturing industries, aviation or in thermal power plants, where electromechanical devices constitute the core of production. As a matter of fact, healthcare sector contains a diverse array of industries, with activities ranging from research to manufacturing to facilities management.

The heart of a predictive maintenance program is based on data acquisition and health indicators monitoring: among rotating machines which are embedded in healthcare system, pumps and bearing are classified as the most critical parts of a mechanical system. To solve possible failure of aforementioned parts, PdM would find fertile ground.

Vibration analysis is the condition monitoring techniques which studies the behaviour of the signal through the frequency excited by each component of the system. In order to monitor these features, the signal can be analyzed in frequency domain with traditional Fast Fourier transform or can be demodulated in Time-Frequency analysis with Hilbert-Huang transform to extract health indicators about the degradation or detection of faults.

The current trends in healthcare is to maintain a high degree of profitability and innovation. Developing a condition monitor model does not prevent the failure, but it can predict the possibility of future failure: this is one of the reasons why medical technology and medical device manufacturers have started to implement predictive maintenance.

Goals of the project

During my experience of internship in ELETTROTECNICA ROLD S.R.L, I faced personally the problem of realizing from scratch the whole experimental set up, from the electronics to collect data, to study the problem of vibration in mechanical fields within Predictive Maintenance scenario, and to apply to real world the signal analysis tools which I studied during my years of Polimi.

To reach the target of this thesis, I firstly made research on Scopus related to vibration analysis, identifying ball bearings as the most critical element undergoing failures: from each paper I extracted information regarding the system acquisitions and the related characteristic frequencies that were detected in order to have an overall initial framework of the problem. A literature review on ball bearing vibration analysis provided me the basic tools to understand the problem of diagnosis of faults.

From these specifics, the implementation of an appropriate data acquisition system followed. This second step began from the choice of an accelerometer from online retailers: a checklist of MEMs was listed and one of them chosen, ensuring a wide range of selectable ODR (Output Data Rate) to perform the acquisition.

Learning *python* language provided me to set properly the accelerometer throught registers in Raspian enviroment, selecting also the communication protocol between MEMs and the board. The core code collects and performs in real-time the transformation from time to frequency domain representation of the signal, by implementing the signal processing tools. Understanding and realizing Hilbert-Huang transform required long time.

After being validated on the bearing, the analysis switched to another device related to medical application. Therefore, Condition monitoring state of art

of medical device needed. As a results, roller pumps was chosen since it is practical and not bulky device, used both in biomedical application and by the company where I stayed.

The whole set up for the project is then realized: identify the behaviour of different object by analysing their vibration using advanced signal processing tools.

Outline

This thesis is structured as follow:

* Chapter 1: the State of Art of maintenance strategies driving the attention to medical devices;
* Chapter 2: steps towards the implementation of the data acquisition system developed;
* Chapter 3: case study of a roller bearing with a review of vibration analysis and signal processing techniques used;
* Chapter 4: experimental set up and theoretical features on the roller pump;
* Chapter 5: results and comparison between different methods;
* Chapter 6: conclusion with future implementations.

1. State of Art

1.1 The need for maintenance in healthcare industry

Today, there are an estimated 2 million different kinds of medical devices on the world market, categorized into more than 22000 devices groups [1].

The complexity of the technological assets found in healthcare facilities, in terms of number and diversity, is reflected in the complexity of technology management, which must be efficient so that the equipment can always be used safely and appropriately [4].

Medical devices are used in many diverse settings, for example, by laypersons at home, by paramedical staff and clinicians in remote clinics, by opticians and dentists and by health-care professionals in advanced medical facilities, for prevention and screening and in palliative care. Such health technologies are used to diagnose illness, to monitor treatments, to assist disabled people and to intervene and treat illnesses, both acute and chronic: any of these complex systems is considered a life support system. The failure of a system or of a single component may put in danger the patient and fail in its primary function as a life support. Medical devices downtime is the most critical aspect a patient is threaten of.

Having a strong and effective medical technology management ensures high-

quality patient care [5] that leads to a high degree of patient safety.

The demand for medical device management is continuously increasing as the number of medical devices increases. Stewart [6] reported that the number of medical equipment increased by 62% over the past 15 years while the average utilization rate of mobile equipment is only 42%: this means in an increasing hospital's acquisition budgets and maintenance costs [2]. Therefore, the development of more effective maintenance programs has achieved prominence [7].

Selecting the most efficient maintenance policy is a significant issue that an industry, as hospitals are, has to deal with to achieve product quality, improved efficiency, safety, productivity and customer satisfaction. As a matter of fact, a key factor is to increase the OEE: the overall equipment effectiveness. If a medical instrument has faults and stops to maintain, it will affect the patients, and even lead to serious medical malpractice [8].

Papers [9, 10] aim to biomedical engineers the responsibility for the correct and safe use of medical devices, underlying how they ought to optimize the best maintenance strategy to reduce the failure rate of medical equipment to improve its reliability. Moreover, proper maintenance management policies can reduce overall medical equipment operation cost, decrease degradation and increase availability.

However, maintenance is a crucial topic in the life cycle management of medical equipment but healthcare is not experiencing excellence maintenance policy compared to other industrial organization [11].

1.2 Maintenance strategies for medical devices

Maintenance of medical equipment consists of two basic activities: scheduled maintenance and corrective maintenance. The first one, also knonw

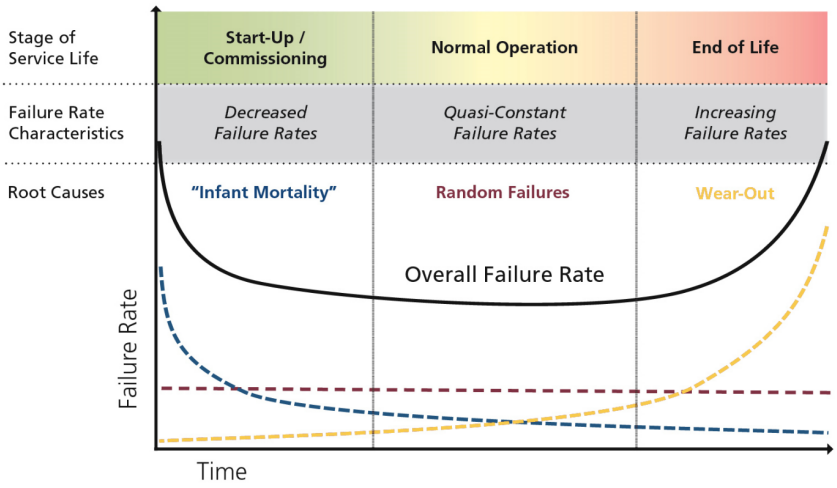

Figure 1.1: *Bathtub curve*

The bathtub curve is widely used in reliability engineering. It describes a particular form of the hazard function which comprises three parts: the first part is a decreasing failure rate, known as early failures; the second part is a constant failure rate, known as random failures; the third part is an increasing failure rate, known as wear-out failures.

as Preventive maintenance (PM) is performed at predetermined intervals to reduce the probability of failure or performance degradation. Preventive maintenance routines, for example, are measured in terms of expected time in each routine performed, depending on operating hours or time intervals [12]. Corrective, instead, is performed when a problem occurs. Both policies assume that machinery follow the so-called *bathtub curve* (1.1) for which scheduled maintenance happens in the wear-out phase in order to reduce the failure rate. This means a tremendous risk to the downtime costs: in healthcare this situation cannot happen, for the aforementioned needs.

The development and increase of the complexity of medical equipment have led to modernizing and updating maintenance techniques and policies.

[4] proposed an Evidence-based maintenance (EBM) combining fault classification and key performance indicator (KPI). This method consists in

continuous monitoring of equipment performance, starting from the current state or from the point of view of fault history and improving its efficiency through the necessary modifications. This process is very important for optimizing the use and allocation of the resources available by the clinical engineering departments.

Knowledge of the history of a failure enables the monitoring and improvement of the current maintenance strategy so that the most appropriate approach can be found [13]: Ridgway [14] classified failures in an attempt to reduce equipment downtime in terms of repair calls gathering both human/environmental interference-related and physical stress-related errors. Authors in [15] prepared maintenance schedules using mean intervals between failures. Taghipour[16] described a periodic inspection optimization model for complex repairable systems while [9] analyzed the technical data from medical devices with support from technology managers. [10] developed a numerical index for each instrument (heart lung machine, ECG recorder, pumps or surgical lamp) combining the risk to which the user is exposed and its function within the hospital.

[14] also noted that PM have some impact on the reliability of some items and therefore it does have some beneficial impact on equipment uptime. To improve the system's reliability, availability and efficiency a reliability-centered maintenance (RCM) approach focuses on design and technology [17]. RCM program is based on systematic assessment of maintenance needs after a complete understanding of the system function and the types of failure causing function losses.

Different maintenance policies have been reviewed in [11] based on three points: determine the criticality of medical equipment based on a multi-criteria analysis, rank the different maintenance strategies based on their (benefits) importance to the hospital and select the optimal maintenance

strategy for each device while keeping the total maintenance costs within a predetermined budget. They identified as crucial element the hemodialysis medical equipment in the hospitals in Africa; ACO as the best technique and they pointed out that the maintenance cost also determine the decision for acquiring new equipment and hospital waste management. The ant colony optimization (ACO) algorithms helps minimizing or removing the Mean Downtime (MDT) and Mean time to repair (MTTR) for a failed hemodialysis machines and improve their reliability.

As pointed in [18], drawbacks in implementing an accurate maintenance program concerns the obsolescence of medical devices: this is one of the most criticized problems of clinical maintenance management. Unlike new high-tech devices, the manufacturers' recommendations for older technology devices are not applicable because of the long usage time and device age [7, 11, 13]: in literature there is a lack of information about the assessment and planning of medical equipment decisions.

1.3 Towards Predictive Maintenance

Although maintenance modeling trend is shifting to Condition-based Maintenance (CBM) and predictive maintenance strategies (PdM), this remains an unexplored area in the healthcare domain.

Large part of the equipment used in the medical field belongs to the category of electromechanical systems: these devices or systems have both mechanical and electrical parts that respectively suffer from both mechanical and electrical failures. In a hospital we can find instruments that fall within this category such as pumps, vitro immunoassay analyzers, ECGs, defibrillators, aspirators, ventilators and operating table and so far.

The application of PdM strategies on these kind of equipment provides ef-

fective diagnosis and prognosis tools to determine its condition continuously prior to failure to reduce the likelihood of failures, evaluate possible faults and estimate when the maintenance should be performed on the equipment. Predictive maintenance is a trend-oriented policy that begins with identifying the states of each component within the equipment, greatly relies on engineering techniques and statistical tools to process the data and analyze the health condition in order to predict possible equipment failure [19].

The analysis of the maintenance technologies focuses on the kind of the critical component that belongs to the system taken into consideration. Two approaches can be implemented in PdM: model-based and data-driven. Physical knowledge about the system might come from mathematical modeling, as in first case, of the system and its faults: understanding system dynamics involves detailed knowledge of relationships among various signals from the machinery (such as input-output relationships among the actuators and sensors), the machine operating range, and the nature of the measurements (for example, periodic, constant or stochastic). However, data-driven approach has significant advantage with respect to the other case mainly because mathematical formulations are not required: the model itself learns the response of the system under different conditions using sensors data, comparing results between health state, different conditions and failures.

The advantage of predictive maintenance is that it does not require manual intervention to determine when the equipment should be maintained [20]. A key step in predictive maintenance algorithm development is identifying condition indicators, features in system data whose behavior changes in a predictable way as the system degrades. To evaluate equipment condition, predictive maintenance utilizes testing technologies such as infrared, acoustic, vibration analysis, sound level measurements, oil analysis, and other specific online tests. Other parameters such as flow rates, voltages, cur-

rents, temperatures are considerably useful to guarantee a wide scenario of the device while providing its current state and performances. Characteristic features are then extracted from data and with signal processing methods are classified according to the vibration signal form, that can be either stationary or non-stationary. For example, FFT (Fast Fourier Transform) is commonly deployed as a health indicator to detect anomaly based on the presence of undesired harmonics in the frequency response of the signal and it requires stationarity and linearity of the vibration signal. Hilbert-Huang transform (HHT) have been developed to deal with non-stationary and non-linear signals [21]. A condition indicator can be any feature that is useful for distinguishing normal from faulty operation (*monitoring* and *diagnosis*) or for (*prognosis*) predicting remaining useful life (RUL) [4]. A useful condition indicator clusters similar system status together, and sets different status apart.

Steps towards PdM implementation are summarized in 1.2.

Figure 1.2: Predictive Maintenance workflow

Among electromechanical devices in medical application, pumps are widely used: different types could be found in heamodialysis treatment, in heart-lungs assistance, even implantable. They are classified as rotating machinery and, therefore, subjected to bearing faults, misalignment, unbalance, gear faults, cavitation, which are common failure cases [22, 23].

In literature can be found example of condition monitoring related to centrifugal pumps, but [23] states that detection of faults and monitoring the

health condition of centrifugal pumps is considered to be important in oil and gas industries [12] only.

Bearings are considered as the major reason for the failure of mechanical equipment[24] in rotating machines. Compared with other mechanical parts, the service lives of bearings can vary greatly in terms of the fault occurrence time, fault type, and severity. This kind of study can be addressed to vibration analysis: defects on bearings, for example, results in specific frequencies that depend on the bearing structure and rotor speed. Each part of bearing has its own characteristics frequency.

[2] proposed using the same vibration analysis to vitro immunoassay analyzer used in one of the largest hospitals in United Arab Emirates. Once identified the belt slippage as the dominant error with a higher failure rate, data were collected by accelerometer and followed by feature extraction both in time and in frequency domain analysis using the same tool. The classification were made by a machine learning algorithm, the support vector machine, SVM, to flag cases into two classes, faulty and healthy. The failures of rotating machineries can be very critical because these lead to machinery damage, production losses and personnel injur [25],

Other authors, for example, perform both preventive and predictive maintenance program based on the type of technology decides within a hospital: preventive maintenance for older ones and PdM to newer high tech devices. Older technology devices comprised of electrocardiography (ECG) devices, infant incubators, defibrillators, surgical aspirators, and electrosurgical units. The second group, newer ones, mostly contained imaging devices. This decision is motivated by the fact that different technologies cannot be managed using the same strategy, due to their incompatible characteristics. The PdM was performed according to the manufacturers' recommendation, reporting daily checks to share with the device support

service if a failure occurred, while periodical performance verification and safety testing (PVST) which includes qualitative and quantitative tests was performed by qualified biomedical personnel on elder devices. The daily check on this group comprised both physical parameters like battery or connector presence and functional test. The reliability of both programs was determined by the failure rate of the tested components: the detection of hidden faults by the two methods ensure the possibility to build a maintenance program comprising both strategies, leading to positive results [7]. Therefore, it can be stated that both preventive and predictive maintenance require a plan for maintaining the availability of proper accessories, as recommended by Ridgway [14].

Lower maintenance costs, extend equipment life and improvement of production quality are key points of Predictive Maintenance. Since history data of devices are convinient in the deployment of a finalized PdM program, a remote storage would be further implemented. The importance of such a strategy in the healthcare industry, as said so far, is primarily due to the complexity and criticality of the equipment.

1.4 Throughout Maintenance

Equipment maintenance involves all activities relating to providing an adequate level of service and limiting down time of a device. If it was seen as an activity to be undertaken only when a breakdown occurred - fix it when it breaks -, as automatization of complex machinery takes place, enabling lowering of manual labor, factories started measuring and tracking the performances of the production output, effectiveness and personnel productivity, introducing periodic and scheduled plan. This regular activity is known as Preventive Maintenance (PM) that mainly focuses on a definite

time interval that cover the life expectancy of a component: once reached, the initial conditions are stored by substituting the component.

Manufacturing industries have pointed out that performing a traditional PM is often unnecessary because it is performed based on a certain interval without considering the actual health condition of a system. PM is a pre-planned, pre-programmed policy that can cause long period of machinery downtime for an industry, meaning a decrease of productivity, thus an increase cost of every operation.

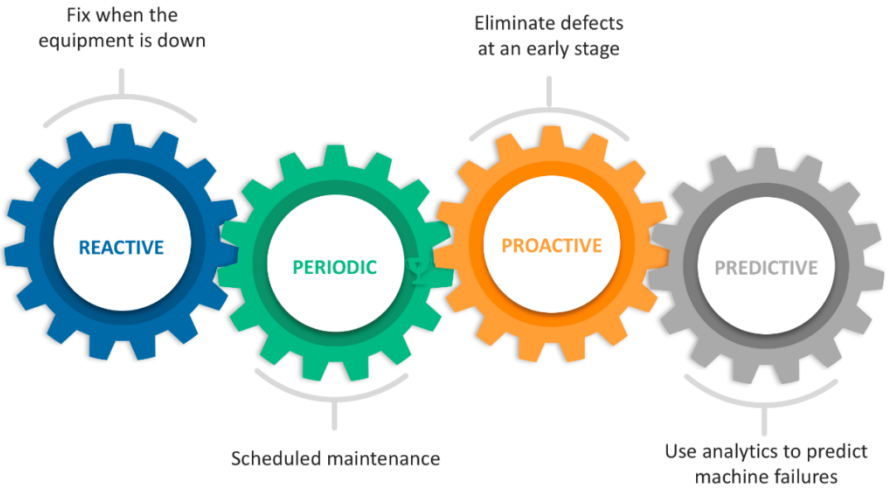

Figure 1.3: Maintenance Strategies

In the last year, instead, the attention is moving toward the operational cost, worker productivity and equipment utilization in term of advanced analytics to predict machine failure. This process goes under the name of Predictive Maintenance (PdM). Differently from PM, which surely broke down the number of failures but still considered too expensive, this newest concept of diagnosis can further reduce equipment failures or unexpected downtime based on the real-time data available, ensuring manufacturers to lower maintenance costs, extend equipment life and improve production quality. It mainly identifies the types of failure of each component within

the system and based on them predict their possible failure.

The key steps to build a good PdM program rely on data acquisition, a robust analytical model to analyze the machine data and decision making. Then, different PdM techniques can be applied to evaluate the condition of the equipment. Techniques such as Proactive or Condition-based Maintenance (CBM) can avoid unplanned stops: the first one drives the attention to identify the critical conditions under which elements are and that could cause dangerous problems to the entire system limiting its service life and substituting them to restore the initial conditions.

CBM model, instead, is based on monitoring the equipment condition during its operation: it requires a good knowledge of the technical failure mechanisms of the equipment in order to plan a proper maintenance program. A practical example from everyday life deals with cars' mileage: this parameter is used as a threshold by constructors to emit notifications to schedule car-services.

Both alternatives impose more emphasis on real-time inspections in order to draw up a correct PdM maintenance program. Other advantages include, besides shorter and fewer "planned stops", optimized handling of spare parts. By relying on the actual condition of a component together with an accurate smart tool for data elaboration, the prediction would become more and more precise over time.

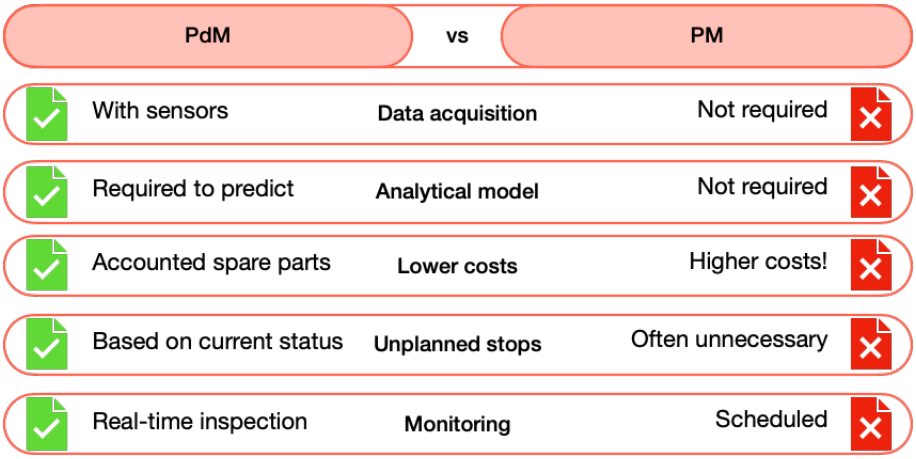

Figure 1.4: PdM vs PM

1.5 Why IoT?

In the new era of Industry 4.0, the Internet of Things is changing the way of living of everyday life. The Internet of Things is the connection between physical objects, the "things", that are embedded with software, sensors and other technologies over at the Internet, in order to acquire and exchange data in real time.[1]

Among the technologies of the 4th wave of Industrial Revolution, the Industrial IoT (IIoT) allows distant isolated objects to be sensed or controlled, thus becoming interconnected, thanks to structured interoperable protocols. Its growth in popularity and application have been possible thanks to the development of sensors capable to gather specific data according to their final goal: ranges of measure span from temperature to acceleration, from noise to pressure. Smart cities, virtual power plants, home appliances, physical devices, vehicles, and other objects embedded with electronics are part of the various IoT applications.

IoT influences companies and industries business and decision makers, with-

[1] "Internet of things", Wikipedia, The Free Encyclopedia

out any evident sign of slowing: its adoption is projected to increase up to a 94% of usage by the end of 2021. Microsoft conducted an online survey with worldwide enterprise companies. As a result, in manufacturing the top use cases for IoT are: automation (48%), quality and compliance (45%), production planning (43%), supply chain logistics (43%), and plant safety and security (33%) [26]. Moreover, it can deliver a return on investment by increasing productivity and production capacity, reducing business expenses, and lowering the chances of human error.

With the introduction of IoT, according to a PWC report, PdM is expected to reduce costs by 12%, increase uptime by 9%, reduce safety, health, environmental, and quality risks by 14% and extend the lifetime of an asset by 20% [27].

The purpose of Internet of Things is to develop a smarter environment and a simplified life-style by saving time, energy and money. These tasks are achieved by an IoT platform, that can be used to present and process data coming from the machines.

Adopters of IoT are already reaping benefits previously mentioned. Examples come from everyday experience: Thames Water is the largest provider of drinking and waste-water services in the UK and is using sensors, analytics and real time data to anticipate equipment failures and respond more quickly to critical situations, such as leaks or adverse weather events [28].

ThyssenKrupp Elevator, leader in elevator distribution, has installed MAX on more than 82000 elevators in the U.S. and 128,000 elevators in 10 countries worldwide, collecting data on components, systems and performance [29]. Thanks to its cloud-based predictive maintenance solution, algorithms can estimate the remaining lifetime of each elevator's components, by decreasing out-of-service situations through online diagnostics.

Detecting potential failure has an economic evaluation: a research con-

ducted by Electric Power Research Institute (EPRI) estimated a cost savings between $75000 to $225000 per event for megawatt-scale turbines, being reliant upon turbine rating and extent of damage (cost of a high-end condition monitoring system is about $20000, which is more than offset by the cost-avoidance savings associated with even one failure!) [30].

Concerning healthcare industries, IoT adoption will help companies in tracking patients, staff and inventory (62%), followed by the remote device and health monitoring, respectively 57% and 55% [26].

Patient care is an obvious application for IoT technologies, from scheduling appointments to monitoring conditions like diabetes. Let's think about wearable devices such as smartwatches or insulin microinfusion sets: Apple worked with Food and Drug Administration (FDA) for a number of years to receive De Novo classification for the ECG app and the irregular heart rhythm notification, making the features available over the counter, available on Apple Watch Series 4 and both a menstrual health-tracking feature and a dedicated Research app added to the Series 5. On 21st September 2020, Series 6 is released with sensor capable to measure O_2 level in blood.

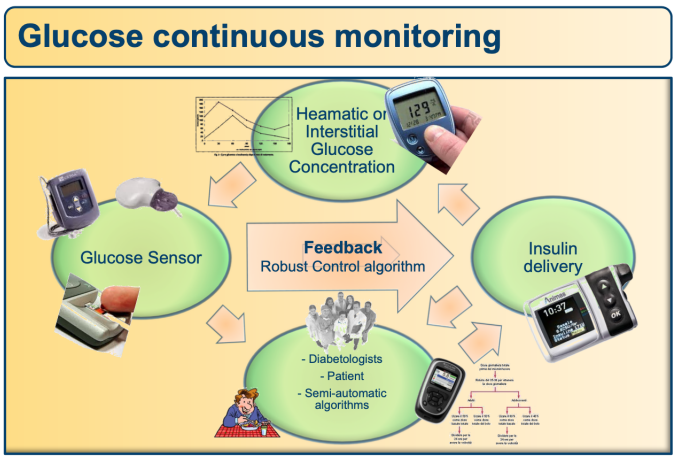

Figure 1.5: Glucose Continuous Monitoring

Devices continuously monitoring the glucose of a patient can supply insulin

when needed thanks to sophisticated algorithms (see Figure 1.5) that not only can connect with doctors but also teach the system how to deal with an increase or decrease of insulin and how to adjust itself.

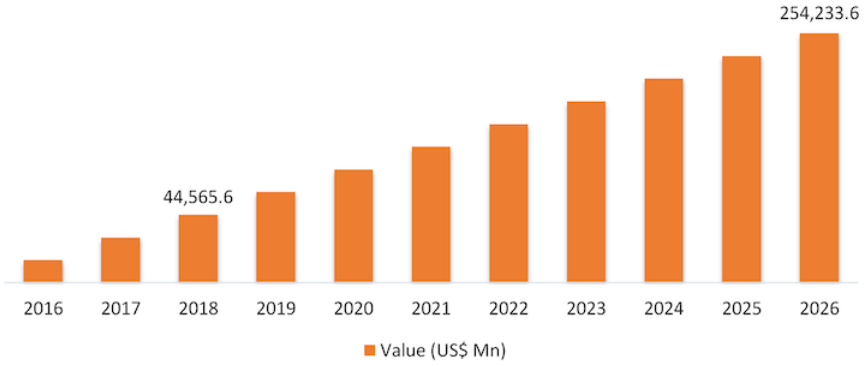

Figure 1.6: Global IoMT Market 2016-2026

The Internet of medical things (IoMT) is expected to increase its connectivity with a global market valued at US$ 44565.6 million in 2018 and to reach US$ 254233.6 million in 2026, growing at a CAGR[2] of 24.4% during the forecast period 2016 - 2026 (1.6). The global IoMT market comprises products, applications and region: in order of importance there are smart wearable devices, real-time monitoring and North America, respectively. IoT can be considered the engine of the present and of the future.

[2]Compound annual growth rate (CAGR) is an index that describes the rate at which an investment would have grown if it had grown the same rate every year and the profits were reinvested at the end of each year of the investment's lifespan.

2. Real-time Monitoring

A key point for Predictive Maintenance implementation is the real-time data collection of the parameters to determine machine condition. This translates into the choice of the correct sensor. The sensor is selected according to the system's failure to monitor: in this first part of the project the accelerometer and ball bearing represent the sensor and the system involved, respectively. Once identified, a data acquisition system should be implemented.

2.1 Data Acquisition System

Data were collected using an acquisition system made up by this components

- a Laptop;
- a triple-axis LIS3DH accelerometer;
- Raspberry Pi4;
- a couple of I2C differential bus extender;
- jumpers, Ethernet and power cables.

Rasperry is a smart and and cost-affordable solution which is nowadays used for many application such as home automation or for IoT solutions. It is possible to control its GPIO header using a number of programming languages and tools.

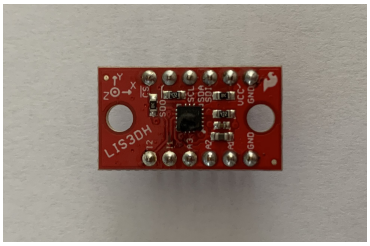

Figure 2.1: LIS3DH accelerometer
This is the first one I used to become familiar with during quarantine: it happily burnt out.

The accelerometer (2.1) was set coding two programs in python language: the first one includes all its registers available and used as a driver, while the second code, the acquisition program, retrieves data in a loop from a queue. Of course, acceleration is not given automatically in m/s^2, but in g: according to the full scale (FS) range selected, a proper conversion is obtained (number of bit and a FS). In order to facilitate post processing data, a first in first out (FIFO) buffer was implemented for each of the three output channels, X, Y, and Z. A watermark level was configured to generate an interrupt in order to know the number of samples stored in the FIFO buffer. A 400Hz frequency sampling and an I2C protocol to transfer data were chosen. The I2C bus speed on Raspberry Pi was set to 400kHz to improve its performance.

Raspberry Pi4 was monitored remotely from a laptop to launch the acquisition program and write data directly in a *.csv* file. The raw data were then imported in MATLAB R2020b to be analyzed. First trials included only a real time analysis implementing both Fast Fourier transform and Hilbert-Huang trasform in Raspian enviroment (they are described later): however, due to higher computational effort, analysis switched to MATLAB. In appendix 6.1 all the code developed to collect and analyze signals are available.

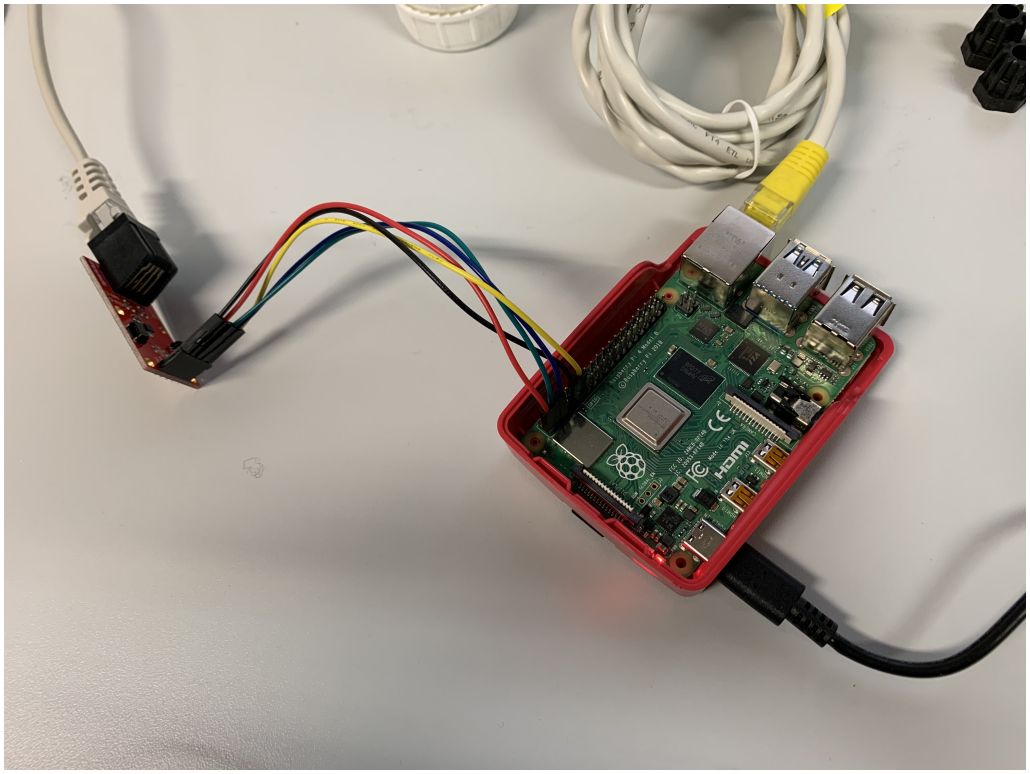

Figure 2.2: Connection between I2C bus extender and GPIO

Jumpers links the accelerometer to the GPIO pins along the board, as seen in figure 2.2: red color for Vcc, black for Ground, green and blu for SDA and SCL respectively, yellow to the interrupt.

LIS3DH's shield was cut and resin glued inside a 3D printed *bussolotto* (2.3a): it was placed inside the bearing pin for bearing tests, back the head of the pump for the second test, as shown in figures 2.3b, 2.3c respectively. A couple of I2C bus extender (fig 2.4) completes the circuit extending both the range of I2C bus and the distance between the devices through Ethernet cable.

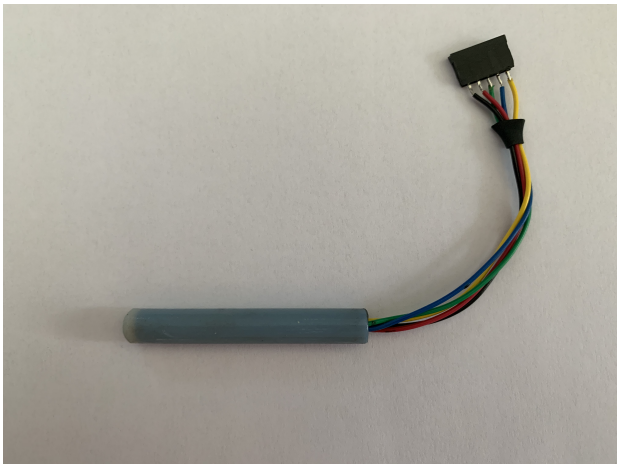

(a) *Bussolotto*

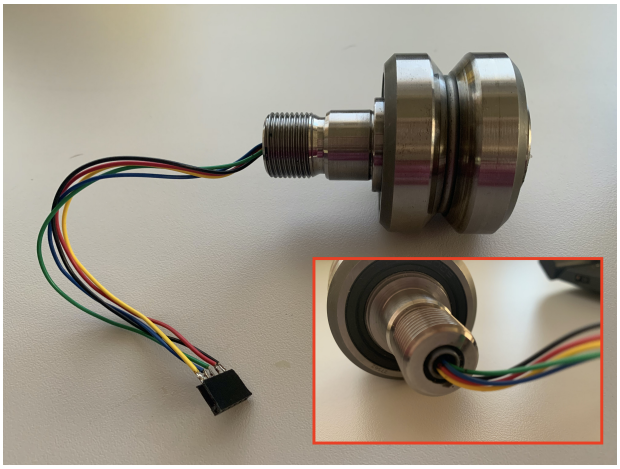

(b) Bearing case

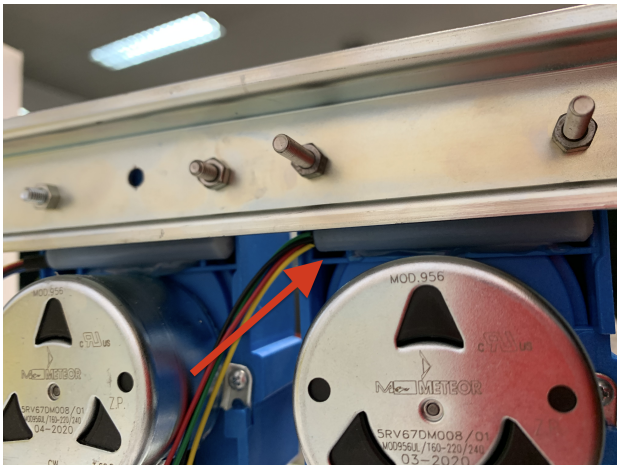

(c) Roller pump case

Figure 2.3: *Bussolotto* and its Position

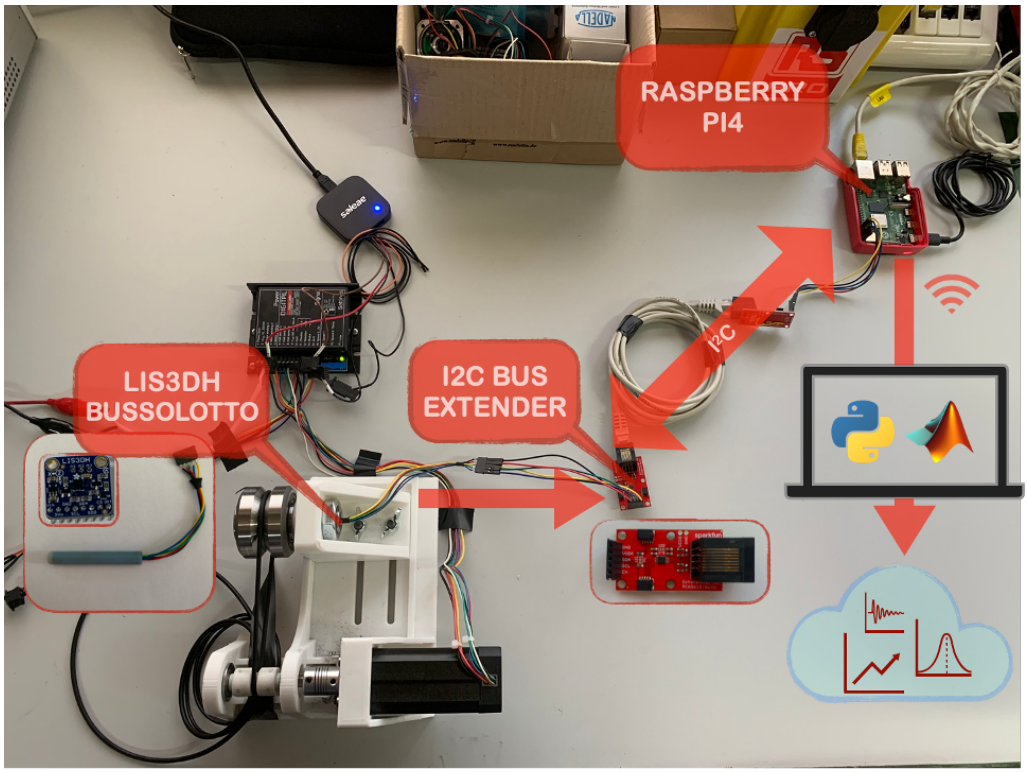

Figure 2.4: Data acquisition configuration

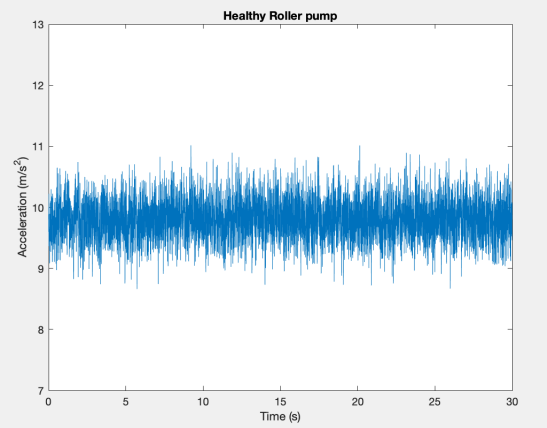

Figure 2.5: Resultant acceleration

2.2 Worflow

As described in 2.1, data are collected for each of the output channel of the accelerometer, X,Y and Z and each signal consists in the resultant acceleration (2.5), $r = \sqrt{X^2 + Y^2 + Z^2}$, expressed in $\mathrm{m/s^2}$. Each signal has been "normalized" in order to have $g = 9,806$ mean.

FFT, Envelope analysis and HHT are then applied to data. FFT shows all the frequency components which characterizes the signal, while the envelope analysis mainly focuses on the impulsiveness of the signal, after filtering. HHT is the used to capture time-frequency dependency of the signal.

The same workflow characterizes both tests: in particular, with bearing theoretical features are known. The identification of a specific trend within each signal is required in order to set a *pattern* able to recognize a particular faulty or healthy condition of the roller pump, instead. The instantaneous energy released by the signal helps in identifying the stressed frequencies.

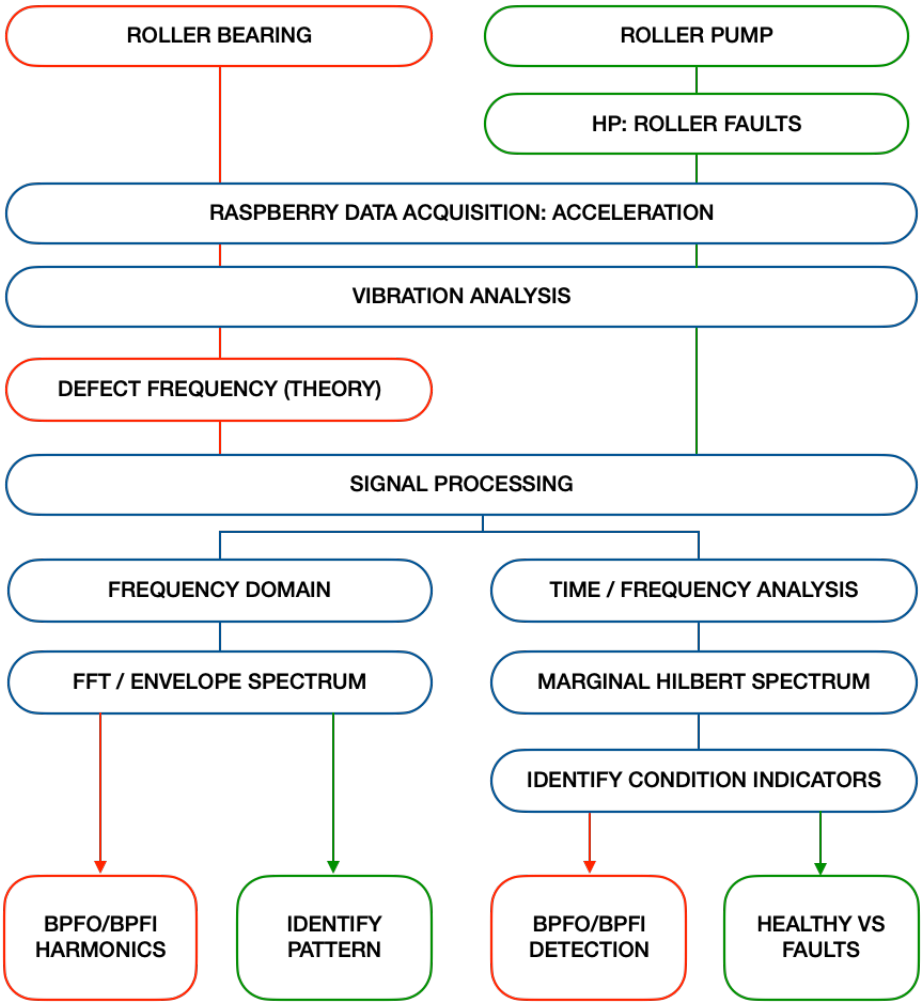

Figure 2.6: Workflow

3. Predictive Maintenance Techniques

Predictive maintenance starts with the periodic or continuous monitoring of the mechanical, electrical or other indicators of the functioning of the systems or processes that can provide the data necessary to ensure the maximum interval between the repair and maintenance works, respectively, to minimize the cost of interruptions of maintenance [12].

Beginning with data that describes the system in a range of healthy and faulty conditions, a detection model (for condition monitoring) or a prediction model (for prognostics) could be implemented. *Diagnosis* concerns the current state of the machine to detect and classify patterns between different failures; *prognosis* aims to predict the future life state of the machine in order to realize the breakdown time.

In 1.3 of first chapter, known PdM techniques have been mentioned: vibration or current monitoring, thermography and tribology. For example, thermography is a predictive maintenance technique that uses instruments that can monitor infrared energy emission to determine operating conditions; tribology techniques concern lubricating oil analysis, spectrographic analysis, ferrography, and wear particle analysis.

Among PdM techniques in literature, **vibration** is identified as one of the key components of machine diagnostics. It has been reliably used to monitor the most critical equipment across a wide range of industrial applications, mainly for the detection of mechanical faults such as bearing, misalignment,

imbalance, bent shaft [22, 23, 25].

Great amount of papers concentrate on ball or cylindrical element bearing vibration monitoring [31–33] because bearings are an important element in a variety of industrial applications. Rolling element bearings are found in almost all types of rotating machinery, ranging from large turbines to slower rotating motors, from relatively simple pumps and fans. An unexpected failure of the bearing may cause significant economic losses: this is the reason why vibration monitoring is one of the most important methods to collect real-time data.

In this chapter an overview of vibration monitoring analysis on roller bearing and signal processing tools are presented together with a case study conducted during the internship. This method is the starting point for the next implementation on the roller pump results.

3.1 Vibration Monitoring

The vibration analysis technique consists of vibration measurement and its interpretation. Beside being a common technique used to evaluate moving parts of an electromechanical system to predict its failures as mentioned before, literature confirmed it as the most effective method for bearing fault diagnosis.

When a machine is operating properly, vibration is small and constant; however, when faults develop and some of the dynamic processes in the machine change, the vibration spectrum also changes: defects on bearings, for example, results in specific frequencies that depend on the bearing structure and rotor speed. Each part of a bearing has its own characteristics frequency:

- FTF, Foundamental Train Frequency of the cage

$$FTF = \frac{1}{2} * f * [1 - \frac{d}{D} * \cos\alpha] \tag{3.1}$$

- BPFO, Ballpass Frequency on Outer race

$$BPFO = \frac{Z}{2} * f * [1 - \frac{d}{D} * \cos\alpha] \tag{3.2}$$

- BPFI, Ballpass Frequency on Inner race

$$BPFI = \frac{Z}{2} * f * [1 + \frac{d}{D} * \cos\alpha] \tag{3.3}$$

- BSF, the frequency rotation of the roller element around its own axis (spin)

$$BSF = \frac{D}{2d} * f * [1 - (\frac{d}{D} * \cos\alpha)^2] \tag{3.4}$$

where D is the pitch diameter, corresponding to the diameter of the cage or $D = \frac{Douter - Dinner}{2}$; d is the ball diameter, α the contact angle, Z the number of ball and f the rotor speed.

3.1.1 Roller Bearing Experimental set up

NADELLA S.p.A., a supplier company for rolling bearings and linear guide components for industrial motion technology, supplied us with two roller bearings to be tested: a healthy bearing, with no sign of damages and an internally damaged one, H and D hereinafter. A NADELLA RKY52 bearing was chosen with the mechanical characteristics listed in table 3.1.

First trials have be conducted in the in-house laboratory room with a 3D printed basement (fig.3.2): since rollers were not subjected to external applied load, results were not very encouraging. Tests moved outside: the rollers were tested within their laboratory, mounted on a test bed machinery with adjustable load cell, as shown in 3.3 and 3.4.

Table 3.1: Mechanical features of RKY52 bearing

MECHANICAL DIMENSION	
D = D cage [mm]	30.45
d = d ball [mm]	5.8
Z [n° ball]	15
α[°] contact angle	14

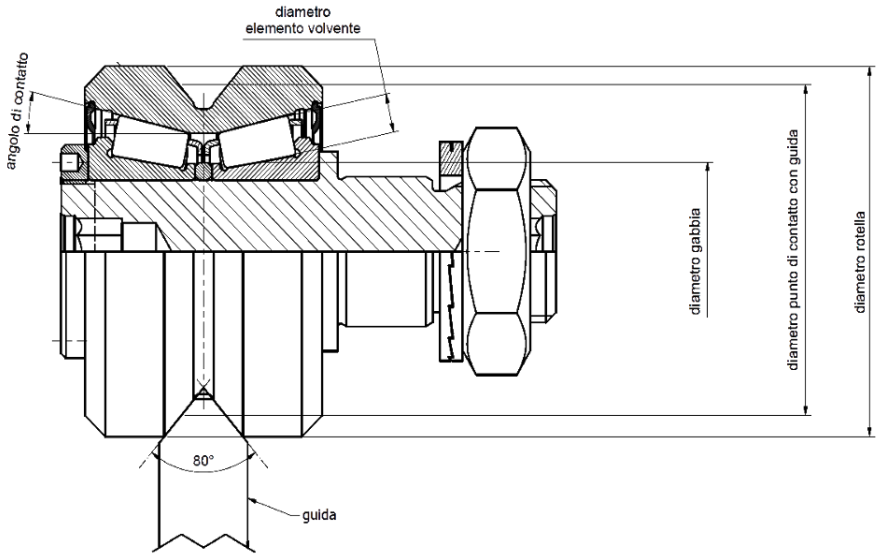

Figure 3.1: Mechanical Drawing of NADELLA RKY52 bearing

The rotational speed was set equal to 1 m/s and axial loads to 4000N and 8000N as suggested by Nadella engineer to be the typical value at which these bearing are subjected during normal working condition.

According to frequency espressions, table 3.1 and the specification about rotational speed (calculated with appropriate trasmission ratio), the characteristics frequencies of the systems are, respectively:

$$FTF = 1.08 \text{ Hz}$$

$$BSF = 6.73 \text{ Hz}$$

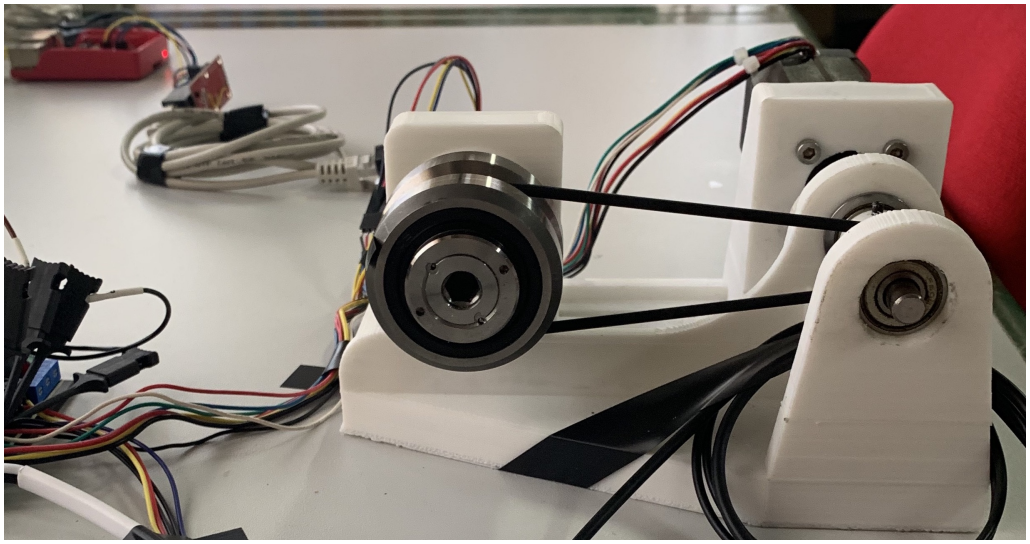

Figure 3.2: Experimental Set Up - First trials

$$BPFO = 16.22 \text{ Hz}$$

$$BPFI = 23.57 \text{ Hz}$$

Data were collected through an accelerometer with a sampling rate set to 400Hz, duration of t=30s. The acquisition system will be further described in Chapter 4. Three kinds of signal processing tools are then used to deal with health indicators match: FFT, Envelope Spectrum and Hilbert Huang transform. In the next section these tools are described reporting results from bearing tests.

Figure 3.3: Experimental Set Up Roller Bearing - 1

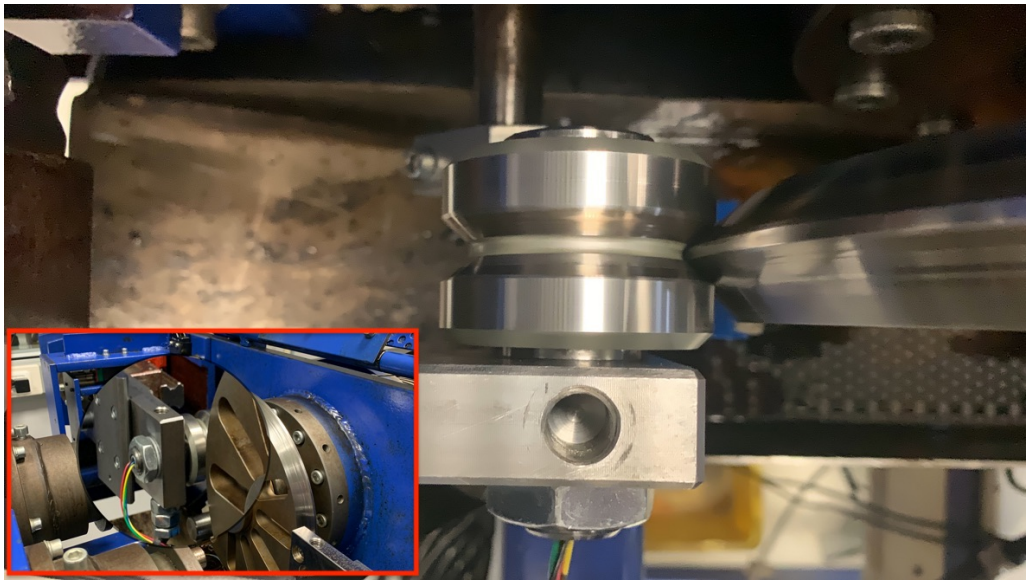

Figure 3.4: Experimental Set Up Roller Bearing - 2

3.2 Signal Processing techniques

Signal processings tecniques are used to analyze, preprocess, and extract features from uniformly and nonuniformly sampled signals. There are three analysis methods to deal with vibration detection:

- Time-Domain Analysis;
- Frequency-Domain Analysis;
- Time-Frequency Analysis.

Each of them is explained considering results from roller bearing tests, elaborated with MATLAB.

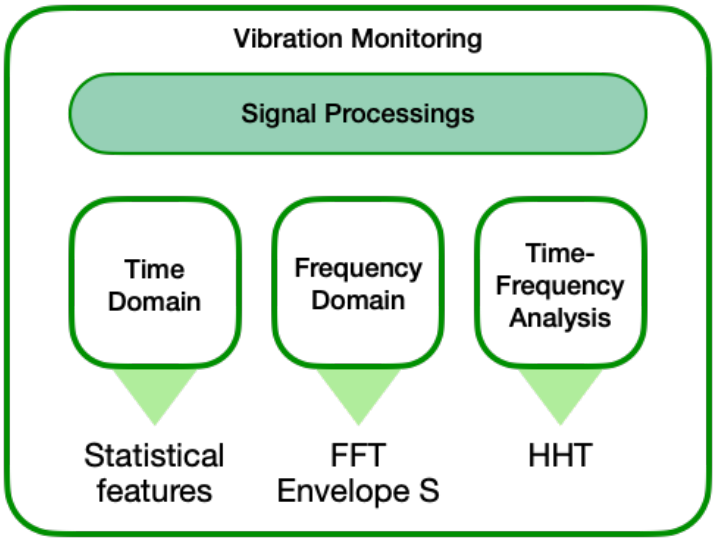

Figure 3.5: Signal Processing techniques

3.3 Time Domain Analysis

Time-domain analysis shows how a signal changes over time and for machine monitoring only calculates time-domain statistical characteristic parameters such as mean value, variance, kurtosis, etc. of the vibration signal. In this cases, all the signal where normalized so to have $g = 9.806$ mean and kurtosis index was calculated automatically in the Envelope Spectrum analysis performed to find the most impulsive band of the signal. However, as stated in [24] using statistical tools only cannot determine the severity of a fault.

3.3.1 Frequency Domain Analysis

Frequency-domain analysis is widely used in such areas as communications, geology, remote sensing, and image processing. While time-domain analysis shows how a signal changes over time, frequency-domain analysis shows how the signal's energy is distributed over a range of frequencies.

The transformation from time to frequency domain of a signal is needed to determine its frequency and phase; moreover in condition monitoring techniques has been proved that some faults, as described previously for bearings fault, have certain frequencies. This operation is provided by Fast Fourier transform.

Another application in frequency-domain analysis is filtering of the signal, useful to emphasise the signal itself over a precise band, removing noise and eliminating useless information with appropriate filters: in Envelope Spectrum analysis a band-pass filter is used to this purpose.

3.3.1.1 Fast Fourier Transform

The conventional technique of Fast Fourier Transform (FFT) is one of the most popular vibration method for fault detection and it has been widely and successfully applied for stationary signals [23]. This algorithm is based on Fourier transform, a mathematical operators that decomposes a function (the analytical signal) into the sum of a (potentially infinite) number of sine wave frequency components. The spectrum of frequency components is the frequency domain representation of the signal. The signal must be converted from continuous to discrete form, through Discrete Time Fourier Transform (DFT) calculated as follow:

$$Y(k) = \sum_{i=0}^{N-1} y(i) * e^{-j\frac{2\pi ik}{N}} \tag{3.5}$$

where $e^{i2\pi/N}$ is a primitive Nth root of 1. This definition directly requires *O(*N^2*)* operations: there are N outputs Y_k, and each output requires a sum of N terms. To accelerate the computation, FFT algorithm is implemented to rapidly compute the same results in *O(NlogN)* operations, meaning high computational speed compared to Fourier transform.

Applying FFT to vibration signal collected from both roller bearings with two different loads, the spectra result in (figs 3.6,3.7):

FFT provides a clear distribution of all frequency components of a given signal. The dashed lines referred to the harmonics of BPFO and BPFI (exception made for the yellow and green ones, respectively indicating the shaft rotation and the BSF).

The difference between H and D bearings is highly visible due to the power amplitudes that mark the D roller compared to H one. In fact, some harmonics match with the theoretical frequency that refers to bearing faults. It can also be noted how the bearing reacts if loaded with different loads.

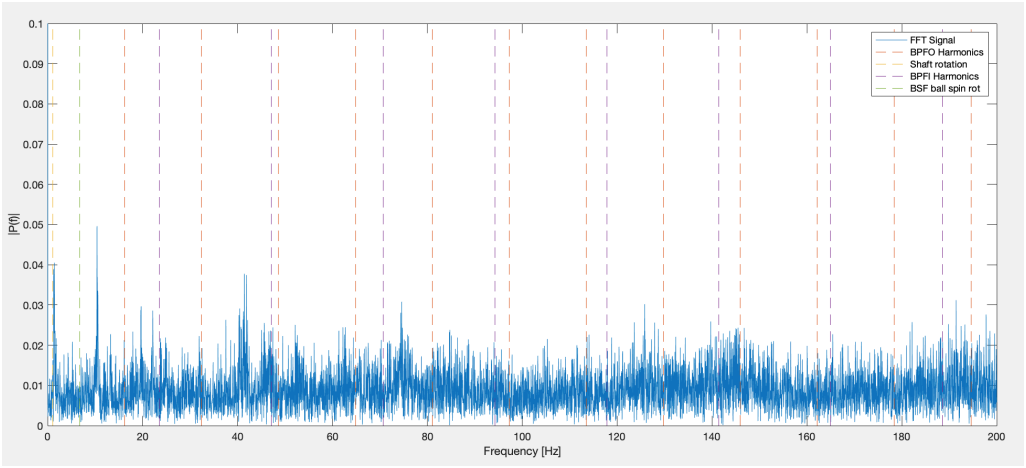

(a) H bearing, L=4000N: FFT

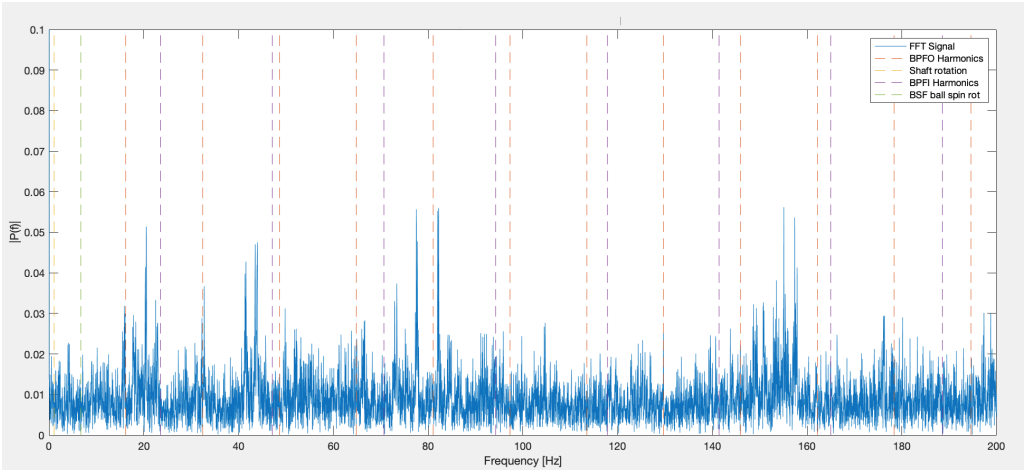

(b) D bearing, L=4000N: FFT

Figure 3.6: Healthy vs Damaged roller bearings, L=4000N: FFT

However, since FFT represents all the frequency content comprised in the signal, some harmonics may be added to the signal due to test bench and other components that might jam the signal and other critical frequencies may be lost in the analysis. This is the main disadvantage of the FFT.

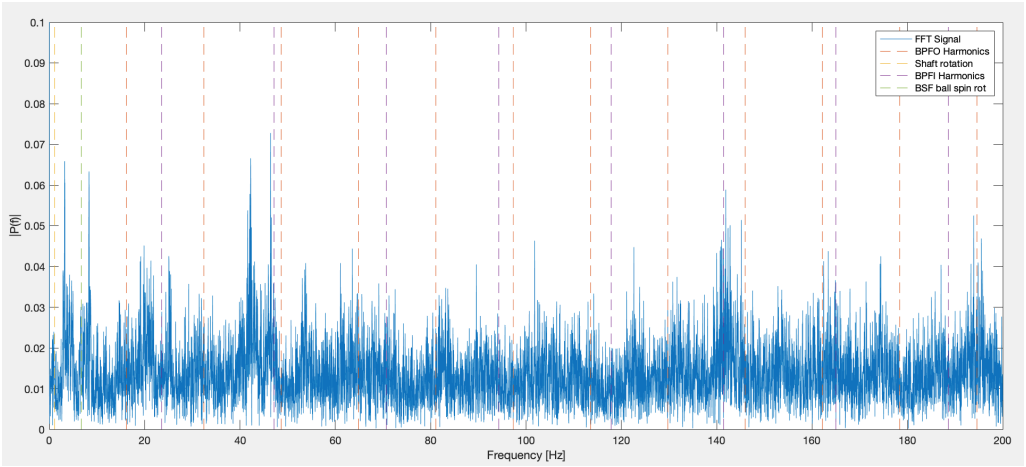

(a) H bearing, L=8000N: FFT

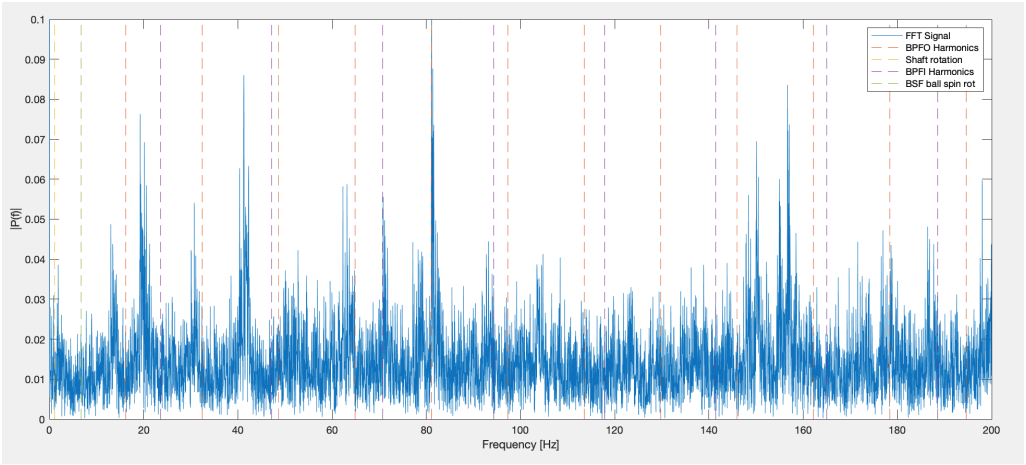

(b) D bearing, L=8000N: FFT

Figure 3.7: Healthy vs Damaged roller bearings, L=8000N: FFT

3.3.1.2 Envelope Spectrum Analysis

Envelope analysis is a technique with certain advantages in roller bearing diagnostics, being very effective in fault identification at early stages [22]. It helps us to extract the bearing fault signal as it enhances the impulsiveness from the background noise. The efficiency of this diagnostic method for rolling element bearings depends on the choice of the most impulsive band for demodulation by band-pass filtering the signal. Briefly,envelope analysis involves steps in 3.8.

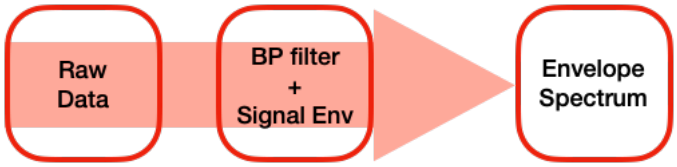

Figure 3.8: Process toward Envelope Spectrum

Applying spectral kurtogram [34] to the signal, the most impulsive bands stand out, giving reference values of filter's center frequency and bandwidth in ordert to select the proper bandpass filter (example in fig 3.9).

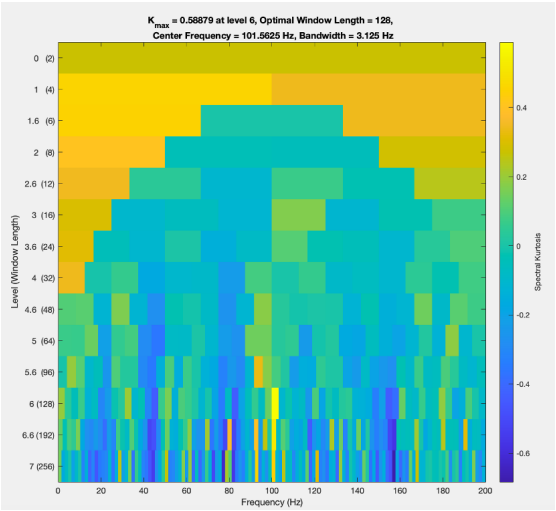

Figure 3.9: Kurtogram on D signal bearing; L=4000N

Looking at figs 3.11b and 3.12b, H bearings does not show any kind of peak related to impulsiveness of the signal, as a confirmation of its health status, while D ones 3.11a and 3.12a highlight some harmonics that both matches with BPFO and BPFI. Same results are shown with fc=1600Hz, where in 3.10 a zoom on 0-300 Hz band shows the impulsiveness of BPFO and BPFI.

However, these methods in frequency domain has flaws and loses some characteristics of nonlinear vibrations, meaning that the monitoring frequency band has a decisive impact on the analysis results. As discussed in [23, 33], in frequency analysis time-related information is lost and it is difficult to classify between the failures precisely: FFT has limited ability in revealing the precise significant frequencies, whereas according to [34] envelope analysis method has the drawback of requiring reference vibration data which are not always available. Therefore the need of alternative methods is required to deal with time-frequency characteristics.

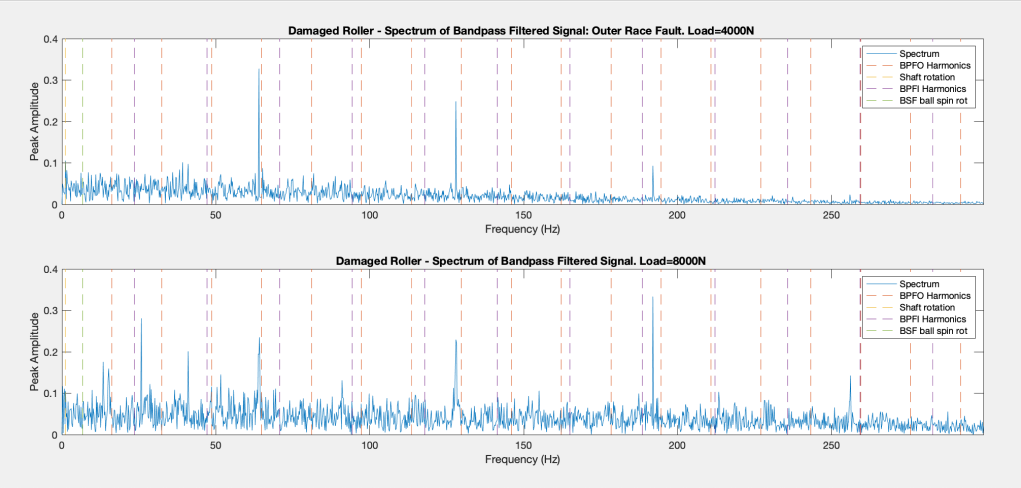

Figure 3.10: Comparison between L=4000N and L=8000N for D roller

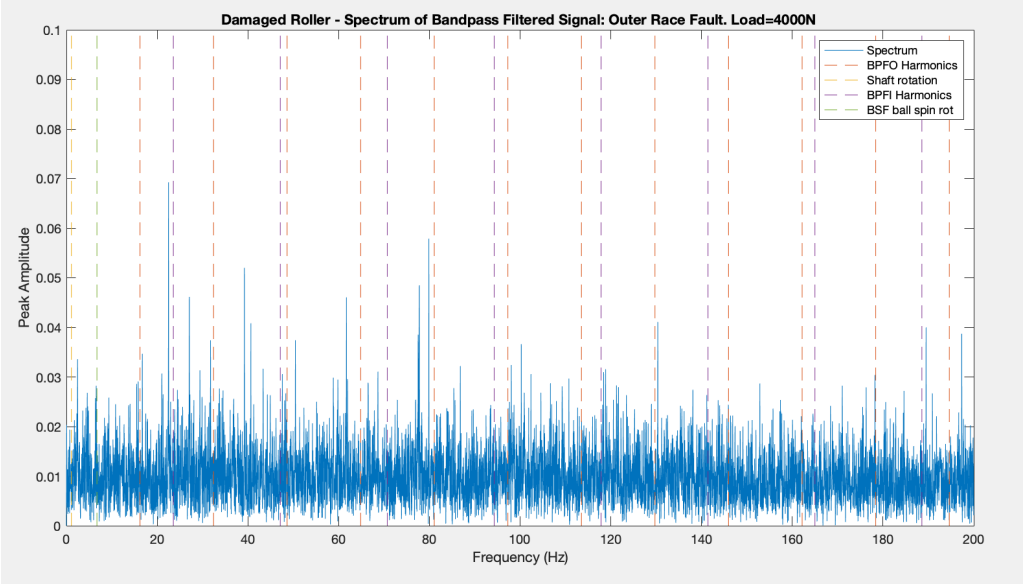

(a) D, L=4000N: Envelope Spectrum

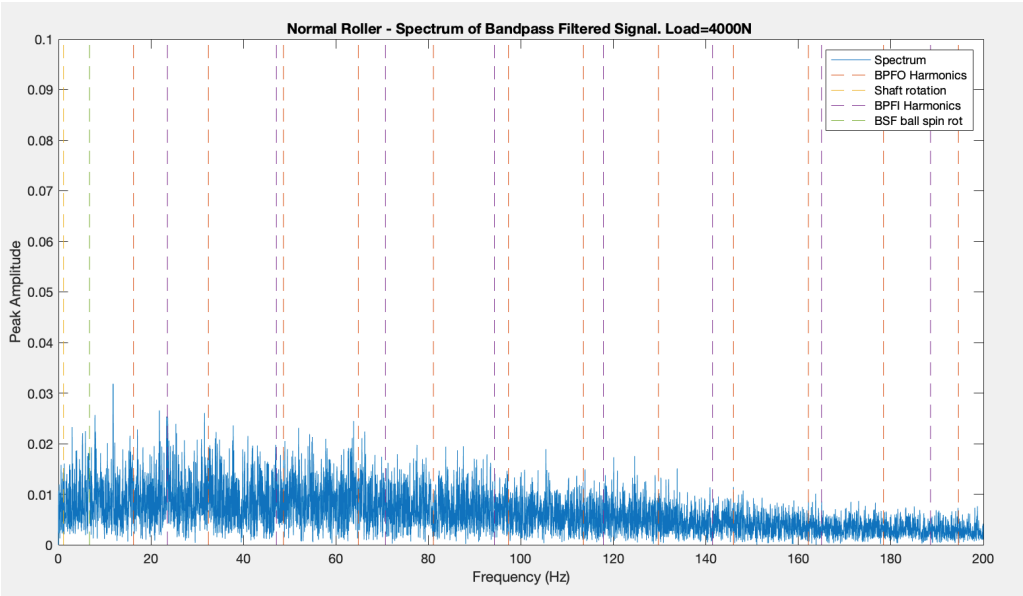

(b) H, L=4000N: Envelope Spectrum

Figure 3.11: H vs D, L=4000N: Envelope Spectrum

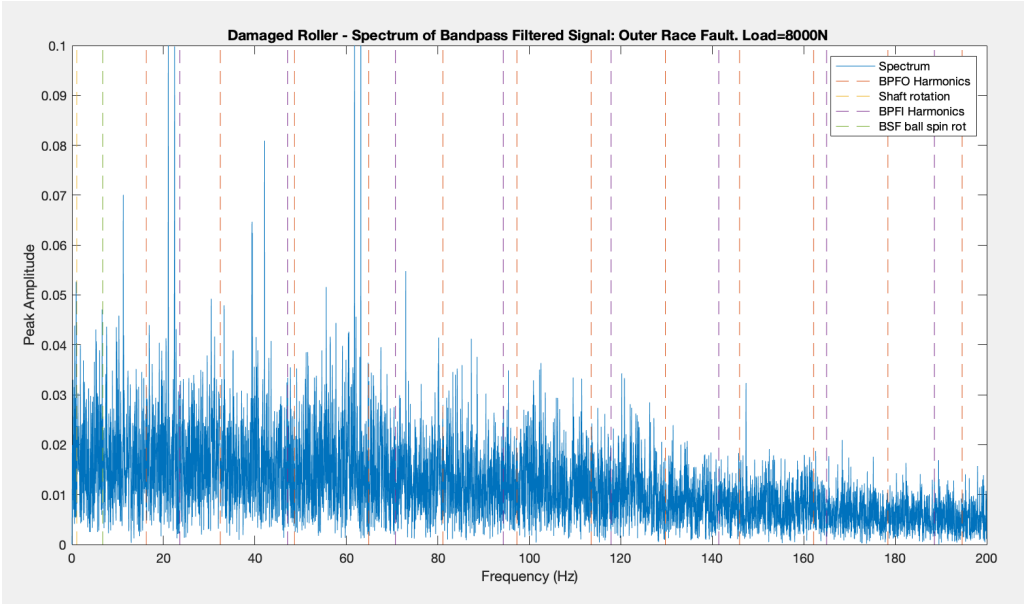

(a) D, L=8000N: Envelope Spectrum

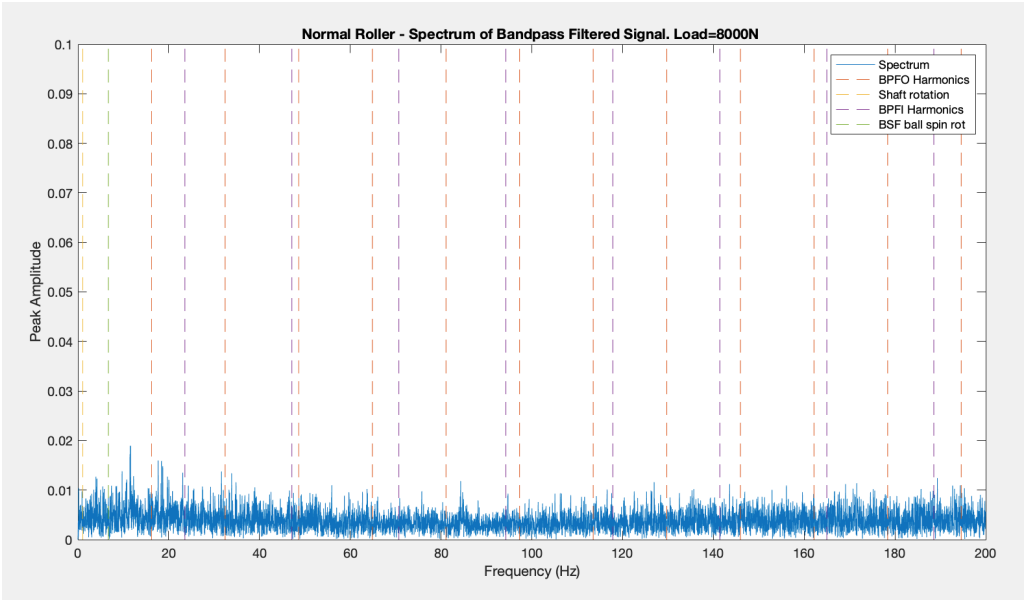

(b) H, L=8000N: Envelope Spectrum

Figure 3.12: H vs D, L=8000N: Envelope Spectrum

3.3.2 Time - Frequency Analysis

When a ball bearing fails, the vibration signal has a tendency to exhibit strong non-stationary and nonlinear characteristics as noted in [24]. That's why a proper techniques is needed to avoid loss of information related to this kind of signals. For this purpose Time-Frequency Analysis has been empirically introduced by Huang [35].

3.3.2.1 Hilbert-Huang Transform

Hilbert-Huang transform is an empirical technique involved in many research fields such as geophysics, image processing, biomedical signal processing and fault detection. Two steps are required to implement this algorithm:

1 Decomposition of the signal in multiple Intrinsic oscillatory mode functions (IMFS);

2 Application of Hilbert transform to each IMF in order to extract instantaneous frequencies and amplitudes of the signal in order to calculate the Marginal Hilbert Spectrum.

Huang [35] introduced the concept of IMFs as functions that require:

- to have the number of extrema and the number of zero-crossings that must either equal or differ at most by one, and
- at any point, the mean value of the envelope defined by the local maxima and the envelope defined by the local minima equal to zero.

Each IMF can have a variable amplitude and frequency as functions of time. In order to extract each intrinsic mode function from the signal, an Empirical Mode Decomposition (EMD) is developed. The EMD requires a sifting

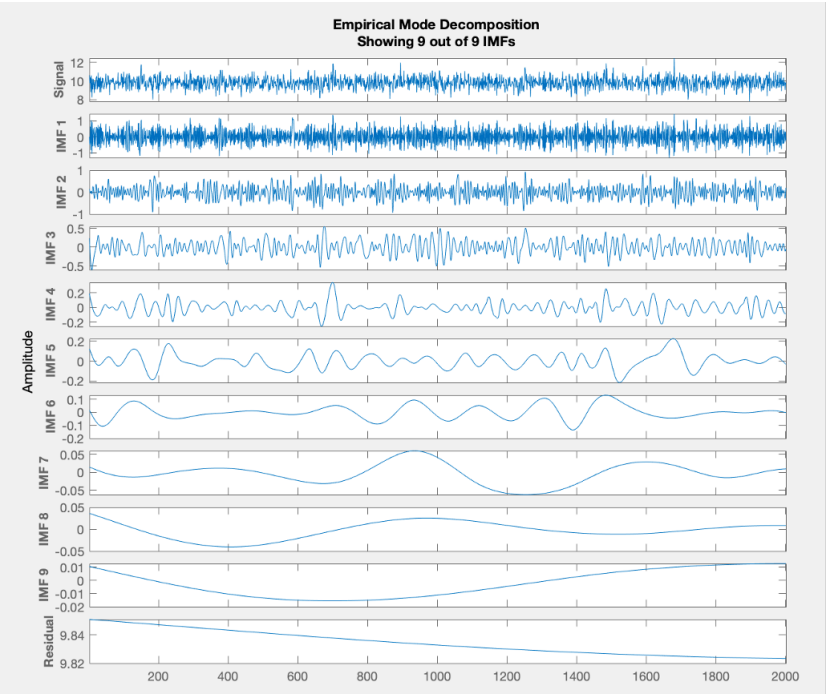

Figure 3.13: EMD - Damaged roller, L=4000N

process that involves, at each step, the identification of the upper envelope and lower envelope of the signal, and iteratively its removal from the signal: the criterion stops after i iterations when the mean envelope is close to zero at each point, or when the signal becomes a monotonic function. The extraction process of IMFs is summarized in fig.3.14; in fig.3.13 EMD has been applied on 5 seconds of vibration record for the damaged bearing. As a result (fig.3.13, each IMFs include frequency bands which range from higher frequency content (shortest period) to lower frequency content, from top to bottom respectively. The frequency band contained in each component is different from a component to another, and these frequencies change according to the signal [21, 35].

Once IMFs have been extracted, next step of HHT algorithm is the application of Hilbert transform to each of them:

$$H[c_i(t)] = \frac{1}{\pi} \int_{-\infty}^{+\infty} \frac{c_i(\tau)}{t-\tau} d\tau \tag{3.6}$$

Thanks to this transform, the analytic signal can be written in a complex conjugate pair $z_i(t)$ that allows to express both amplitude and phase of the signal [35]:

$$z_i(t) = c_i(t) + jH[c_i(t)] \tag{3.7}$$

which can be expressed as:

$$z_i(t) = a_i(t)e^{j\omega_i(t)} \tag{3.8}$$

where a_i is the amplitude and $\theta_i(t)$ the phase defined as:

$$a_i(t) = \sqrt{c_i(t)^2 + H[c_i(t)]^2} \tag{3.9}$$

$$\theta_i(t) = \arctan\left(\frac{H[c_i(t)]}{c_i(t)}\right) \tag{3.10}$$

The instantaneous frequency is therefore given by:

$$\omega_i(t) = \frac{d\theta_i(t)}{dt} \tag{3.11}$$

Toward the last point of Hilbert-Huang algorithm, the original signal can be expressed as:

$$x(t) = \mathrm{Re} \sum_{i=1}^{n} a_i(t) e^{(j \int \omega_i(t) dt)} \tag{3.12}$$

where $\mathrm{r}_n(t)$ has been left out.

Eq. 3.7 lets to represent in a three-dimensional plot the amplitude and the instantaneous frequency, designating this time-frequency distribution a the Hilbert-Huang Spectrum *H(ω,t)*:

$$H(\omega, t) = \mathrm{Re} \sum_{i=1}^{n} a_i(t) e^{(j \int \omega_i(t) dt)} \tag{3.13}$$

Last point concerns the definition of Marginal Hilbert Spectrum *h(ω)*:

$$h(\omega) = \int_0^T H(\omega, t) dt \tag{3.14}$$

which is also defined as the squared amplitude of the signal, that is the instantaneous energy of the signal.

This is what is known as Hilbert-Huang transform, which offers a measure of amplitude contribution from each frequency and time, giving the exact occurrence time of that oscillation with Hilbert-Huang spectrum, while with the marginal Hilbert spectrum (MHS) offers a measure of the total amplitude (or energy) contribution from each frequency value [21].

[36] stated that the frequency in *h(ω)* has a totally different meaning from the Fourier spectral analysis. Here the existence of energy at a frequency ω means that a component has higher probability [21, 33] to appear locally in the time-frequency distribution, whereas in Fourier the frequency existence means that a component of a sine or a cosine wave is persisting the time span of the data, thus losing time-related information.

This method has been applied also on the two bearings: the first four IMFs have been selected to bearing purpose, then MHS has been calculated. The last IMFs are not considered since they lose physical meaning.

At a first sight, the impact of the rollers from Hilbert Spectrum is highly noticeable: if we compare every imfs, the healthy roller spectrum shows less

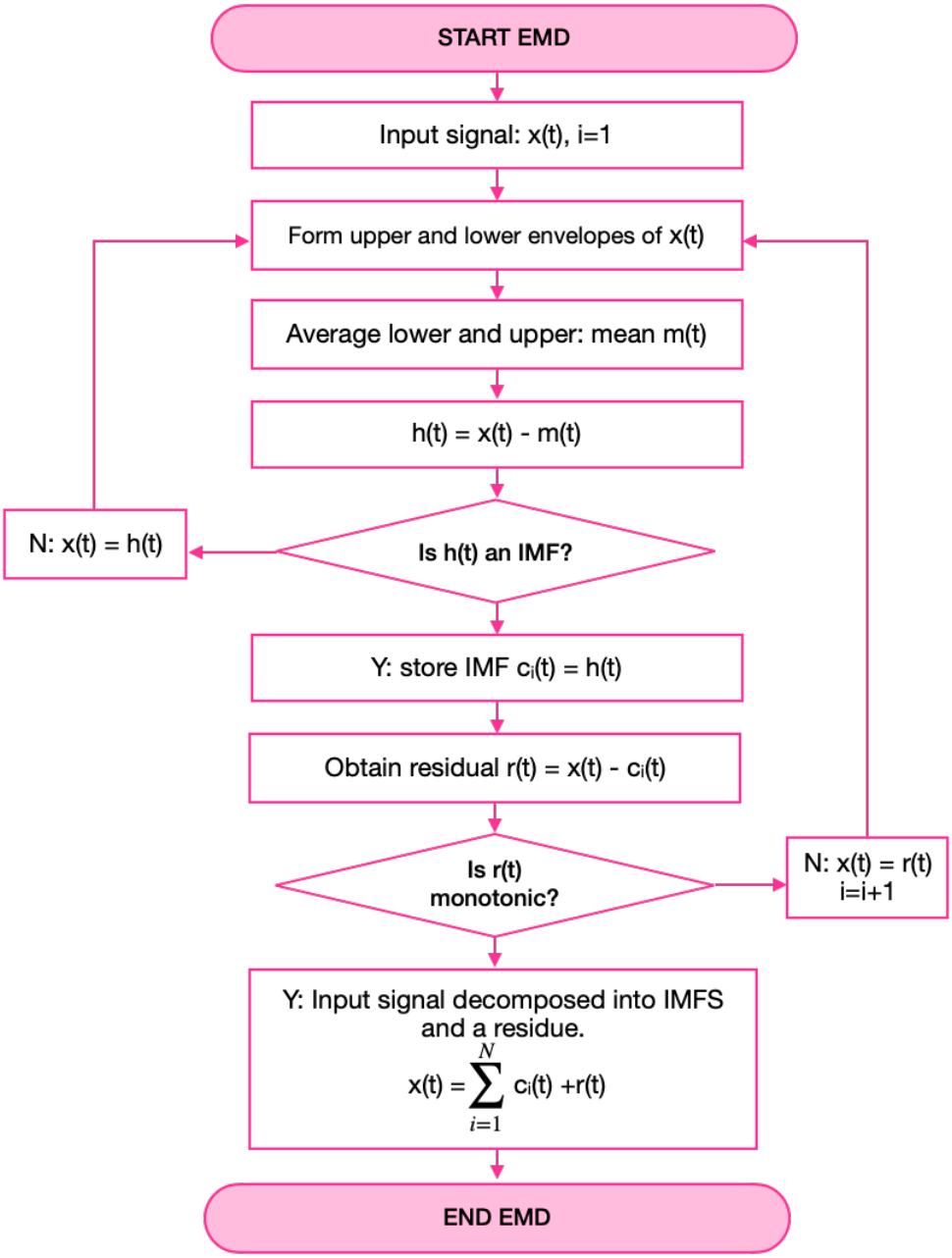

Figure 3.14: EMD flowchart

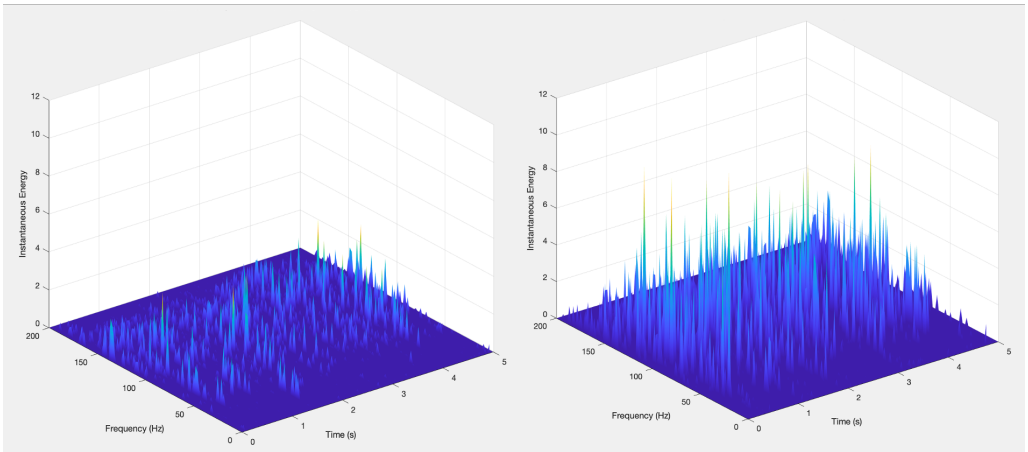

(a) HHS 1, D

Left: L=4000N; right: L=8000N

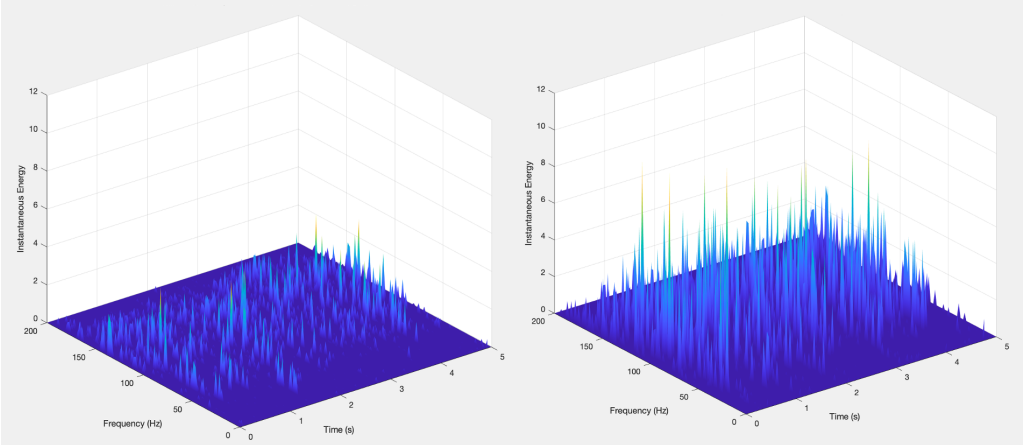

(b) HHS 1, H

Left: L=4000N; right: L=8000N

energy contribution than the damaged roller one. It happens also if the the bearings are subjected to the higher load.

By making MHS, we are able to extract at every single time-point of the signal its instantaneous frequency and energy. As said before, the energy calculated estimates the probability to find such frequency in a precise band, by summing its contribution over time.

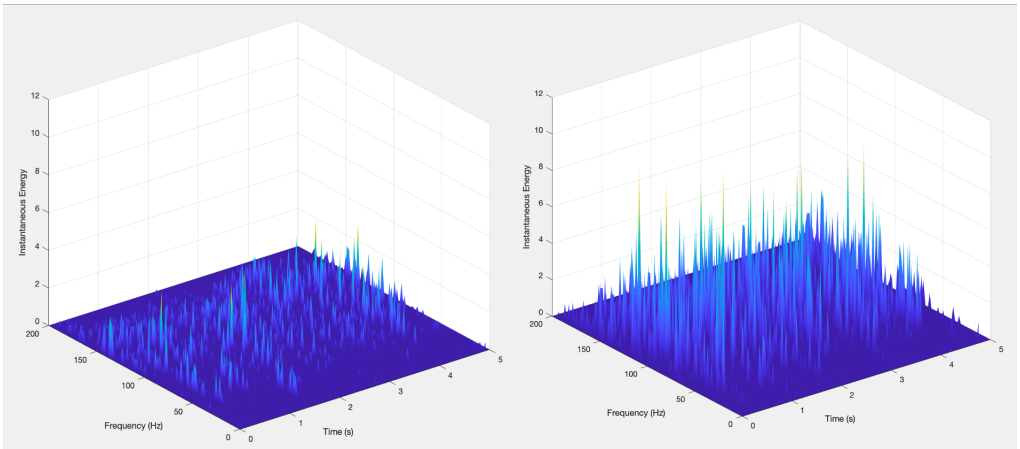

Figure 3.16: HHS 2, D

Left: L=4000N; right: L=8000N

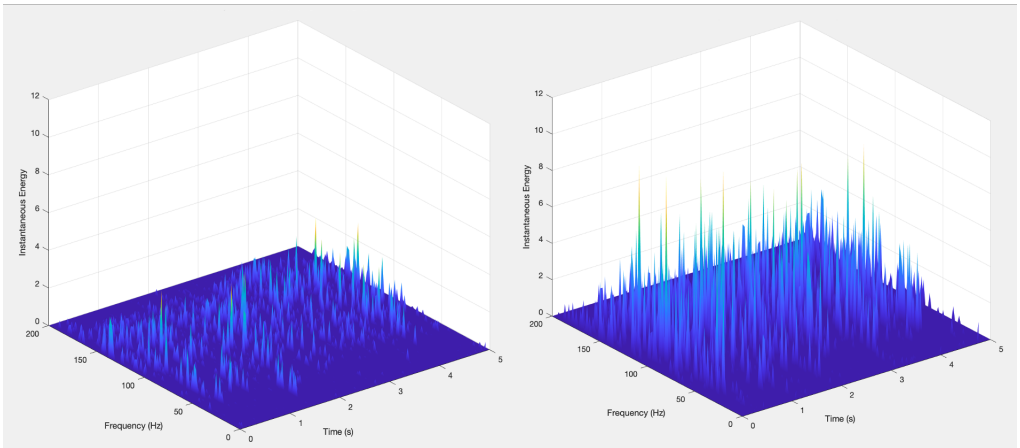

Figure 3.17: HHS 2, H

Left: L=4000N; right: L=8000N

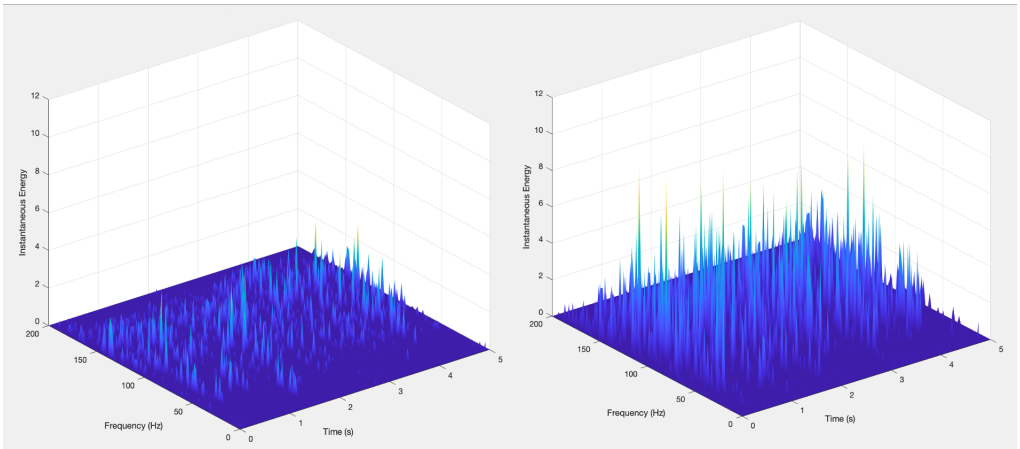

Figure 3.18: HHS 3, D

Left: L=4000N; right: L=8000N

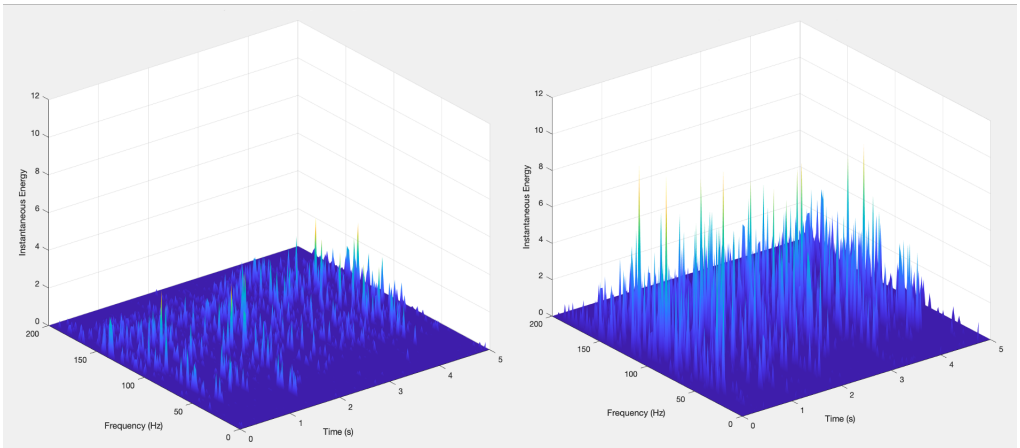

Figure 3.19: HHS 3, H

Left: L=4000N; right: L=8000N

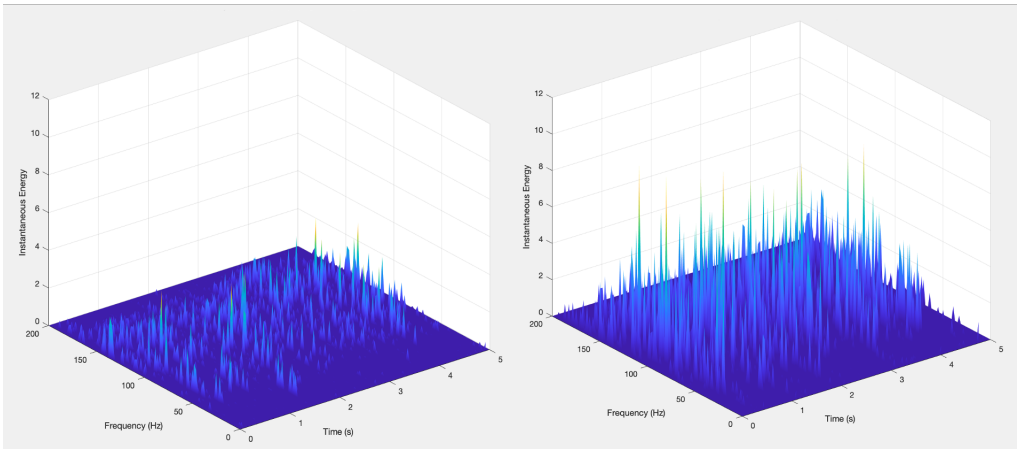

Figure 3.20: HHS 4, D

Left: L=4000N; right: L=8000N

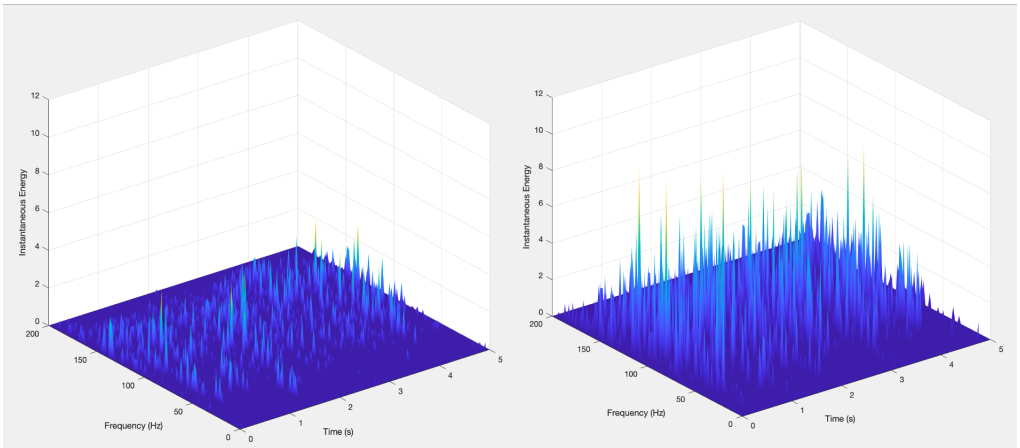

Figure 3.21: HHS 4, H

Left: L=4000N; right: L=8000N

Table 3.2: Marginal Hilbert Spectrum: BPFI

BPFI	D 4000N	H 4000N	D 8000N	H 8000N
IMF 1	0,0226	0,0329	0	0,3227
IMF 2	0,0013	0,5610	0,6699	1,7102
IMF 3	0,5114	0,3110	1,3987	0,9377
IMF 4	0	0	0	0

Table 3.3: Marginal Hilbert Spectrum: BPFO

BPFO	D 4000N	H 4000N	D 8000N	H 8000N
IMF 1	0	0	0,1204	0
IMF 2	0,1774	0,0798	0	0
IMF 3	1,2116	0,1755	1,7843	1,0601
IMF 4	0,0137	0,0022	0,1492	0,0106

As summarized tables 3.3 3.2, the instantaneous energy values corresponding to the characteristics frequency are lower for Hs (as expected) with respect to Ds case, both 4000N and 8000N case respectively. Remind that BPFO = 16.22 Hz and BPFI = 23,57 Hz The highest contributions are given in the 3rd IMFS: this as a confirmation that BPFO and BPFI are located in this frequency band. Summing their weights over time, the total amplitude of the frequency we are interested in is found.

These techniques have been proved on roller bearing. Results from this analysis shows how FFT is useful as a first attempt to provide a clear distribution of all frequency components of the signal, but loose time-related information; the Envelope Spectrum is able to recognize and extract bearing faults as it enhances the impulsiveness from the background noise. The decomposition of the signal through HHT enanches the selection of the correct IMF according to bearing indicators to predict time-frequency behavoiur of the signal. The probability energy density in bearing cases shows an increasing trend for both BPFO and BPFI frequency, from Damaged to Healthy case for both loading case, in lower frequency components of IMFs. The damaged bearing, however, was damaged on both internal and external race, for which I was not able to find a clear damage profile. These tools were validated in order to propose the same techniques on another device which is not so widely cited in literature for this application: the roller pump. By studying its vibration in different condition, some clues to monitor the roller pump health status would be detect.

4. Roller Pump Test

In the previous chapter vibration monitoring is discussed, focusing on the mathematical formulation of the three algorithms used together with their validation and effectiveness on detecting ball bearing characteristics BPFO and BPFI. In this chapter, the second part of the thesis is presented. An overview on roller pumps in medical application is given before showing the second experimental set up and the results.

4.1 Roller pumps

Peristaltic pumps, commonly known as roller pumps, are a type of positive displacement pump used for pumping fluids.

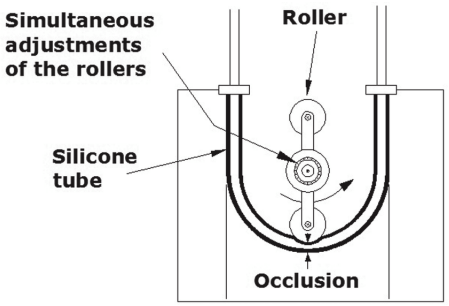

Figure 4.1: Schematic of a roller pump

The working principle of a peristaltic pump is based on the pressure and release of the hose, or tube, by the roller holder, which is moved by the

motor. The double action of pressure and release of the tube generates a suction force along the tube that sucks the fluid and pushes it to the delivery path: this continuous alternating of compression and relaxation is called peristalsis. Where the pressure has been released the hose or tube recovers creating a vacuum. The fluid flows within a flexible tube set inside a peristaltic case, squeezed by the rollers: the roller pump rotates and delivers a constant volume at each rotation, depending of the dimension of the tube. For this reason they belong to volumetric continuous pumps family.

The outlet flow rate is proportional to number of rotation of motor, volume and number or rollers and can be calculated as follow:

$$Qroller = n * V * N \tag{4.1}$$

where n = number of rollers, V = volume, N = rpm, rotation per minute.

The working condition of the pump is defined by the the internal characteristics of the device itself, and on the external ones, determined by the downstream part of the circuit. The internal characteristics are vertical lines expressed in ΔH vs G graph (see Figure 4.2), function of the number of revolution of the rollers. The external ones, instead, depend on the hydraulic downstream resistance. Both should be coupled in order to set properly the prevalence, the energy provided by pump to win over gravitational forces. As a direct consequence, one of the advantage of roller pumps is that they are totally afterload - independent, able to pump against high resistance without reducing flow.

On the other hand, disadvantages include the need to assess occlusiveness (the amount of squeeze applied to hose), capability for pumping large volumes of air, and ability to create large positive and negative pressures. Roller pumps continuously run or may be indexed in partial revolutions to deliver controlled and smaller amounts of fluid.

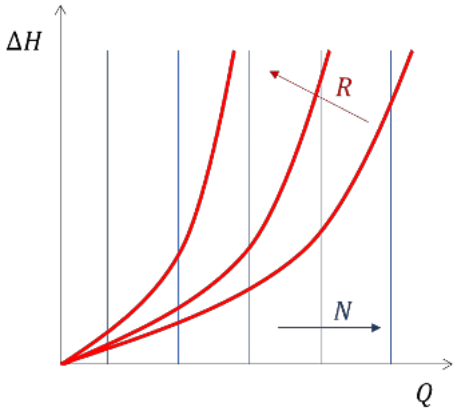

Figure 4.2: Internal and External Characteristics of a roller pump

The internal characteristics of the volumetric pump are vertical: with an increasing number of revolutions (N), the flow rate increases. For each flow rate, the pump will be capable to pump the same flow rate whatever the hydraulic resistances are. The pump has to provide a flow with a sufficient pressure to reach a certain flow rate and decide the outlet value of the pressure: this is the intended use. The circuit displays a certain amount of pressure drops (localized and distributed). The external characteristics ($\propto \rho\frac{v^2}{2} \propto Q^2$, local pressure drops have a quadratic trend) show a quadratic behavior and they increase with the hydraulic resistances (R). If hydraulic resistances increase downstream, the pump will continue to pump and the tubes will explode and the connection between the tubes will collapse, because the energy given to blood is increasing.

4.1.1 Roller pumps in medical application

Roller pumps are widely used in biomedical applications: the common factor is the need to drive blood from the body, through the circuit and back to the patient. Even if roller pumps are characterized by a continuous flow, not physiological as pulsatile flow is, their use is motivated by the fact that these devices are safe, very versatile, easy to set and low cost.

The patient is part of the circuit and his/her safety is the main important aspect to take account of. In particular, any variation on his/her resistances

may produce a variation in the flow rate: the use of roller pump allows to control the amount of volume constantly. As mentioned above, internal characteristics of the device are vertical lines that ensure constant Q for every rpm set, with respect to hydraulic R.

Example can be found in dialysis, cardiopulmonary bypass (CPB) or heart-lung assistance (ECMO, extracorporeal membrane oxygenator). The use of a roller pump during the haematic circuit of dialysis (blood flow rate is in the order 350cc) is mandatory to guarantee the same constant flow rate since everything in the circuit is programmed in order to have a specific exchange of mass and specific concentration over the length of the dialyzer. During CPB higher flow rate are processed, 5 lpm, and head pumps can be placed also 1 meter far away from the operating bed. Fluid is of course primed with saline solution because of the length of the circuit and for physiological reason: blood outside the body has to be treated with anticoagulant to avoid cots. If the patient is sedated, roller pumps are preferred to e.g. centrifugal pumps in ECMO procedures: since the patient is part of the circuit, any variation on his resistances may produce a variation in the flow rate.

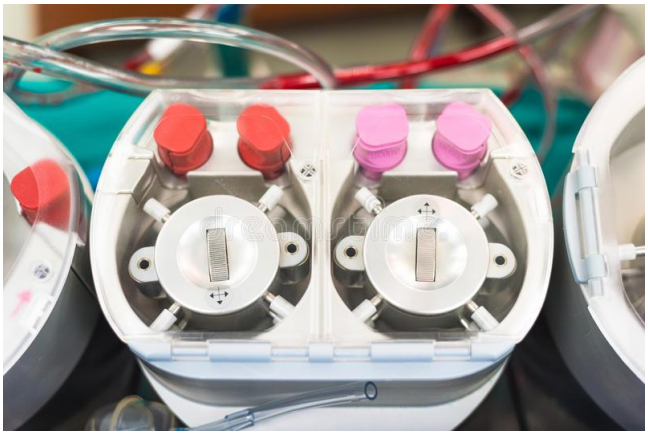

Figure 4.3: Medical roller pums

4.1.2 Roller Pumps problems in medical application

The main disadvantage related to the use of roller pump is the damage of blood due to high shear stresses on cell membranes. Haemolysis is the rupture of the membrane of the red blood cells (due to the elderly of the red blood cells). RBCs live 120 days and when they die, they undergo to physiological hemolysis. Besides factors such as chemical, thermal or mechanical that are responsible to this phenomenon, heamolysis induced by shear stresses is determined by rate of application of these stresses: it is like the RBCs are undergoing to fatigue testing but with different loads and times of application. These kind of stresses lead to premature aging of red blood cells (RBCs), releasing hemoglobin into the plasma. In order to reduce the hemolytic effect, roller pumps are not used in a complete occlusive configuration but meati are left (small holes through which RBCs can pass along the tube). Blood does not undergo hemolysis during hemodialysis treatments thanks to the compromise between long duration treatment and low blood flow rate processed.

Dealing with the mechanical elements that constitute a roller pump, the peristaltic hose and the rollers are the main responsible for this problem. Rollers may loss their efficiency showing a damage on surfaces that may stress the fluid badly. If blood is concerned, hemolysis would take place.

Occlusion is the second aspect to take care of while setting a roller pumps. It is the minimum gap between the roller and the housing that determines the maximum squeeze applied on the tubing. The amount of squeeze applied to the tubing affects pumping performance and the tube life. A fully occlusive configuration, since roller pump is after load independent, could cause rapture of the device due to the high pressure.A not proper set of the roller pump may cause, of course, haemolysis and may not deliver the

correct amount of blood throughout the circuit.

Having healthy and well positioned rollers would benefit in terms of health status of the machine itself and proper working condition.

4.2 Experimental Set Up

For the purpose of this thesis, a small size roller pump for dish-washer is used, the one shown in figure 4.4.

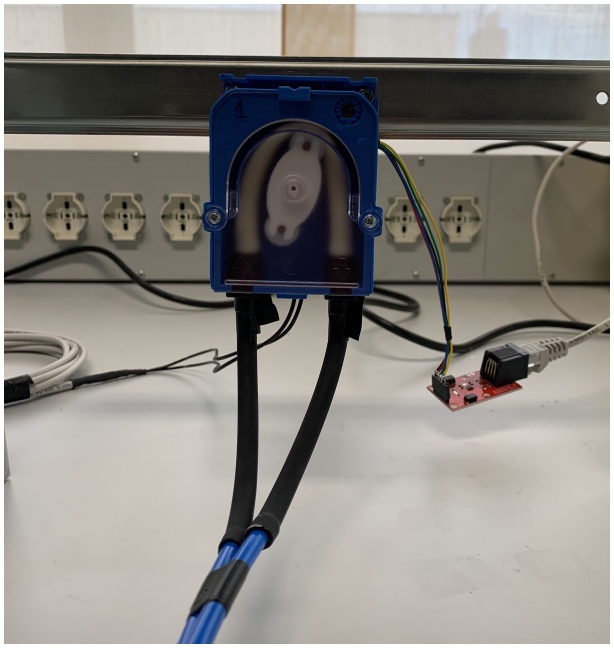

Figure 4.4: Peristaltic Pump

The vibration signals are measured under healthy and faulty conditions. Firstly, the signal of normal condition is acquired when the pump is healthy, without any faults. Faulty conditions, instead, concern how the rollers and their housing interacts with the surrounding cage. Three different records have been made for every case: 15, 30 and 45 seconds. The same procedure has been done for both water and water diluted with hand liquid soap.

Neither tubes nor leakages are considered in this work.

4.2.1 Roller Pumps and Damages

Two roller pumps have been positioned in the laboratory room. The characteristics for both devices are gathered in the following table 4.1:

Table 4.1: Mechanical features of selected roller pumps

MECHANICAL FEATURES	
Qmax [L/h]	3,0
V [Vac]	230
N [rpm]	21
n rollers	2

At first attempt, pumps were placed directly in contact with the surface of the table, but initial recordings were too noisy, so the decision to fix them to a bar over the table. Water and the solution made with water and liquid soap flows from a tank to another, both placed on floor. Rigid blue air hoses complete the circuit. Each pump works one after the other for cycles of 1 or 2 minutes long according to acquisition duration.

In order to have a framework of patterns associated to a particular case, faulty conditions have been organized as follow (figs 4.6, 4.5):

1 number of faulty rollers and how they are damaged;

   (a) 1D: one face of a roller damaged;

   (b) 2D: double-damaged face of a roller;

   (c) DC: Circumferentially damaged roller;

   (d) DD: means that holder contains rollers which are both damaged

2 +R: internal consumption of the roller holder;

Figure 4.5: Healthy rollers and holder

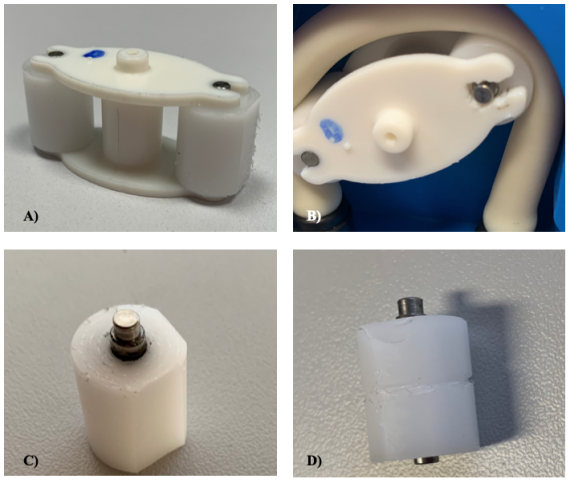

Figure 4.6: Types of Damages
A)1D case; B)+R: internal wear out of the holder; C)2D case; D)Dc case

3 BR, blocked roller: a piece of tape stops the roller to reproduce its slippage on the tube;

4 O: obstruction in the delivery path tightening it with a rubber band.

Since rollers and their holder are interchangeable, this enables to have different possible cases.

Each test consists in acquiring vibration data per different combination of the faulty conditions already described.

With the help of the tutor that follow me during my internship, the components of the roller pumps have been milled with a milling machine (4.7)

and drilled. Beside vibration, current consumption was measured for each case with a digit multimeter.

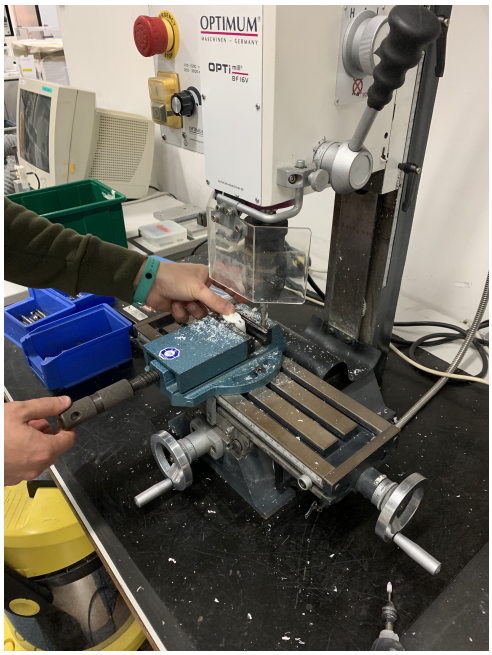

Figure 4.7: Milling machine

5. Results and Discussion

In this chapter, results are presented and compared: the aim is to find some patterns that enable to recognize a specific faulty case. Each pump worked one after the other for 1 or 2 minutes, then released for few minutes, time to store a certain condition and then plugged again.

Every signal has been processed with all the methodology discussed in chapter 3 in this way: a first approach is given by FFT and Envelope Spectrum, then a section dedicated to Hilbert Huang transform analysis.

Table 5.1: Analysis

ANALYSIS		
	FIRST	SECOND
Healthy	H	H
Faulty	1D, 2D, BR, O, +R	1D[1], DC, 2D, BR, O, +R
fc [Hz]	400	400
t [s]	30	15, 30, 45
Signal Proc.	FFT, ENV, HHT	FFT, ENV, HHT
Fluid	Water	Water vs Liquid Soap

FirstAnalysis refers to a set of acquisition of 30 seconds each, one per combination; *SecondAnalysis* gathers three time-based acquisition of 15,

[1] 1D and BR cases only for Water case

30 and 45 seconds per each of the same combination proven in the previous set (5.1).
Signal Processing and Predictive Maintenance toolbox offered by MATLAB R2020b are used to the experimental analysis of this thesis.

5.1 Results: FFT & ENV

Each acquisition lasts 30 seconds and a sampling frequency (fc) set to 400Hz, thus the frequency representation covers frequencies up to half fc. The first fluid taken into consideration is water.

5.1.1 First Analysis

As first, one pump was made working without the peristaltic hose: from its frequency spectrum (5.1) the highest peak frequency, related to the natural frequency of the system, at f=1.1Hz (black arrow) is visible and other harmonics of 12 Hz probably due to the presence of the holder (red ones) or to the mechanical support and test bench 53.9Hz, 67.1Hz (green).

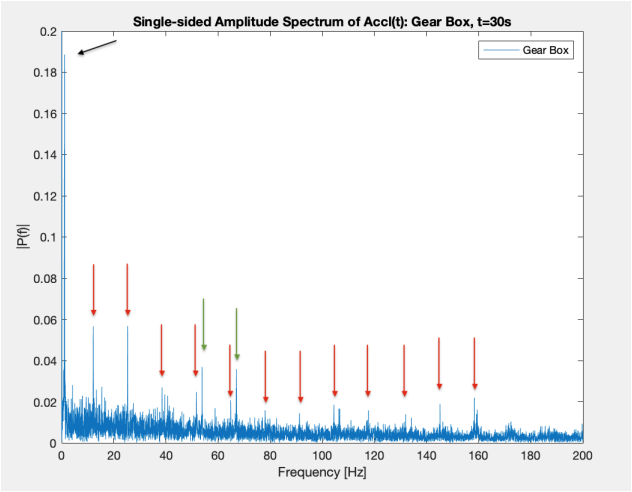

Figure 5.1: FFT - Gear box + hose

5.1.1.1 Healthy pump

From now on, peristaltic hose has been positioned, and water is pumped through the circuit. First tests on the healthy pump (H hereinafter) show some frequency components in the FFT spectrum 5.2a. The black arrow points toward the peak frequency found as the highest in the previous case. In particular, 12 Hz harmonics are always visible (red arrow points to the first one). In the last band 160 – 200 Hz, 159.7Hz, 172.9Hz and 184.5Hz appear. The envelope spectrum (5.2b), however, does not show any relevant frequency components if a healthy pump is considered.

5.1.1.2 1D case: one damaged roller inside the holder

Differently from the H case, having a damage on one roller results in both the frequency spectra. On the left, FFT spectrum highlights some 21Hz harmonics (21Hz, 63.2Hz, 84.2Hz, 105.3Hz, 168Hz, 189.5Hz, red arrows in 5.3a), exception made for f=56Hz (green) and 153Hz. These harmonics are justified in the envelope spectrum on the right (not visible the 2x and 8x harmonics, 42Hz and 168Hz respectively). Moreover, 56Hz stands in the envelope spectrum in 1D case (5.3a).

5.1.1.3 2D case: two-sided damaged roller

2D case presents an FFT spectrum (5.4a) slightly different from the 1D case: the only frequency components more visible are 84.2Hz 105.2 and 126.3, the 21Hz harmonics identified in the previous case. Beside, the envelope spectrum (5.4b) fully represents all the harmonics in all the available frequency range. 56Hz that characterizes the 1D case disappears in this situation. Peak amplitude of 21Hz is higher with respect to the previous case.

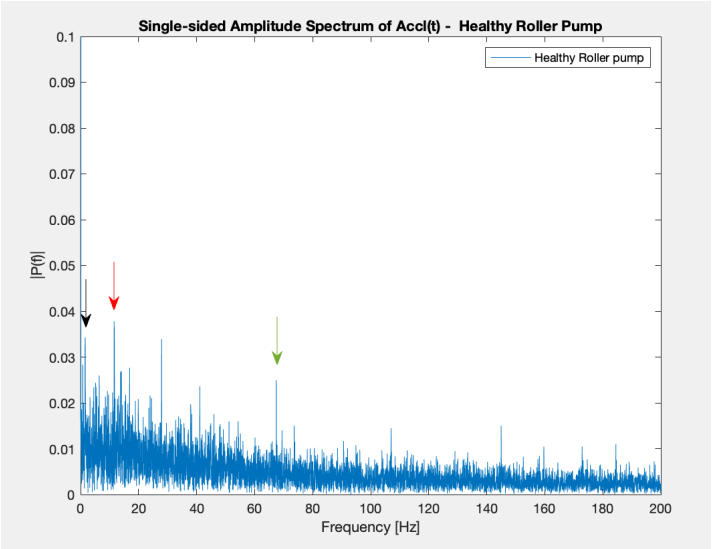

(a) H: FFT

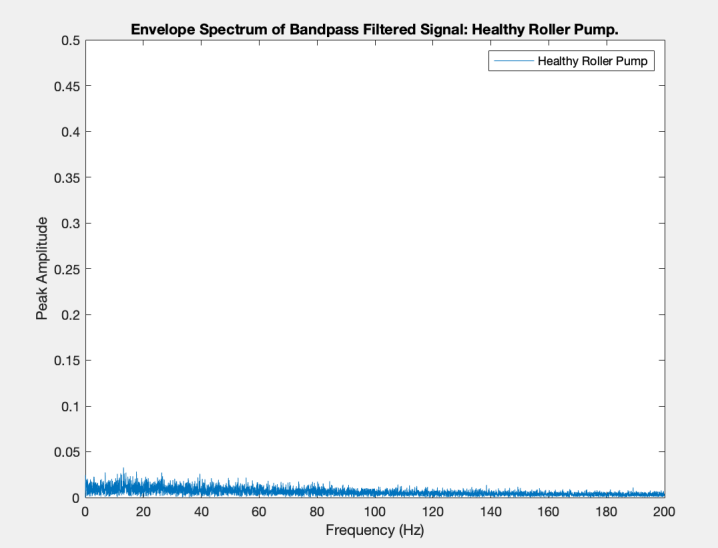

(b) H: Envelope Spectrum

Figure 5.2: Healthy Pump

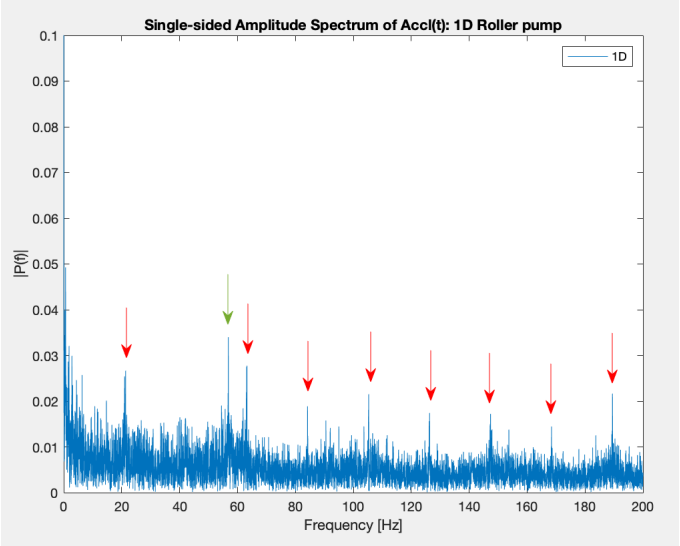

(a) 1D: FFT

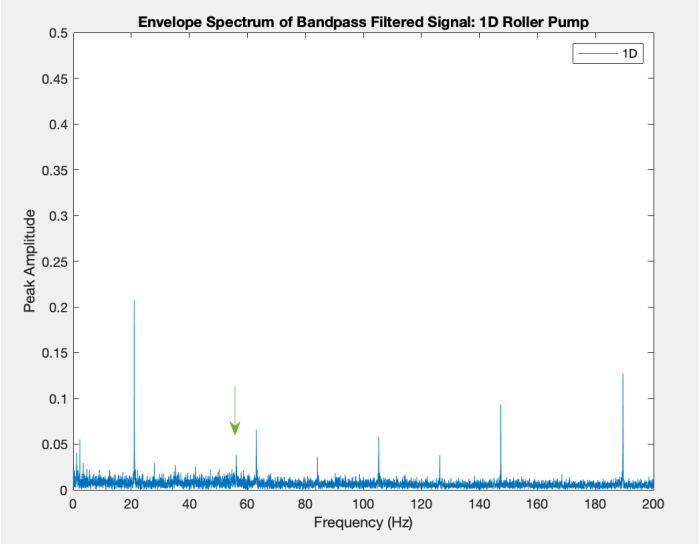

(b) 1D: Envelope Spectrum

Figure 5.3: 1D case

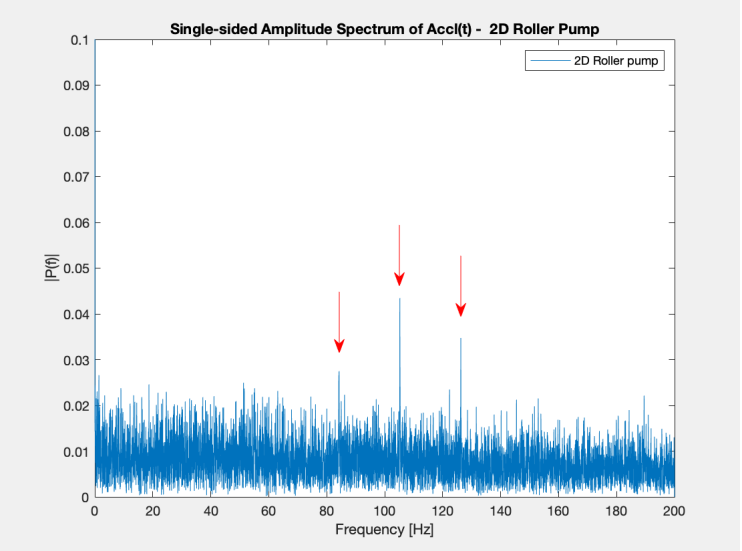

(a) 2D: FFT

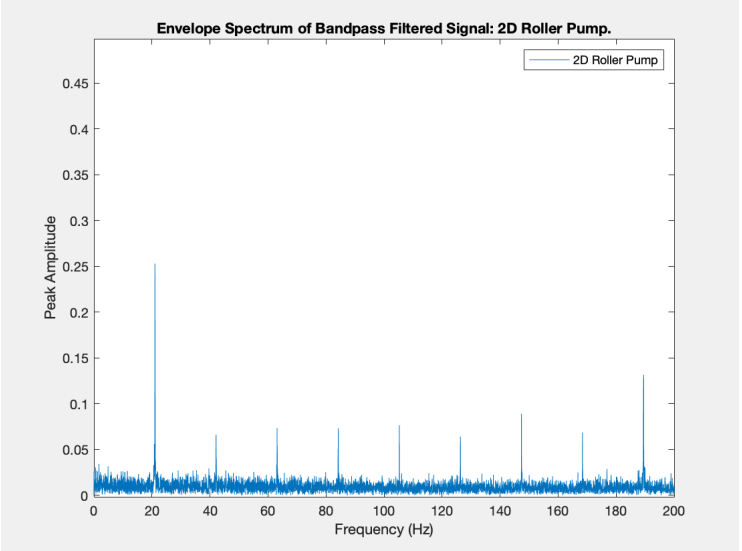

(b) 2D: Envelope Spectrum

Figure 5.4: 2D case

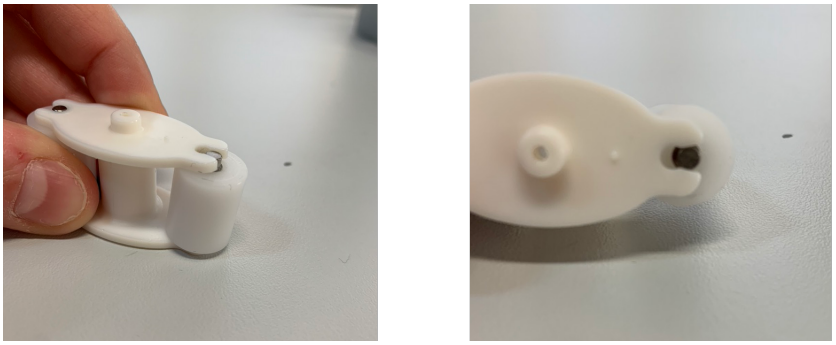

Figure 5.5: Roller out

5.1.1.4 DD: Both damaged rollers, combination of the 1D and 2D case

Combining the previous damaged case, one expects that in the FFTt spectrum the frequency components of each case would sum up: experimentally this seems not to happen. The FFT spectrum (5.6a) does not show any important frequency components, whereas it seems to be a non – faulty case. Applying the envelope analysis, the spectrum sums both the previous case adding a 35Hz frequency (5.6b). Again, peak amplitude of each component is still higher in magnitude comparing to other cases.

5.1.1.5 Roller out

In this configuration, the roller is not perfectly aligned and in position, as shown in fig. 5.5. This solution was not so easy to perform and maintain during the working of the pump, because once plugging the pump, the combination of both pressure of the water in the hose against the roller, and the other way around, put the roller, in some cases, back in position. The only weird case is related to the combination DD+Roller out (5.10a, 5.10b). As seen, both FFT and Envelope spectra do not show any features that would lead to recognize this condition. In the other cases, this solution only con-

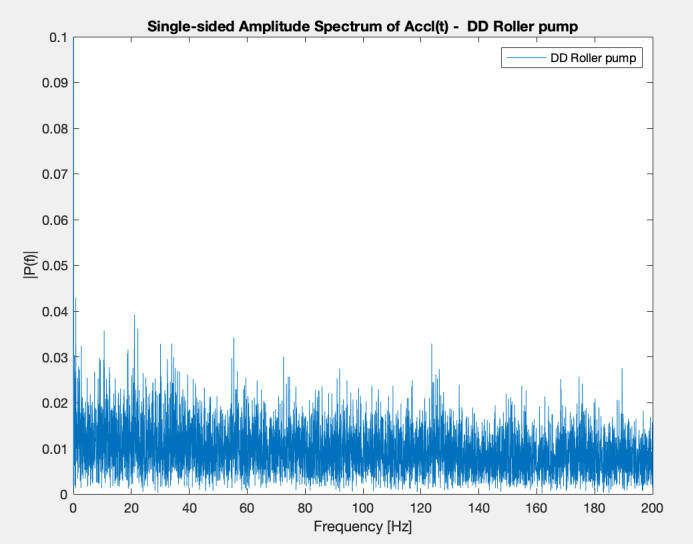

(a) DD: FFT

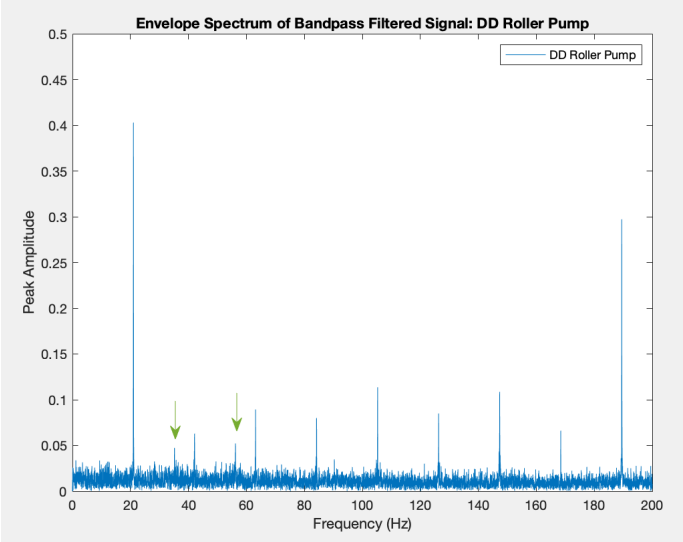

(b) DD: Envelope Spectrum

Figure 5.6: DD case

tributes to emphasize the well-known 21Hz harmonics.
Concerning the H+R case (5.7a,5.7b), if H has a complete plain envelope spectrum, here the combination with a misalignment stresses 63Hz,84Hz and 189.5Hz, even if their magnitude (too low) is not comparable with the damaged cases. In the first frequency range a 0.6Hz characterizes H+R condition. 56Hz identifies 1D case in the envelope spectrum (5.8b), as already found out.

5.1.1.6 BR: blocked roller

During normal working condition, the rollers turn around their own axis pushing the hose to let the fluid moves. In this situation, a piece of tape wraps the roller around the vertical axis of the roller itself in order to let it not turning but slipping on the tube. As a result, the envelope spectrum highlights the harmonics in the central part of the frequency band available (84Hz, 105Hz,126Hz,147Hz in pink in 5.11b).

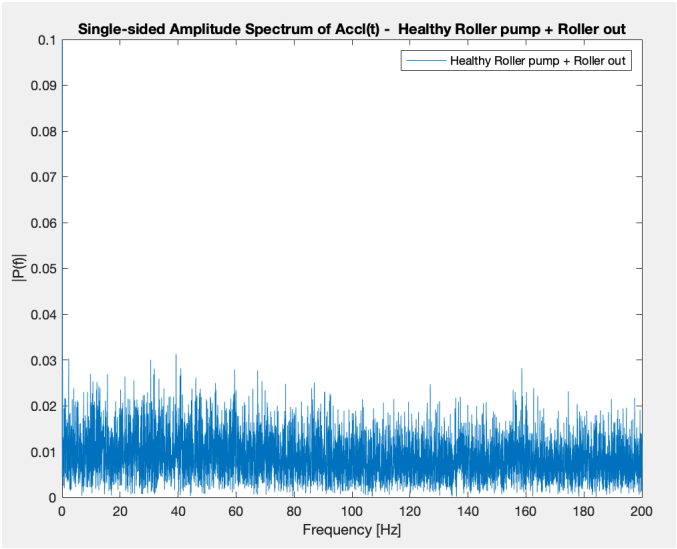

(a) H+R: FFT

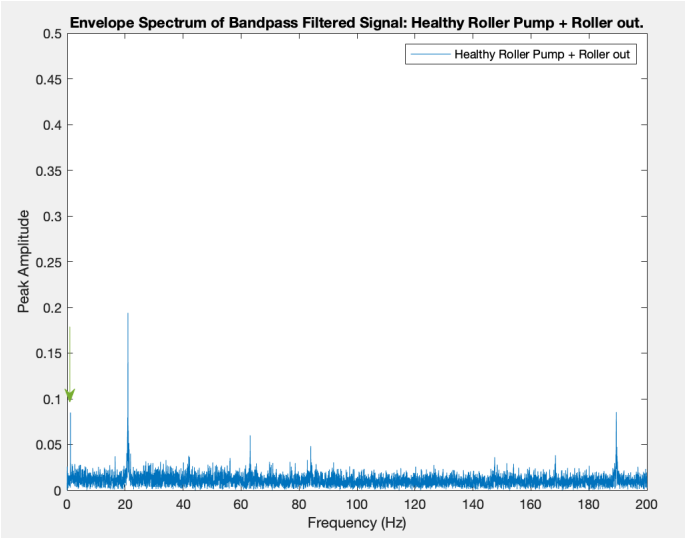

(b) H+R: Envelope Spectrum

Figure 5.7: H+R case

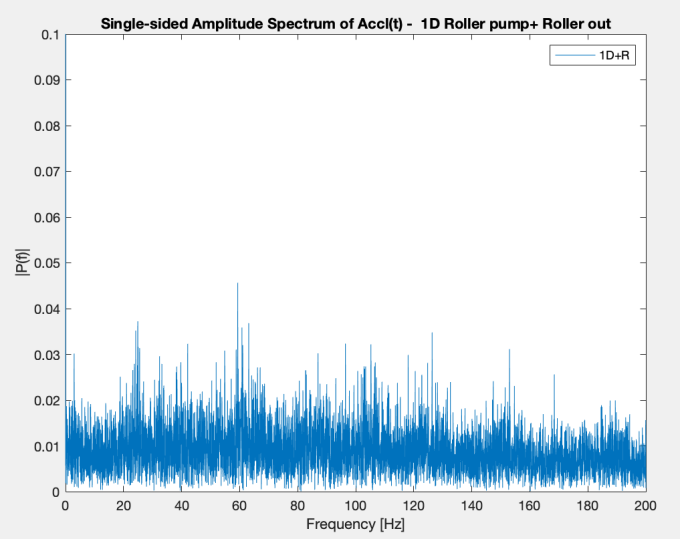

(a) 1D+R: FFT

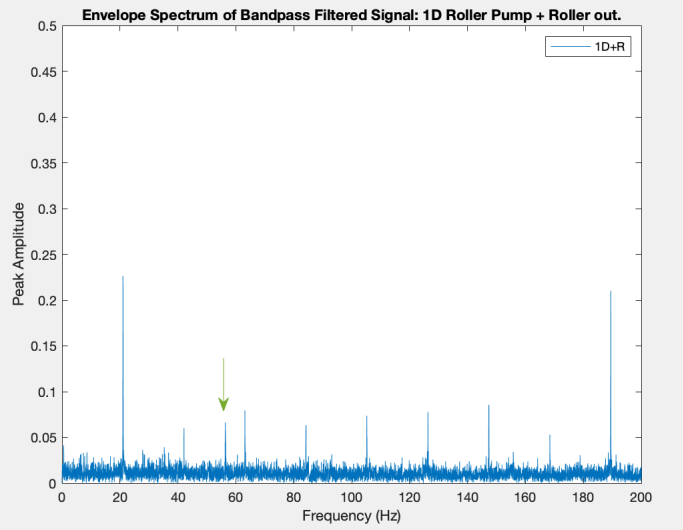

(b) 1D+R: Envelope Spectrum

Figure 5.8: 1D+R case

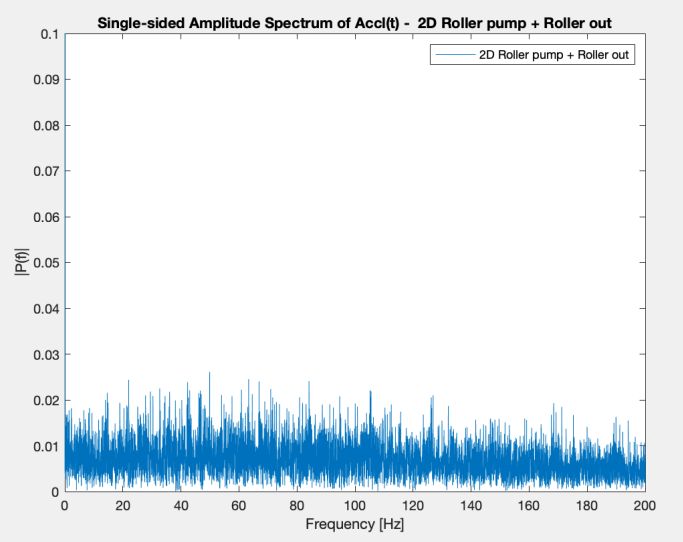

(a) 2D+R: FFT

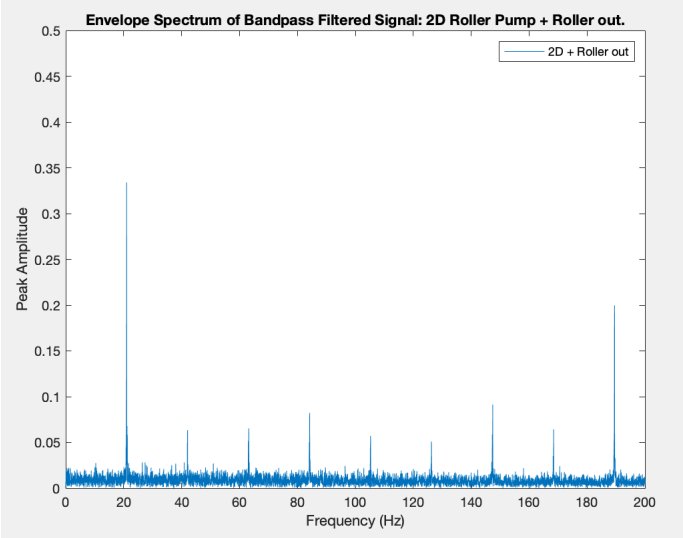

(b) 2D+R: Envelope Spectrum

Figure 5.9: 2D+R case

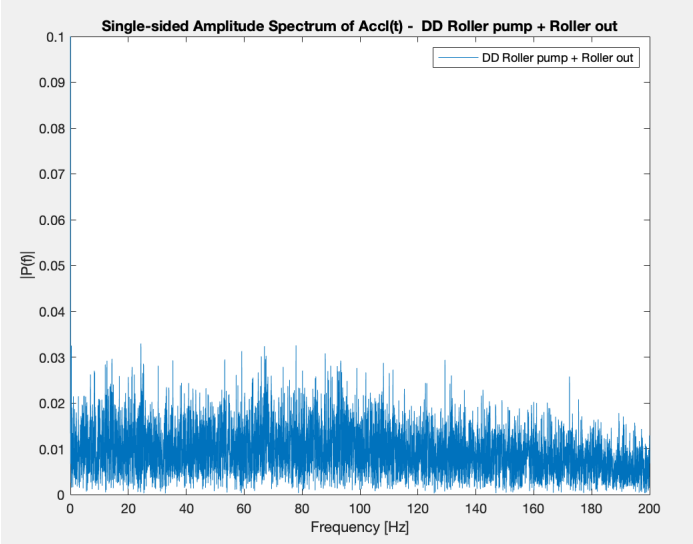

(a) DD+R: FFT

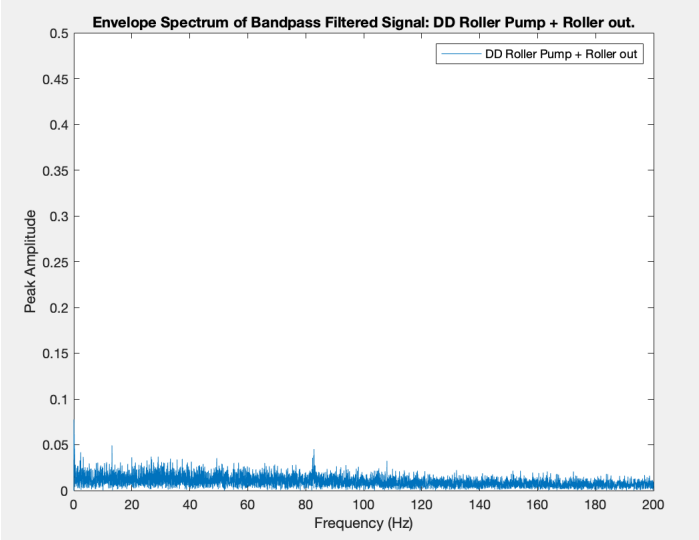

(b) DD+R: Envelope Spectrum

Figure 5.10: DD+R

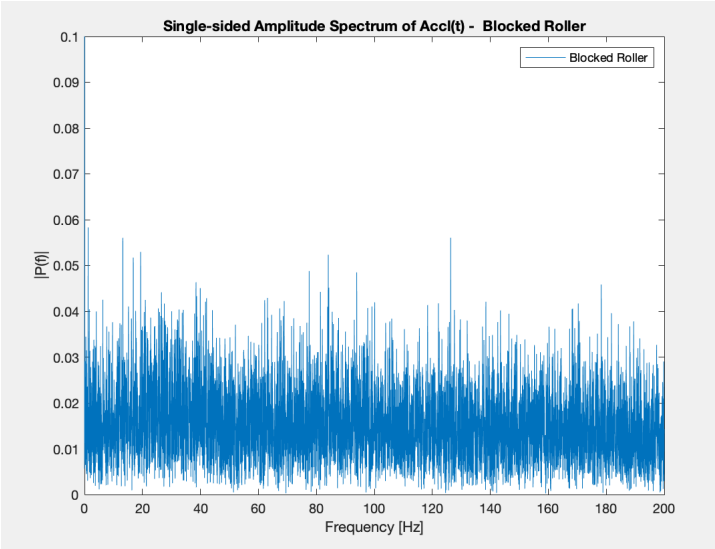

(a) BR: FFT

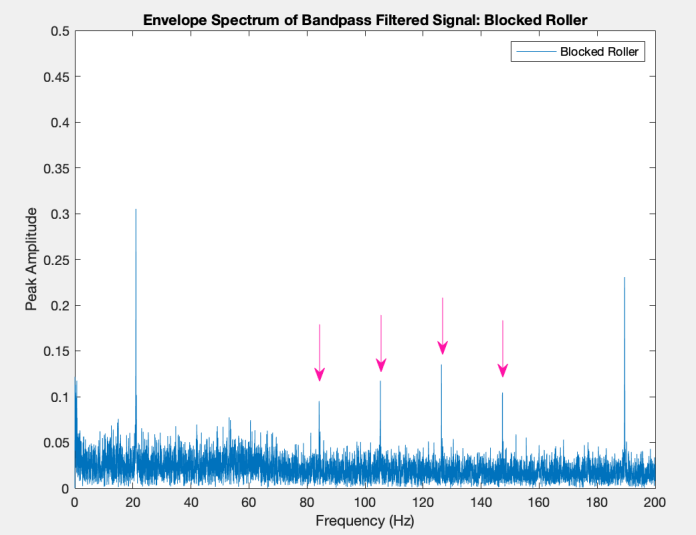

(b) BR: Envelope Spectrum

Figure 5.11: BR case

5.1.2 Second Analysis

In the previous section, patterns of healthy and faulty cases have been presented. In this section, results of the same combination are presented for tests that differ for the time duration of the acquisition and the type of fluid the pumps are sucking.

5.1.2.1 Water

5.1.2.1.1 Healthy pump

FFT spectrum does not show ant relevant frequency components in all the three cases (5.12a,5.12b,5.12c). In the frequency band 0-5 only a component of 3.2 Hz clearly dominates the frequency spectrum.

Concerning the envelope spectrum (5.13a,5.13b,5.13c), instead, the system seems to be impulsive only at 21Hz in each time-window acquisition. Moreover, in the frequency band 0-50, the first two harmonics of 0.6 Hz are visible, related to the rotation of both rollers. 21Hz can be considered as a health indicator for this kind of pump.

5.1.2.1.2 1D

Frequency spectrum of 1D case, with respect to H case, shows clearly some frequency components. Red arrows point to harmonics of 21Hz (5.14a) that can be found in all the FFT spectra, except for 2x harmonics of 42Hz that is not stressed like the others (5.14b,5.14c).

Considering the envelope spectra, all the harmonics previously found are still present, but 2x and 8x (42Hz and 168H respectively) are not. Other frequencies that characterize the envelope spectra of both t=15s and t=30s are 28Hz 35Hz and 56Hz (5.15a). However, if we consider the latter case, t=45s, we cannot appreciate these frequencies in the envelope spectrum,

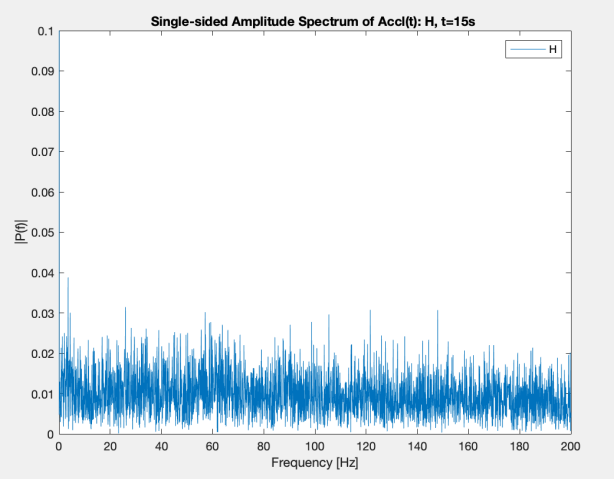

(a) H 15s: FFT

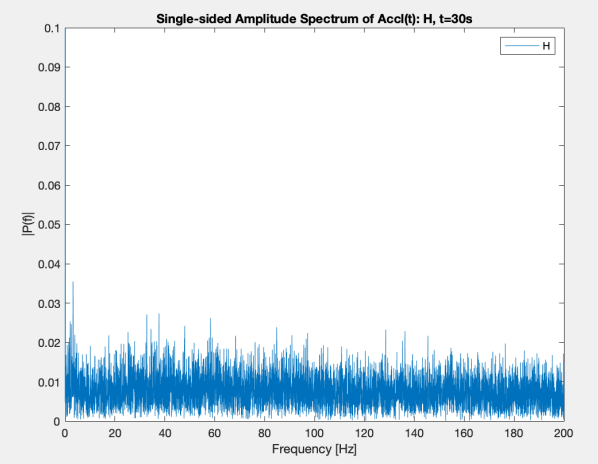

(b) H 30s: FFT

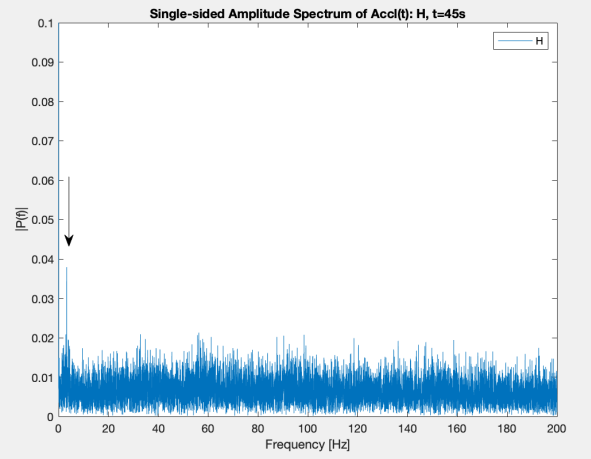

(c) H 45s: FFT

Figure 5.12: H: FFT

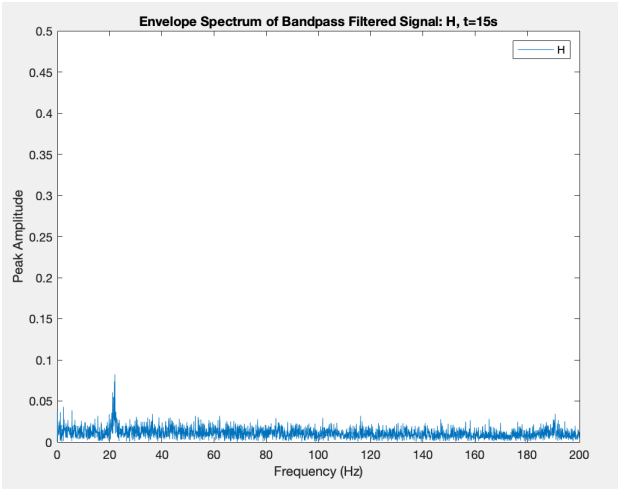

(a) H 15s: ENV

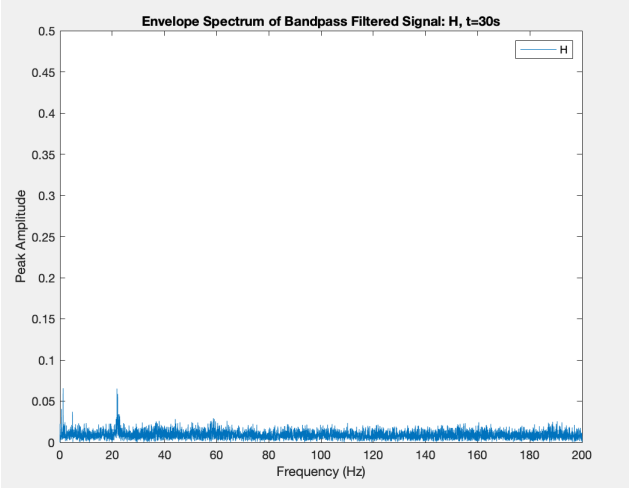

(b) H 30s: ENV

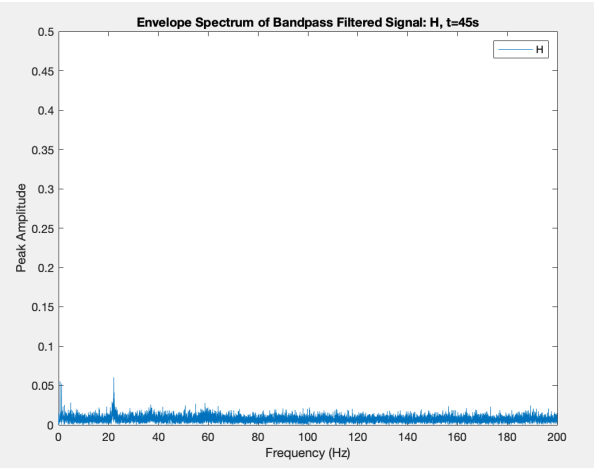

(c) H 45s: ENV

Figure 5.13: H: Envelope Spectrum

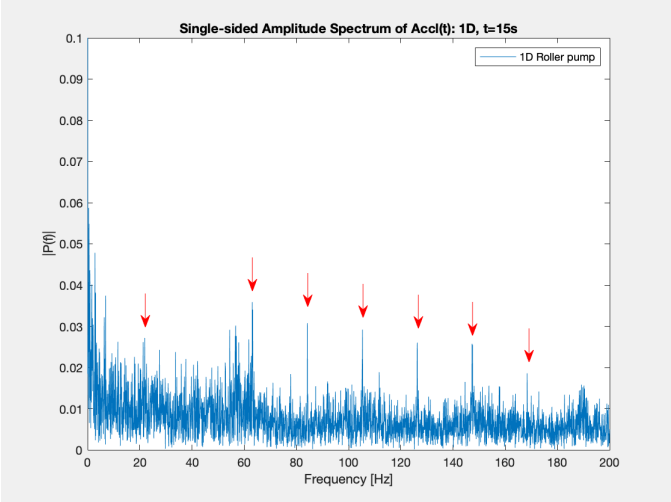

(a) 1D 15s: FFT

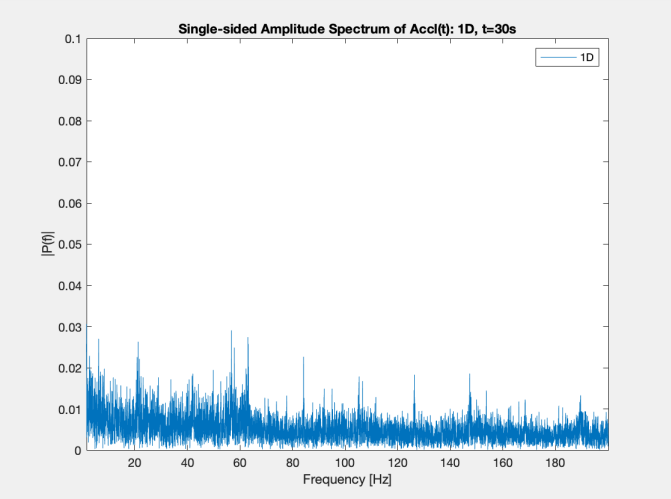

(b) 1D 30s: FFT

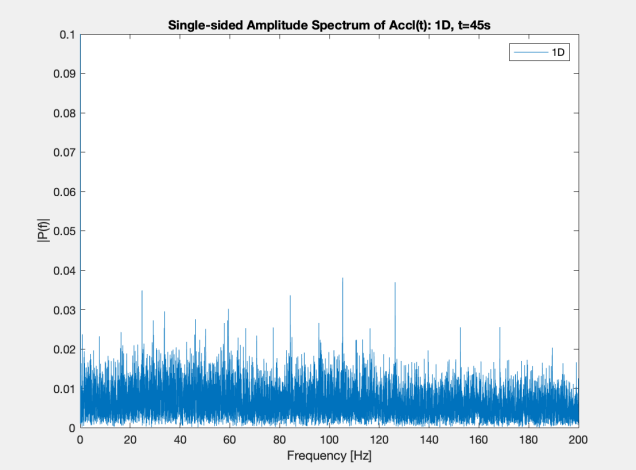

(c) 1D 45s: FFT

Figure 5.14: 1D: FFT

while in FFT the same are hidden among other components. 1D pattern can be recognize by the presence of (in envelope spectrum):

1 Frequency components 56Hz (green arrow in 5.15a,5.15b,5.15c);

2 Absence of 2x and 8x;

5.1.2.1.3 2D

Even in this case, frequency harmonics of 21Hz are still present, emphasized mainly in frequency bands 30-70Hz and 140-180Hz. Differently from 1D case, a 4.2Hz component in FFT spectrum dominates the first 0-10 Hz band (5.16a,5.16b,5.16c).

In the envelope spectrum instead, we can notice that the two missing harmonics in 1D spectrum are now visible. Indeed, in order to identify this kind of damage, we can rely on the fact that 105Hz and 126Hz have peak amplitude lower compared to the other harmonics (5.17a,5.17b,5.17c).

With respect to H case, having a damaged roller impact the frequency content of the vibration signal. In particular, from the envelope spectrum it seems that having a one-faced or double-faced damaged roller emphasizes in amplitude some harmonics with respect to others.

5.1.2.1.4 DC

DC case is obtained from 1D roller which has been damaged adding a circumferential trace along its surface, thus DC case is then reproduced. DC FFT spectra are quite plain, but f=4.2Hz peak is higher. (5.18a,5.18b,5.18c).

However, looking at the envelope spectrum (5.19a,5.19b,5.19c), this case is characterized by the absence of 105Hz and 126Hz harmonics.

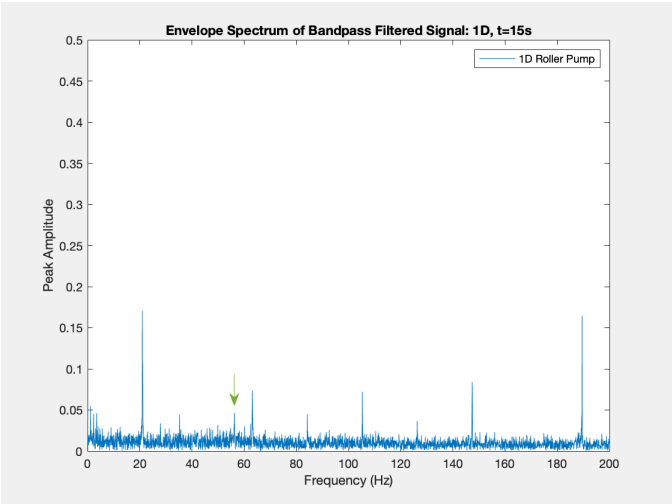

(a) 1D 15s: ENV

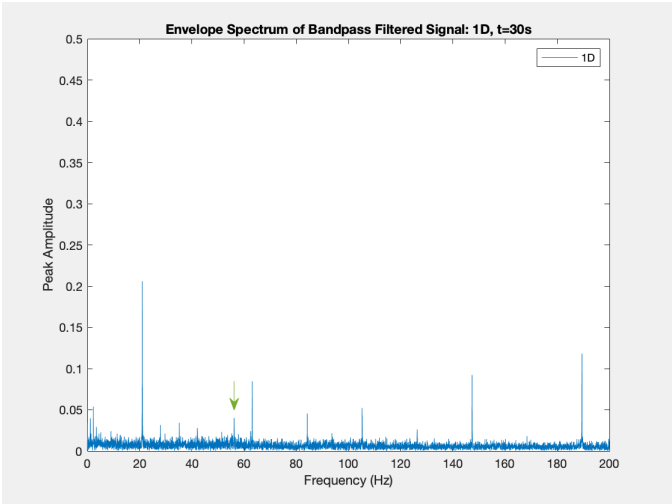

(b) 1D 30s: ENV

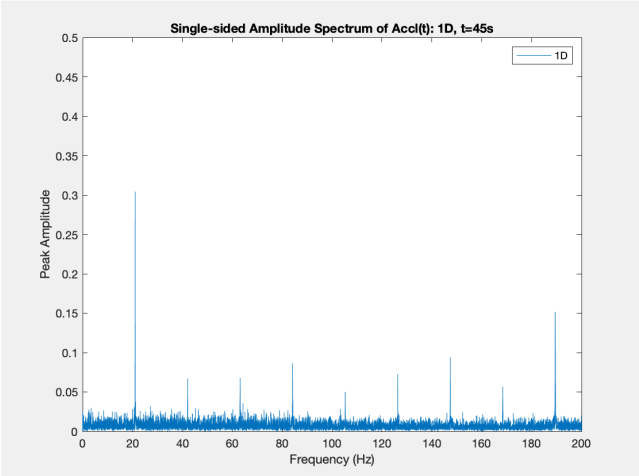

(c) 1D 45s: ENV

Figure 5.15: 1D: Envelope Spectrum

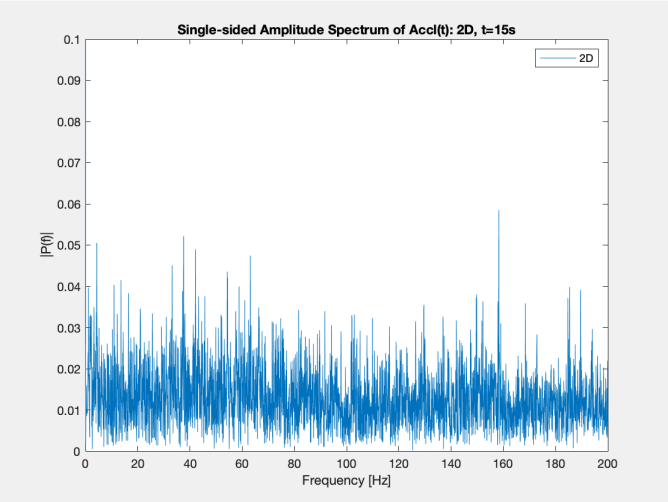

(a) 2D 15s: FFT

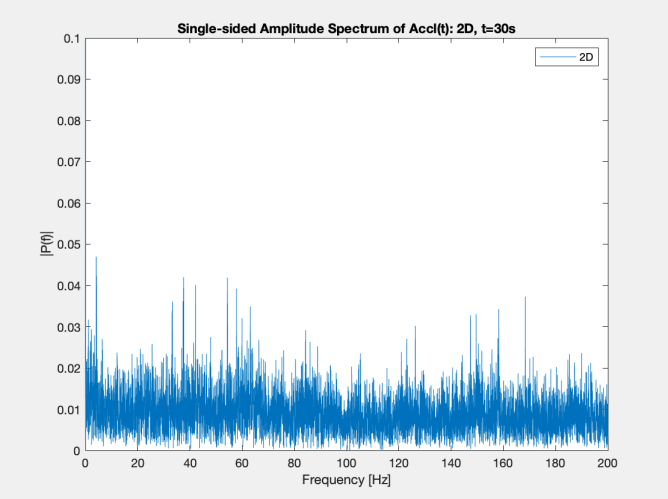

(b) 2D 30s: FFT

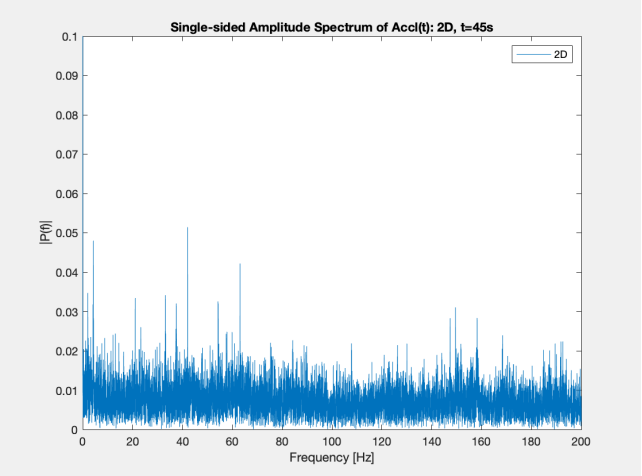

(c) 2D 45s: FFT

Figure 5.16: 2D: FFT

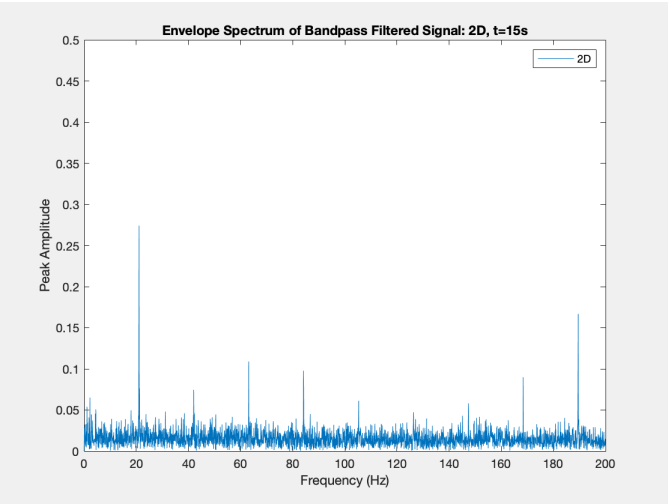

(a) 2D 15s: ENV

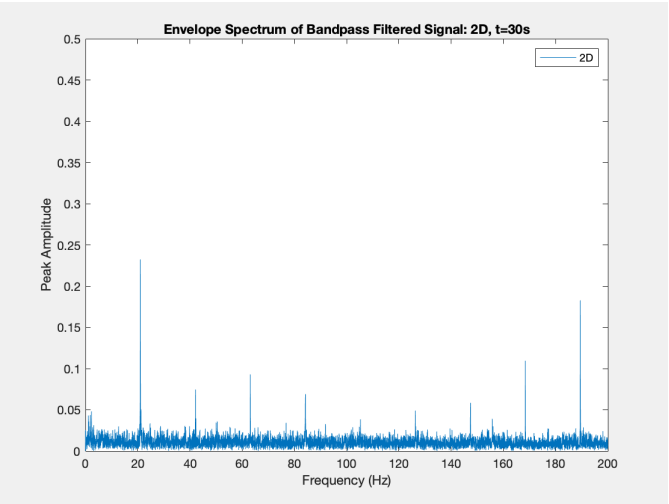

(b) 2D 30s: ENV

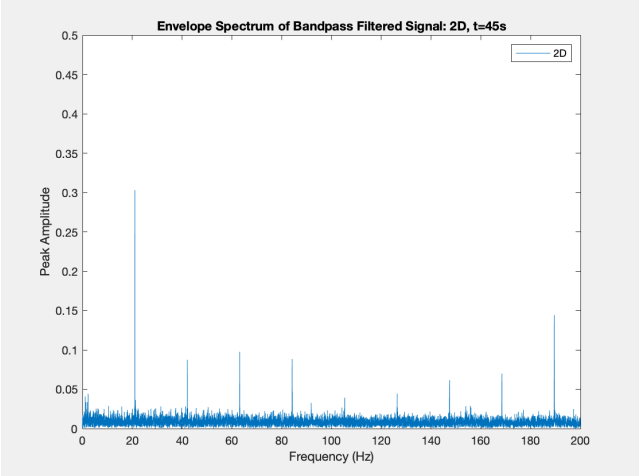

(c) 2D 45s: ENV

Figure 5.17: 2D: Envelope Spectrum

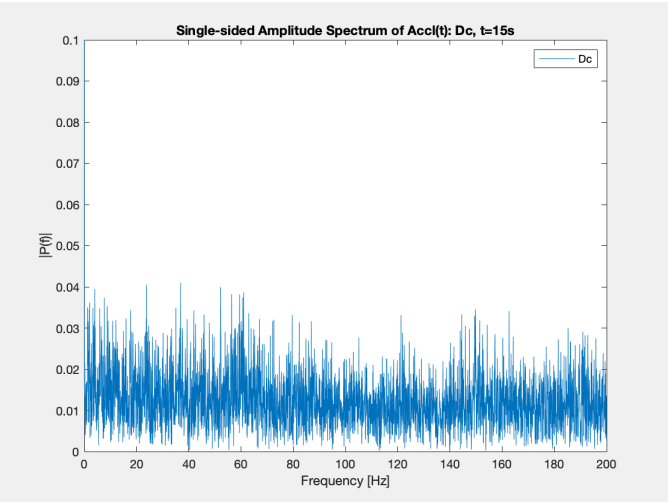

(a) DC 15s: FFT

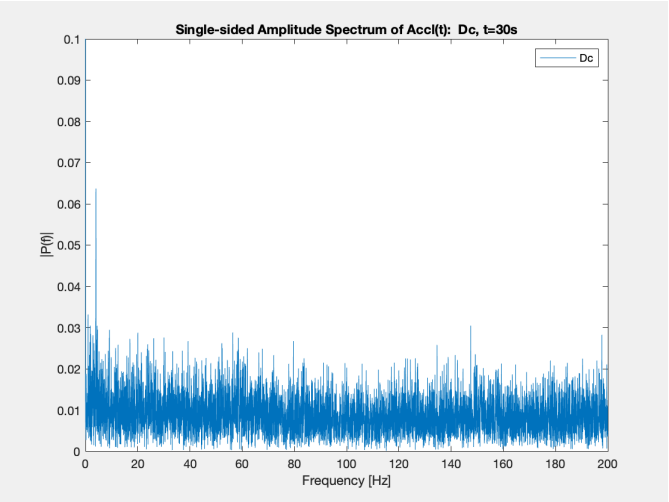

(b) DC 30s: FFT

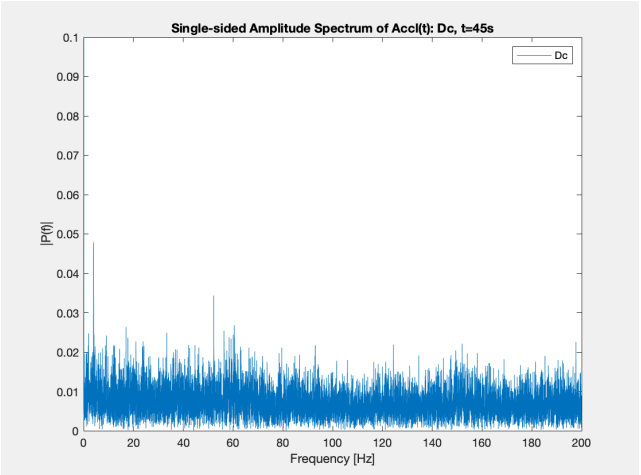

(c) DC 45s: FFT

Figure 5.18: DC: FFT

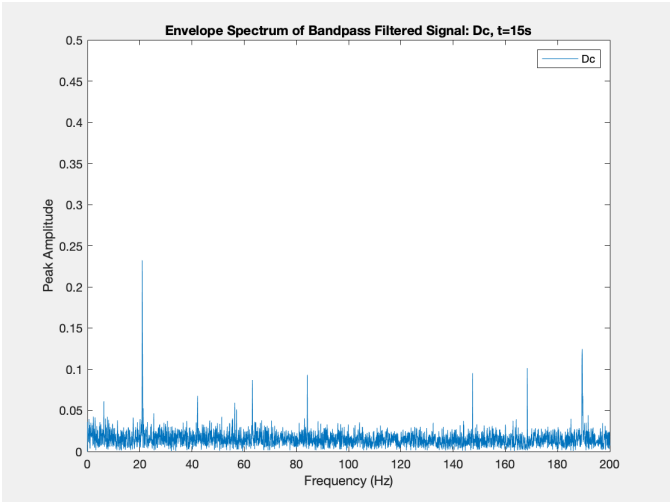

(a) DC 15s: ENV

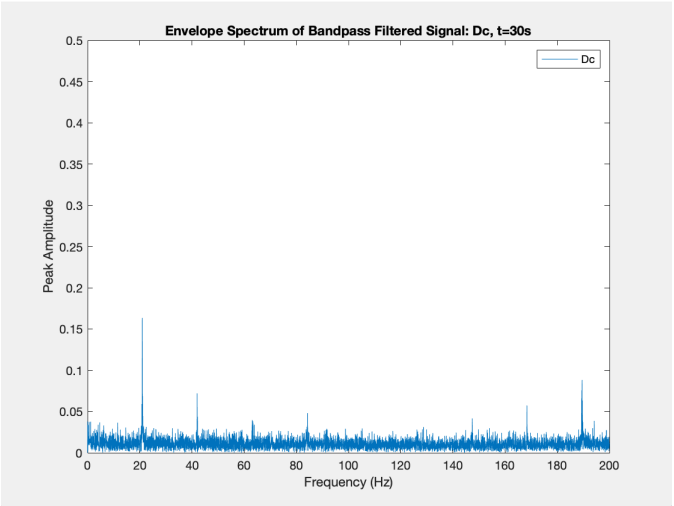

(b) DC 30s: ENV

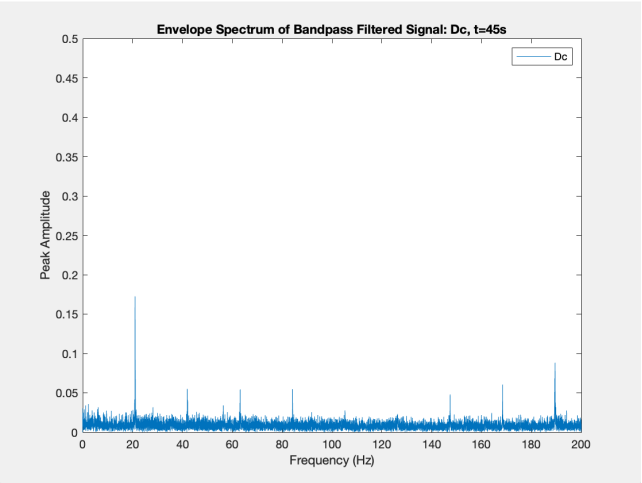

(c) DC 45s: ENV

Figure 5.19: DC: Envelope Spectrum

5.1.2.1.5 DD

The holder, in this case, hosts both rollers that are completely damaged. All the harmonics of 21 Hz figure out in FFT spectrum (5.20b,5.20c), not so evident in t=15s frame (5.20a). This leads to have an envelope spectrum for each time frame gathering both DC and 2D frequency components, all but f=35Hz (5.21a, 5.21b, 5.21c).

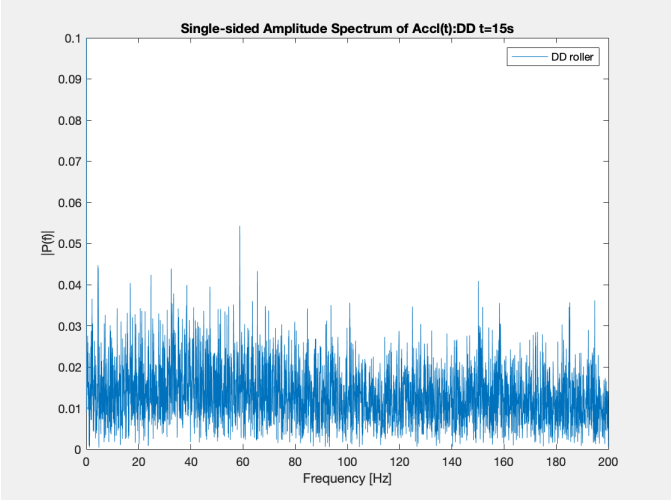

(a) DD 15s: FFT

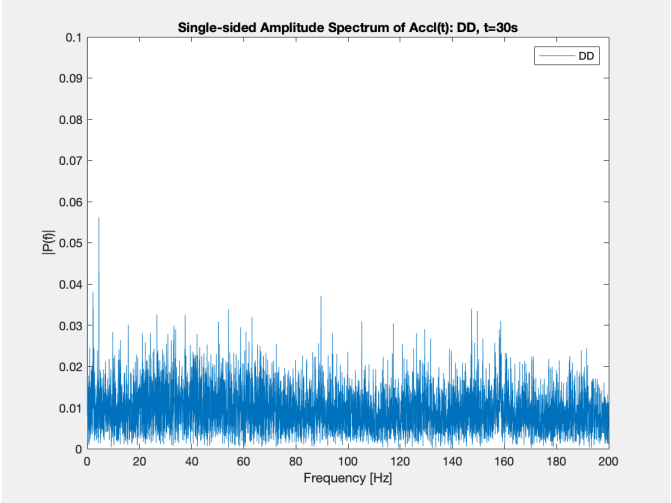

(b) DD 30s: FFT

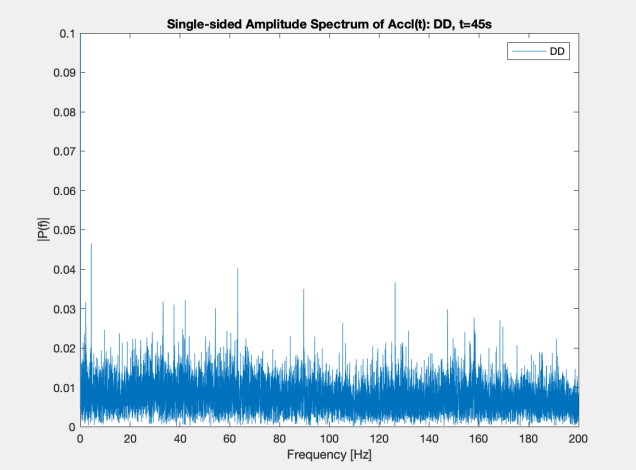

(c) DD 45s: FFT

Figure 5.20: DD: FFT

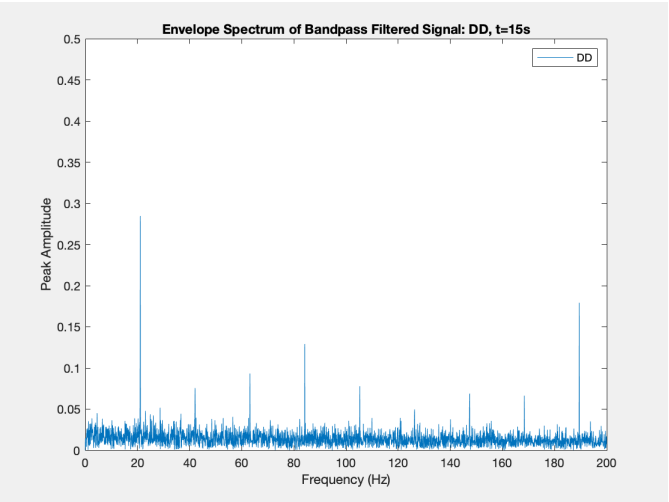

(a) DD 15s: ENV

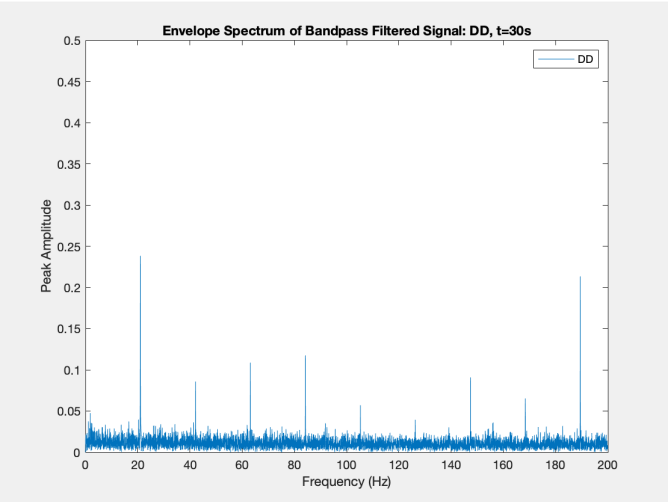

(b) DD 30s: ENV

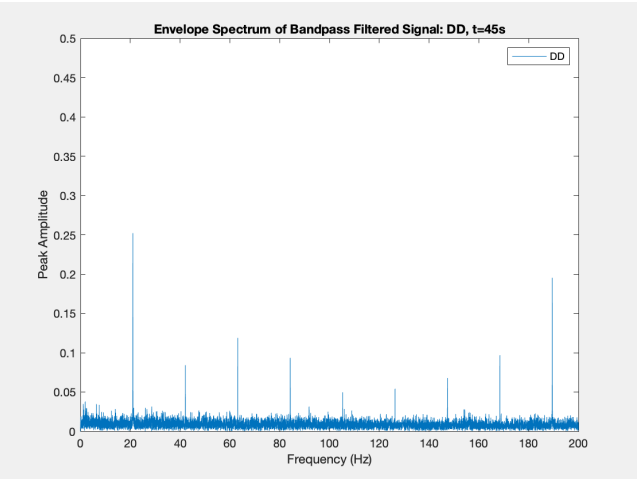

(c) DD 45s: ENV

Figure 5.21: DD: Envelope Spectrum

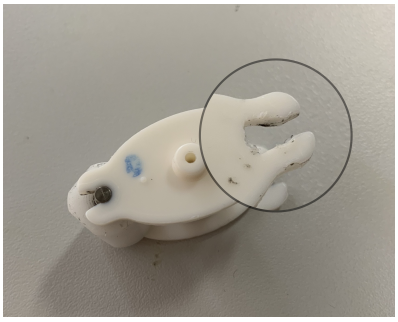

Figure 5.22: Internal consumption of the roller
The internal part has been drilled as zoomed in the figure

5.1.2.1.6 +R

In paragraph 5.1.1.5, replacing a misalignment of the roller was considered quite difficult to manage. In order to see whether a wrong positioning of the roller may impact on the frequency domain, that solution was replaced drilling the internal part of the holder (5.22). In this way, both the misalignment of the roller and the material consumption of the holder was proved.

In H+R case the only component that stands in the FFT spectrum is f=42Hz, exception made in t=45s, where the same component seems to be hidden among other components. Exception made for t=45s (5.24c) where the central band does not show any peaks, the other envelope spectra are stressed all over the band (5.24a, 5.24b), the opposite of H case.

1D+R case, instead, shows peaks mainly at f=21Hz, 63Hz and 126Hz, all harmonics of 21Hz (5.25a, 5.25b, 5.25c). In its envelope spectrum, f=56Hz still characterizes 1D case, independently from +R condition (5.26a, 5.26b, 5.26c).

The remaining cases have FFT results which are different for any time acquisition, thus ineffective to realize which case is: for example both 2D+R (5.27a,5.27b,5.27c)and DC+R results have f=4.3Hz (5.28b,5.28c) only that

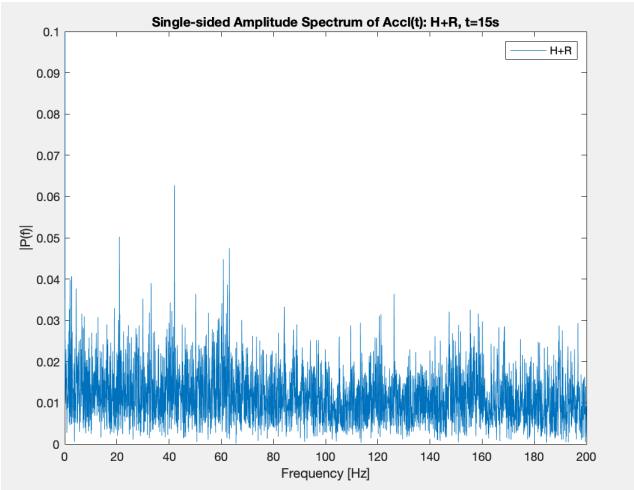

(a) H+R 15s: FFT

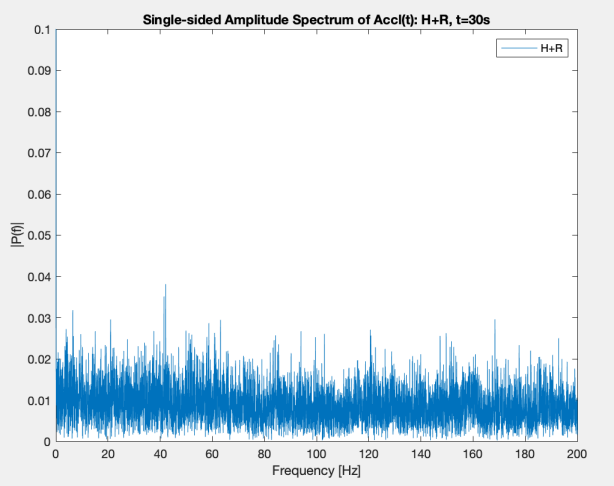

(b) H+R 30s: FFT

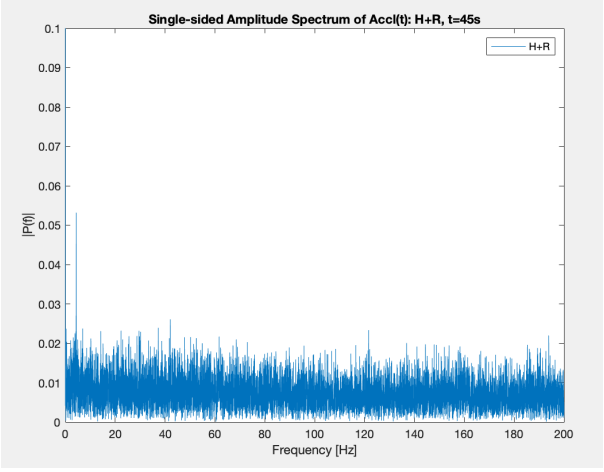

(c) H+R 45s: FFT

Figure 5.23: H+R: FFT

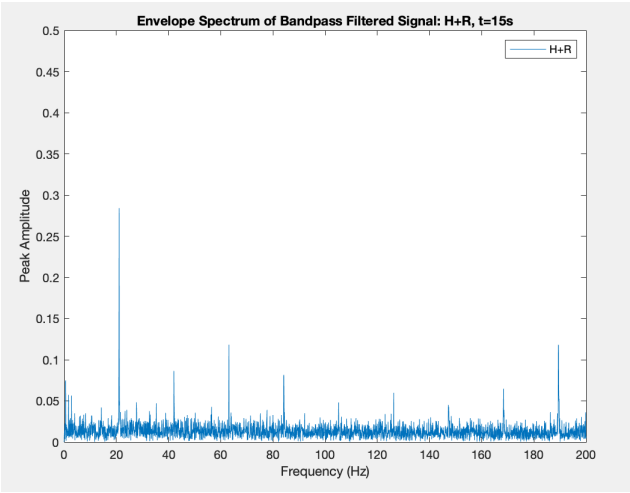

(a) H+R 15s: ENV

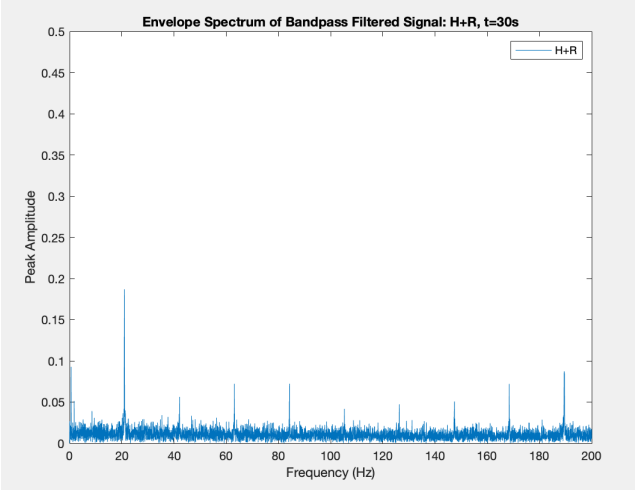

(b) H+R 30s: ENV

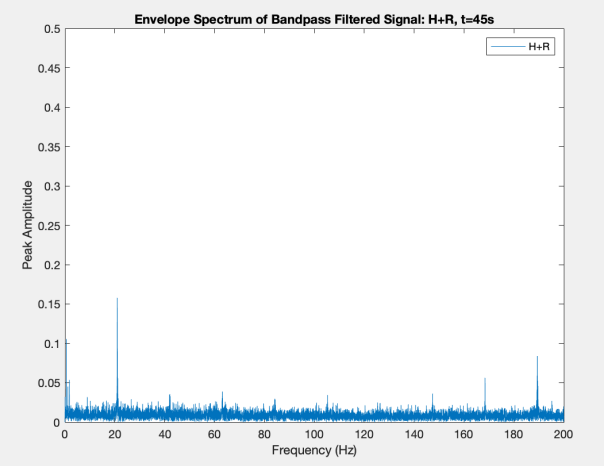

(c) H+R 45s: ENV

Figure 5.24: H+R: Envelope Spectrum

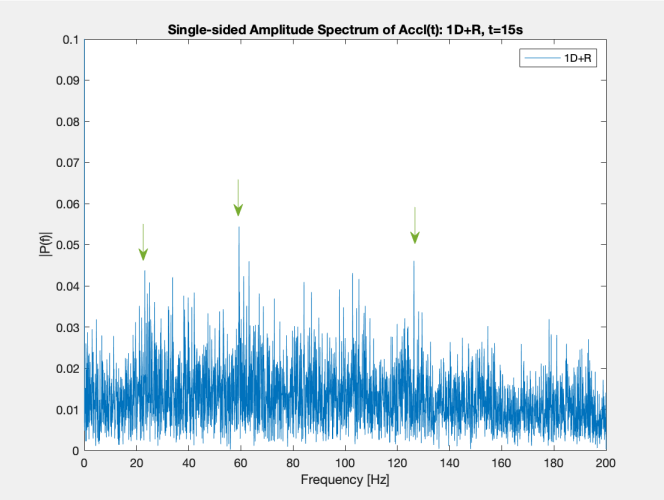

(a) 1D+R 15s: FFT

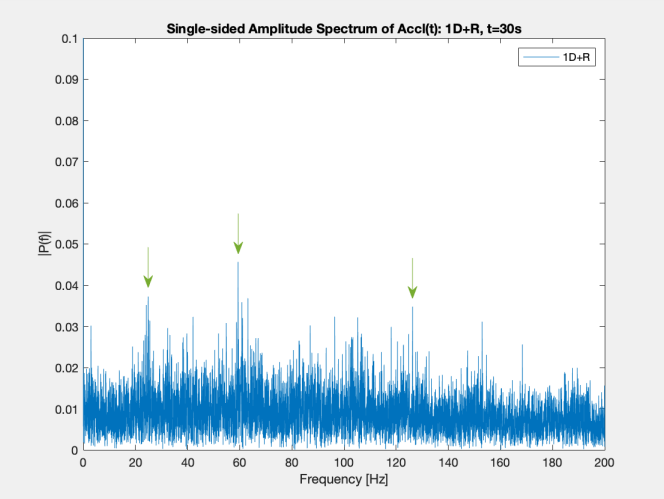

(b) 1D+R 30s: FFT

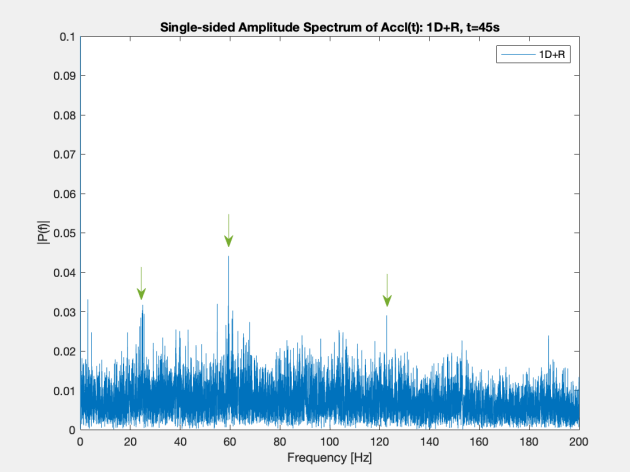

(c) 1D+R 45s: FFT

Figure 5.25: 1D+R: FFT

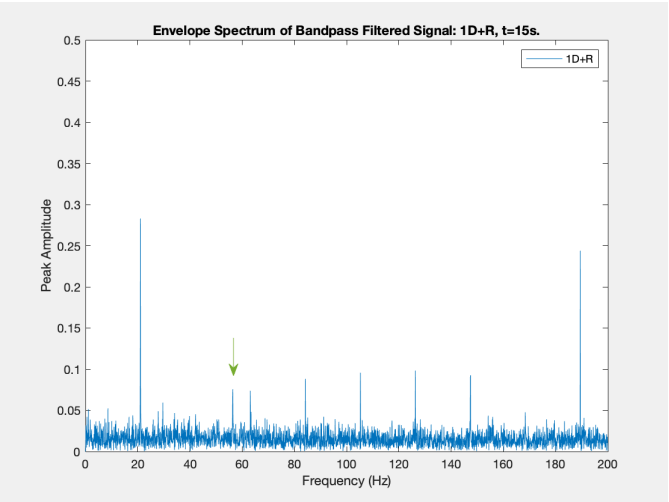

(a) 1D+R 15s: ENV

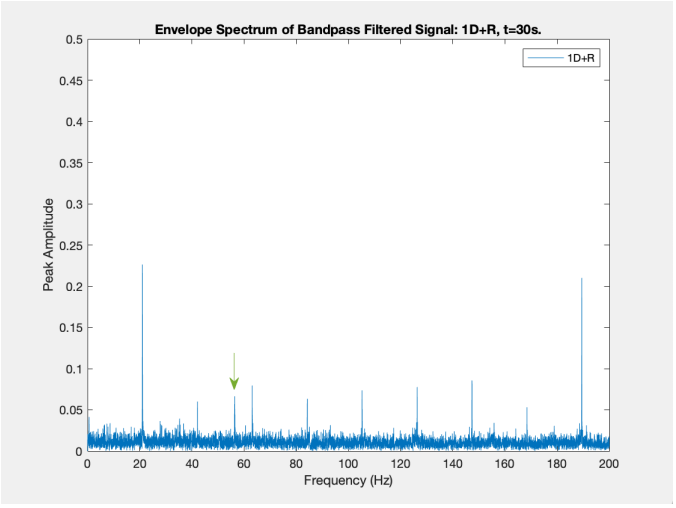

(b) 1D+R 30s: ENV

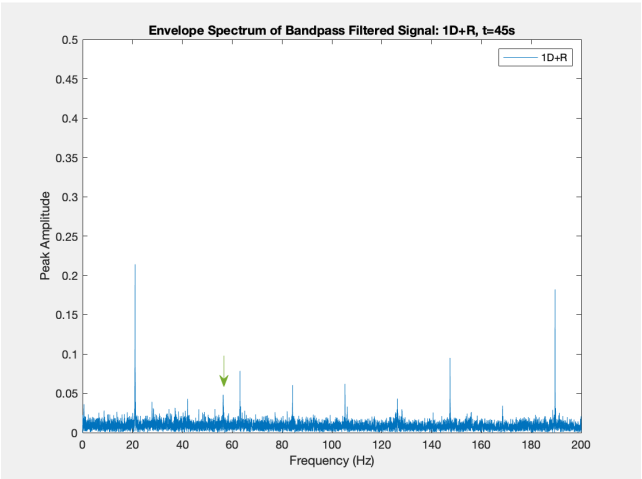

(c) 1D+R 45s: ENV

Figure 5.26: 1D+R: Envelope Spectrum

arises from FFT spectrum (not in t=15s for DC+R 15 5.28a).

Regarding the envelope spectrum, each of them heterogeneously stresses the same (or not) frequencies: in particular 2D+R (5.29a,5.29b,5.29c). DD+R (5.30a,5.30a,5.30a), on the other hand, can be recognized due to the absence of frequency peaks near f=100Hz.

In DD+R FFT spectrum (5.31a,5.31b,5.31c), compared to DD case (5.20b), the same frequencies have steeper peak amplitude. Also the envelope spectrum (5.32a,5.32b,5.32c) underlines all the harmonics.

5.1.2.1.7 BR

Together with +R in the previous section case, replying the slipping of the roller on the tube was not so easy to perform: every time I used to try this configuration, a newer piece of tape wraps the roller. This may lead in not finding a specific pattern.

5.1.2.1.8 O

The obstruction of the delivery path was obtained binding a rubber band along the tube.

Again, FFT differs between the 3 time duration (5.35a,5.35b,5.35c), while the envelope spectrum (5.36a,5.36b,5.36c) shows higher peaks in the first half of the spectrum, mainly in 0.6Hz, 11.2Hz, and harmonics of 21Hz up to 100Hz, with respect to the second half between 100 and 200Hz, where the the only meaningful peak is in 189.5Hz.

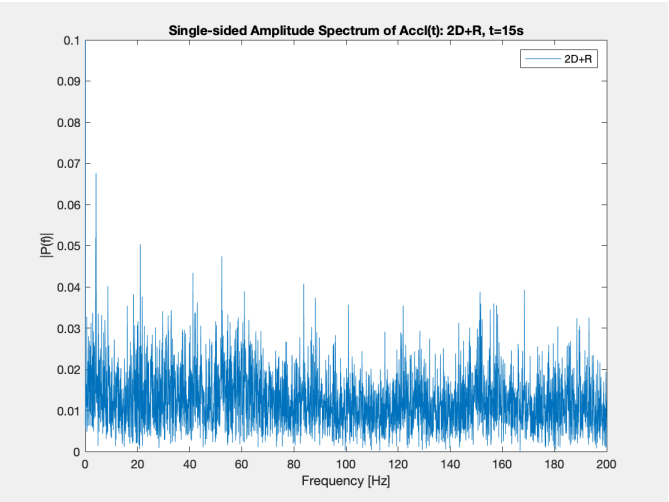

(a) 2D+R 15s: FFT

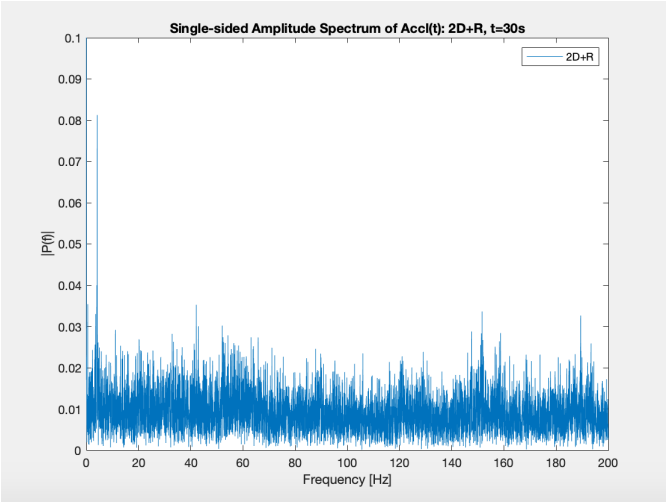

(b) 2D+R 30s: FFT

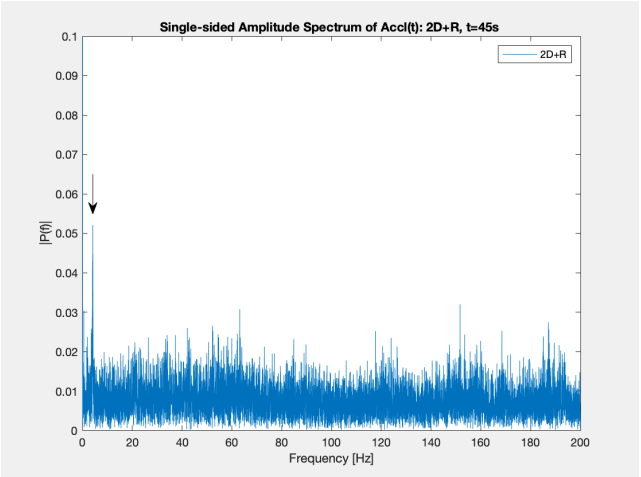

(c) 2D+R 45s: FFT

Figure 5.27: 2D+R: FFT

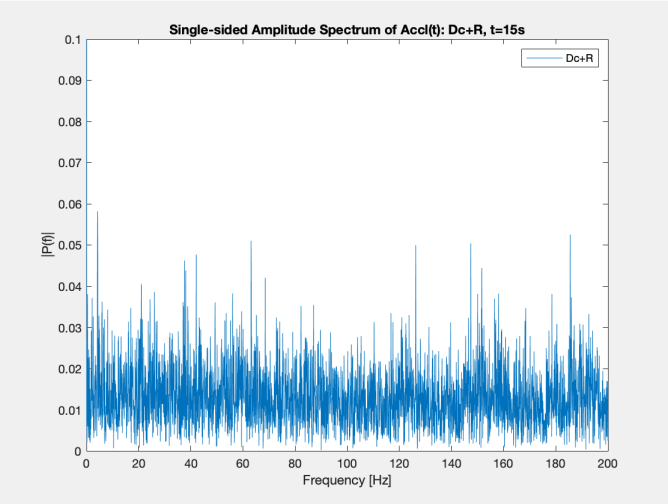

(a) DC+R 15s: FFT

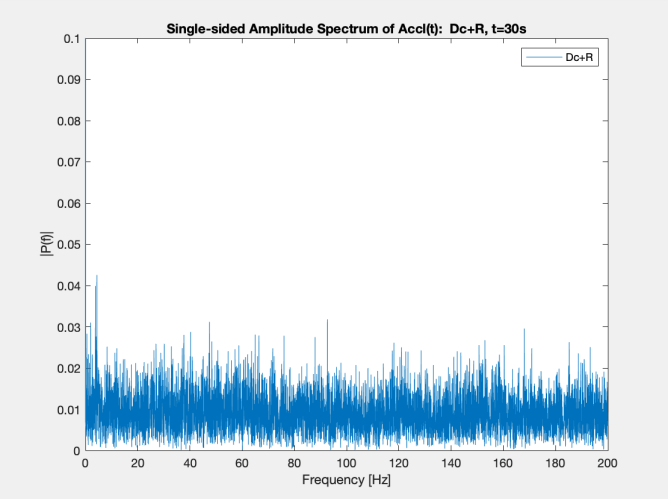

(b) DC+R 30s: FFT

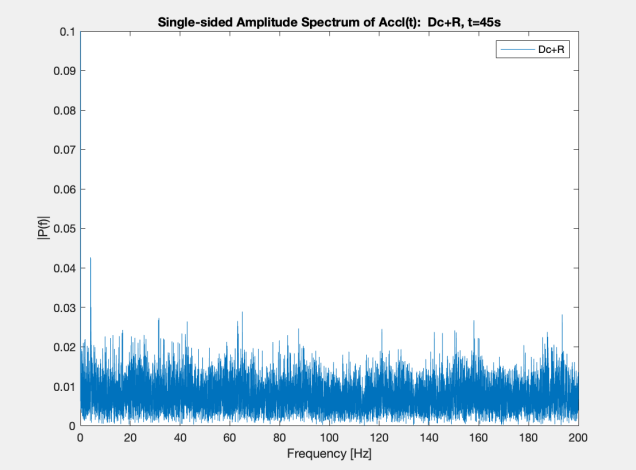

(c) DC+R 45s: FFT

Figure 5.28: DC+R: FFT

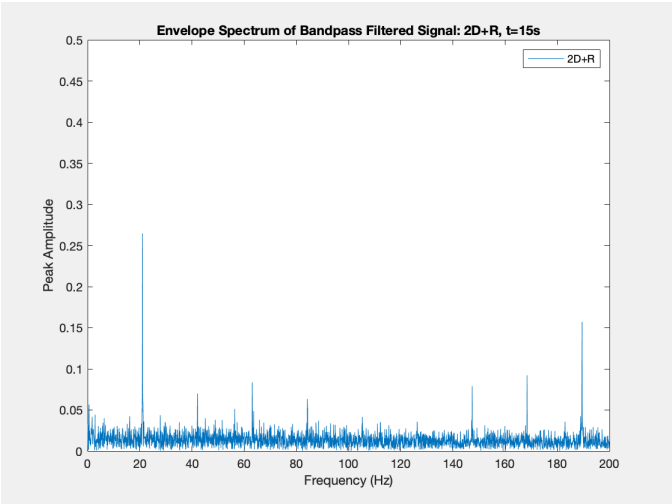

(a) 2D+R 15s: ENV

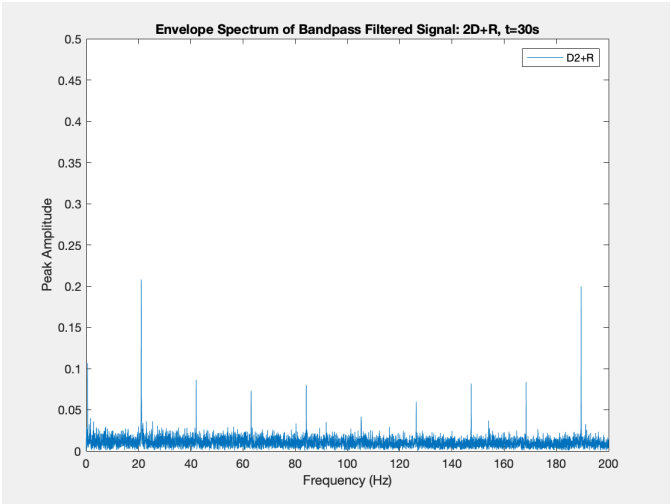

(b) 2D+R 30s: ENV

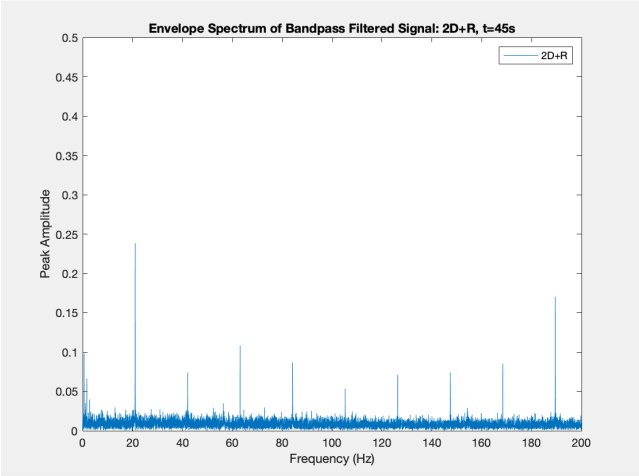

(c) 2D+R 45s: ENV

Figure 5.29: 2D+R: Envelope Spectrum

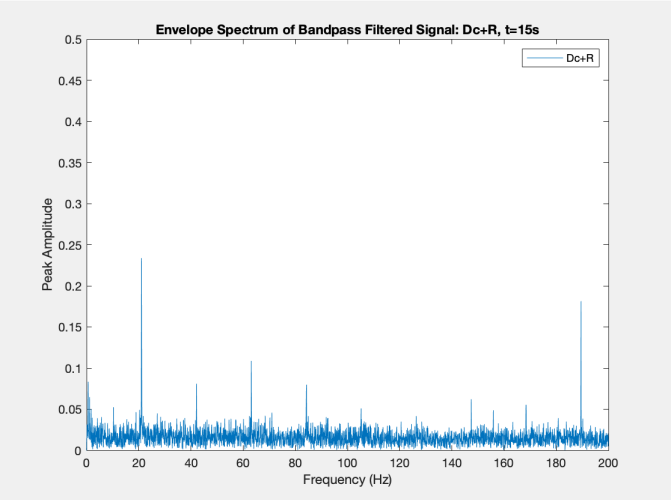

(a) DC+R 15s: ENV

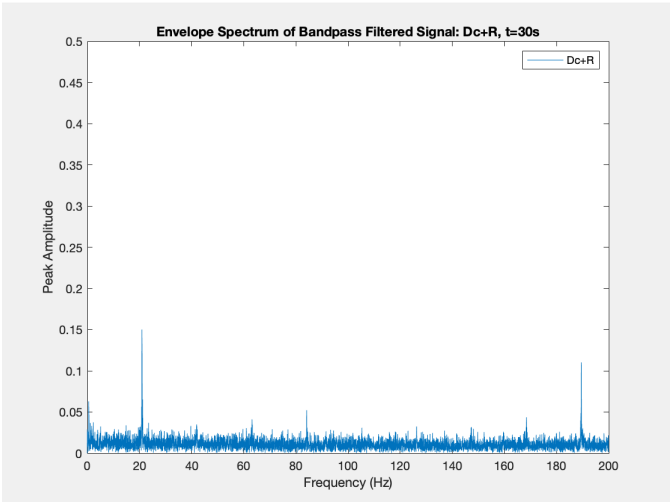

(b) DC+R 30s: ENV

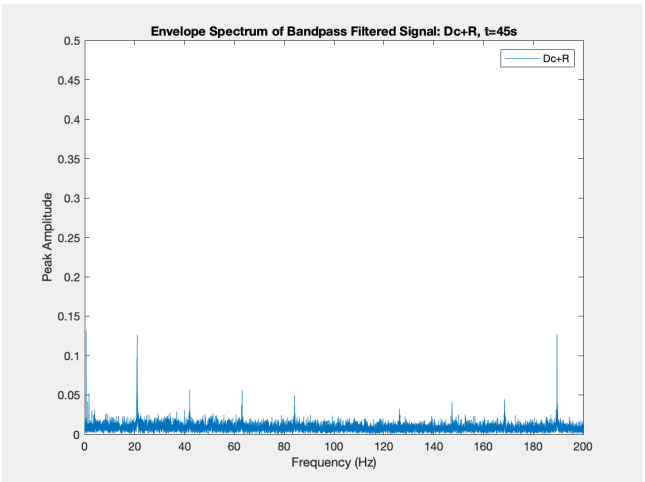

(c) DC+R 45s: ENV

Figure 5.30: DC+R: Envelope Spectrum

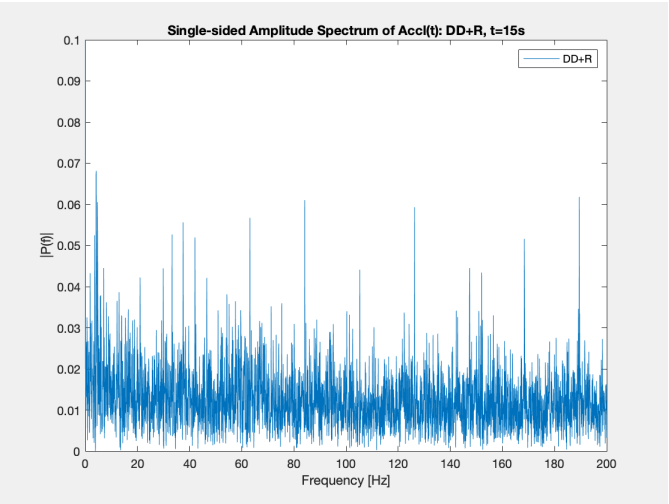

(a) DD+R 15s: FFT

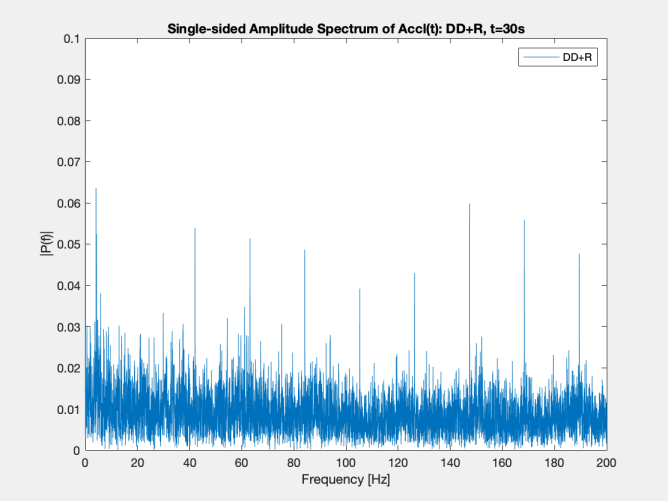

(b) DD+R 30s: FFT

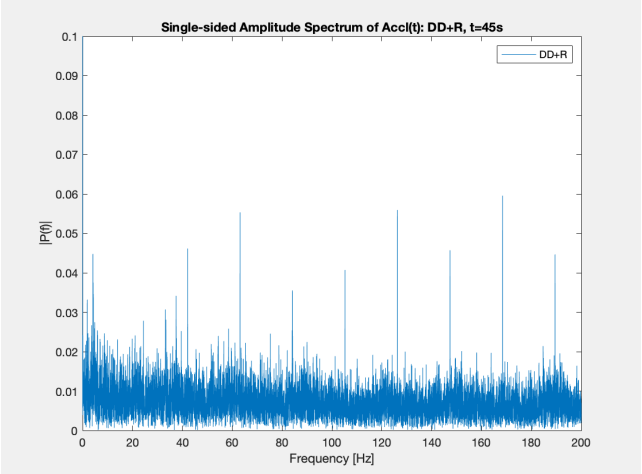

(c) DD+R 45s: FFT

Figure 5.31: DD+R: FFT

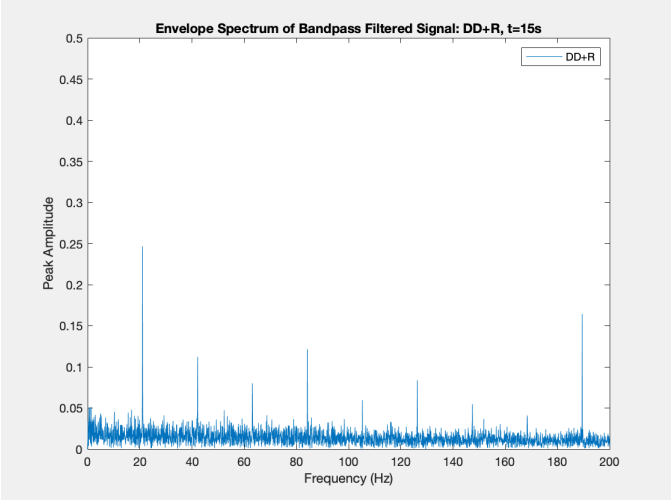

(a) DD+R 15s: ENV

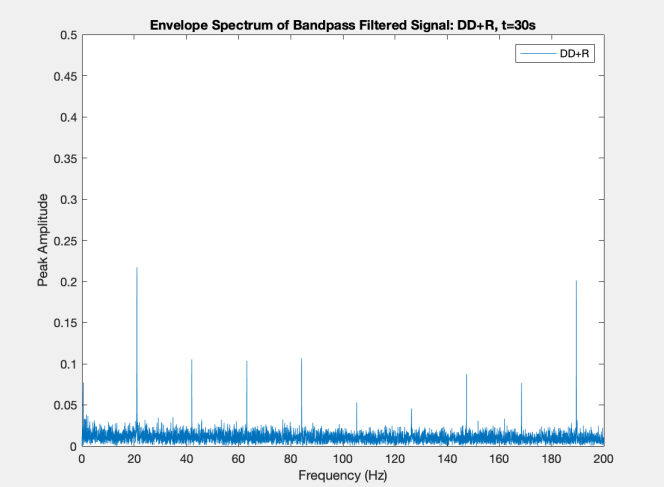

(b) DD+R 30s: ENV

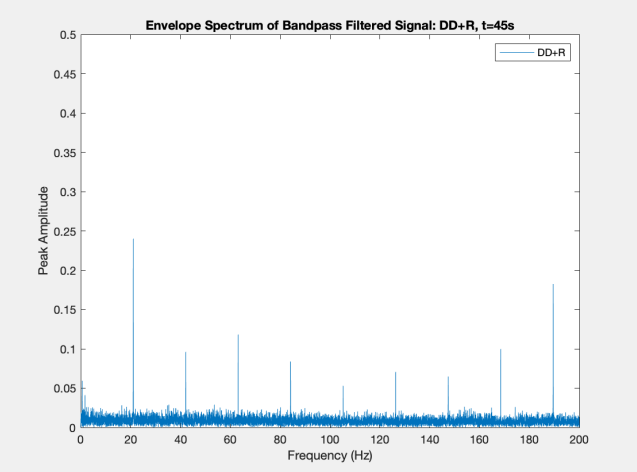

(c) DD+R 45s: ENV

Figure 5.32: DD+R: Envelope Spectrum

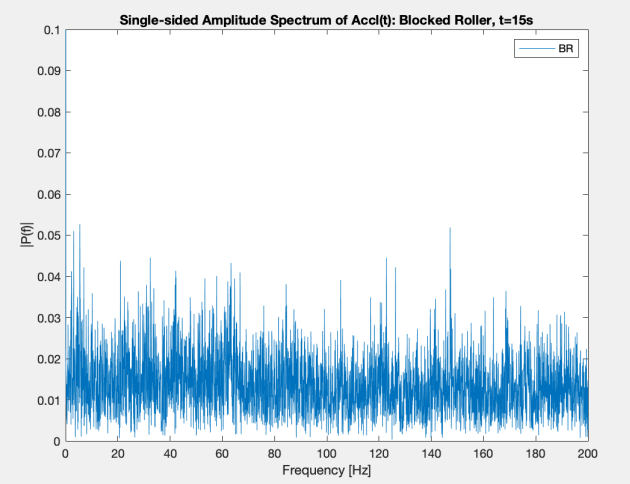

(a) BR 15s: FFT

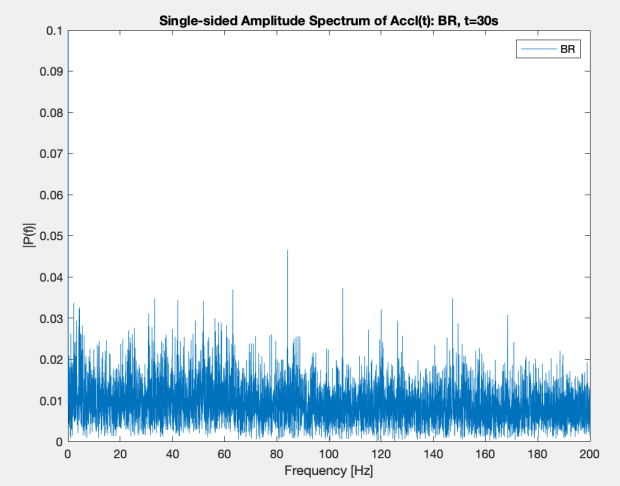

(b) BR 30s: FFT

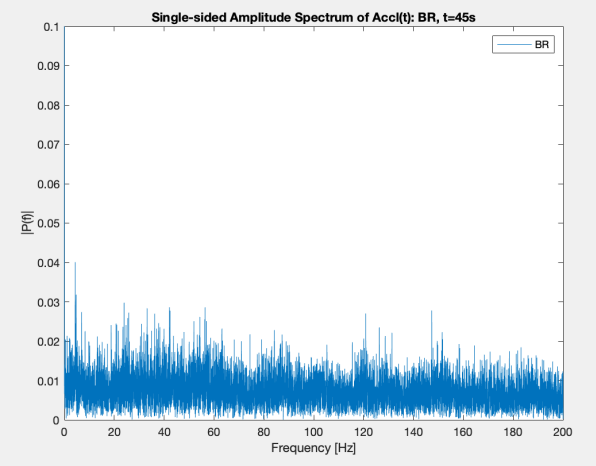

(c) BR 45s: FFT

Figure 5.33: BR: FFT

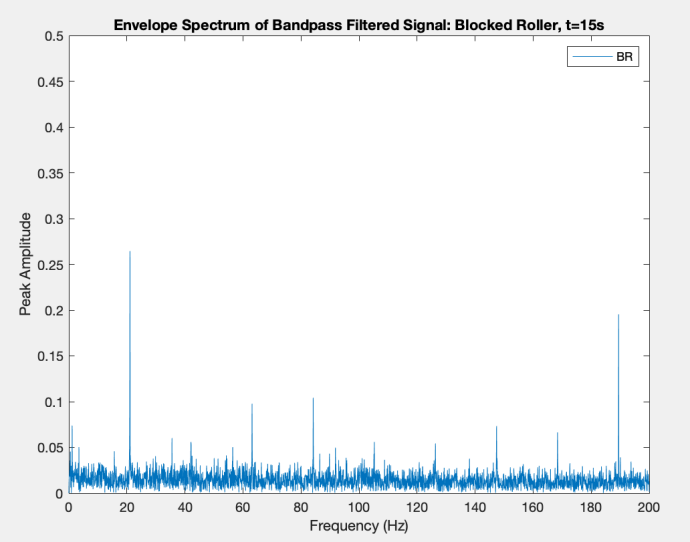

(a) BR 15s: ENV

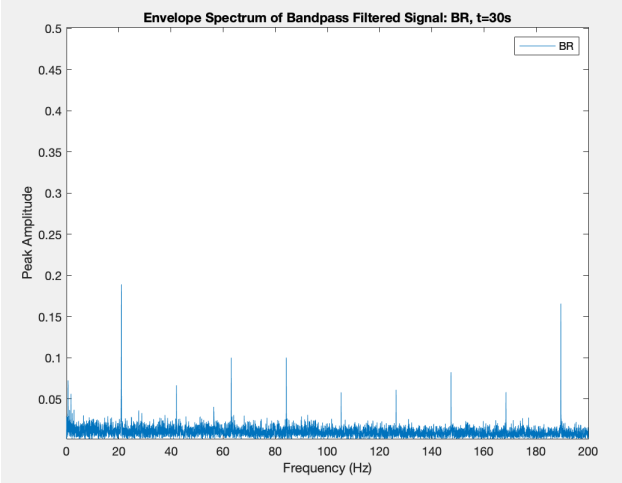

(b) BR 30s: ENV

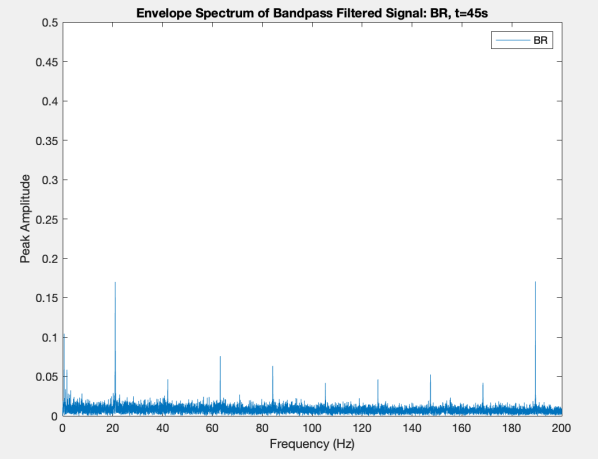

(c) BR 45s: ENV

Figure 5.34: BR: Envelope Spectrum

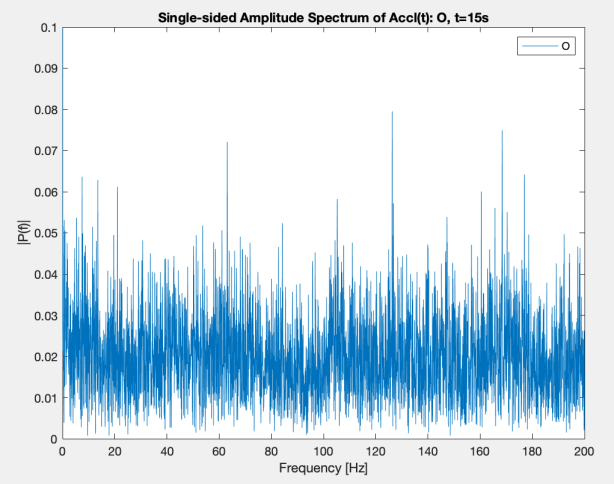

(a) O 15s: FFT

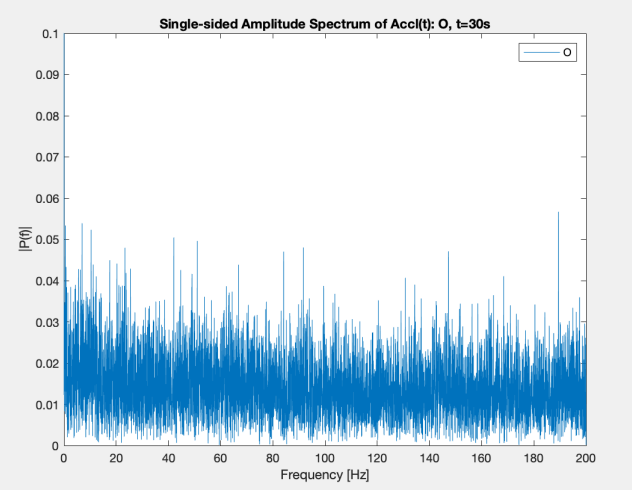

(b) O 30s: FFT

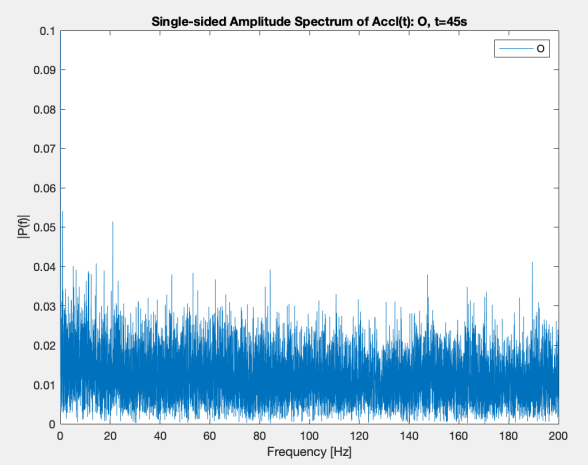

(c) O 45s: FFT

Figure 5.35: O: FFT

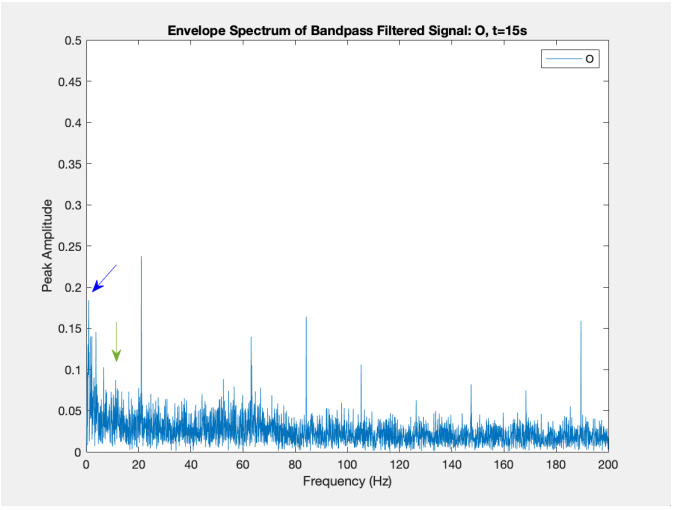

(a) O 15s: ENV

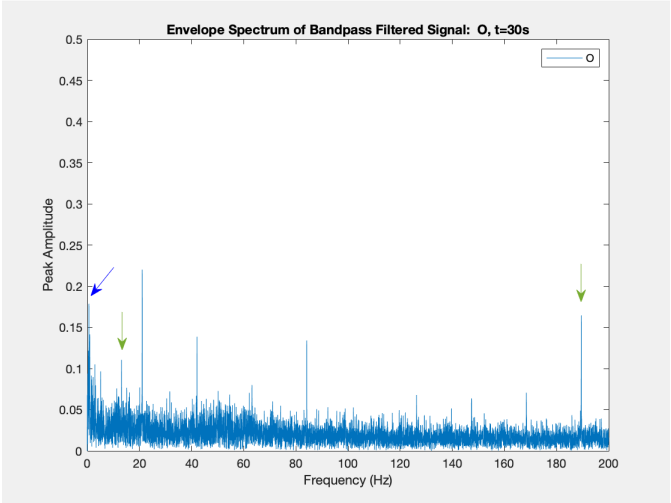

(b) O 30s: ENV

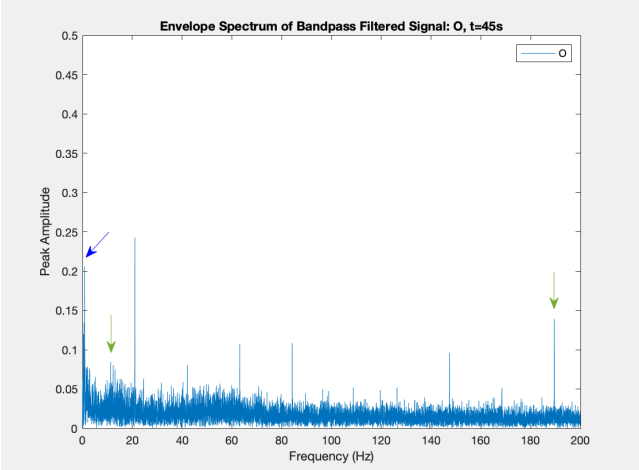

(c) O 45s: ENV

Figure 5.36: O: Envelope Spectrum

5.1.2.2 Water + LiquidSoap

One tank was filled with 2l water adding 200ml of liquid hand soap.

5.1.2.2.1 Healthy pump

Pump is firstly working under healthy condition pumping a new fluid. This kind of solution brings to the formation of bubbles in the tank, with the risk that the pump would suck also bubbles. At a first sight, the FFT spectrum (5.37a,5.37b,5.37c) of the healthy pumps shows higher peaks with respect to the corresponding case using water. Peaks cover the whole available range: 1.7Hz and 3.8Hz are the highest, in the middle band peaks that repeat in all the three cases are 21Hz,37Hz, 58Hz, 86Hz, 121Hz and near 150Hz, whereas in the envelope spectrum high impact is given by the well-known f=21Hz. Beside this frequency, in the envelope spectrum (5.38a,5.38b,5.38c) of each case there are some hidden frequency up to 100Hz and a peak at f=189Hz in the second half of the frequency range.

5.1.2.2.2 DC

Dealing with FFT (5.39a, 5.39b, 5.39c) of DC case, peaks cover the central band, in particular 105Hz is the highest. The other frequency components have the same stressed in 1D case, but higher in amplitude. In t=15s and t=30s frames, a 33Hz peak stands, whereas in the last case this frequency is hidden between the first two 21Hz harmonics.

Envelope spectrum in 5.40a,5.40b,5.40c emphasises a set of three consecutive peaks (27.8Hz, 35.2Hz, 42Hz), 56 Hz inherited from 1D case and 155Hz.

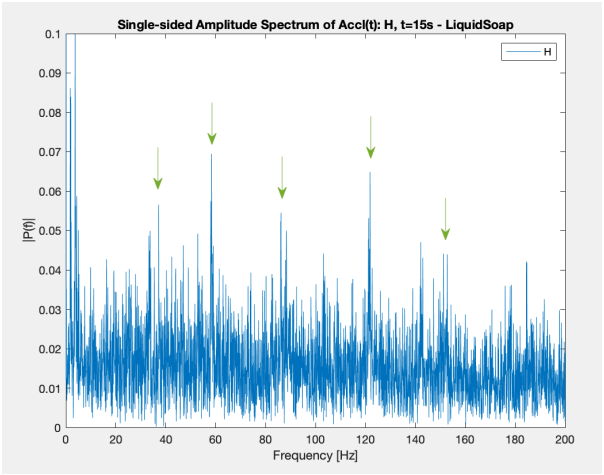

(a) H wLS 15s: FFT

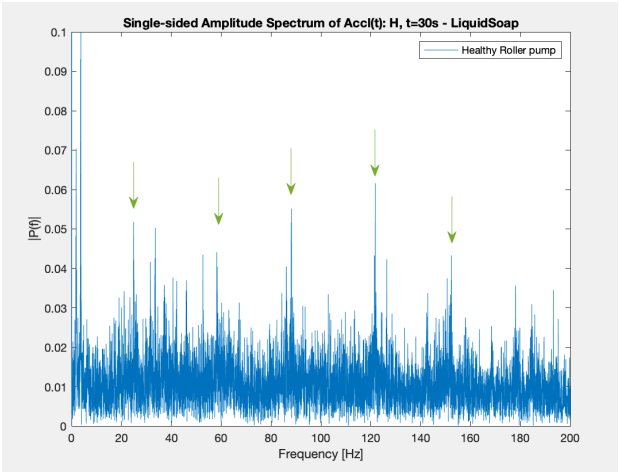

(b) H wLS 30s: FFT

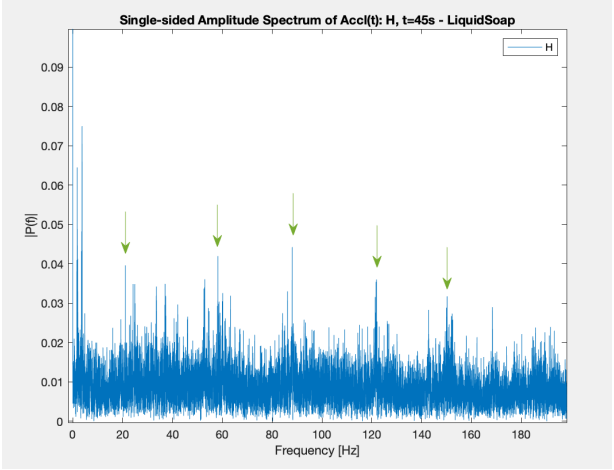

(c) H wLS 45s: FFT

Figure 5.37: H wLS: FFT

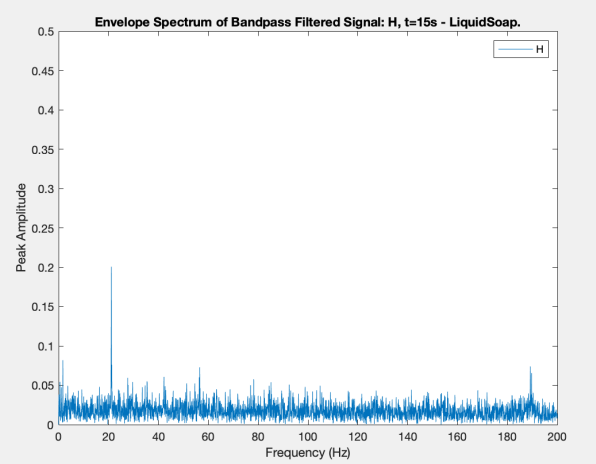

(a) H wLS 15s: ENV

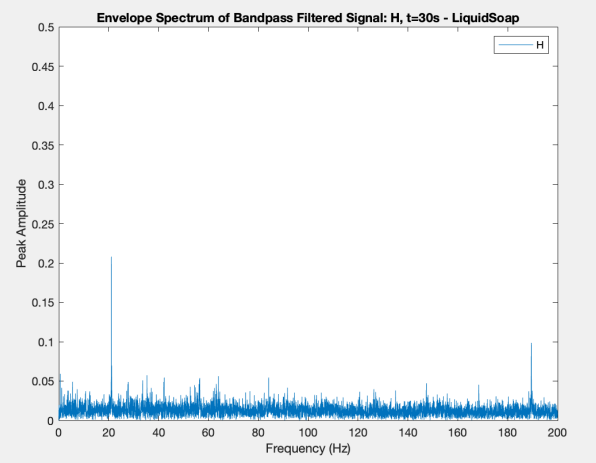

(b) H wLS 30s: ENV

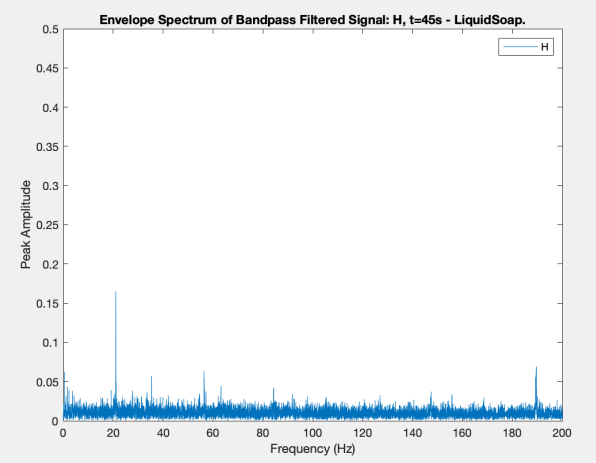

(c) H wLS 45s: ENV

Figure 5.38: H wLS: Envelope Spectrum

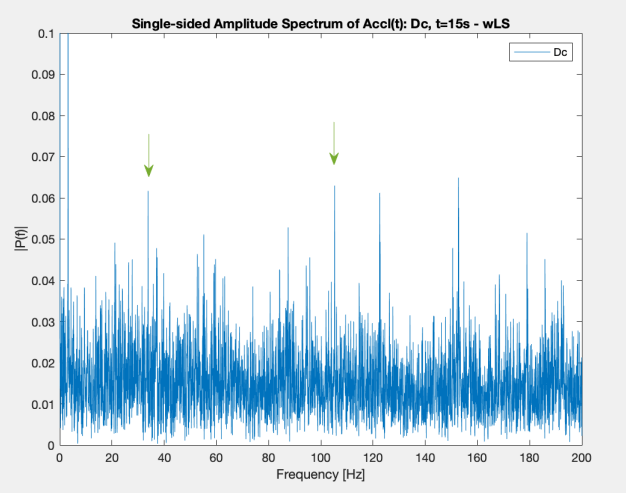

(a) DC wLS 15s: FFT

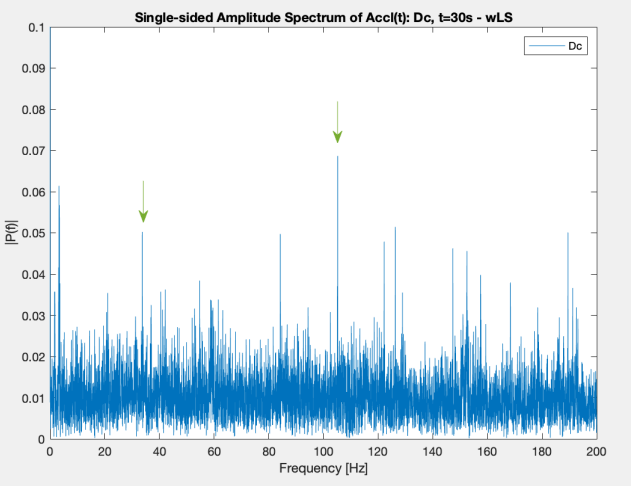

(b) DC wLS 30s: FFT

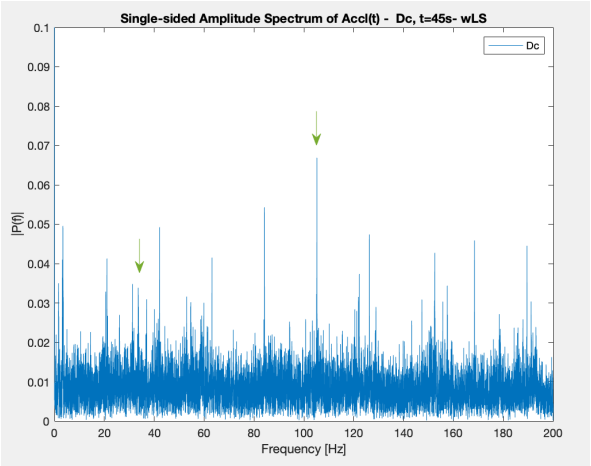

(c) DC wLS 45s: FFT

Figure 5.39: DC wLS: FFT

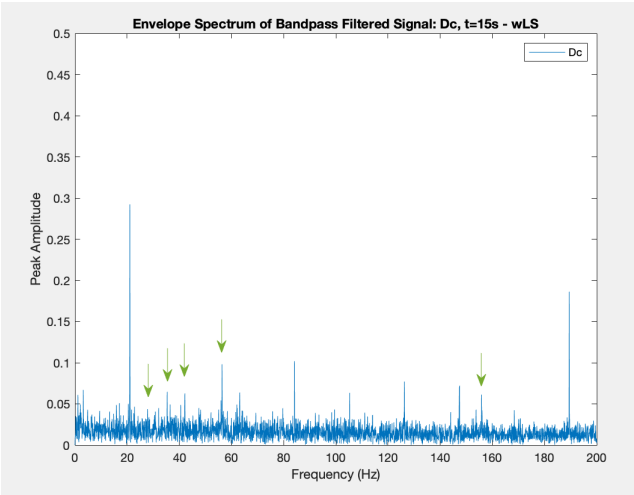

(a) DC wLS 15s: ENV

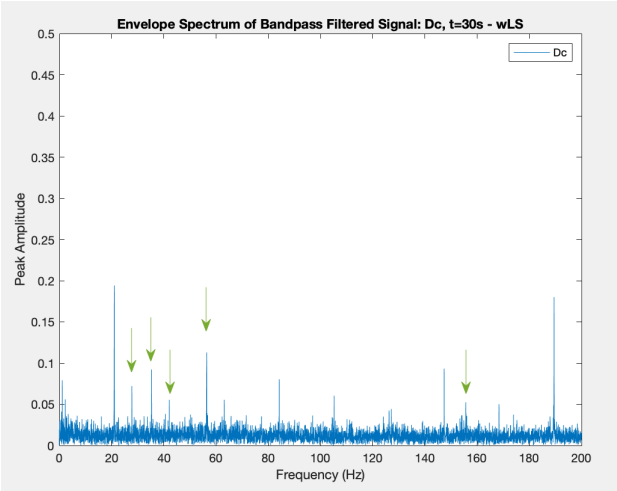

(b) DC wLS 30s: ENV

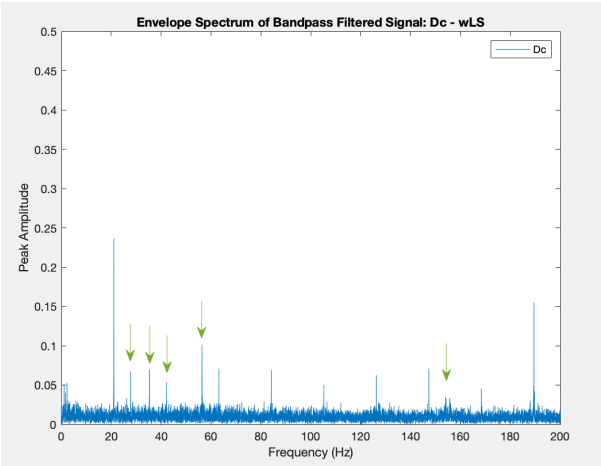

(c) DC wLS 45s: ENV

Figure 5.40: DC wLS: Envelope Spectrum

5.1.2.2.3 2D

Beside some harmonics of 21Hz, a component of 37Hz dominates both t=15s and t=30s. In the latter case, the highest peak in FFT spectrum is given by 60.4Hz (in pink 5.41a,5.41b,5.41c).

In the envelope spectrum (5.42a,5.42b,5.42c), the pattern found in the same case with water is no more valid: in that case we could rely on the fact that both 105 and 126 Hz components had lower contribute in magnitude. With liquid soap, this condition is confirmed only in t=15s case; in the other time frames, instead, arrows in figs 5.42b,5.42c point toward the same components that characterized one of the set found for DC case, discussed in section 5.1.2.2.2.

5.1.2.2.4 DD

FFT has sharp frequencies at f=4Hz, 63Hz and in the range 140-180Hz (5.43a,5.43b,5.43c). It shows lower peaks with respect to DD water case. The envelope spectrum (5.44a,5.44b,5.44c) combines 2D and DC case for small contributes given by the range 90-120Hz and 56Hz peak presence respectively.

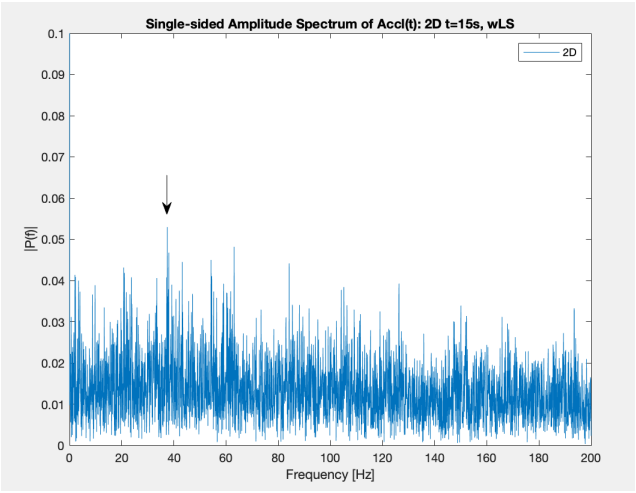

(a) 2D wLS 15s: FFT

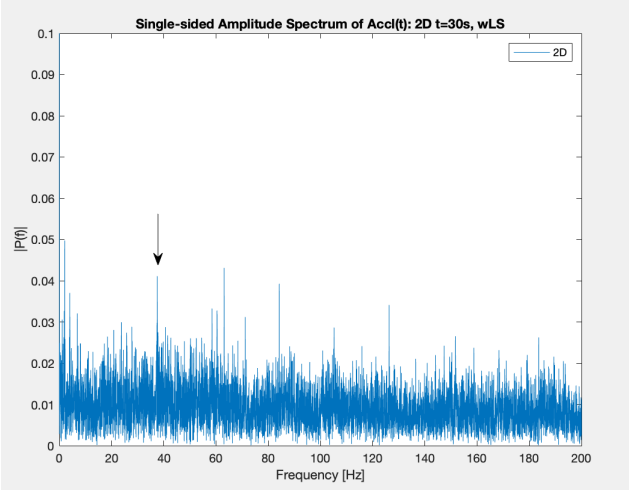

(b) 2D wLS 30s: FFT

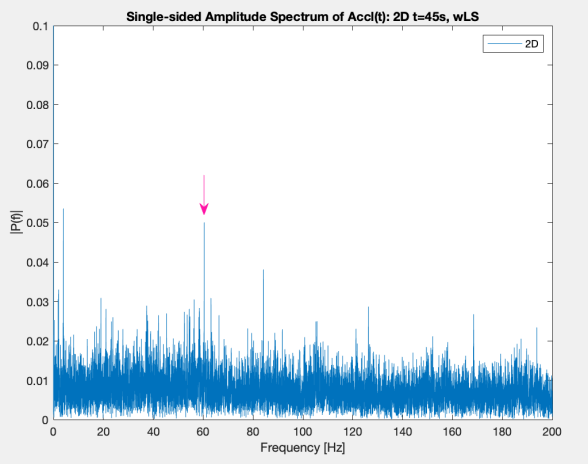

(c) 2D wLS 45s: FFT

Figure 5.41: 2D wLS: FFT

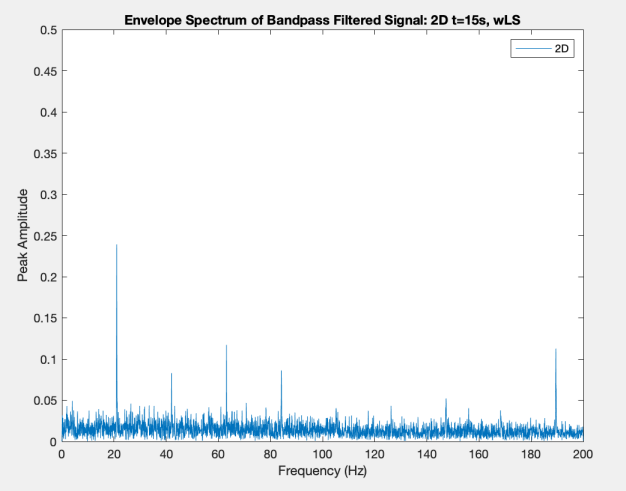

(a) 2D wLS 15s: ENV

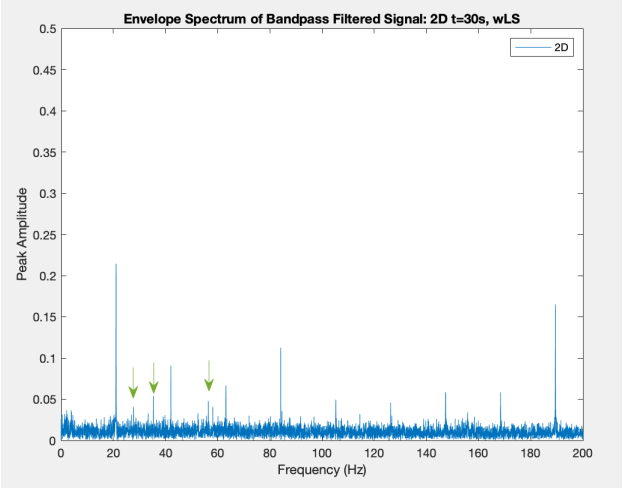

(b) 2D wLS 30s: ENV

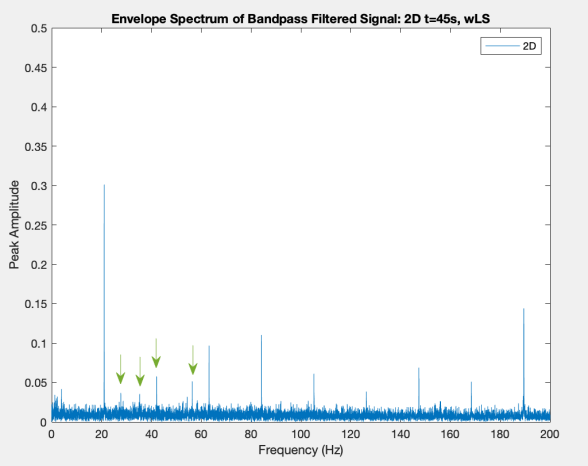

(c) 2D wLS 45s: ENV

Figure 5.42: 2D wLS: Envelope Spectrum

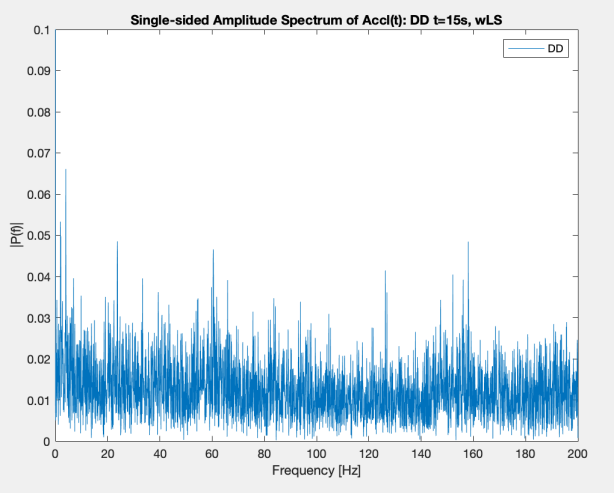

(a) DD wLS 15s: FFT

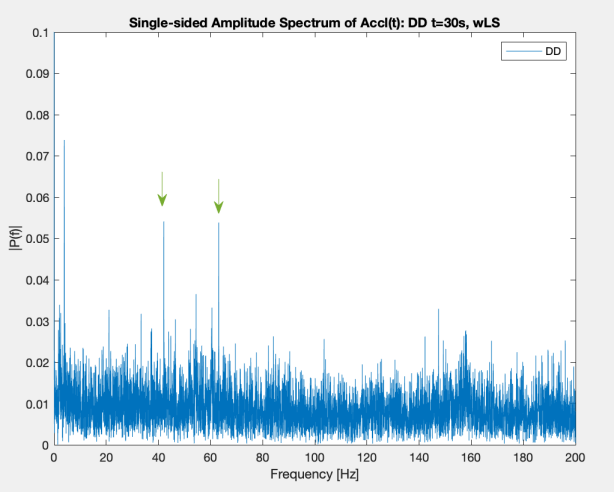

(b) DD wLS 30s: FFT

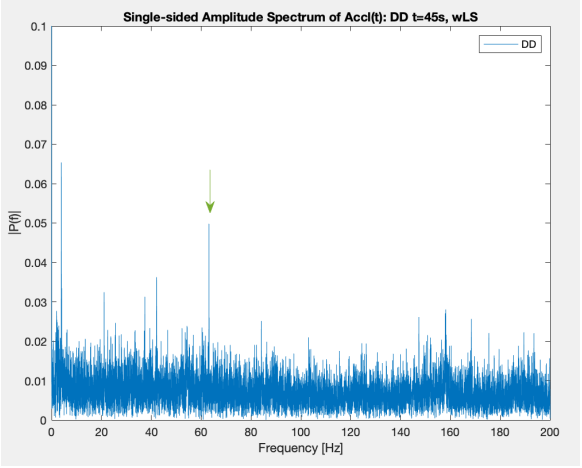

(c) DD wLS 45s: FFT

Figure 5.43: DD wLS: FFT

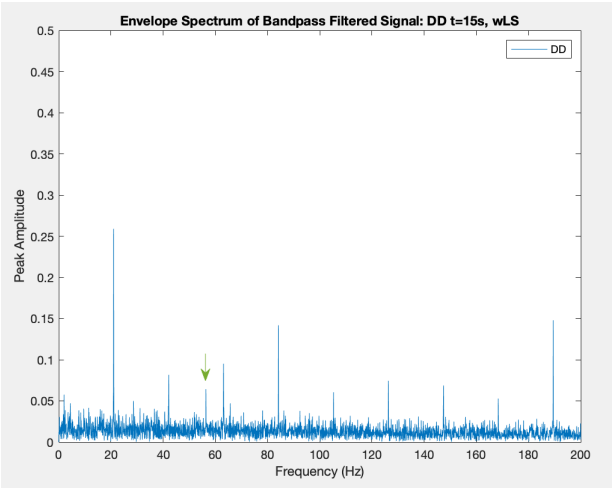

(a) DD wLS 15s: ENV

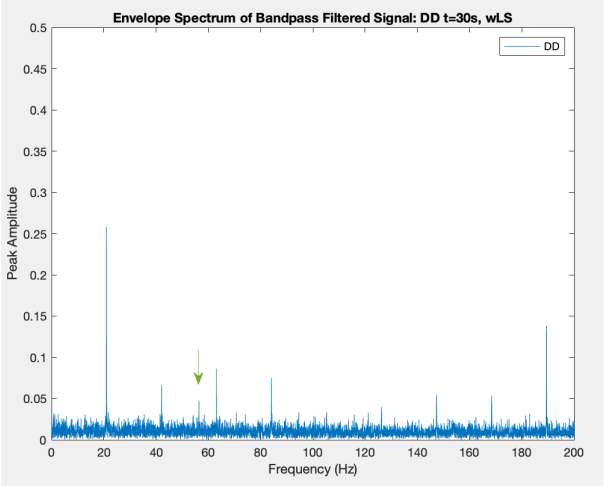

(b) DD wLS 30s: ENV

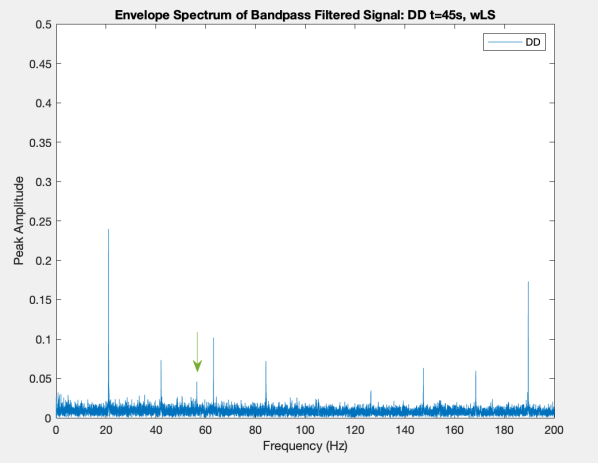

(c) DD wLS 45s: ENV

Figure 5.44: DD wLS: Envelope Spectrum

5.1.2.2.5 +R

If H+R case is considered, one can notice that, with respect to H case, peaks are highly dominant in the first half of FFT spectrum (5.45a, 5.45b, 5.45c), in particular at f=33Hz.

However, this frequency is not stressed in the envelope spectrum (5.46a, 5.46b, 5.46c): it shows only higher peaks for those frequency that in H case were not stressed.

Apart from 4-4.8Hz, only four frequencies characterizes FFT 2D+R spectrum, whereas the central band lower peaks intensity (5.47a, 5.47b, 5.47c). In the envelope spectrum (5.48a, 5.48b, 5.48c) all the 21Hz harmonics are stressed.

Also in Dc+R case the side band frequency are more stressed with respect to the central domain, mainly 33Hz and 54Hz a part from 21Hz harmonics (5.49a, 5.49b, 5.49c); the central harmonics of 126Hz gives the lowest contribute in magnitude in the envelope spectrum (5.50a, 5.50b, 5.50c).

DD+R is the only case with a plain FFT frequency distribution (5.51a, 5.51b, 5.51c), which is reflected in an envelope spectrum with lower magnitude intensity (5.52a, 5.52a, 5.52a).

5.1.2.2.6 O

As the other damaged cases, FFT (5.53a, 5.53b, 5.53c) has higher sideband frequencies and the envelope spectrum (5.54a,5.54b,5.54c) does not great contribution in understanding which frequency has greater impact. From these representation, O can be confused with +R cases.

Tables 5.2 and 5.3 summirezes the main differences between the cases for what concerns the First Analysis only; tables 5.4 and 5.5 respectively FFT and Envelope analysis for the second analysis related of each cases in three time duration.

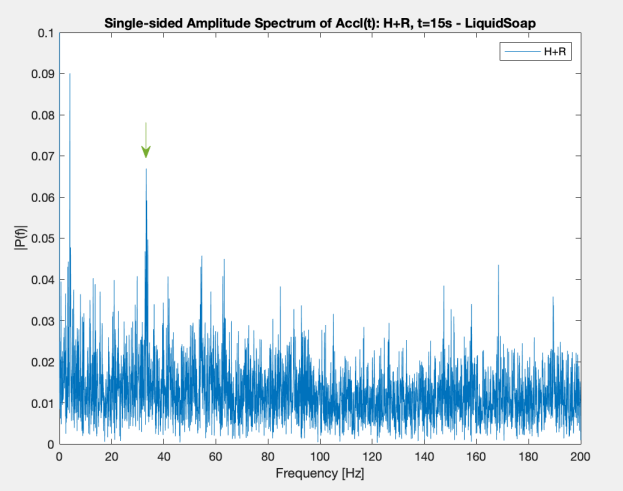

(a) H+R wLS 15s: FFT

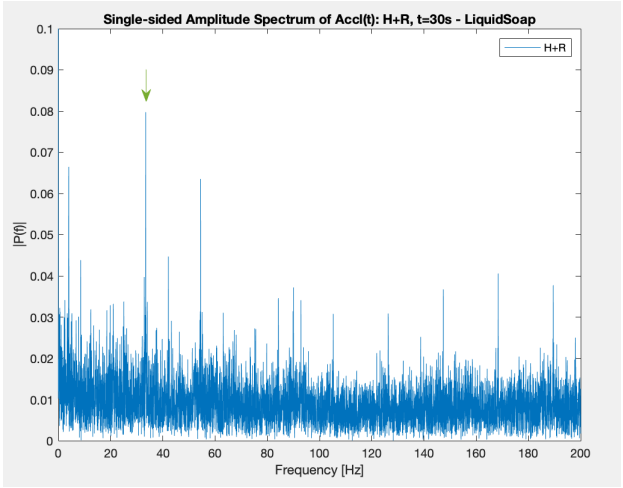

(b) H+R wLS 30s: FFT

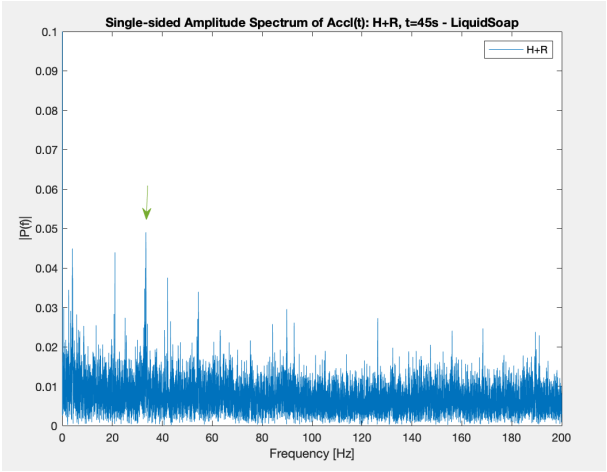

(c) H+R wLS 45s: FFT

Figure 5.45: H+R wLS: FFT

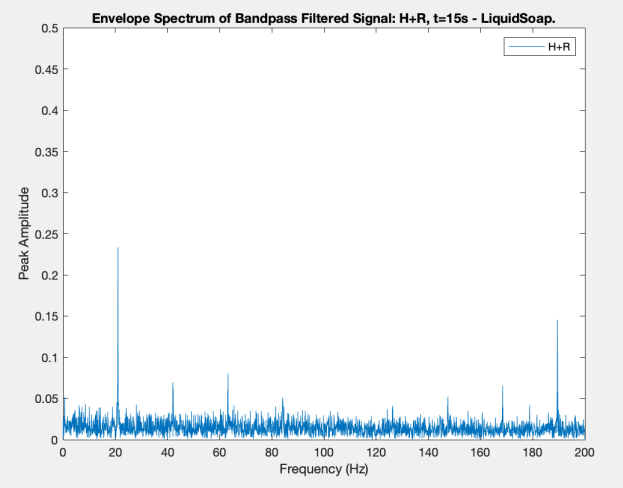

(a) H+R wLS 15s: ENV

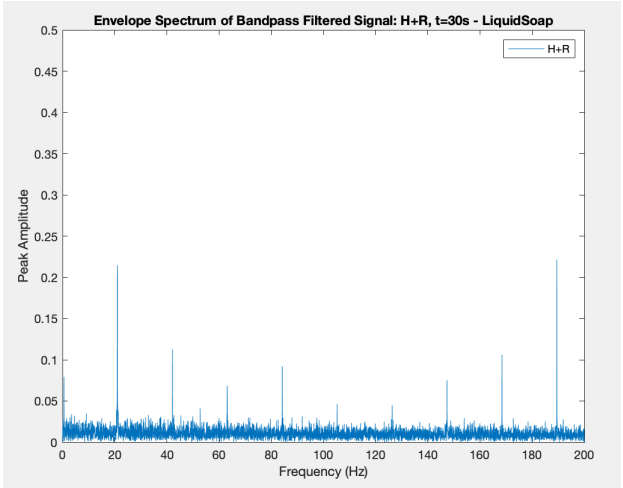

(b) H+R wLS 30s: ENV

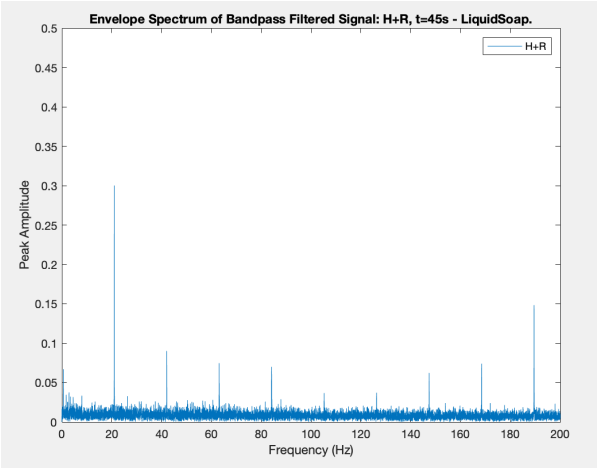

(c) H+R wLS 45s: ENV

Figure 5.46: H+R wLS: Envelope Spectrum

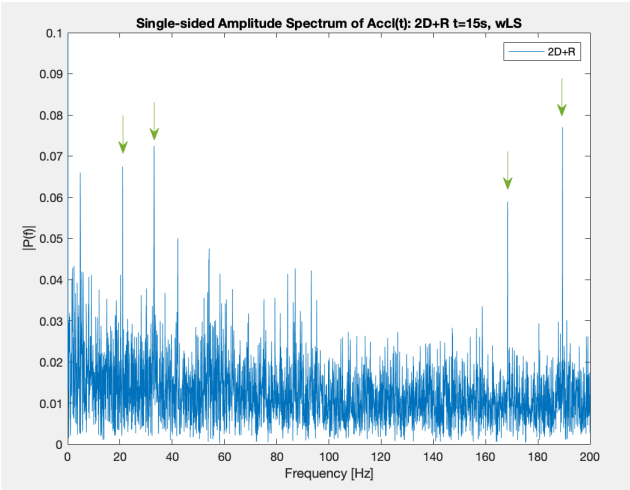

(a) 2D+R wLS 15s: FFT

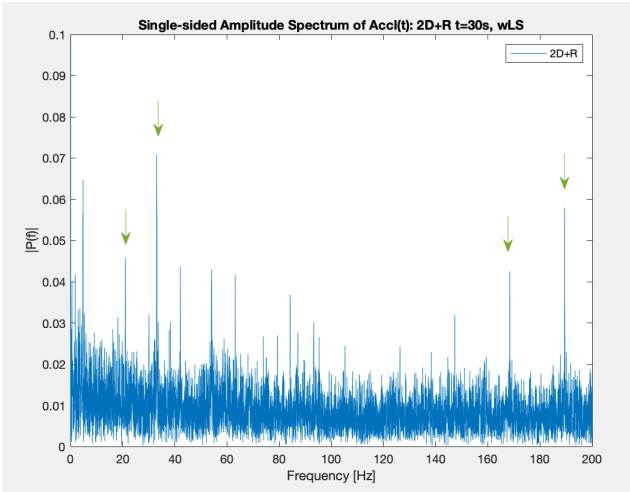

(b) 2D+R wLS 30s: FFT

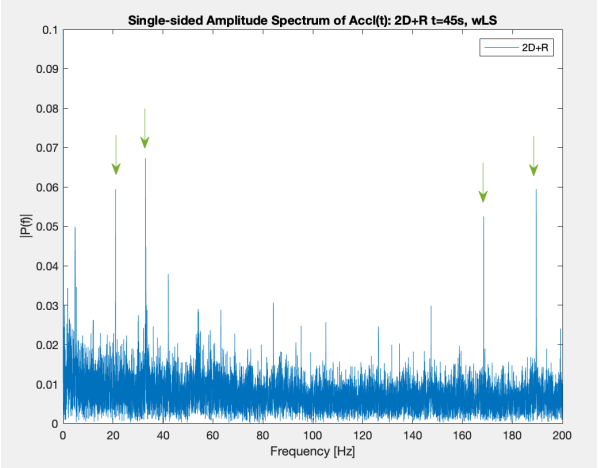

(c) 2D+R wLS 45s: FFT

Figure 5.47: 2D+R wLS: FFT

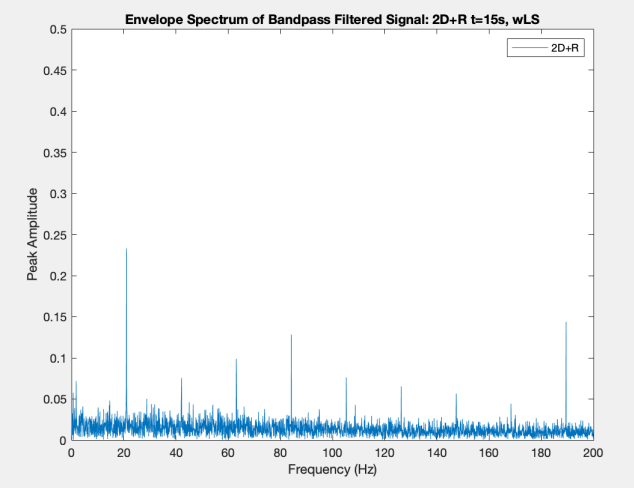

(a) 2D+R wLS 15s: ENV

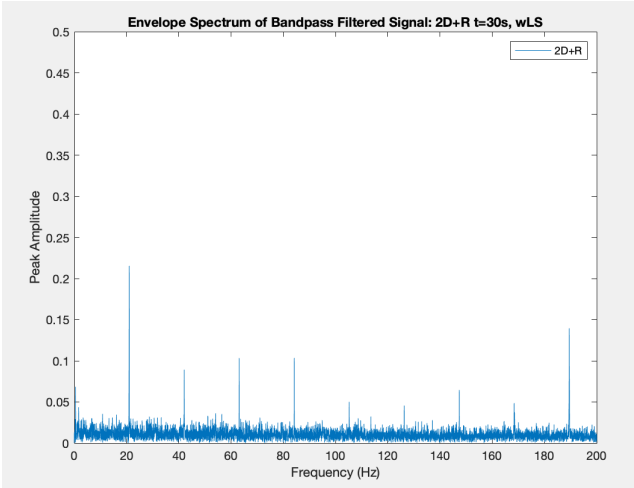

(b) 2D+R wLS 30s: ENV

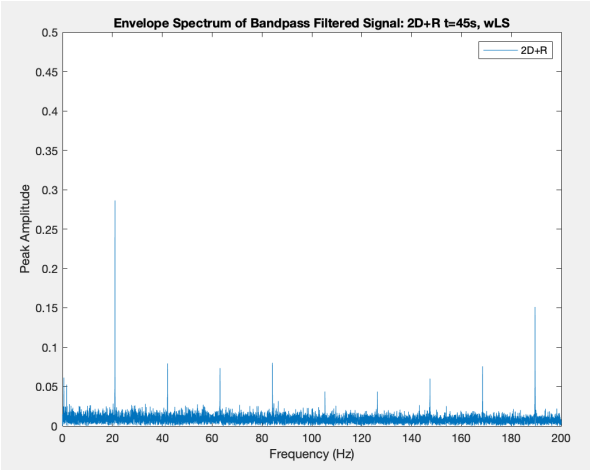

(c) 2D+R wLS 45s: ENV

Figure 5.48: 2D+R wLS: Envelope Spectrum

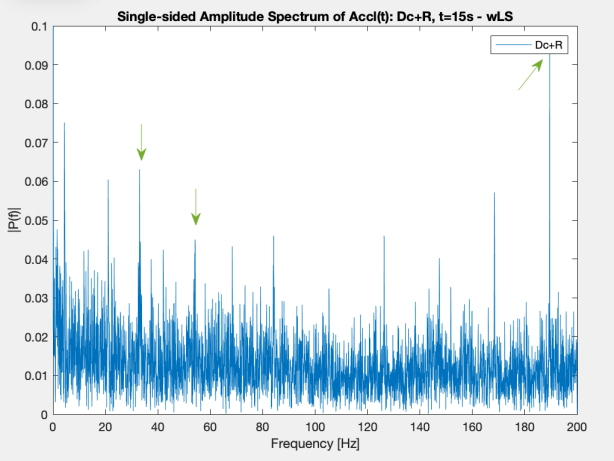

(a) DC+R wLS 15s: FFT

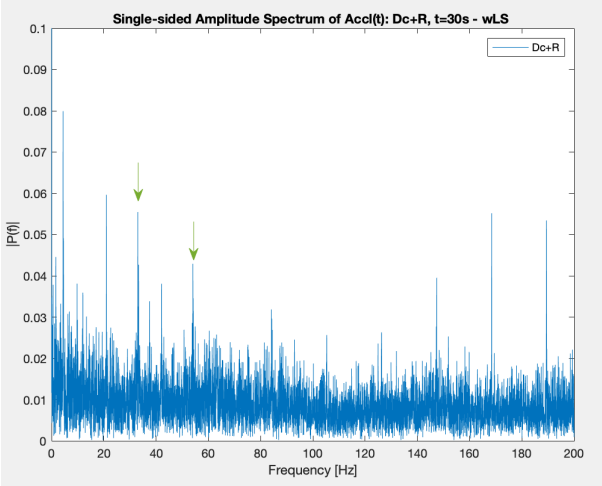

(b) DC+R wLS 30s: FFT

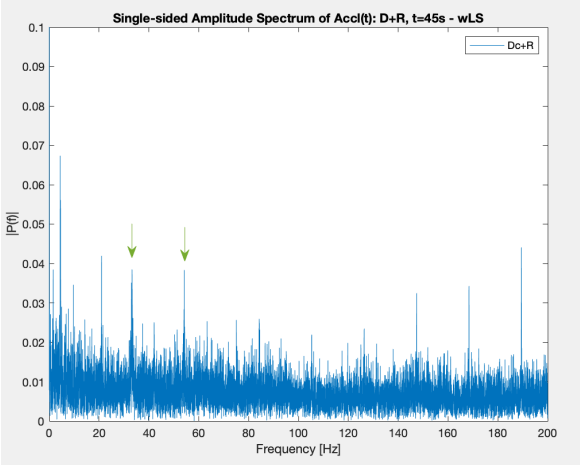

(c) DC+R wLS 45s: FFT

Figure 5.49: DC+R wLS: FFT

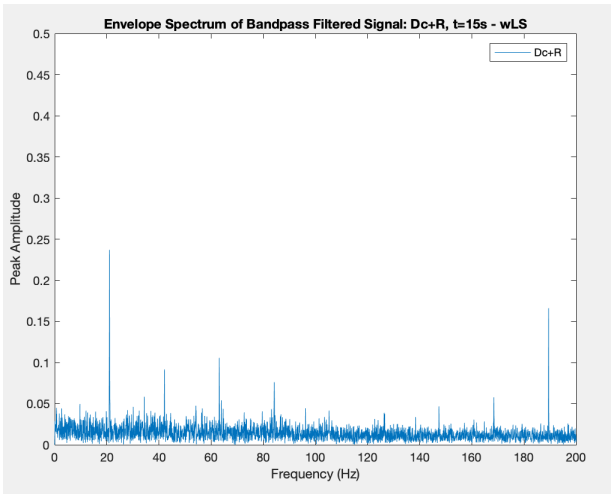

(a) DC+R wLS 15s: ENV

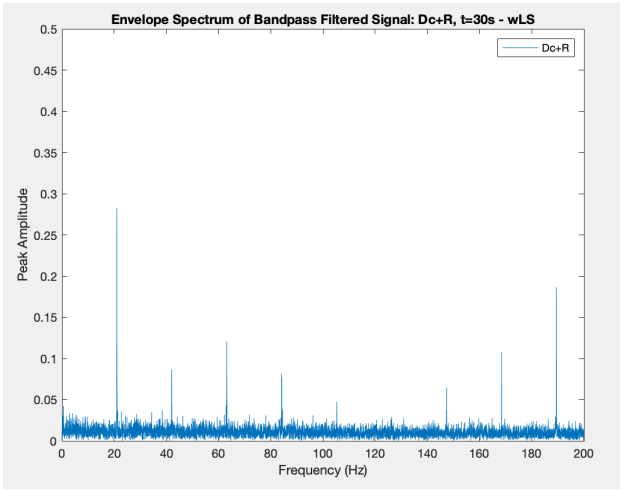

(b) DC+R wLS 30s: ENV

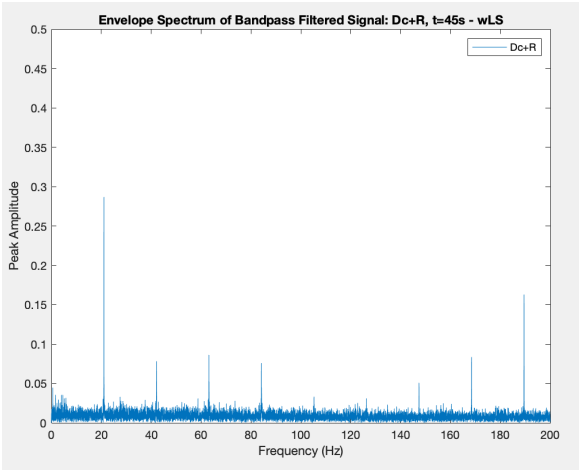

(c) DC+R wLS 45s: ENV

Figure 5.50: DC+R wLS: Envelope Spectrum

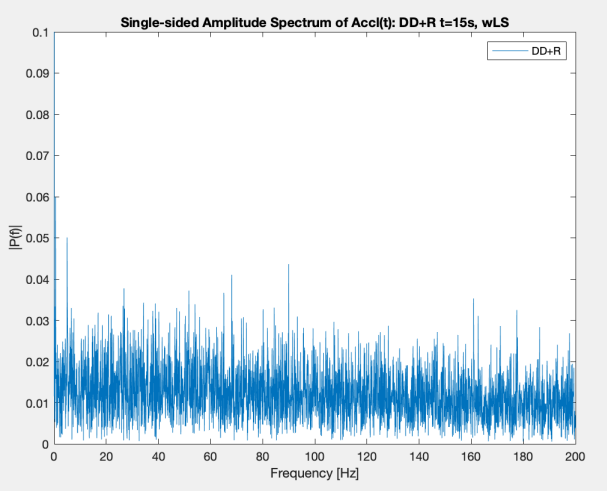

(a) DD+R wLS 15s: FFT

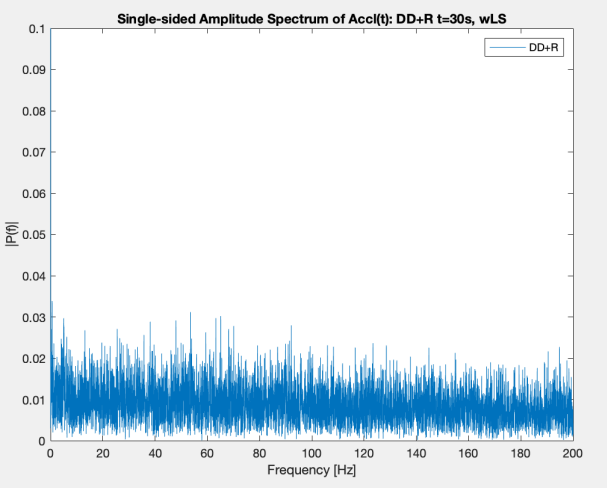

(b) DD+R wLS 30s: FFT

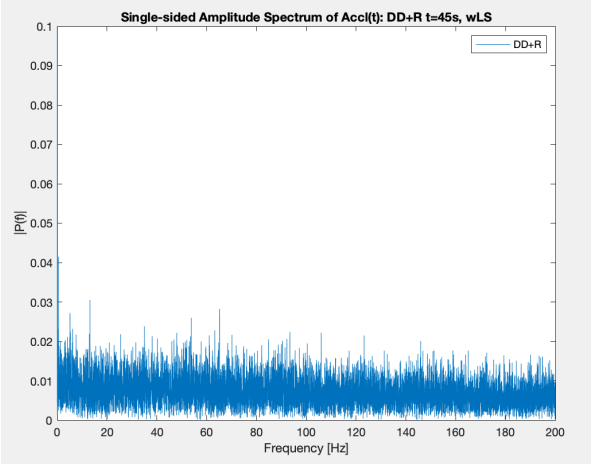

(c) DD+R wLS 45s: FFT

Figure 5.51: DD+R wLS: FFT

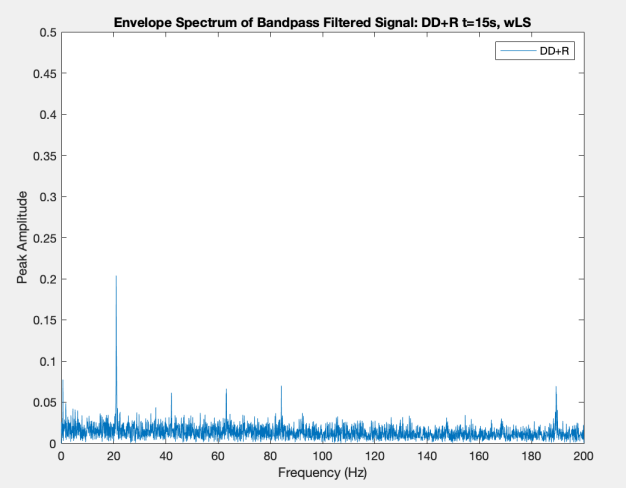

(a) DD+R wLS 15s: ENV

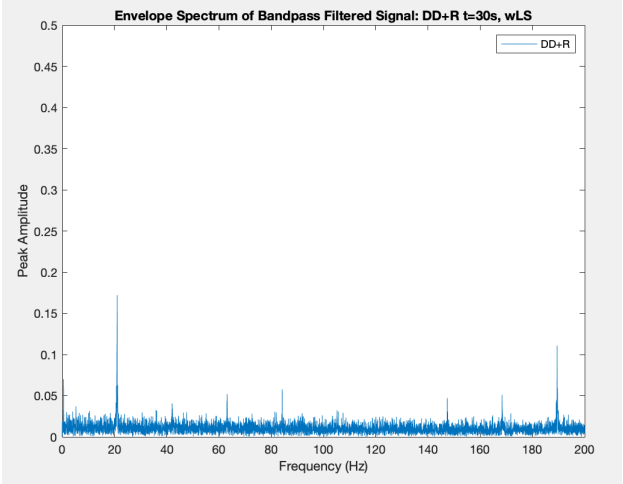

(b) DD+R wLS 30s: ENV

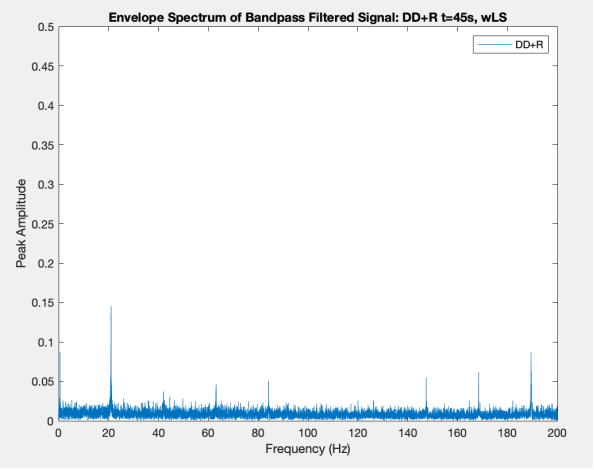

(c) DD+R wLS 45s: ENV

Figure 5.52: DD+R wLS: Envelope Spectrum

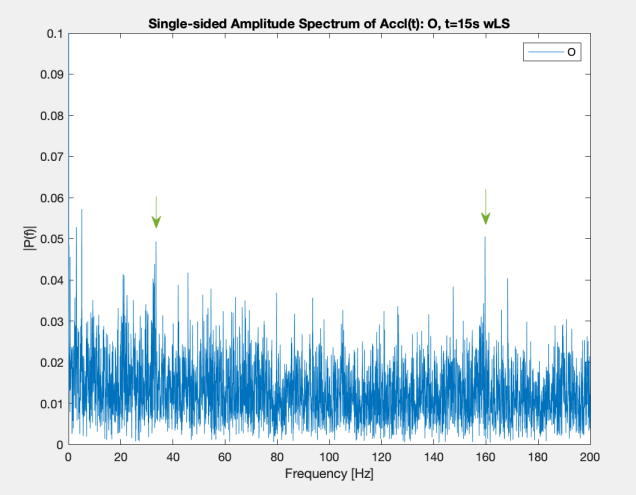

(a) O wLS 15s: FFT

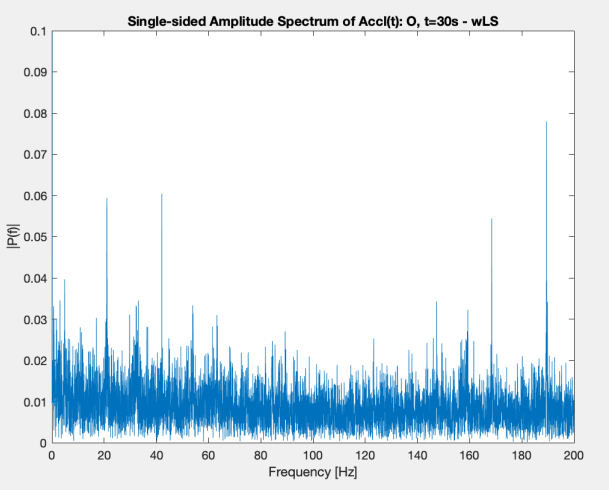

(b) O wLS 30s: FFT

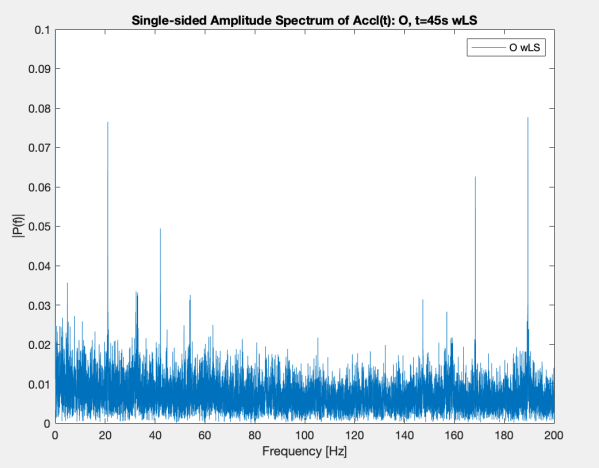

(c) O wLS 45s: FFT

Figure 5.53: O wLS: FFT

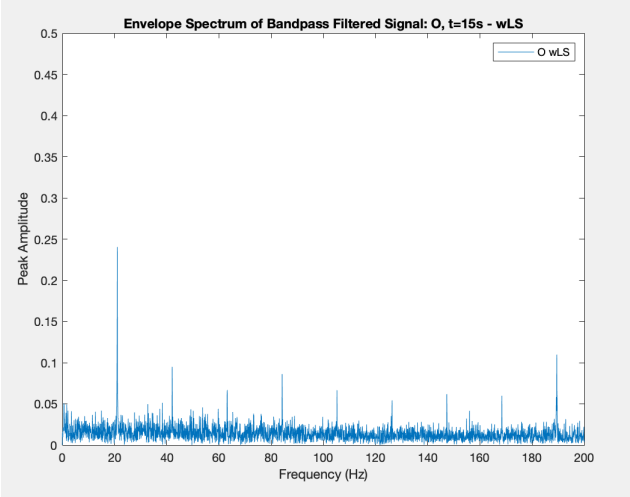

(a) O wLS 15s: ENV

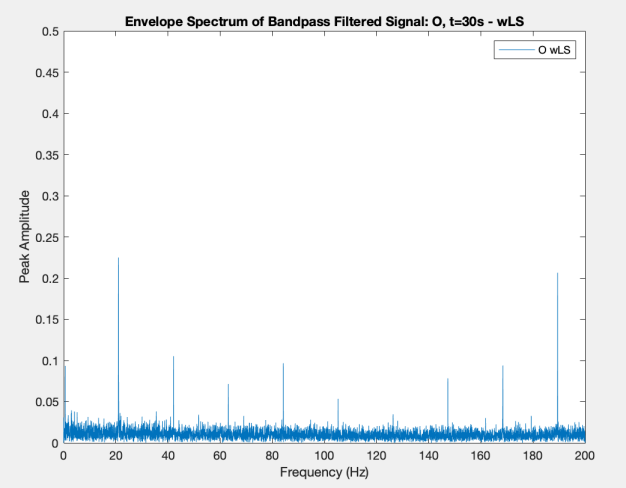

(b) O wLS 30s: ENV

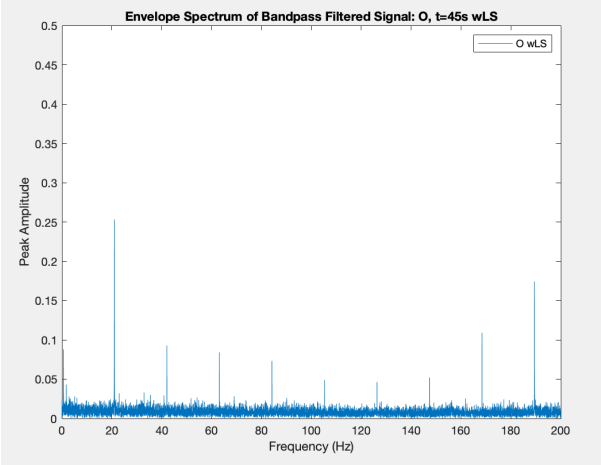

(c) O wLS 45s: ENV

Figure 5.54: O wLS: Envelope Spectrum

Table 5.2: FFT comparison: First Analysis

FFT	**FIRST ANALYSIS : WATER**
H	12Hz harmonics all over spectrum
1D	Impact of 21Hz harmonics
2D	84Hz,105Hz,126Hz stand in all domain
DD	Not relevant frequencies that have important peaks
+R	+R seems not to influence the frequency content; highest peak is found in 1D+R case at f=56Hz
BR	Some peaks but FFT representation is quite similar to +R case

Table 5.3: Envelope Spectrum comparison: First Analysis

ENV	**FIRST ANALYSIS : WATER**
H	Plain spectrum, no evidence of impacting f
1D	Presence of f=56hz, all 21Hz harmonics but 2x and 8x
2d	21Hz harmonics have higher peaks, no presence of 56Hz
DD	Sums previous faulty cases, introducing f=35Hz
+R	Only in H+R a f=0.6Hz is stressed higher wrt other case; highest peak is found in 1D+R case at f=56Hz. DD+R has totally plain spectrum (not expected)
BR	Peaks in central band: 84Hz,105Hz,126 and 147Hz

Table 5.4: FFT comparison: Second Analysis

SECOND ANALYSIS		
FFT	**WATER**	**W wLS**
blackH	All plain spectrum. Highest peakat 3.2Hz	Higher peaks all over band wrt to W
1D	Presence of 21Hz harmonics, allbut 2x	-
DC	Same trend as 1D	Highest p:33Hz and 105Hz
2D	Only 4.2 Hz	Highest p:37Hz e 60.4Hz
DD	Spectra differs for different t, butall present a central band with sovrasting peaks	Sharp frequencies located at 4Hz, 42Hz and 63Hz
H+R	Only f=42 Hz as characteristics	Higher wrt H, wrt to W (in particular first half) and f peak at 33 Hz
1D+R	Peaks at 21Hz, 63Hz,126Hz	-
2D+R DC+R	Only 4.3 Hz and Sided band highly emphatized	
DD+R	Frequency are steeper in all domain	Plain spectra
BR	Heterogeneous spectra	-
O	Results similar to BR	High sided band, confused with +R

Table 5.5: ENV comparison: Second Analysis

SECOND ANALYSIS		
ENV	**WATER**	**WATER wLS**
H	21Hz peak only	21Hz and 189Hz peaks only
1D	f=28Hz and 35Hz in addition to characteristic 56Hz	-
DC	Absence of f=105Hz, 126Hz	Three sets of f 27.8 + 35.2 + 42 Hz 56Hz and 155Hz
2D	f=105Hz, 126Hz lowest	The same as W only for t15, the others show DC pattern
DD	All component but 35Hz	Smaller contribution of band 90-120Hz and peak at 56Hz
H+R	Totally opposite scenario wrt H with noticeable peak at 0.6Hz	
1D+R	Presence of known 56Hz peak	-
2D+R	Similar content, all harmonics empathized in all domain	
DC+R	Low components emphatized in particular at 105/126Hz	Sided band highly emphatized
DD+R	Absence of f=100Hz and lower overall peaks	
BR	Heterogeneous spectra, no specific pattern	-
O	0.6Hz and 11.2Hz peaks in lower band and 189.5 highest	Heterogeneous spectra, no specific pattern

As we can see, FFT and Envelope spectrum gives information of impulsiveness of the signal considering its vibration. For each case, some frequencies identify a precise case: for example, 1D case is always recognized by the presence of a peak ampliture corresponding to f=56Hz. In other conditions, e.g. BR and O, there is not a clear pattern able to identify them, but their spectrum gives however the idea that something wrong is happening to the system. Moreover, the consumption of the holder does not stress a particular frequency, but contribute to rise up or lower the peak amplitude all over the domain. Another direct consequence relies on the liquid that has been pumped: if soap is added to water, this leads to the production of bubbles that can be sucked and produce noisier vibration in the system.

5.2 Results: HHT

The EMD method decomposes the signal into several intrinsic mode functions (IMFs) as 5.55 illustrates. Each IMF includes different frequency bands that range from the component of the shortest period to longer period, from the first IMF at higher frequency to latter with lower frequency. Each component differs according to the input signal. Only five out of nine, or ten according to the EMD process, have been analyzed focusing the attention on the first and the third one, which represent respectively the highest frequency band available up to 200Hz and a smaller band (in fig.5.56). Health indicators are monitored from the normal state of the pump.

In sections 5.1.2.1.1, in which normal working condition of the pump are considered, a f=21Hz stands to be a good candidate as a health indicator for the device. In the following results, this value is set as a reference to compare its importance between the cases. The Hilbert spectrum offers

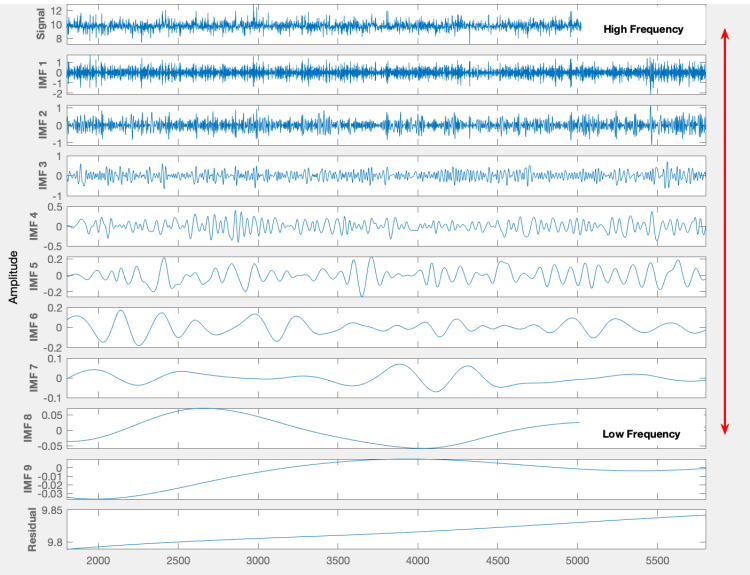

Figure 5.55: Example of EMD decomposition

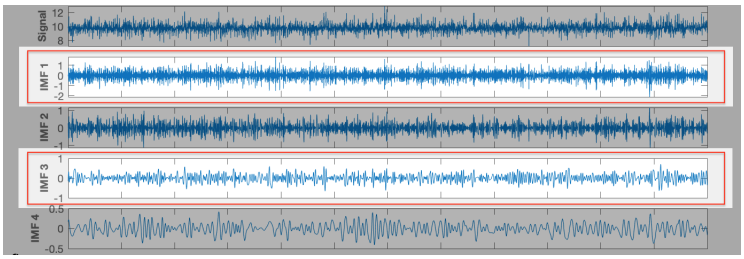

Figure 5.56: IMFs selection

a measure of amplitude contribution from each frequency and time, while the marginal spectrum offers a measure of the total amplitude (or energy) contribution from each frequency.

Dealing with bearings, characteristic frequencies are well-known and they can be easily calculated because they depend on physical parameters (dimensions) and on shaft rotation, thus the choice of the IMFs is quite immediate, relying on the frequency band in which the frequencies are expected to be located in.

In this case, since theoretical features are not provided, I choose to focus the MHS calculation on the 1st and 3rd intrinsic mode functions because they see

Table 5.6: MHS @21Hz, First Analysis on water only

FIRST ANALYSIS

MHS @21Hz	H	1D	2D	DD	H+R	1D+R	2D+R	DD+R	BR
#1	1.70	3.20	2.26	4.25	4.08	5.39	2.74	2.16	18.74
#3	14.91	23.30	34.76	66.27	39.20	57.06	21.77	39.95	190.27

different frequency frameworks: the first one covers all the domain available (representation is up to $\frac{fc}{2}$), the latter has narrower band in which f=21Hz falls, reference found in previous analysis. So, differently from FFT and Envelope Spectrum, results are proposed in backwards, presenting prior the Marginal Hilbert Spectrum (I remember that it is purely a number which gives an idea of the energy acquired by the signal in time @ certain f), then figures showing Hilbert Spectrum. From figures it is easy to discriminate at sight the different faulty conditions over time thanks to the energy intensity given by mesh colourmap: after MHS discussion, the frequency at which there is the maximum instantaneous energy is tagged in next figures.

From table 5.6 the contribution given by 21Hz differs between #1 and #3 IMFS: as expected, the instantaneous energy grows from H case to damaged cases, meaning higher probability to find such frequency in those bands depicted by IMFs if a injury occurs. However, +R case seems to lower the magnitude with respect to their corresponding cases without consumer of roller. Blocked roller highlights its presence in both IMFs (highest values)

From the instantaneous energy amplitude of each case we can find the frequency: tables 5.7 show marginal spectrum calculated for those frequencies at which there is the maximum energy amplitude. There is the same increasing trend as before if IMF1 is concerned, whereas dealing with IMF3 only few faulty cases respect what said. According to the choice of an intrinsic mode function, the system responds stressing distinct frequencies whose

Table 5.7: MHS @ f(IEmax), First Analysis on water only

FIRST ANALYSIS

MHS IMF 1	H	1D	2D	DD	H+R	1D+R	2D+R	DD+R	BR
IEmax	1.17	1.93	5.35	8,04	9.66	4.95	5.06	7.38	46.09
***f* (IEmax)**	72	114	106	59	103	82	100	96	111
MHS @*f*	6.33	13.48	35.27	35.93	30.68	34.44	32.10	71.62	192.94
MHS IMF 3									
IEmax	0.40	0.22	0.45	0.835	0.82	0.50	0.37	0.85	4.85
***f*(IEmax)**	10	13	23	15	12	15	13	11	16
MHS @ *f*	37.19	26.40	26.40	68.88	2.54	40.38	21.15	48.25	36.33

contribution determines its influence.

Switching to *SecondAnalysis*, the choice of diluting water with soap was motivated by discovering if the system would behave depending on the type of fluid processed. Adding soap to water, of course, bubbles form and may change the results. Water and Water + liquid soap (W and WwLS from here on) are compared in the next tables.

In fact, from tables 5.8 and 5.9 the impact of the two fluids in the different time frames differs. Starting from f=21Hz, in IMF #1, depending on the time over which data are collected, healthy state of the pump presents lower contribution with respect to each damaged case if water is concerned. Sucking soaps, it seem that the pump 21Hz is highly emphatized in H case only, whereas in the damaged cases, the same frequency is less involved. The other way around IMF #3 behaves: the second fluid highlights this frequency with respect to water, but in some cases eg 2D the intensity is lower with respect to healthy condition. Looking at the energy we could understand, based on reference values on normal state, whether the pump

Table 5.8: MHS 1 @21Hz, Comparison between W and WwLS

SECOND ANALYSIS

MHS 1 @21Hz	**H**	**DC**	**2D**	**DD**	**H+R**	**DC+R**	**2D+R**	**DD+R**	**O**
W 15	0.77	2.09	0.97	1.17	1.82	1.79	1.57	0.34	0.73
WwLS 15	1.66	1.74	2.32	0.33	2.27	1.38	2.29	0.36	1.26
W 30	2.68	6.88	2.51	3.58	2.45	4.37	1.65	0.98	22.93
WwLS 30	7.86	1.30	2.73	2.91	2.27	3.88	3.50	1.12	1.33
W 45	3.62	8.06	5.45	5.77	3.05	5.38	3.49	3.47	38.56
WwLS 45	8.95	2.39	3.68	4.19	4.88	8.24	5.22	2.59	3.08

is working properly or not.

Cases in 5.10 are not comparable since 1D case processing soap there is not (switched to DC instead).

Again, the maximum energy of the signal identifies the most stressed frequency, in 15s,30s and 45s recordings, enabling to read the data. Tables 5.11, 5.12, 5.13 for IMF #1, tables 5.14, 5.15, 5.16 for IMF #3.

From these last tables, the first consideration concerns the instantaneous energy: whit the increasing of the time duration of each test, this parameter increases for the corresponding case. However, the frequency changes, but within a narrowed band. Among the cases it is not always possible notice, as for f=21Hz, the increasing trend between the healthy condition and the faulty ones. This time-related information, together with Hilbert Spectrum, provides the identification of localized features.

Table 5.9: MHS 3 @21Hz, Comparison between W and WwLS

SECOND ANALYSIS

MHS 3 @21Hz	**H**	**DC**	**2D**	**DD**	**H+R**	**DC+R**	**2D+R**	**DD+R**	**O**
W 15	12.08	26.10	23.73	29.86	23.38	24.38	24.17	22.31	64.52
WwLS 15	32.93	37.75	29.24	21.39	24.51	33.34	23.99	21.19	28.78
W 30	22.21	52.94	53.35	47.05	45.72	42.95	48.40	42.15	145.20
WwLS 30	66.13	56.37	46.99	42.19	50.87	61.61	46.44	41.65	54.77
W 45	37.89	75.88	73.33	71.27	65.68	69.09	71.93	62.34	214.84
WwLS 45	88.14	94.32	72.58	65.78	71.45	81.85	75.73	58.45	85.05

Table 5.10: MHS @21Hz Non comparable cases

SECOND ANALYSIS: WATER ONLY

MHS 1 @21Hz	**t 15**	**t 30**	**t 45**
1D	1.82	3.21	4.89
1D+R	2.73	5.39	5.80
BR	0.79	4.26	4.25

MHS 3 @21Hz	t 15	t 30	t 45
1D	10.08	29.60	21.37
1D+R	23.30	57.06	39.83
BR	76.22	85.11	64.04

Table 5.11: MHS of IMF 1 @ f(IEmax), Second Analysis, comparison W vs WwLS 15sec

SECOND ANALYSIS - MHS of IMF1 - W vs WwLS

WATER 15s	H	DC	2D	DD	H+R	DC+R	2D+R	DD+R	O
IEmax	2.87	7.07	6.74	5.42	5.44	7.05	5.56	7.57	98.86
***f* (IEmax)**	105	80	117	107	64	120	106	111	77
MHS @*f*	10.67	19.91	30.14	28.46	11.49	29.7	18.98	54.37	242.42

WwLS 15s	H	DC	2D	DD	H+R	DC+R	2D+R	DD+R	O
IEmax	6.66	10.20	7.35	8.02	6.75	5.28	6.22	5.21	7.50
***f*(IEmax)**	92	136	91	120	133	83	111	101	98
MHS @ *f*	37.81	34.98	20.61	15.35	22.21	17.31	22.69	22.92	27.52

Table 5.12: MHS of IMF 1 @ f(IEmax), Second Analysis, comparison W vs WwLS 30 sec

SECOND ANALYSIS - MHS of IMF1 - W vs WwLS

WATER 30s	H	DC	2D	DD	H+R	DC+R	2D+R	DD+R	O
IEmax	3.52	7.04	7.02	8.42	5.81	9.66	6.10	7.57	160.10
***f* (IEmax)**	116	80	104	118	138	105	83	111	58
MHS @*f*	31.81	47.30	39.52	57.04	45.12	48.39	18.57	54.37	222.86

WwLS 30s	H	DC	2D	DD	H+R	DC+R	2D+R	DD+R	O
IEmax	8.35	7.85	7.25	6.61	11.83	4.88	6.21	5.8	7.27
***f*(IEmax)**	118	98	96	96	100	106	110	116	83
MHS @ *f*	59.18	43.08	42.95	21.87	44.12	45.58	35.56	47.47	31.38

Table 5.13: MHS of IMF 1 @ f(IEmax), Second Analysis, comparison W vs WwLS 45 sec

SECOND ANALYSIS - MHS of IMF1 - W vs WwLS

WATER 45s	H	DC	2D	DD	H+R	DC+R	2D+R	DD+R	O
IEmax	3.61	7.04	7.03	8.41	7.87	8.15	7.82	7.57	86.17
***f* (IEmax)**	128	80	104	118	99	91	139	111	72
MHS @*f*	71.95	47.30	59.06	73.05	49.49	57.27	80.73	71.59	159.39

WwLS 45s	H	DC	2D	DD	H+R	DC+R	2D+R	DD+R	O
IEmax	12.86	11.59	7.19	7.26	11.82	7.03	17.45	10.71	7.40
***f*(IEmax)**	97	109	88	109	100	127	116	101	118
MHS @ *f*	106.46	117.14	46.82	53.18	72.69	63.62	56.09	67.96	59.27

Table 5.14: MHS of IMF 3 @ f(IEmax), Second Analysis, comparison W vs WwLS 15sec

SECOND ANALYSIS - MHS of IMF3 - W vs WwLS

WATER 15s	H	DC	2D	DD	H+R	DC+R	2D+R	DD+R	O
IEmax	0.30	0.57	0.58	0.86	0.75	0.37	0.51	0.59	8.44
***f* (IEmax)**	22	20	11	17	13	16	9	12	13
MHS @*f*	11.49	28.32	9.50	31.09	18.90	24.04	7.04	23.74	103.14

WwLS 15s	H	DC	2D	DD	H+R	DC+R	2D+R	DD+R	O
IEmax	1.18	0.68	0.44	0.63	0.53	0.89	0.62	0.84	0.65
***f*(IEmax)**	19	12	21	11	13	16	13	13	18
MHS @ *f*	44.68	15.47	29.24	17.28	25.56	34.36	20.49	29.75	31.30

Table 5.15: MHS of IMF 3 @ f(IEmax), Second Analysis, comparison W vs WwLS 30 sec

SECOND ANALYSIS - MHS of IMF3 - W vs WwLS

WATER 30s	H	DC	2D	DD	H+R	DC+R	2D+R	DD+R	O
IEmax	0.28	0.59	0.58	0.58	0.54	0.73	0.53	0.76	4.45
***f* (IEmax)**	22	13	11	21	30	24	17	11	18
MHS @*f*	22.91	47.10	22.61	47.05	8.78	32.03	41.79	37.13	184.41

WwLS 30s	H	DC	2D	DD	H+R	DC+R	2D+R	DD+R	O
IEmax	0.60	0.82	0.62	0.71	0.74	0.90	0.76	0.92	0.59
***f*(IEmax)**	20	19	17	16	13	15	8	15	13
MHS @ *f*	70.09	58.03	55.41	52.10	50.41	53.86	28.61	39.95	43.09

Table 5.16: MHS of IMF 3 @ f(IEmax), Second Analysis, comparison W vs WwLS 45 sec

SECOND ANALYSIS - MHS of IMF3 - W vs WwLS

WATER 45s	H	DC	2D	DD	H+R	DC+R	2D+R	DD+R	O
IEmax	0.74	0.61	0.59	0.80	0.75	0.63	0.532	0.76	0.96
***f* (IEmax)**	16	13	11	15	16	20	17	11	14
MHS @*f*	76.85	65.06	29.65	67.78	76.86	74.27	70.00	54.54	179.21

WwLS 45s	H	DC	2D	DD	H+R	DC+R	2D+R	DD+R	O
IEmax	1.08	0.82	0.70	0.72	0.79	0.91	2.62	0.90	0.67
***f*(IEmax)**	16	18	13	16	16	13	24	18	17
MHS @ *f*	103.86	97.47	51.15	75.97	90.57	72.51	46.89	71.77	100

5.2.1 Hilbert Spectrum

Next figures show Hilbert Spectrum: the colour of the mesh determines in a three-dimensional plot the energy intensity over time. Every mesh can be seen as sequence of consecutive slice each of which plots the amplitude of $h(\omega)$ (3.14).

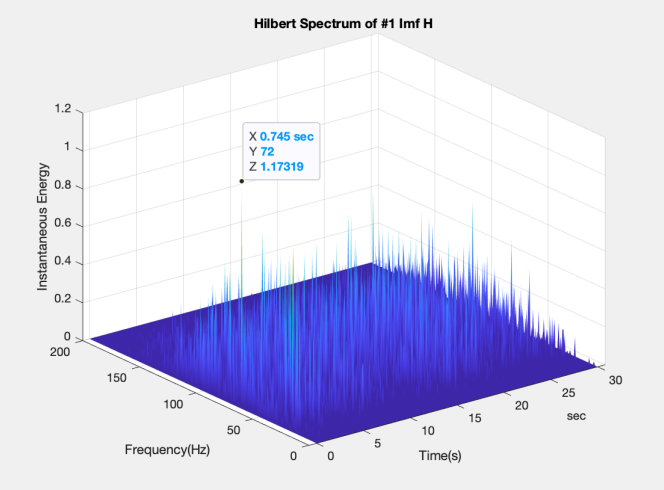

(a) H: HHS 1

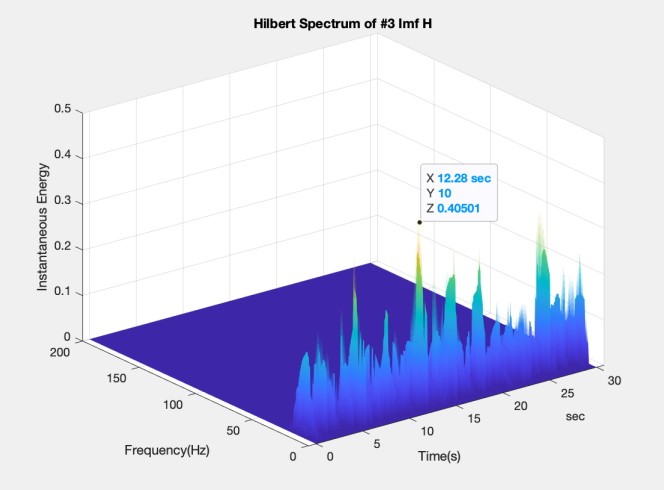

(b) H: HHS 3

Figure 5.57: H: HHS

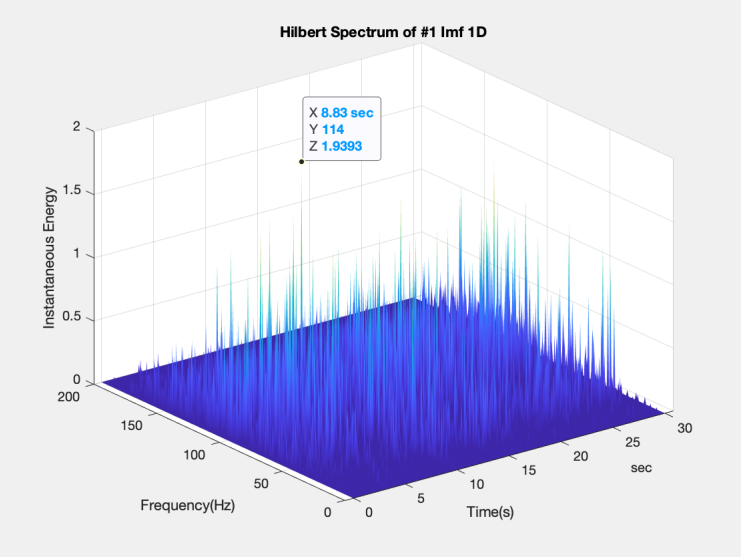

(a) 1D: HHS 1

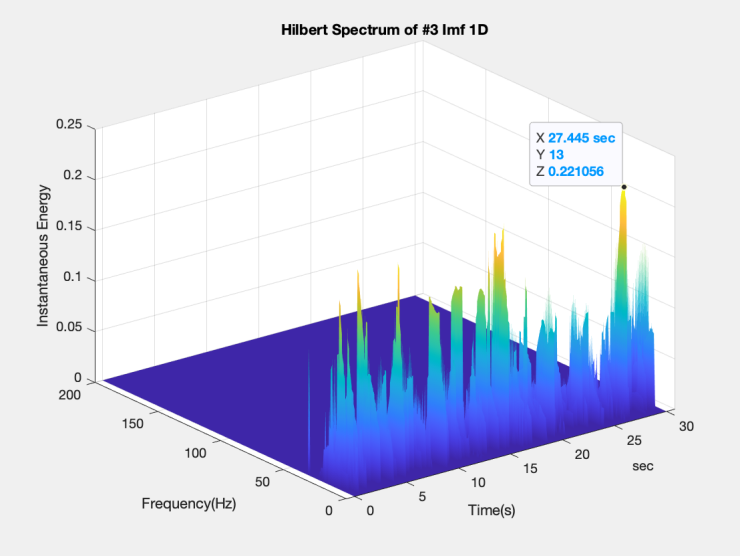

(b) 1D: HHS 3

Figure 5.58: 1D: HHS

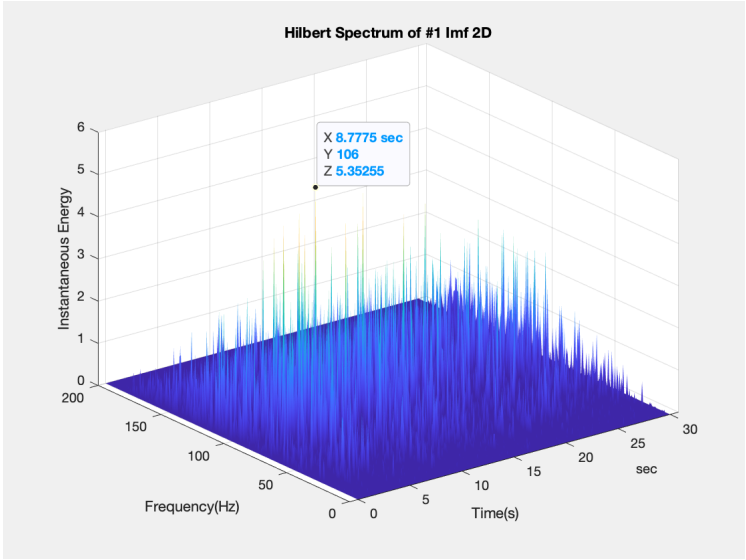

(a) 2D: HHS 1

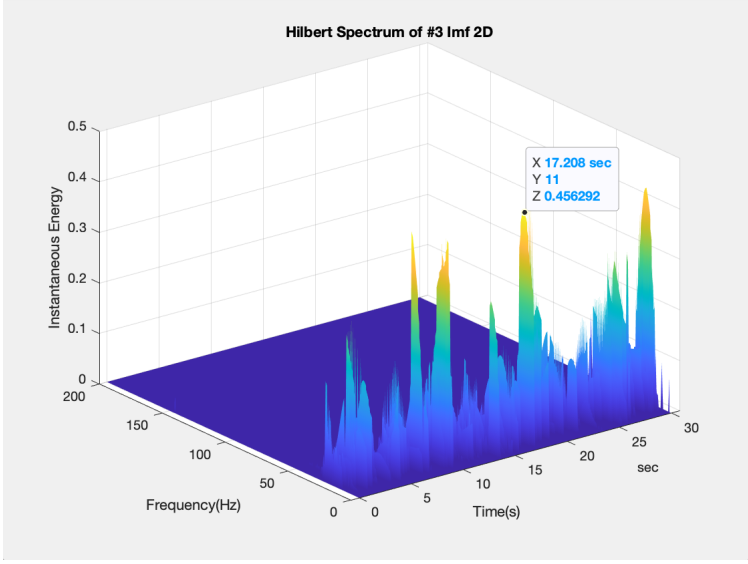

(b) 2D: HHS 3

Figure 5.59: 2D: HHS

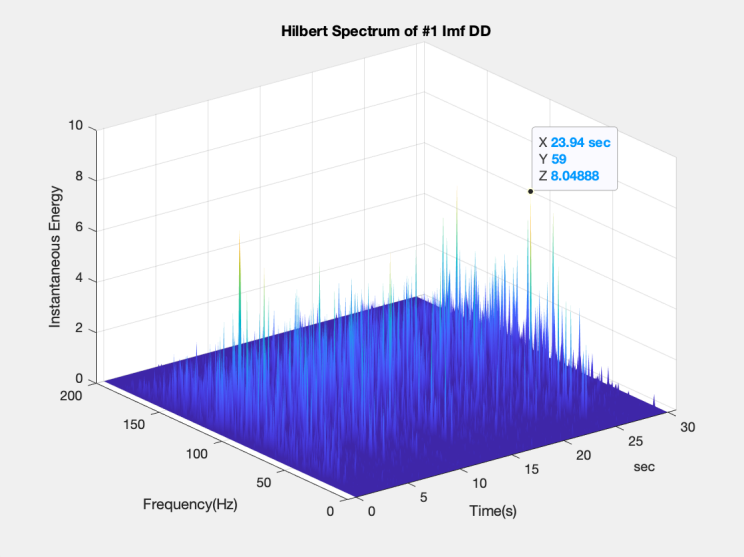

(a) DD: HHS 1

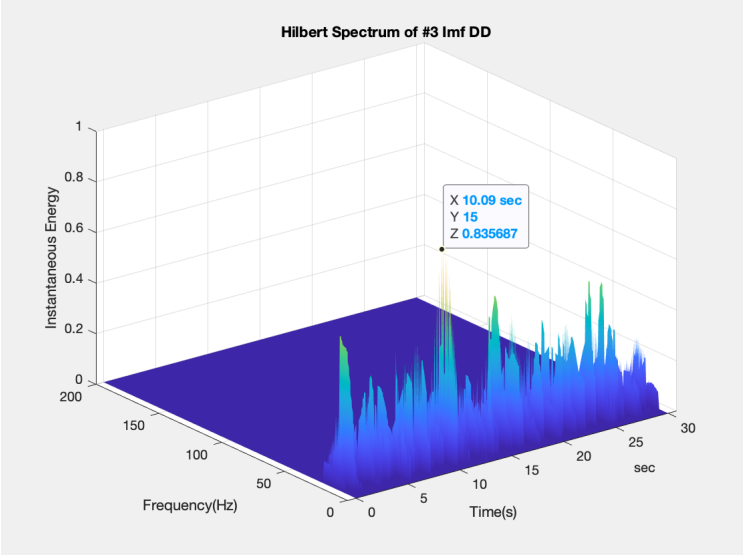

(b) DD: HHS 3

Figure 5.60: DD: HHS

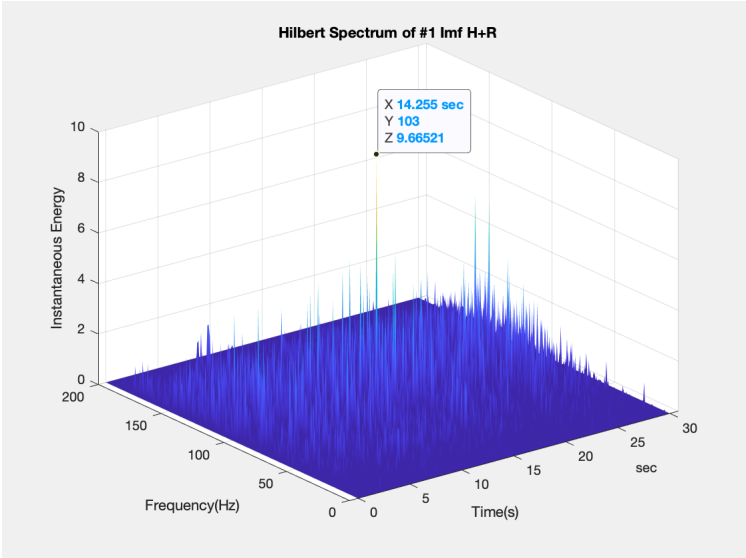

(a) H+R: HHS 1

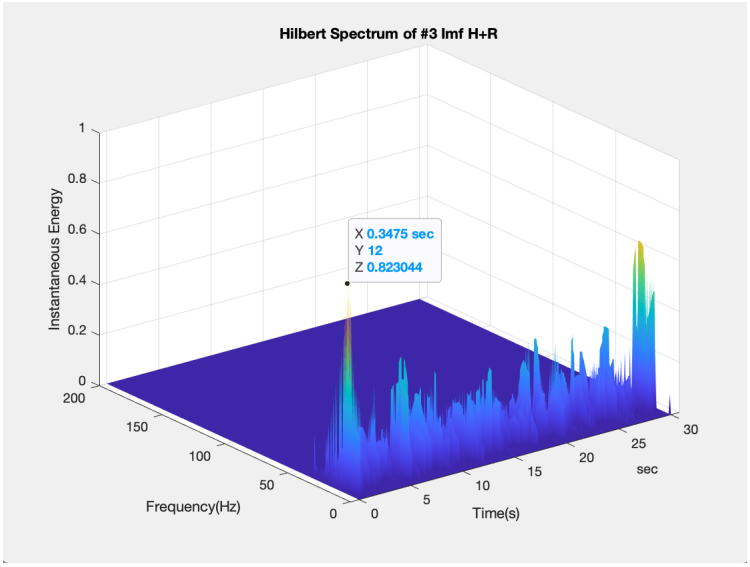

(b) H+R: HHS 3

Figure 5.61: H+R: HHS

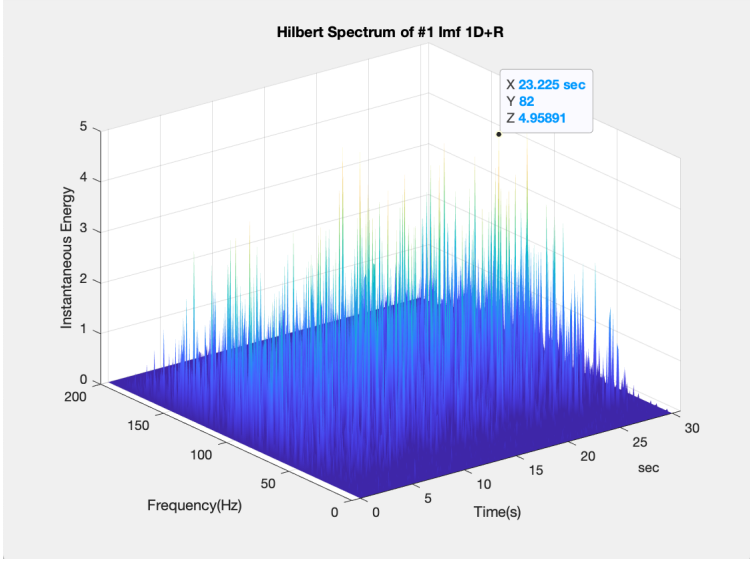

(a) 1D+R: HHS 1

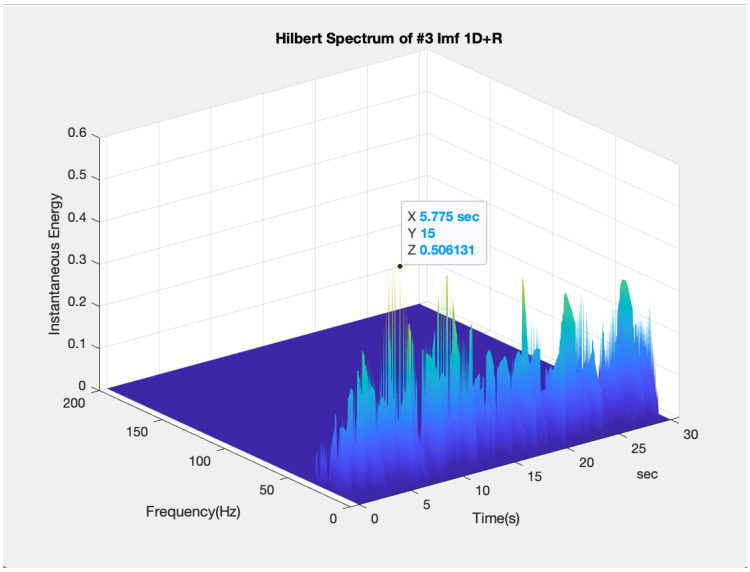

(b) 1D+R: HHS 3

Figure 5.62: 1D+R: HHS

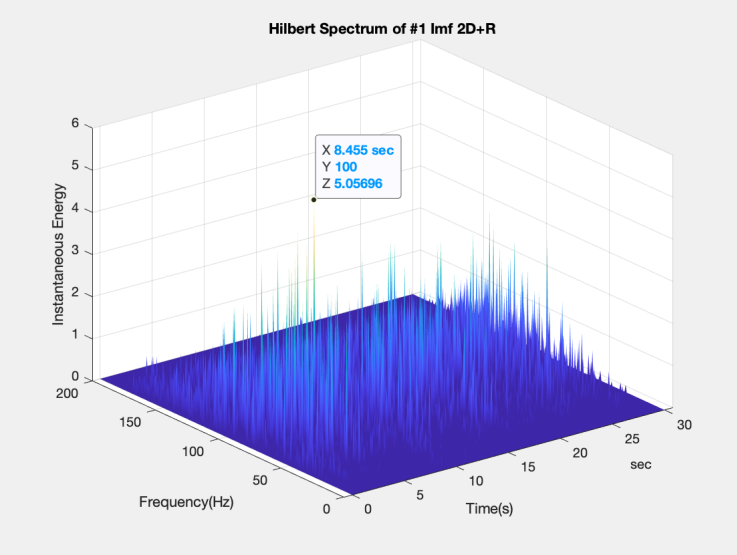

(a) 2D+R: HHS 1

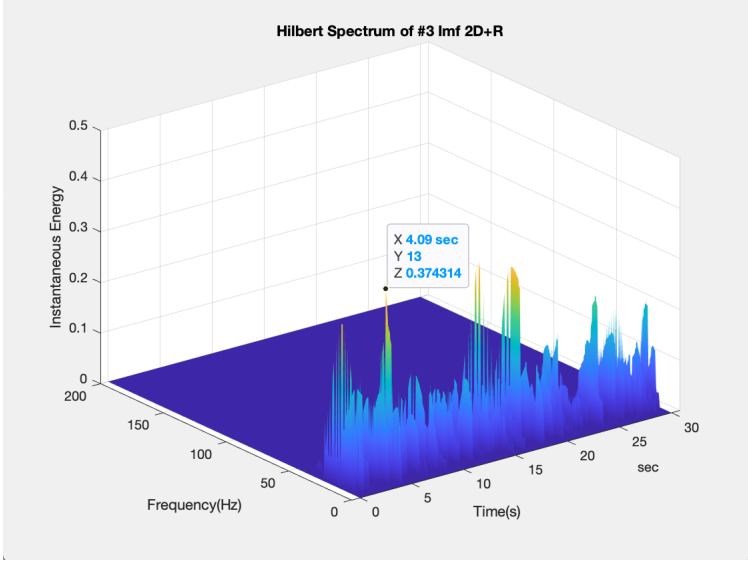

(b) 2D+R: HHS 3

Figure 5.63: 2D+R: HHS

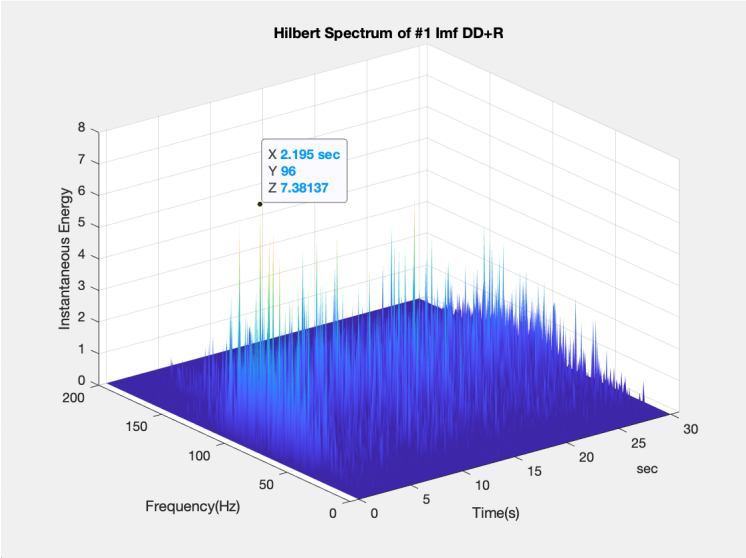

(a) DD+R: HHS 1

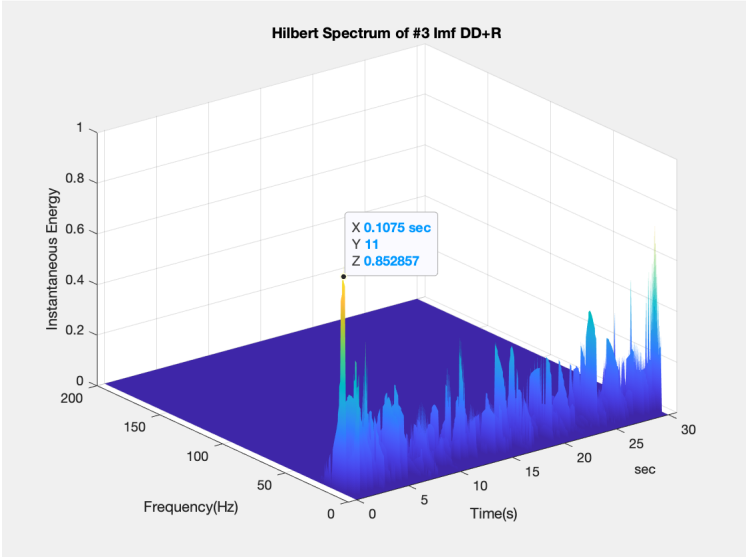

(b) DD+R: HHS 3

Figure 5.64: DD+R: HHS

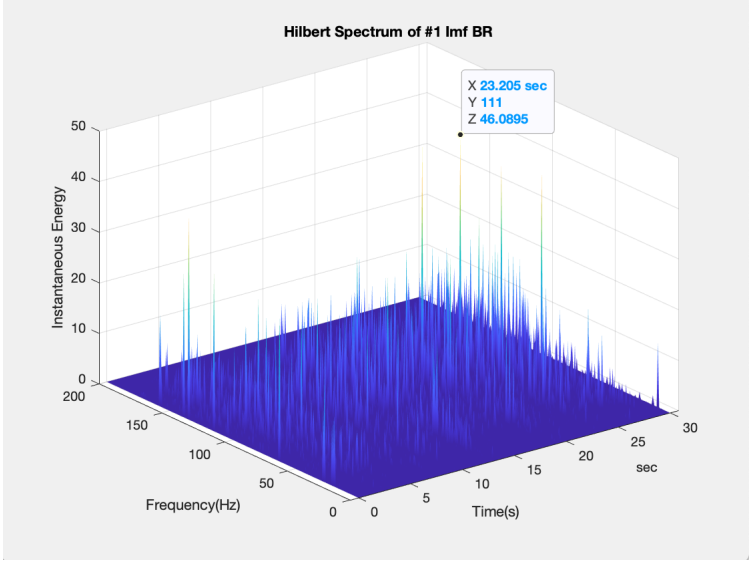

(a) BR: HHS 1

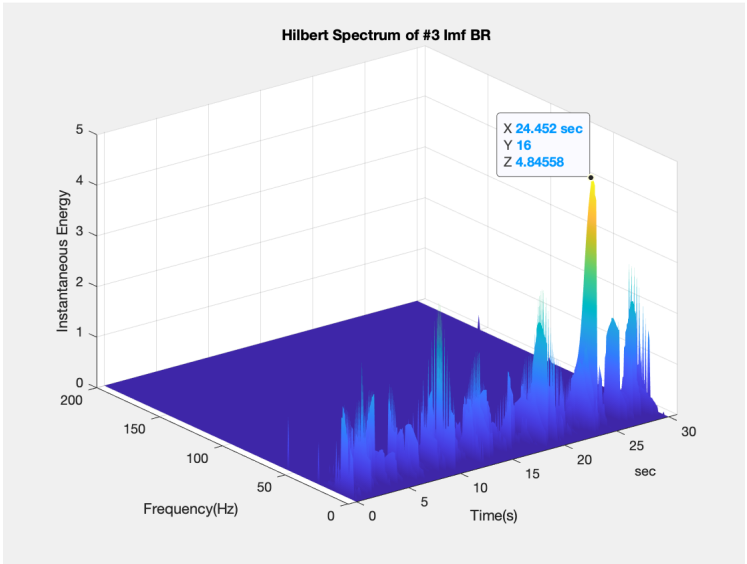

(b) BR: HHS 3

Figure 5.65: BR: HHS

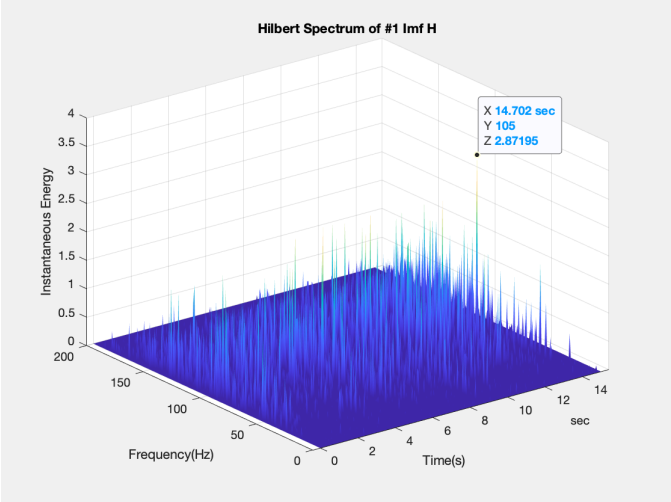

(a) H 15s: HHS 1

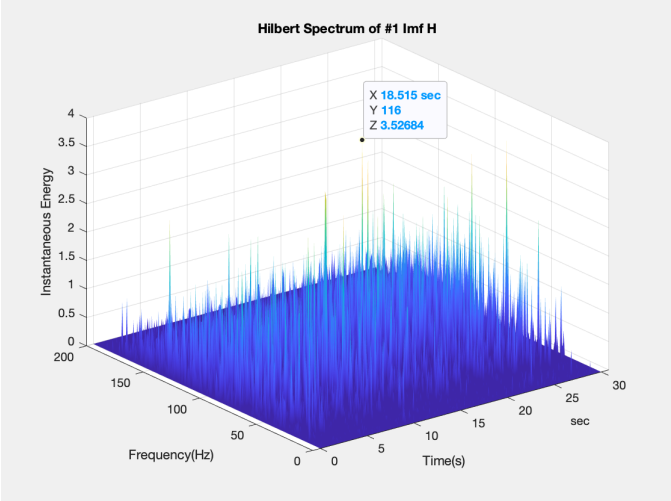

(b) H 30s: HHS 1

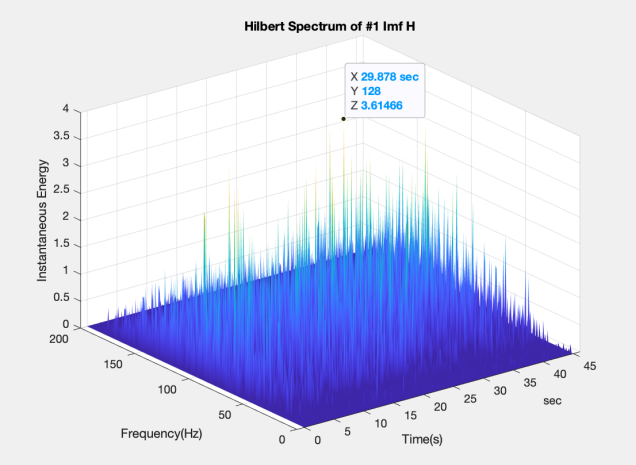

(c) H 45s: HHS 1

Figure 5.66: H: HHS 1

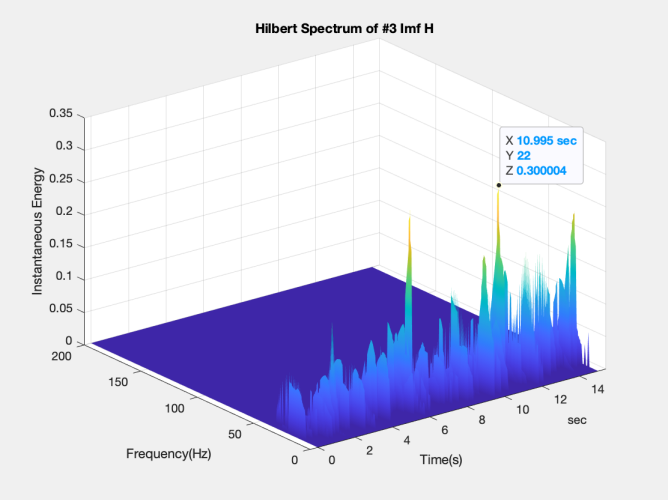

(a) H 15s: HHS 3

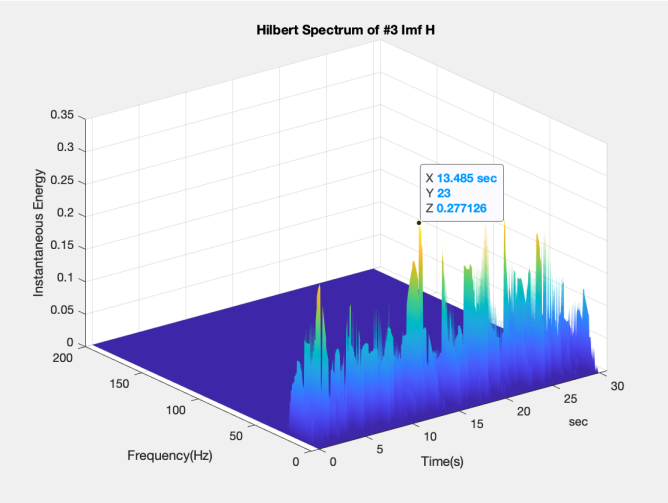

(b) H 30s: HHS 3

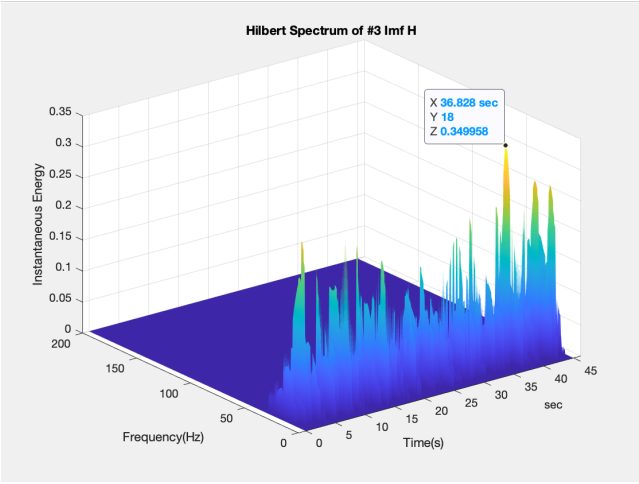

(c) H 45s: HHS 3

Figure 5.67: H: HHS 3

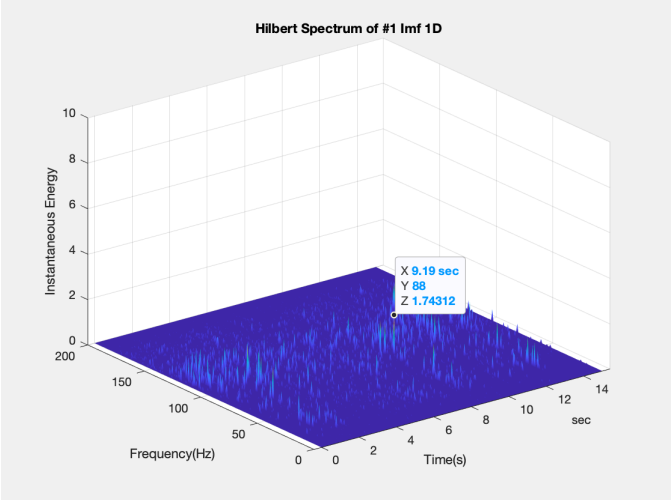

(a) 1D 15s: HHS 1

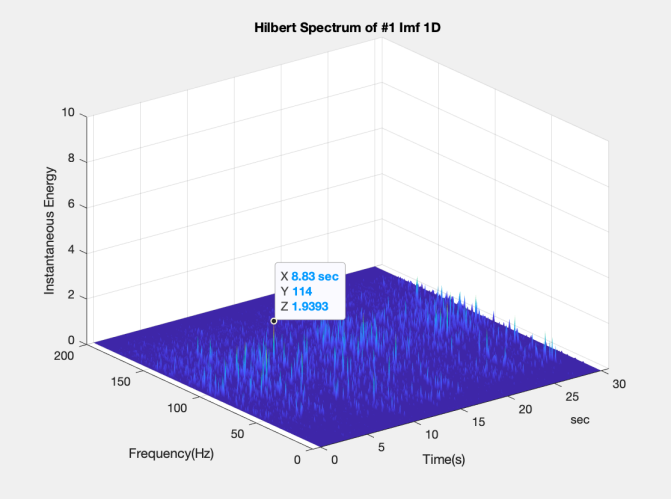

(b) 1D 30s: HHS 1

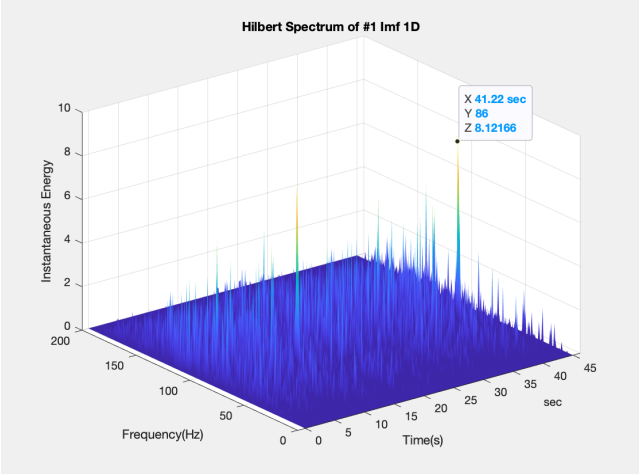

(c) 1D 45s: HHS 1

Figure 5.68: 1D: HHS 1

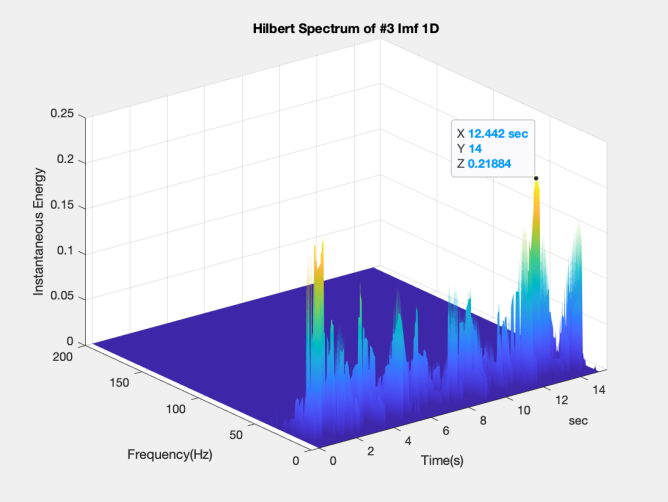

(a) 1D 15s: HHS 3

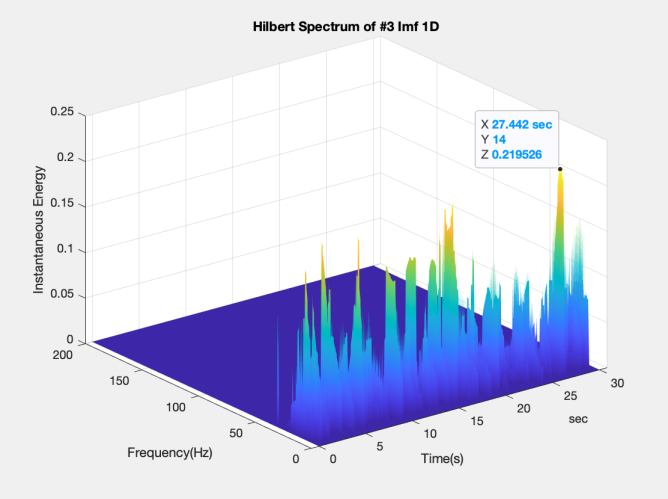

(b) 1D 30s: HHS 3

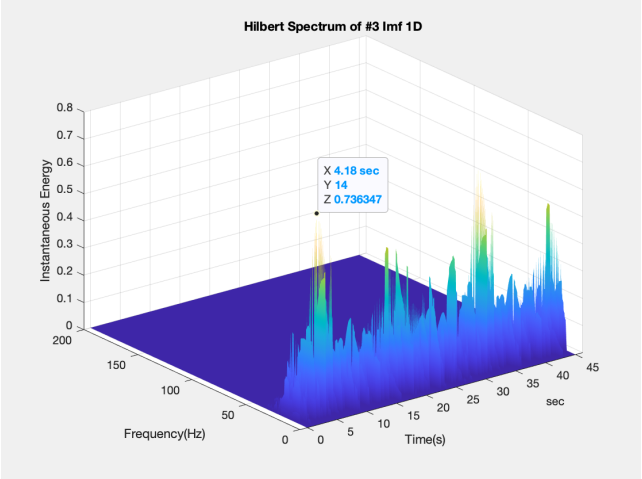

(c) 1D 45s: HHS 3

Figure 5.69: 1D: HHS 3

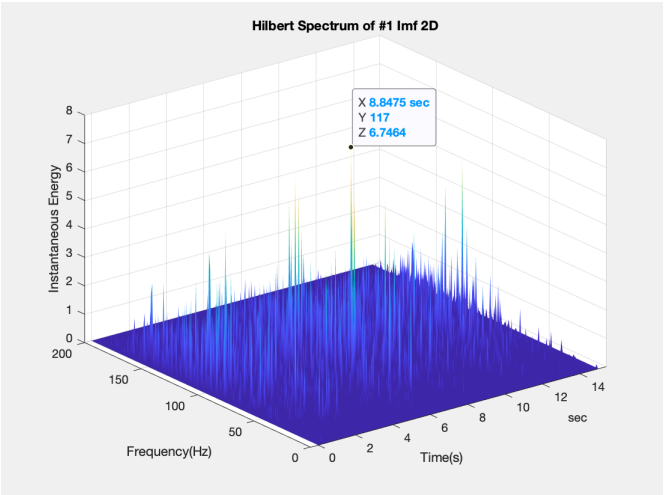

(a) 2D 15s: HHS 1

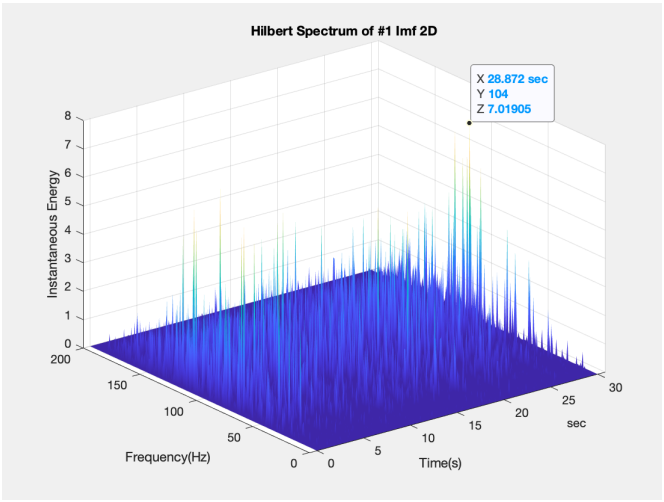

(b) 2D 30s: HHS 1

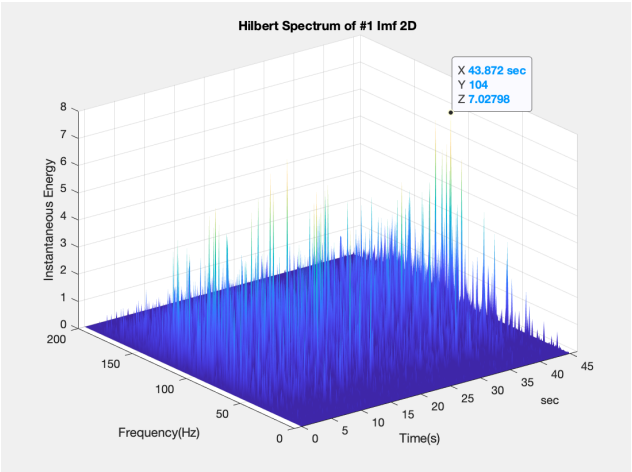

(c) 2D 45s: HHS 1

Figure 5.70: 2D: HHS 1

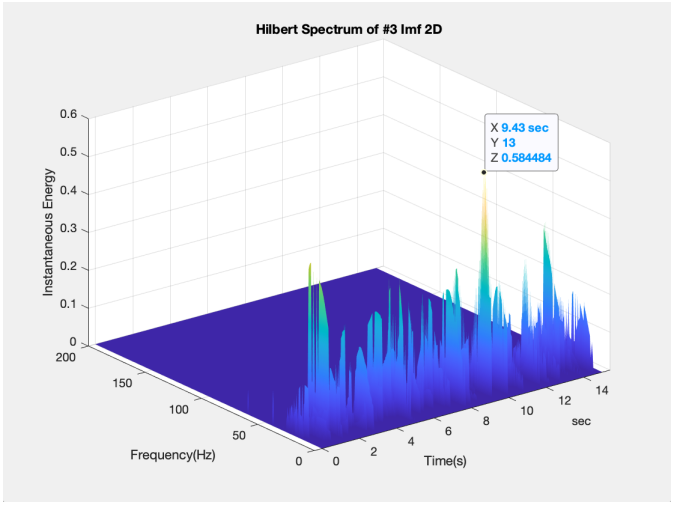

(a) 2D 15s: HHS 3

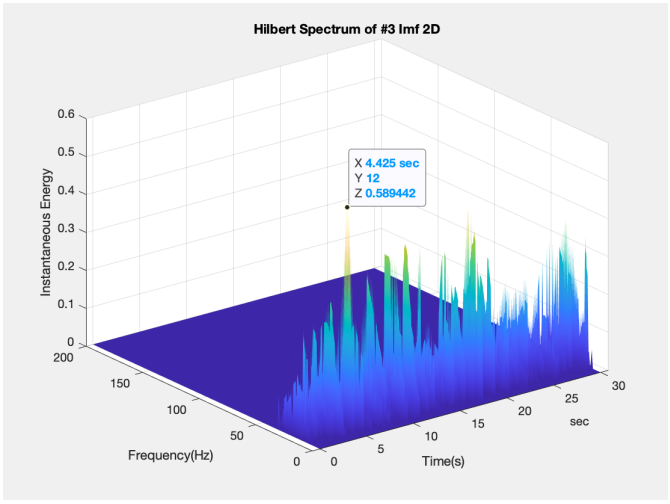

(b) 2D 30s: HHS 3

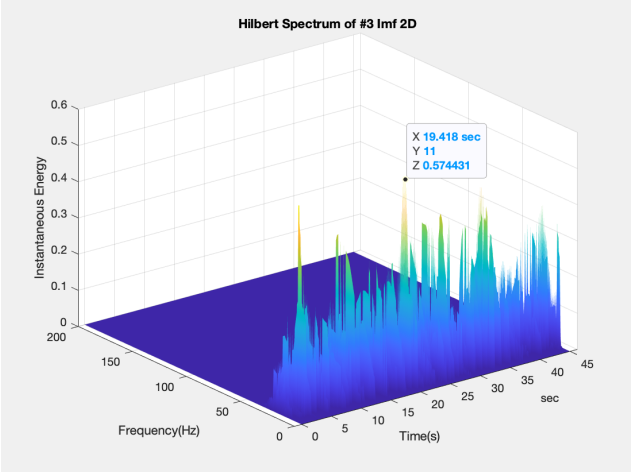

(c) 2D 45s: HHS 3

Figure 5.71: 2D: HHS 3

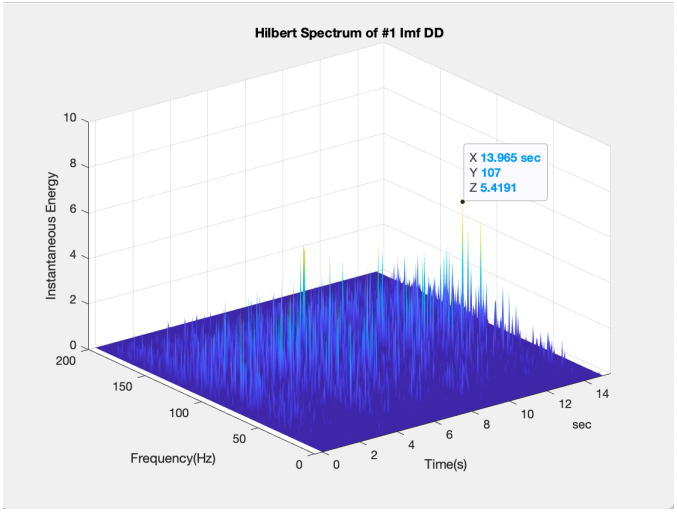

(a) DD 15s: HHS 1

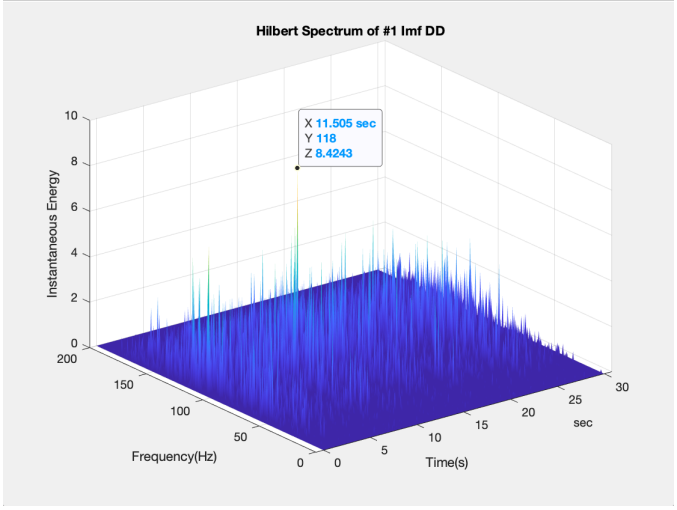

(b) DD 30s: HHS 1

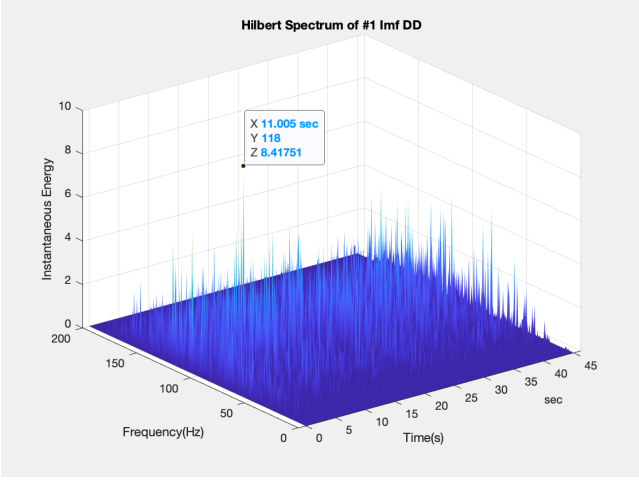

(c) DD 45s: HHS 1

Figure 5.72: DD: HHS 1

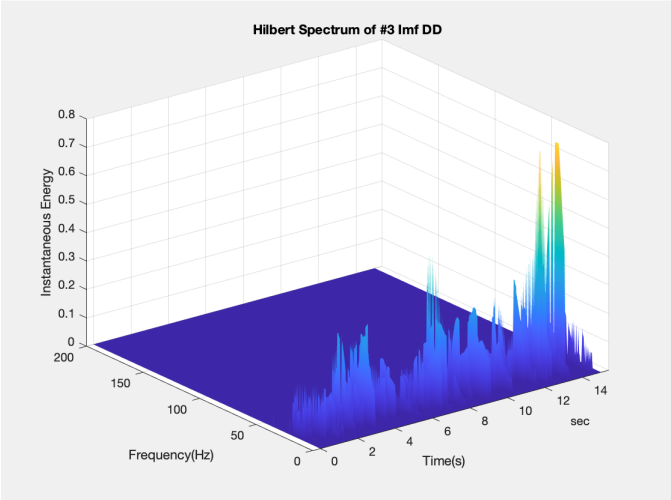

(a) DD 15s: HHS 3

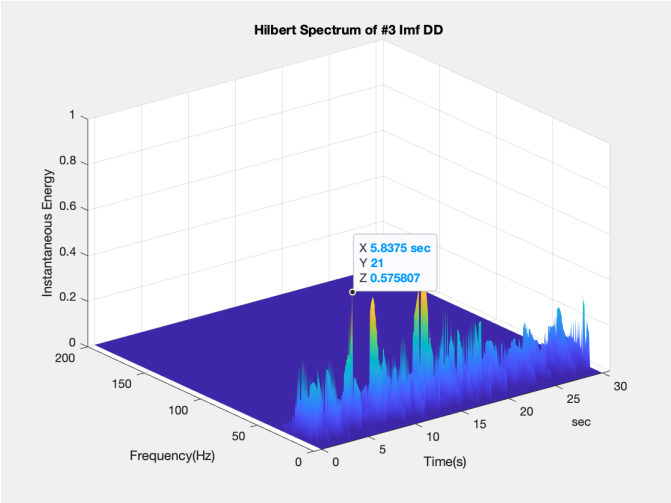

(b) DD 30s: HHS 3

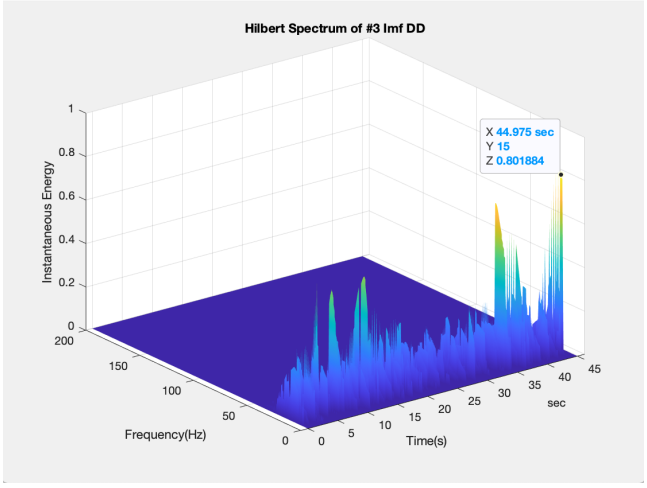

(c) DD 45s: HHS 3

Figure 5.73: DD: HHS 3

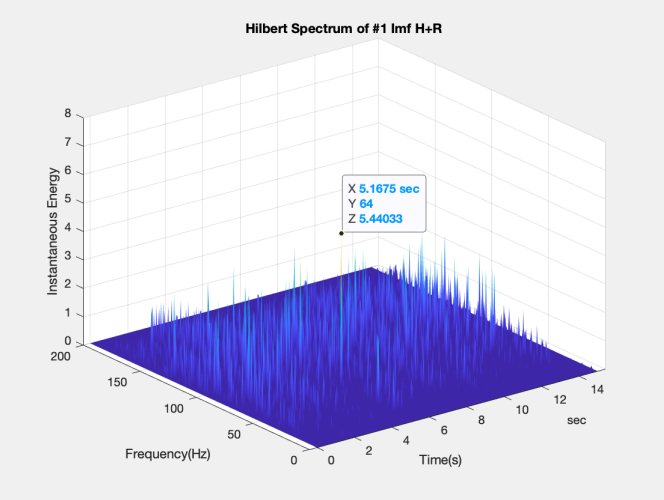

(a) H+R 15s: HHS 1

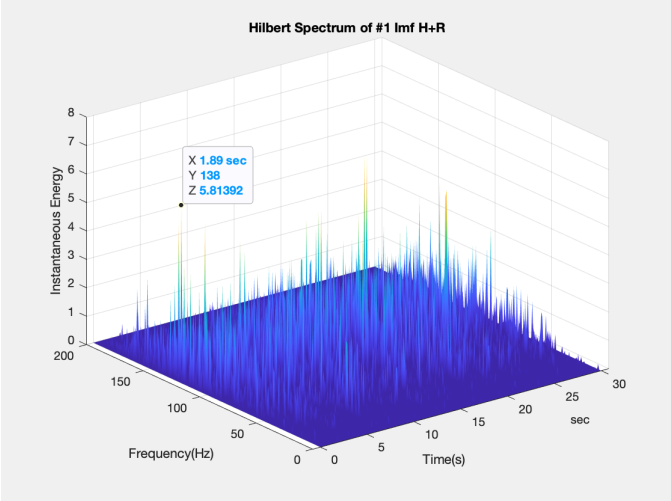

(b) H+R 30s: HHS 1

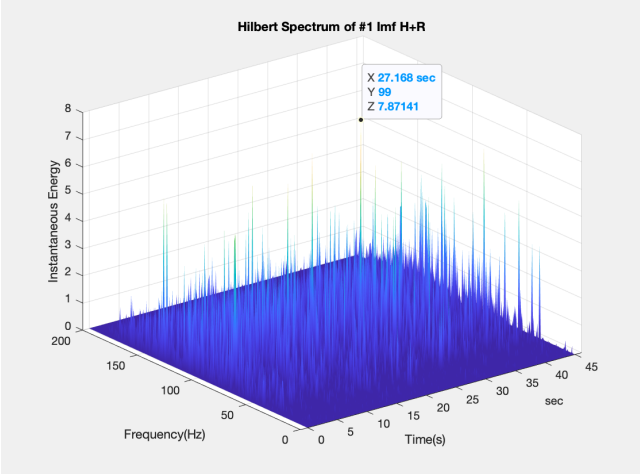

(c) H+R 45s: HHS 1

Figure 5.74: H+R: HHS 1

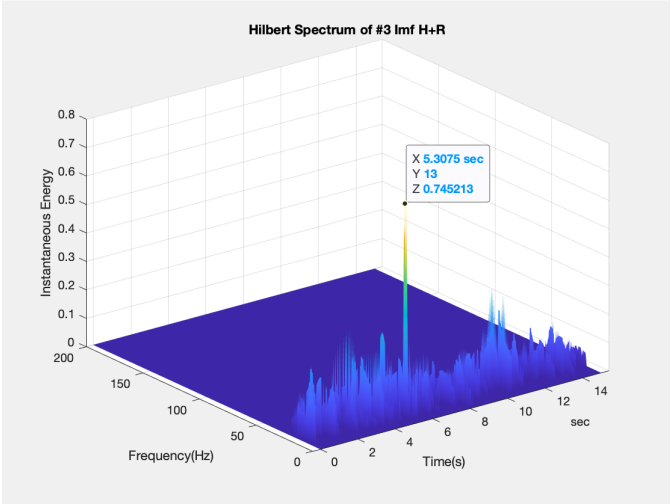

(a) H+R 15s: HHS 3

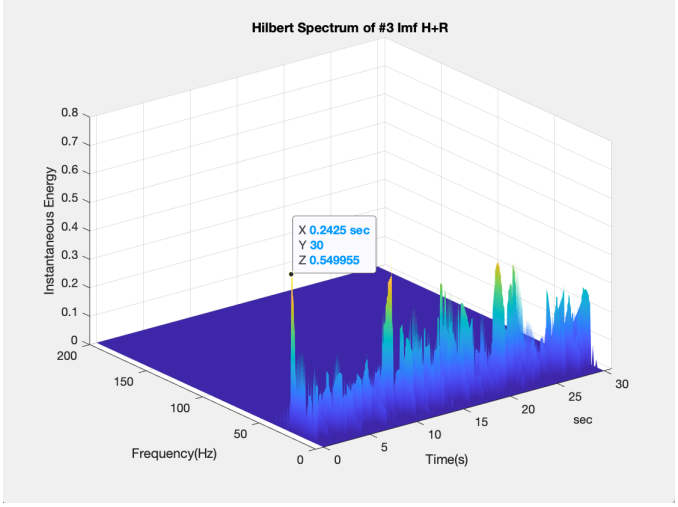

(b) H+R 30s: HHS 3

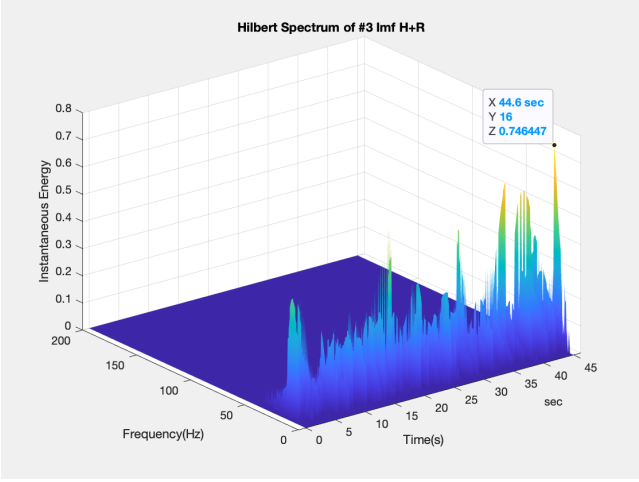

(c) H+R 45s: HHS 3

Figure 5.75: H+R: HHS 3

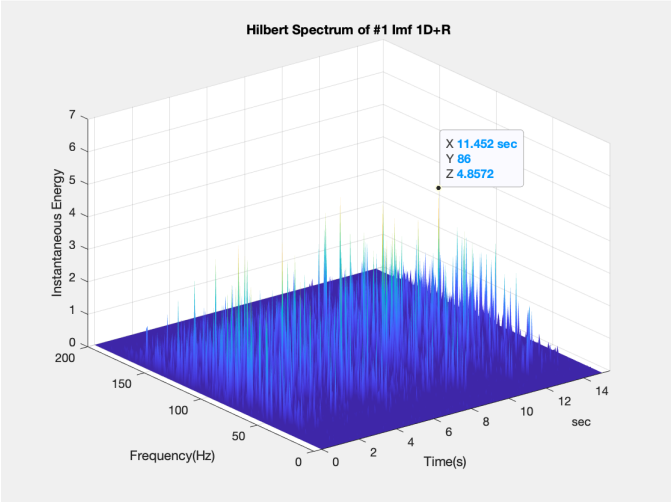

(a) 1D+R 15s: HHS 1

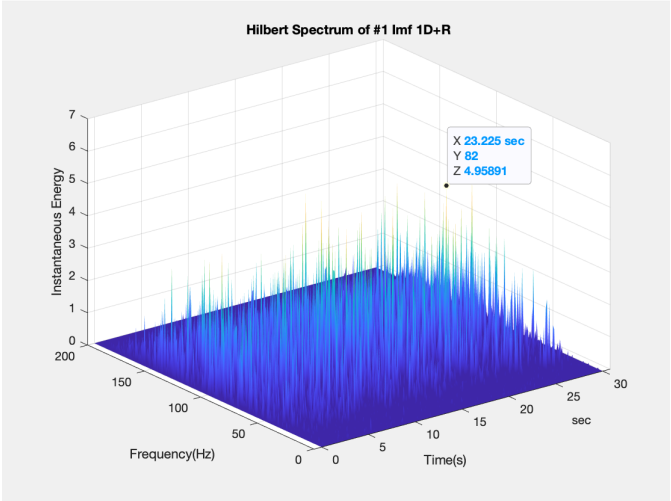

(b) 1D+R 30s: HHS 1

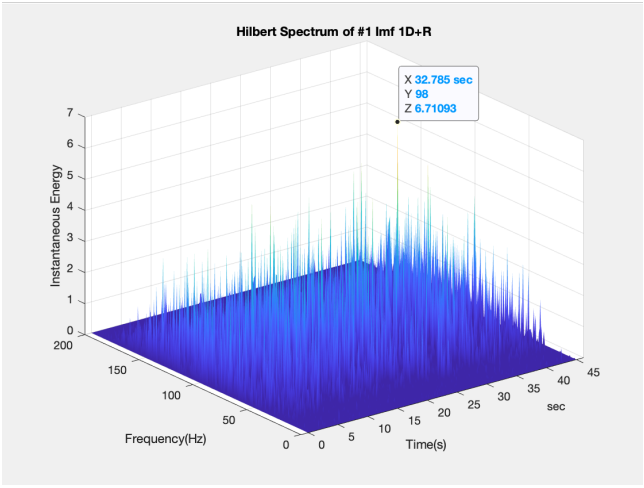

(c) 1D+R 45s: HHS 1

Figure 5.76: 1D+R: HHS 1

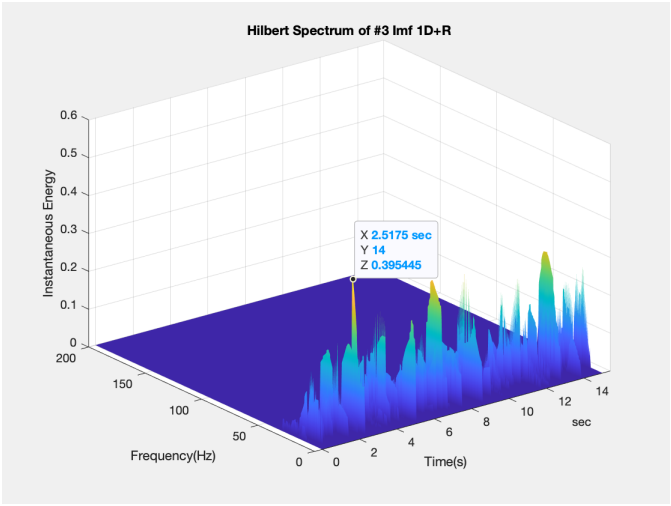

(a) 1D+R 15s: HHS 3

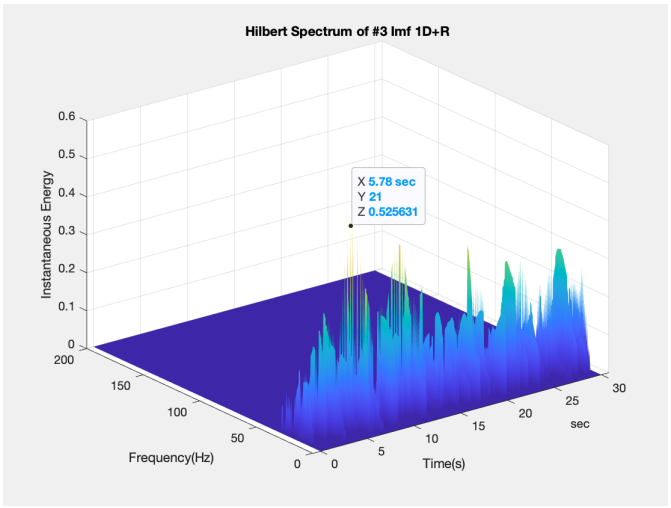

(b) 1D+R 30s: HHS 3

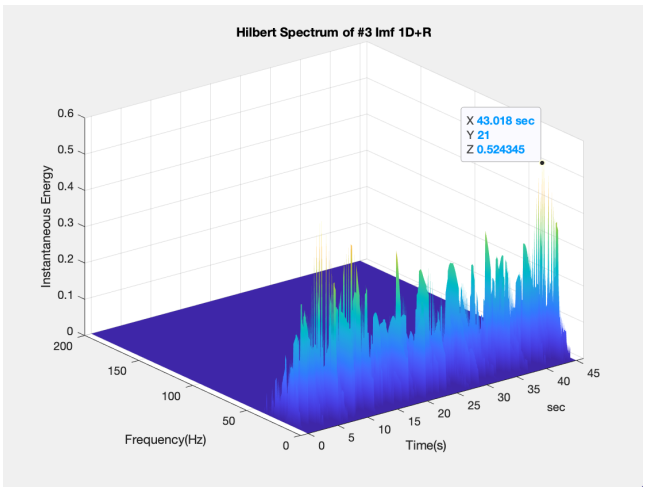

(c) 1D+R 45s: HHS 3

Figure 5.77: 1D+R: HHS 3

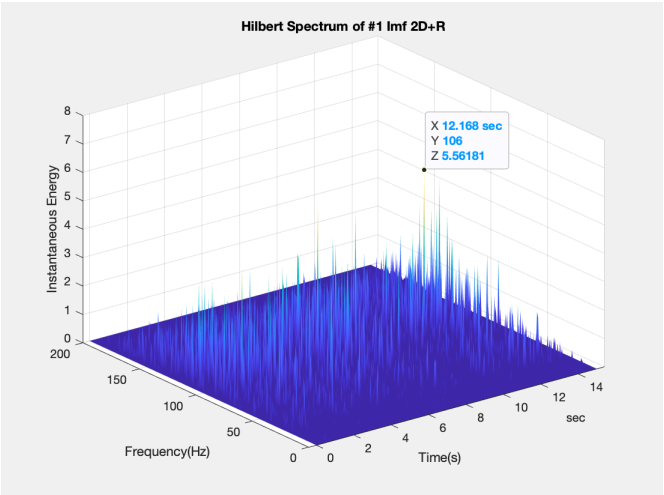

(a) 2D+R 15s: HHS 1

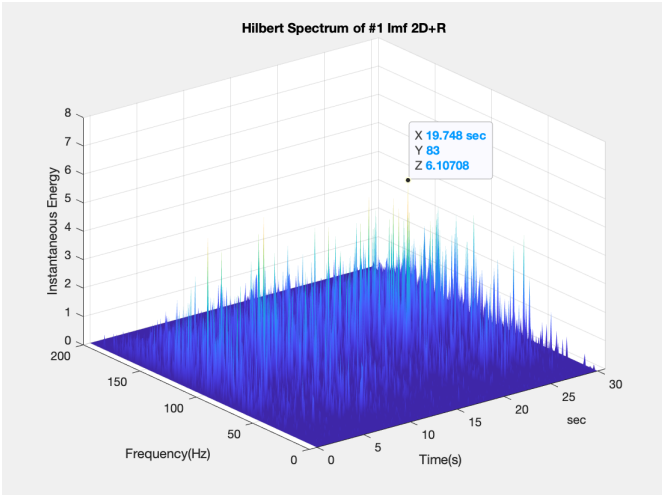

(b) 2D+R 30s: HHS 1

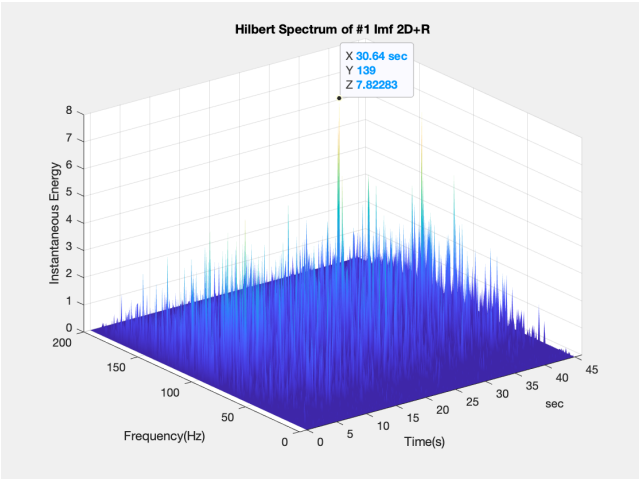

(c) 2D+R 45s: HHS 1

Figure 5.78: 2D+R: HHS 1

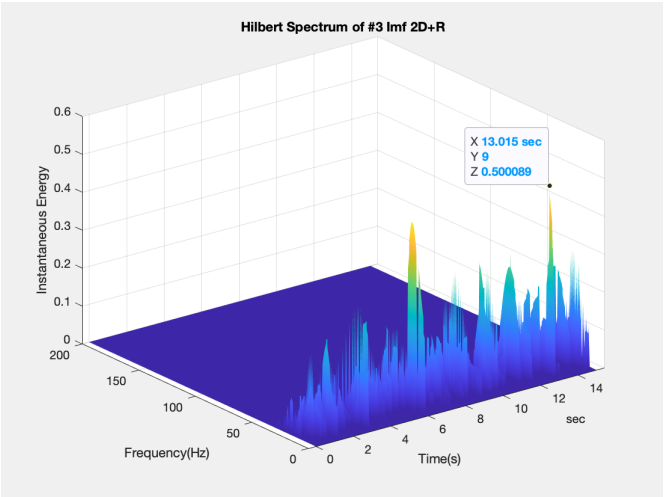

(a) 2D+R 15s: HHS 3

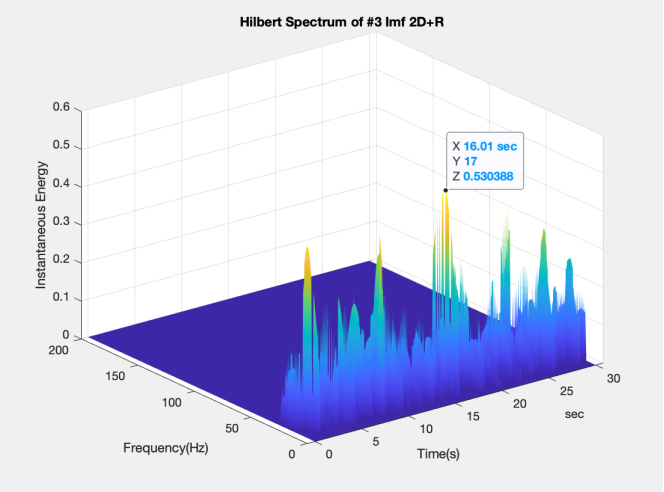

(b) 2D+R 30s: HHS 3

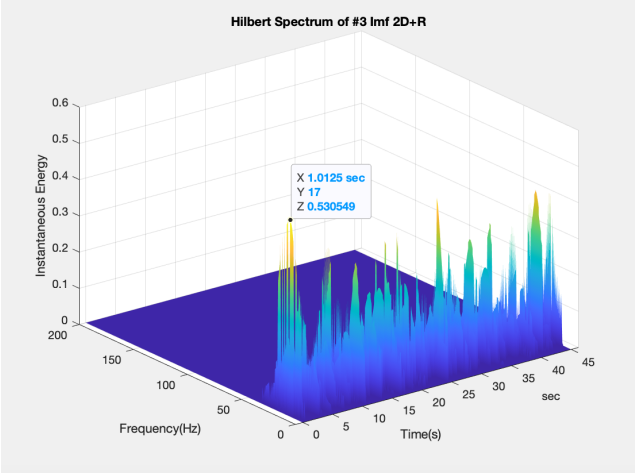

(c) 2D+R 45s: HHS 3

Figure 5.79: 2D+R: HHS 3

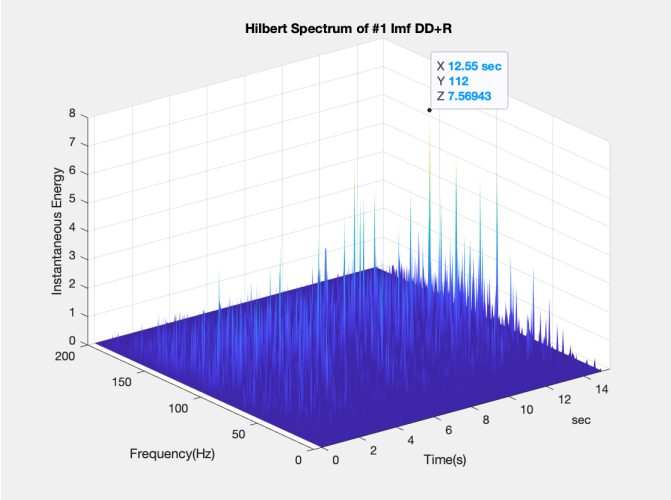

(a) DD+R 15s: HHS 1

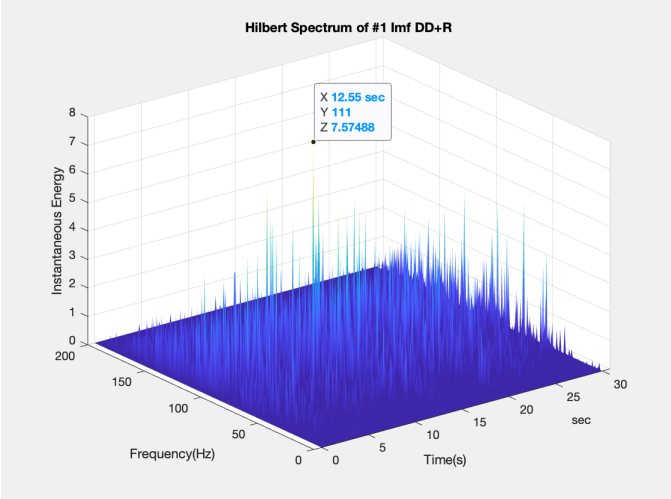

(b) DD+R 30s: HHS 1

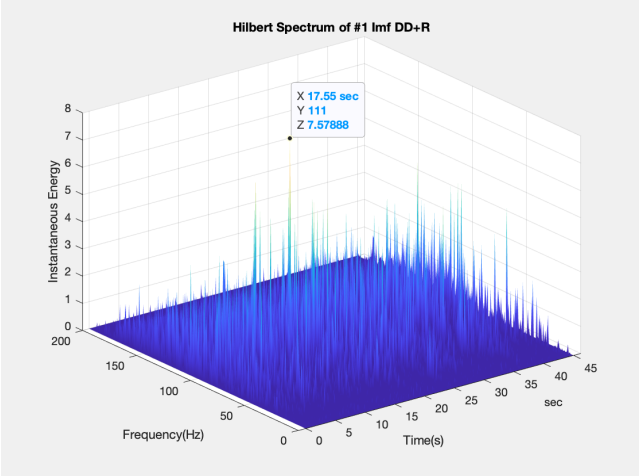

(c) DD+R 45s: HHS 1

Figure 5.80: DD+R: HHS 1

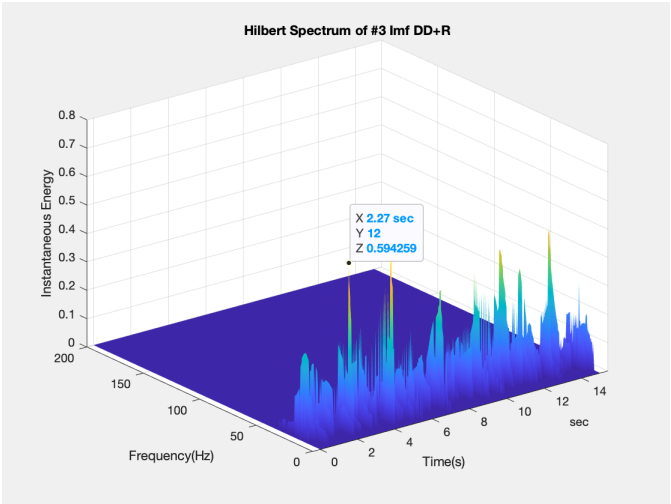

(a) DD+R 15s: HHS 3

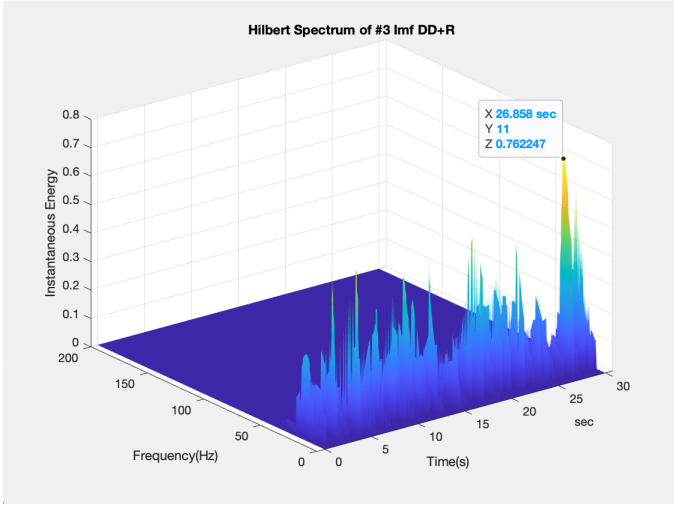

(b) 2D+R 30s: HHS 3

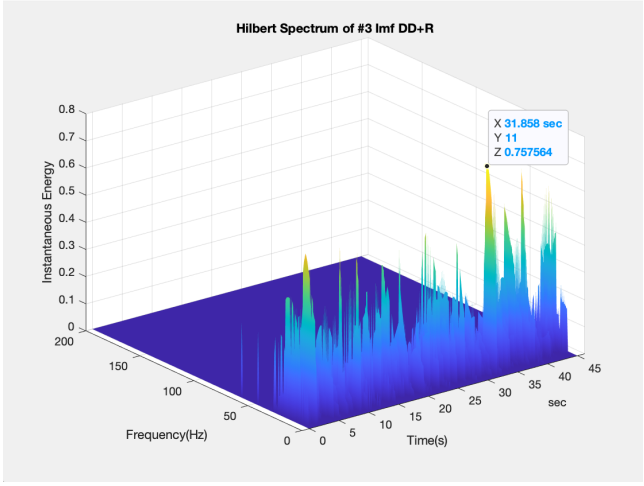

(c) DD+R 45s: HHS 3

Figure 5.81: DD+R: HHS 3

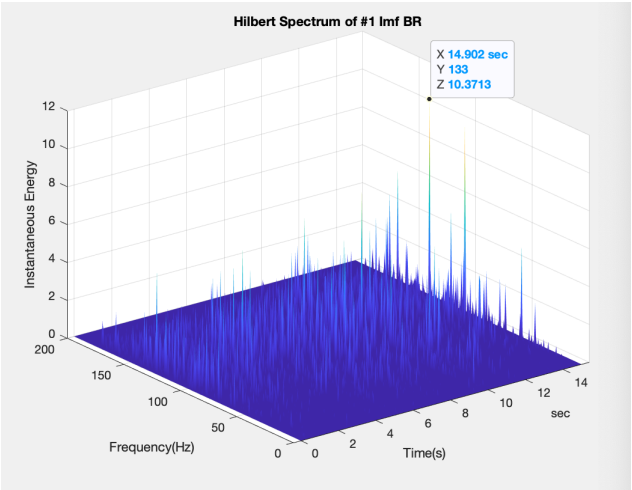

(a) BR 15s: HHS 1

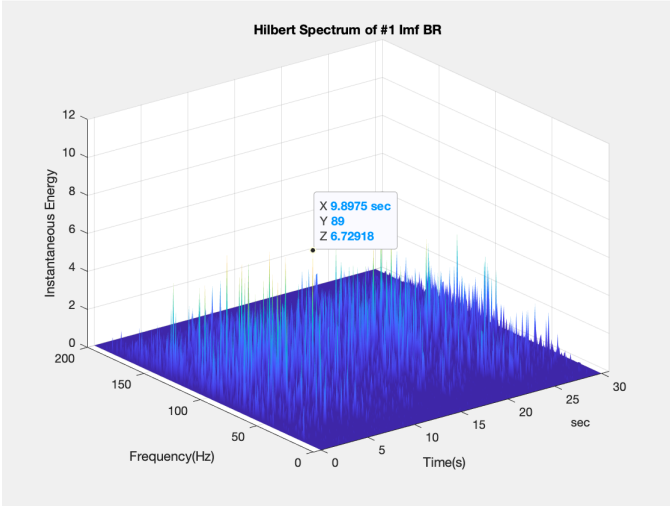

(b) BR 30s: HHS 1

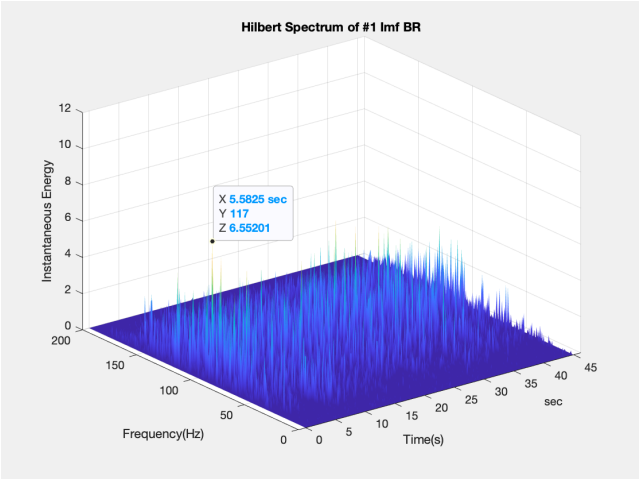

(c) BR 45s: HHS 1

Figure 5.82: BR: HHS 1

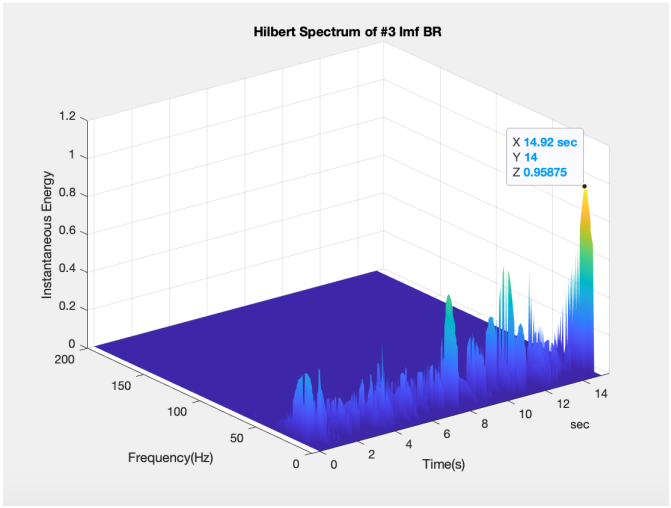

(a) BR 15s: HHS 3

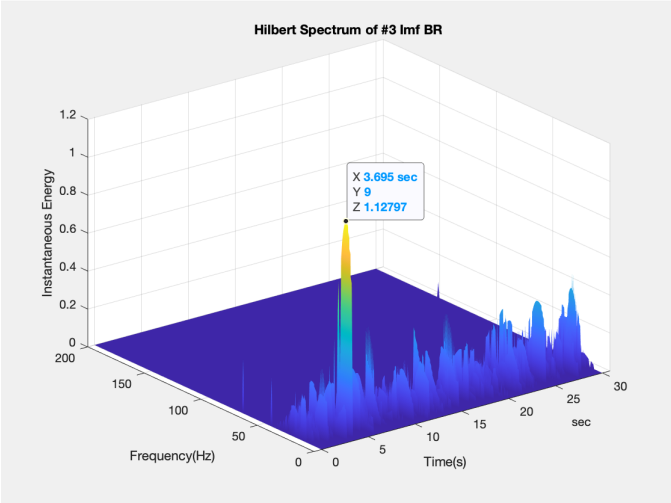

(b) BR 30s: HHS 3

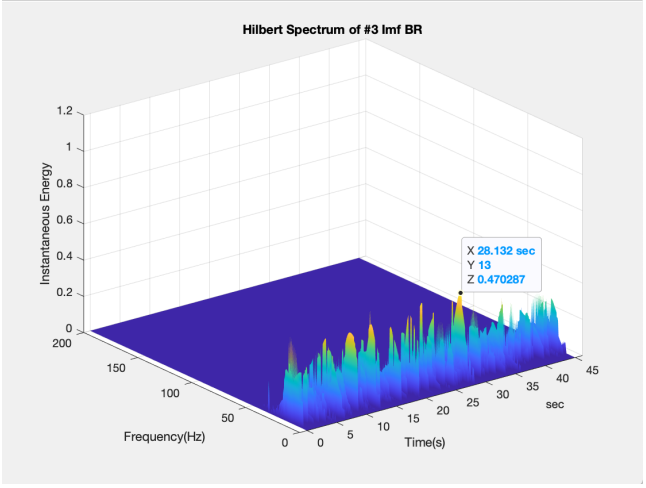

(c) BR 45s: HHS 3

Figure 5.83: BR: HHS 3

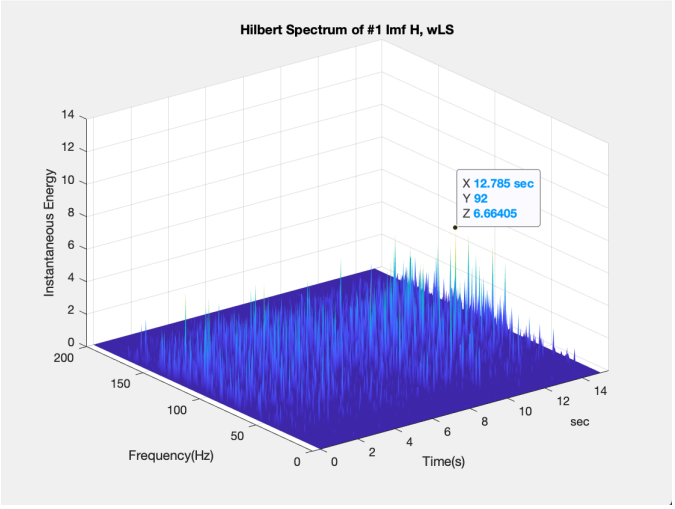

(a) H wLS 15s: HHS 1

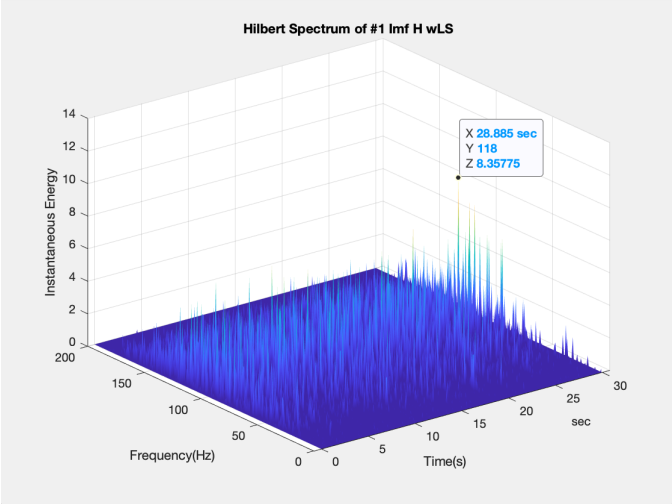

(b) H wLS 30s: HHS 1

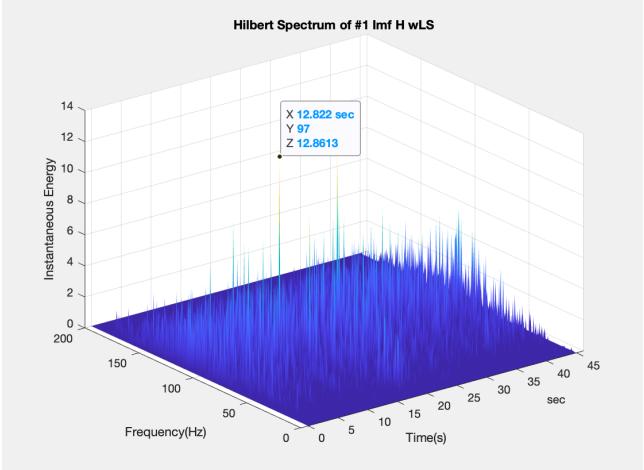

(c) H wLS 45s: HHS 1

Figure 5.84: H wLS: HHS 1

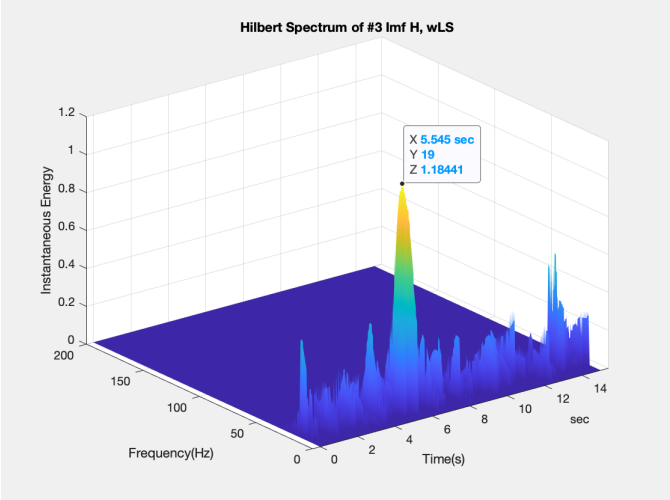

(a) H wLS 15s: HHS 3

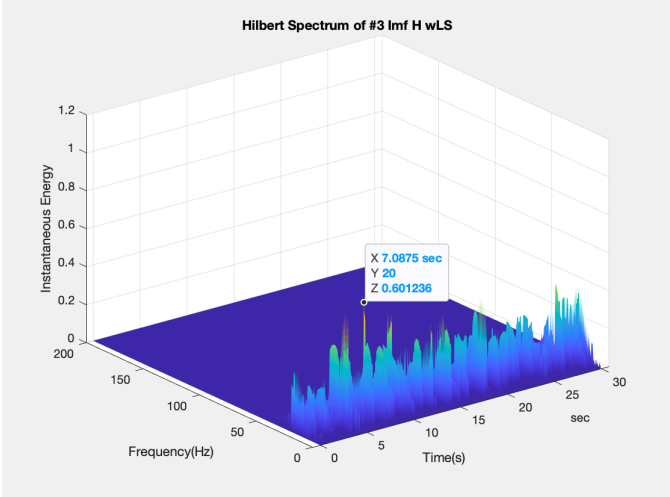

(b) H wLS 30s: HHS 3

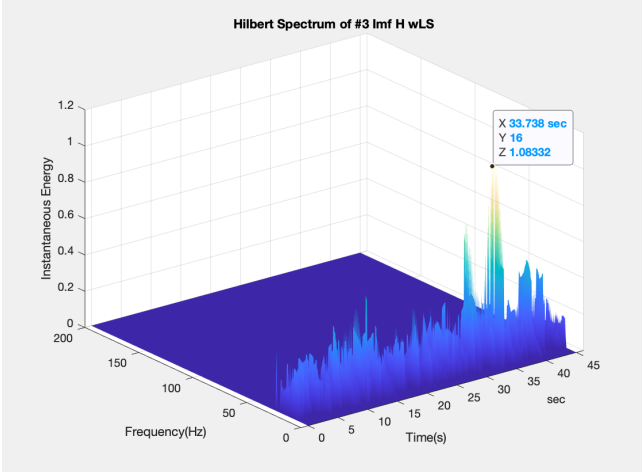

(c) H wLS 45s: HHS 3

Figure 5.85: H wLS: HHS 3

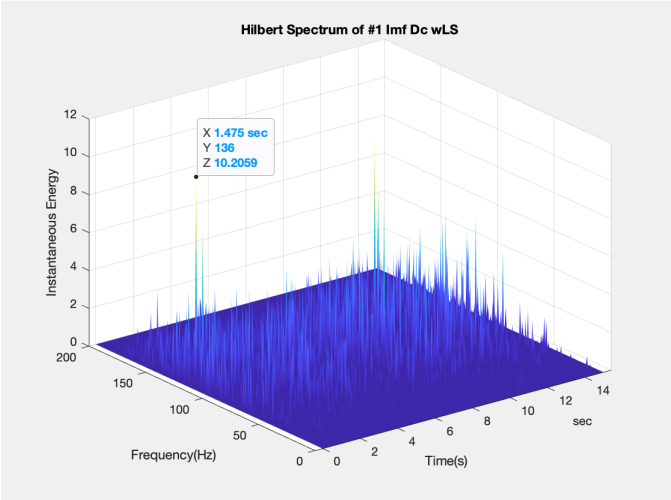

(a) DC wLS 15s: HHS 1

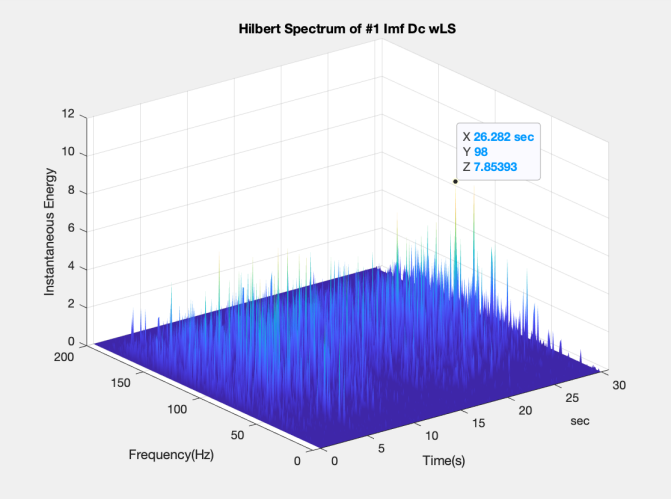

(b) DC wLS 30s: HHS 1

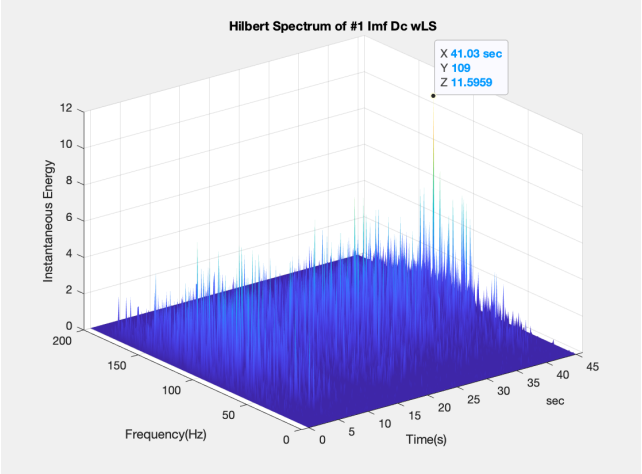

(c) DC wLS 45s: HHS 1

Figure 5.86: DC wLS: HHS 1

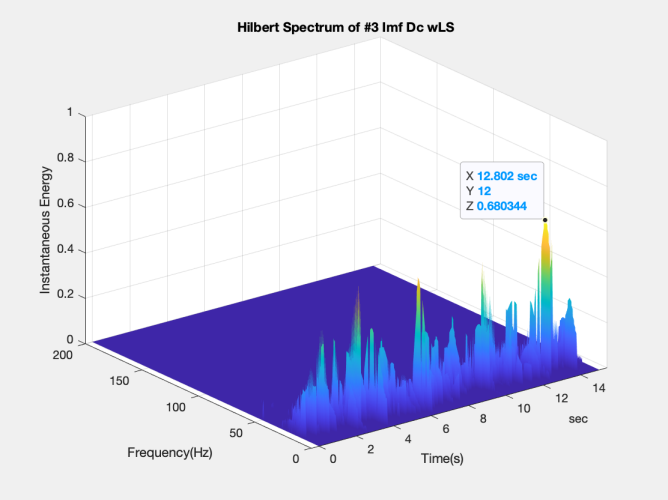

(a) DC wLS 15s: HHS 3

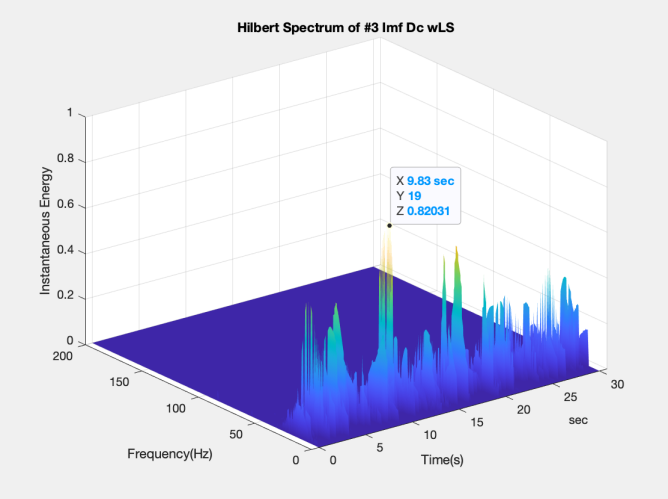

(b) DC wLS 30s: HHS 3

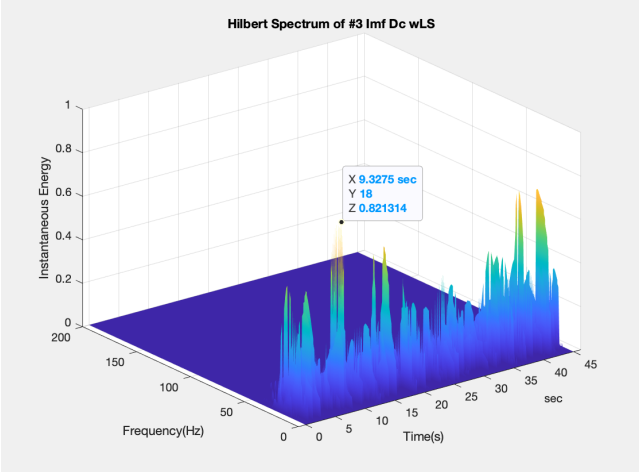

(c) DC wLS 45s: HHS 3

Figure 5.87: DC wLS: HHS 3

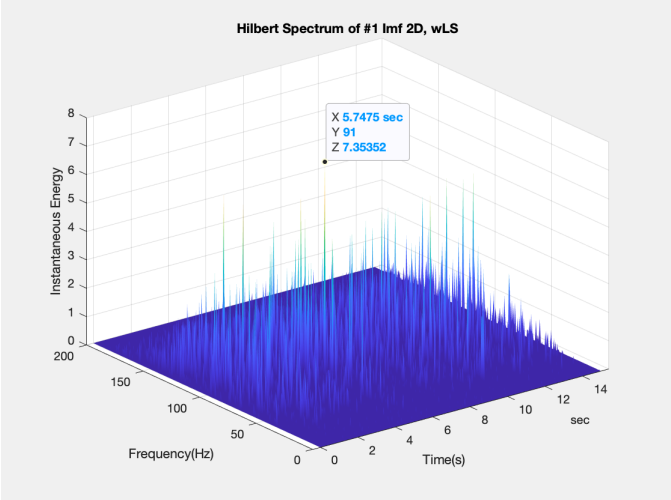

(a) 2D wLS 15s: HHS 1

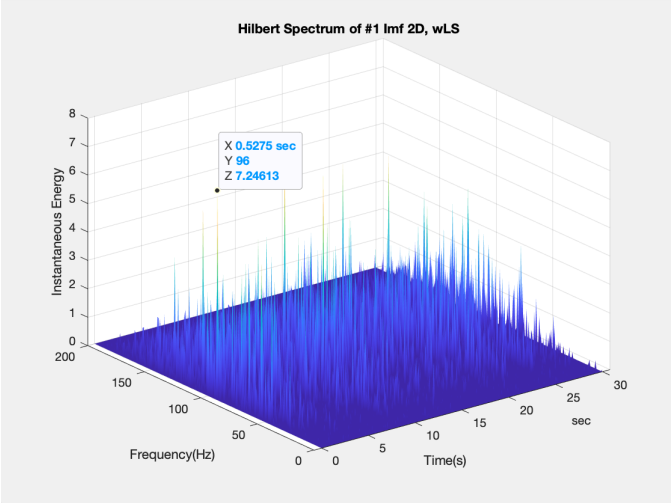

(b) 2D wLS 30s: HHS 1

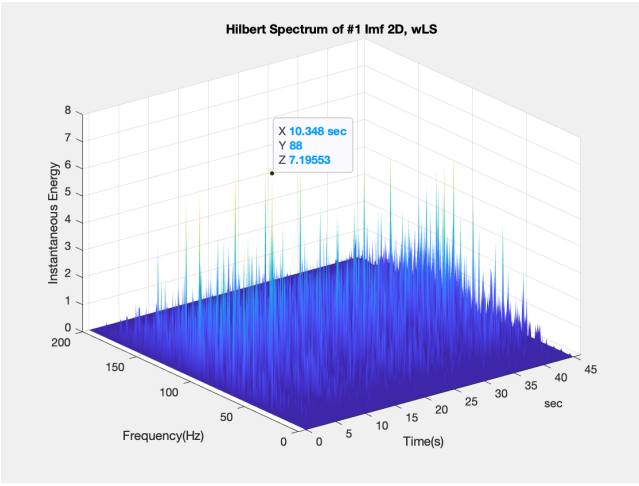

(c) 2D wLS 45s: HHS 1

Figure 5.88: 2D wLS: HHS 1

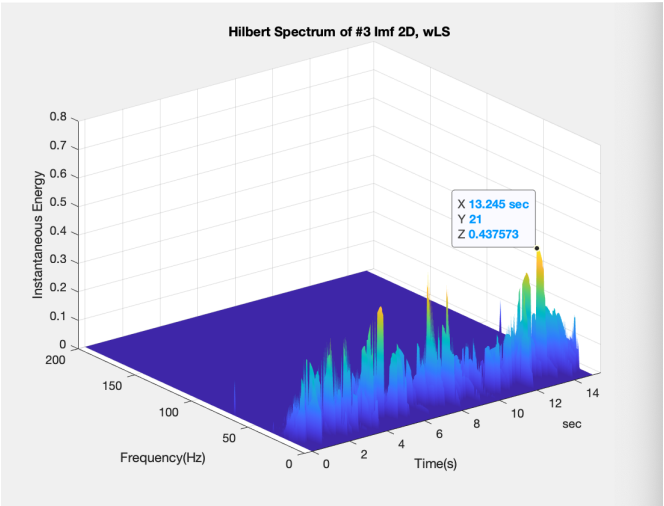

(a) 2D wLS 15s: HHS 3

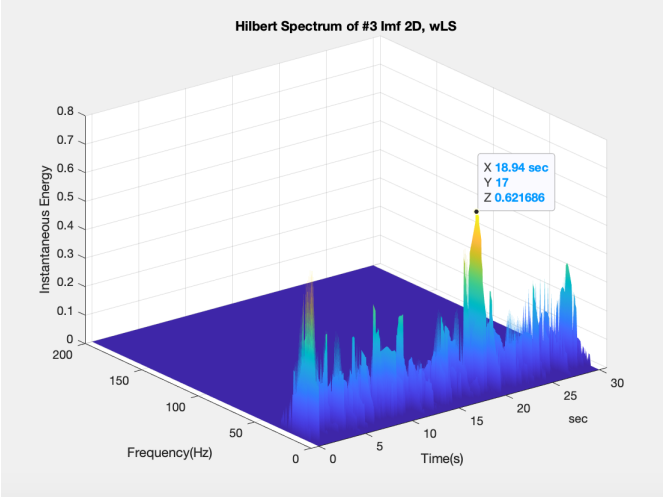

(b) 2D 30s: HHS 3

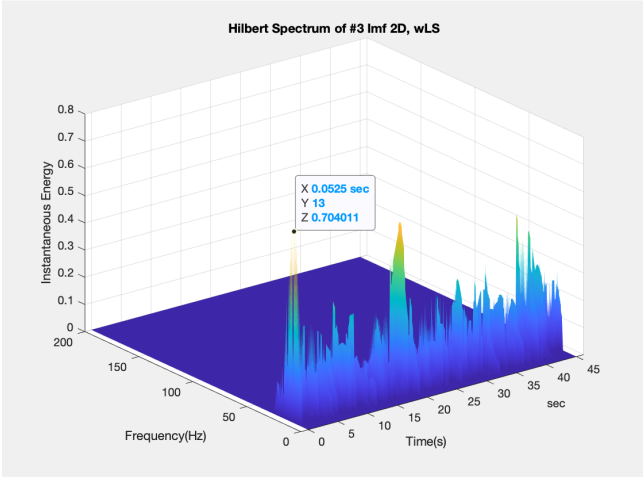

(c) 2D wLS 45s: HHS 3

Figure 5.89: 2D wLS: HHS 3

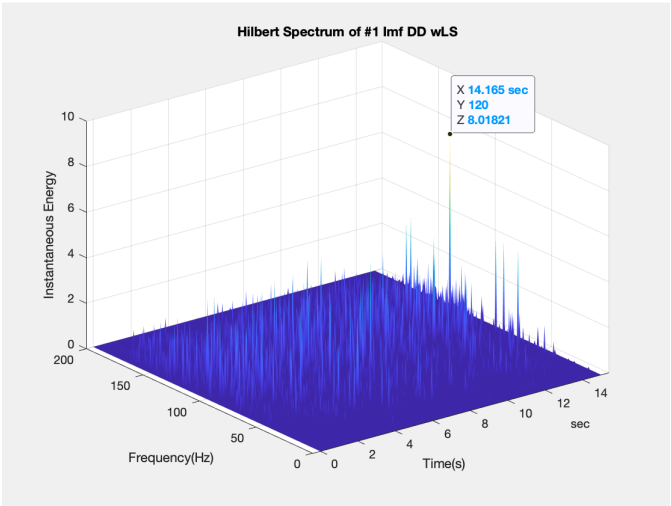

(a) DD wLS 15s: HHS 1

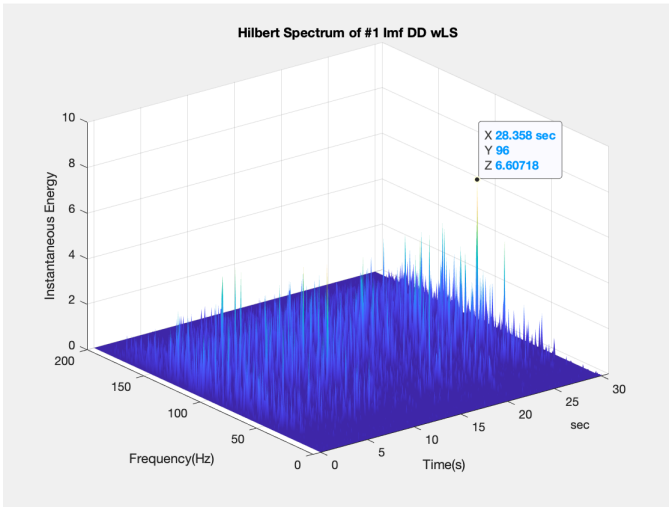

(b) DD wLS 30s: HHS 1

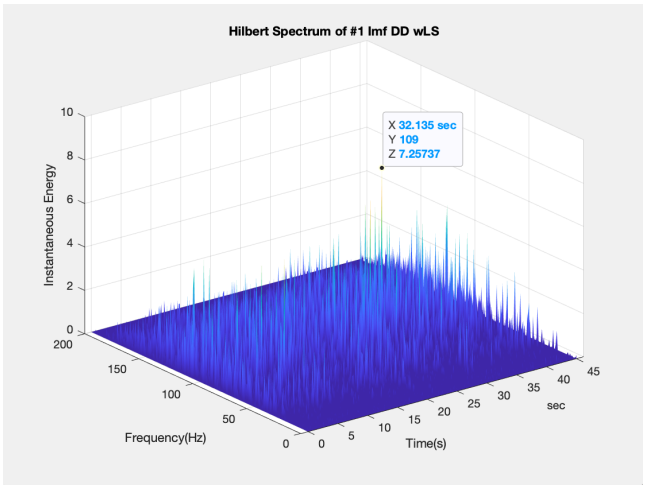

(c) DD wLS 45s: HHS 1

Figure 5.90: DD wLS: HHS 1

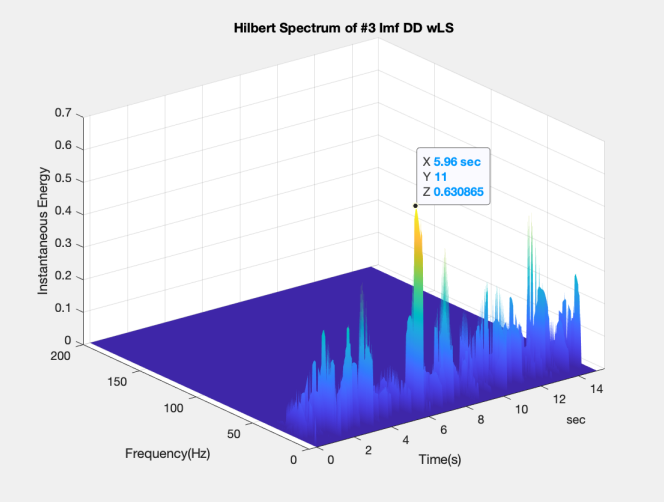

(a) DD wLS 15s: HHS 3

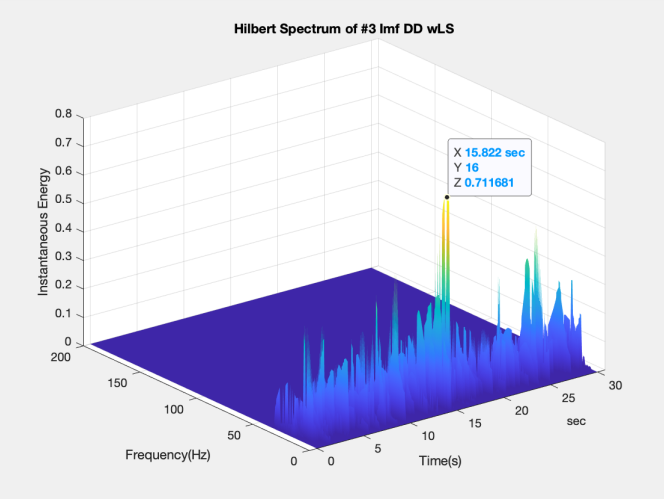

(b) DD wLS 30s: HHS 3

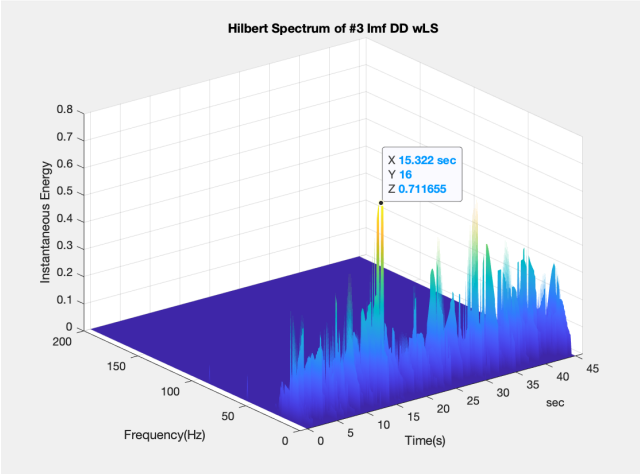

(c) DD wLS 45s: HHS 3

Figure 5.91: DD wLS: HHS 3

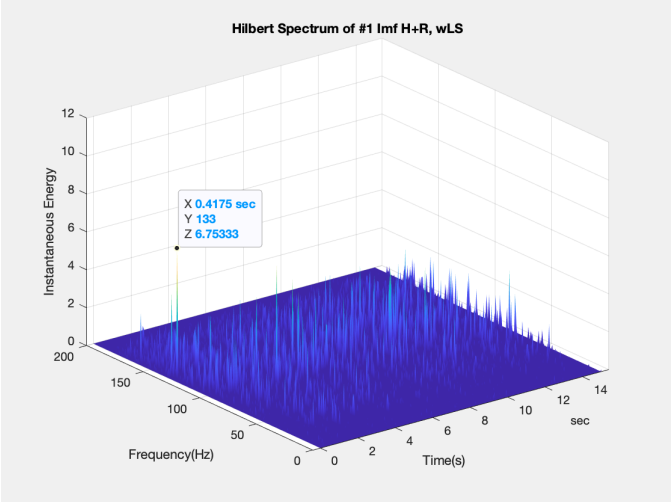

(a) H+R wLS 15s: HHS 1

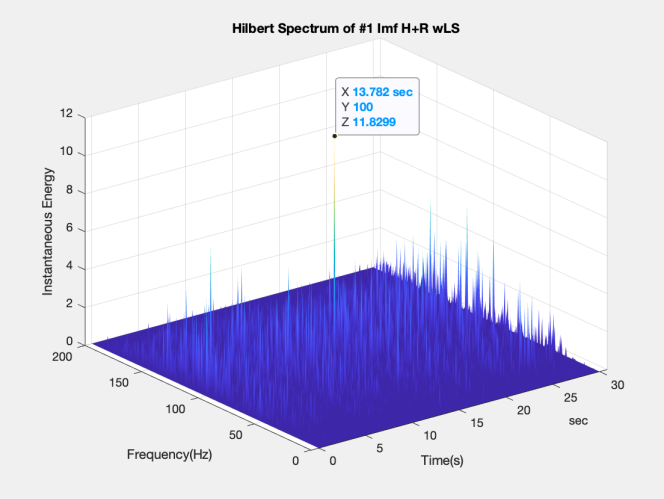

(b) H+R wLS 30s: HHS 1

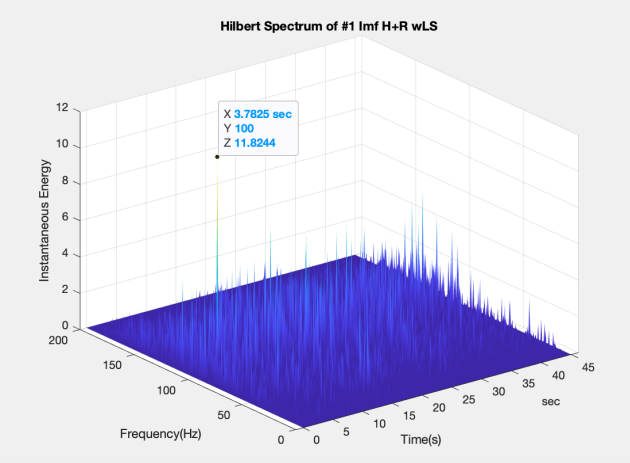

(c) H+R wLS 45s: HHS 1

Figure 5.92: H+R wLS: HHS 1

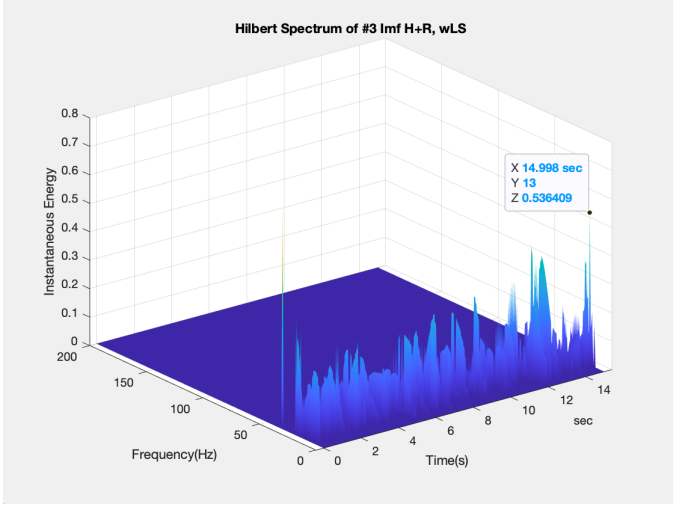

(a) H+R wLS 15s: HHS 3

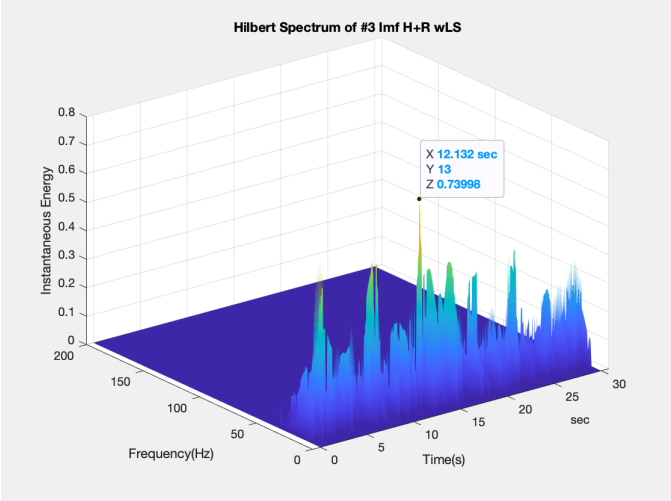

(b) H+R wLS 30s: HHS 3

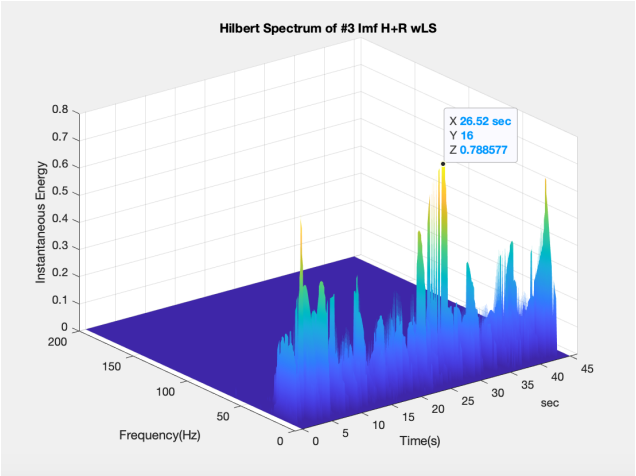

(c) H+R wLS 45s: HHS 3

Figure 5.93: H+R wLS: HHS 3

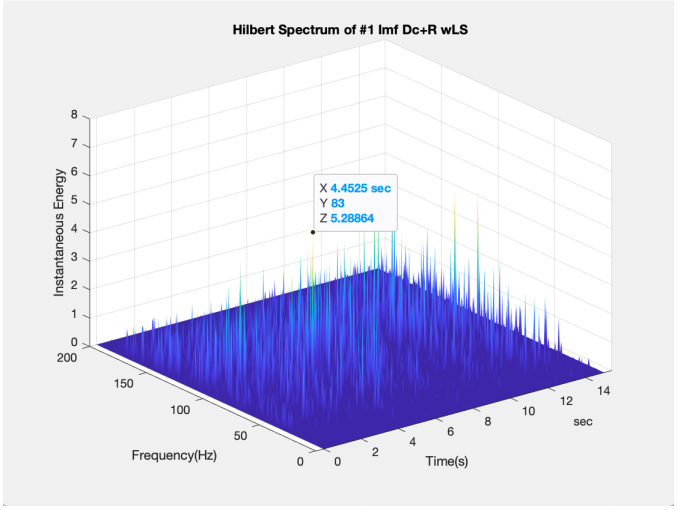

(a) DC+R wLS 15s: HHS 1

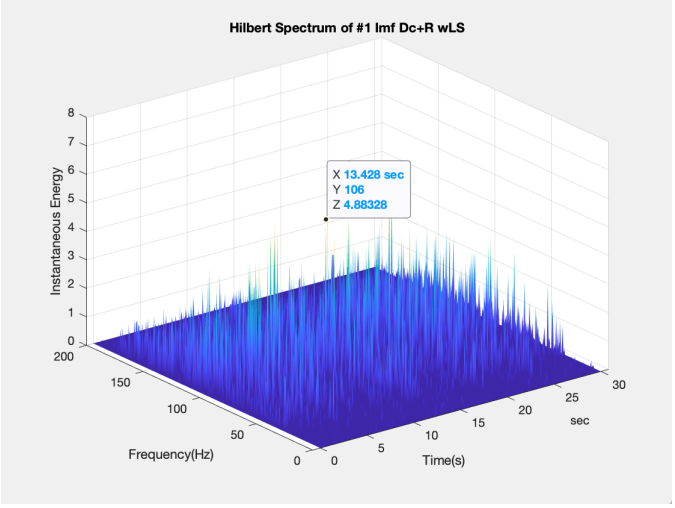

(b) DC+R wLS 30s: HHS 1

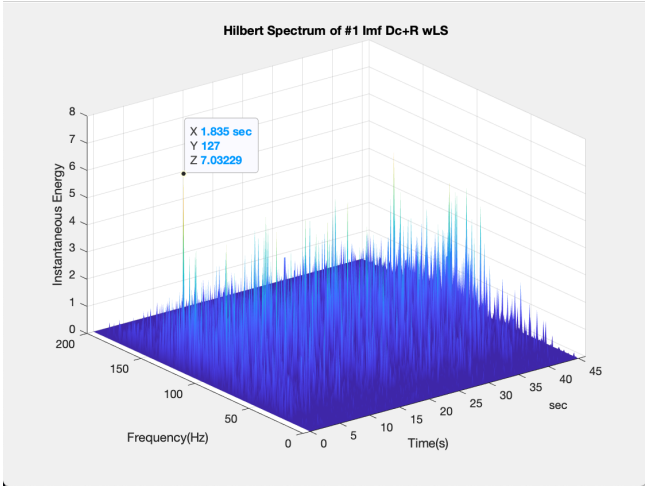

(c) DC+R wLS 45s: HHS 1

Figure 5.94: DC+R wLS: HHS 1

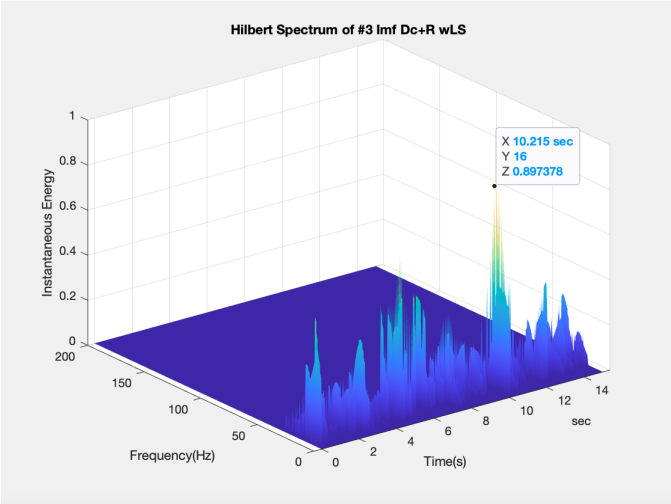

(a) DC+R wLS 15s: HHS 3

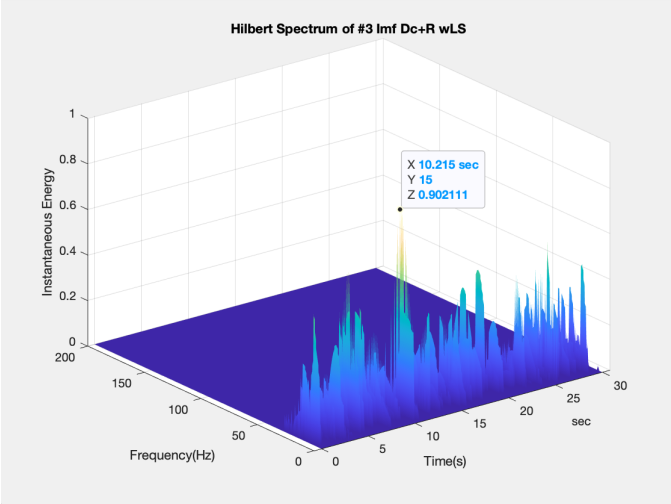

(b) DC+R wLS 30s: HHS 3

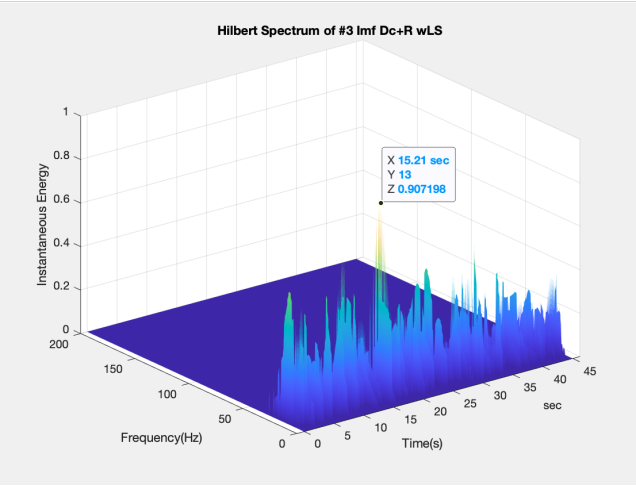

(c) DC+R wLS 45s: HHS 3

Figure 5.95: DC+R wLS: HHS 3

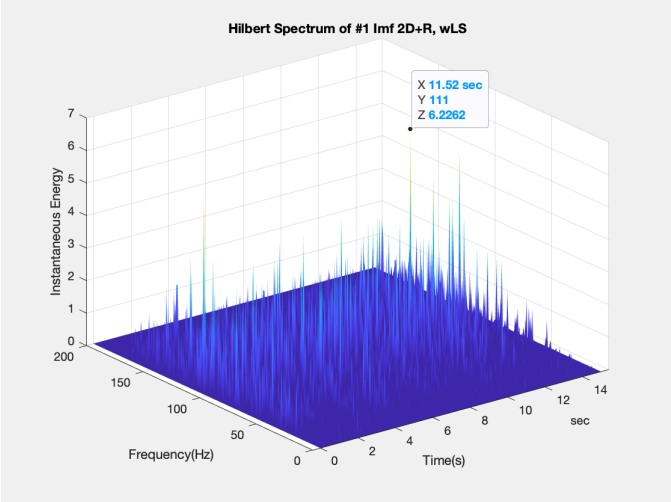

(a) 2D+R wLS 15s: HHS 1

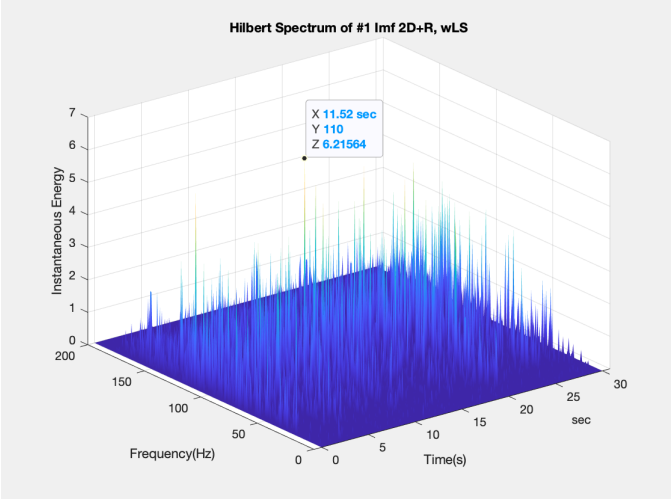

(b) 2D+R wLS 30s: HHS 1

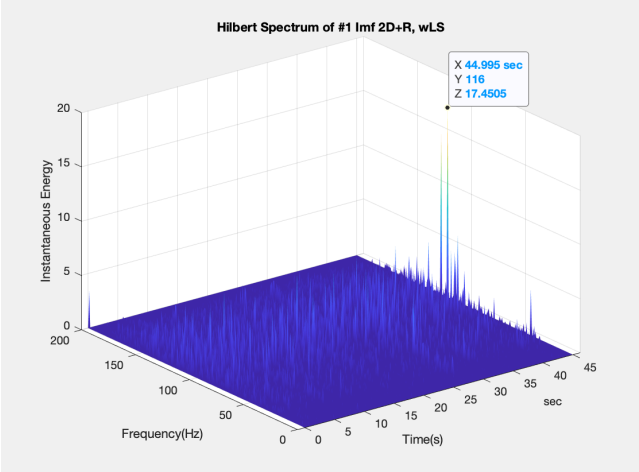

(c) 2D+R wLS 45s: HHS 1

Figure 5.96: 2D+R wLS: HHS 1

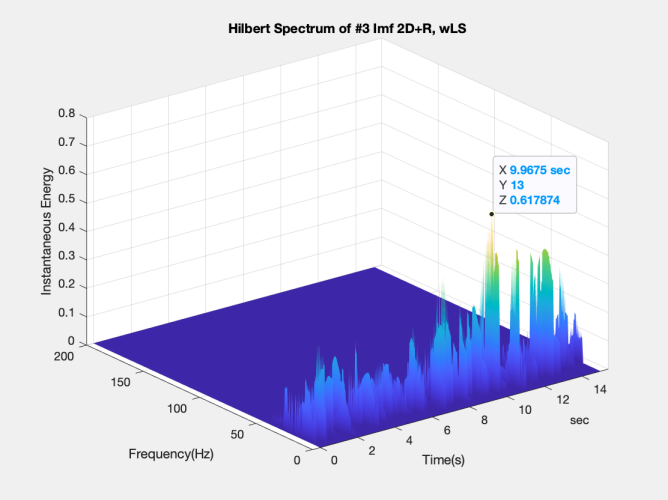

(a) 2D+R wLS 15s: HHS 3

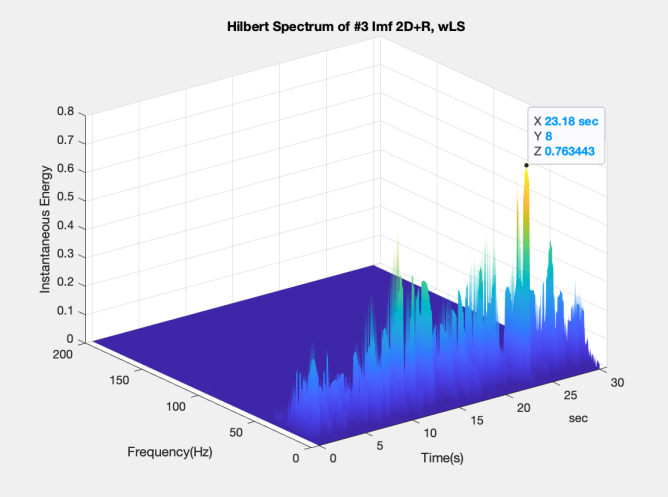

(b) 2D+R wLS 30s: HHS 3

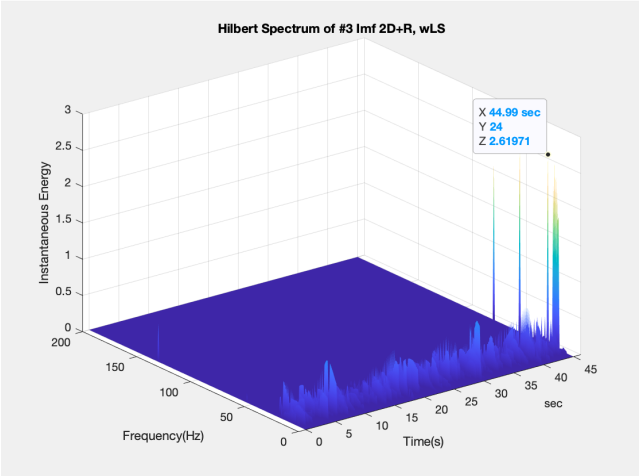

(c) 2D+R wLS 45s: HHS 3

Figure 5.97: 2D+R wLS: HHS 3

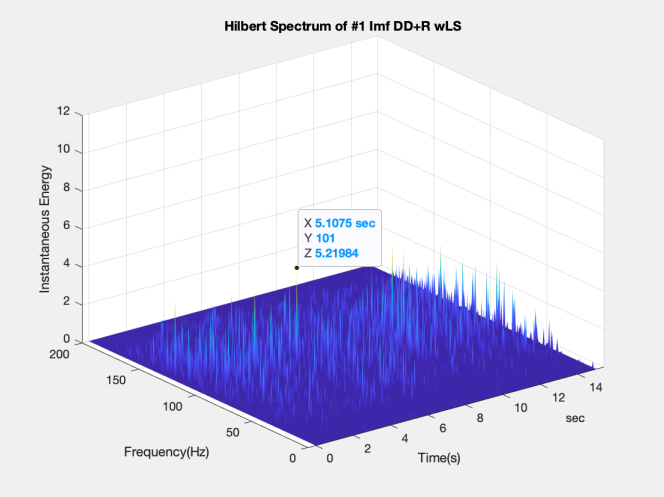

(a) DD+R wLS 15s: HHS 1

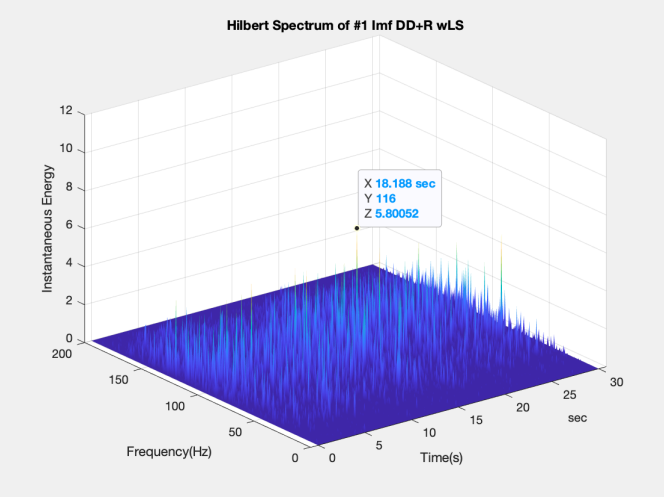

(b) DD+R wLS 30s: HHS 1

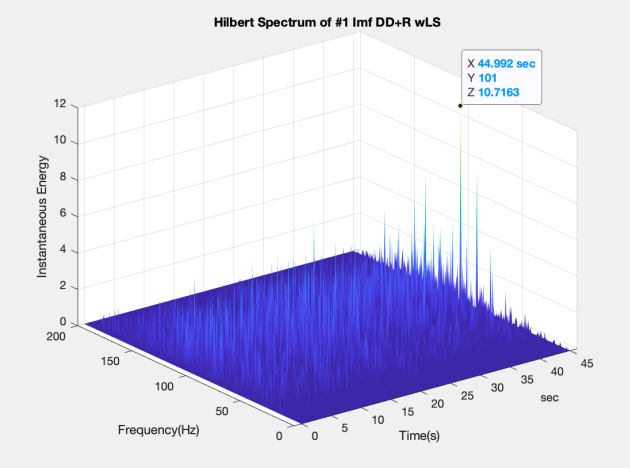

(c) DD+R wLS 45s: HHS 1

Figure 5.98: DD+R wLS: HHS 1

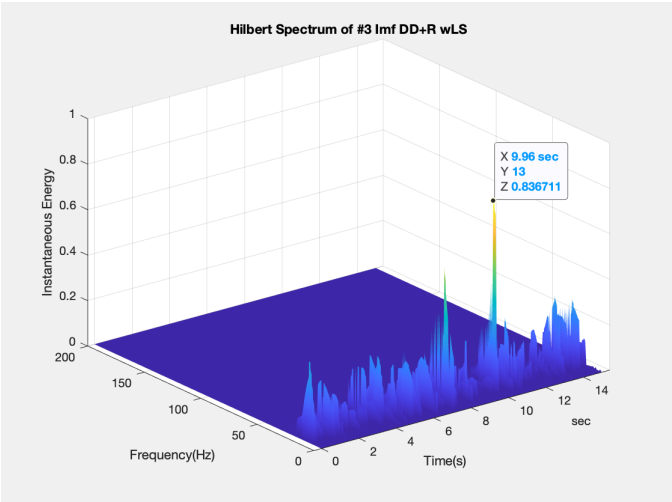

(a) DD+R wLS 15s: HHS 3

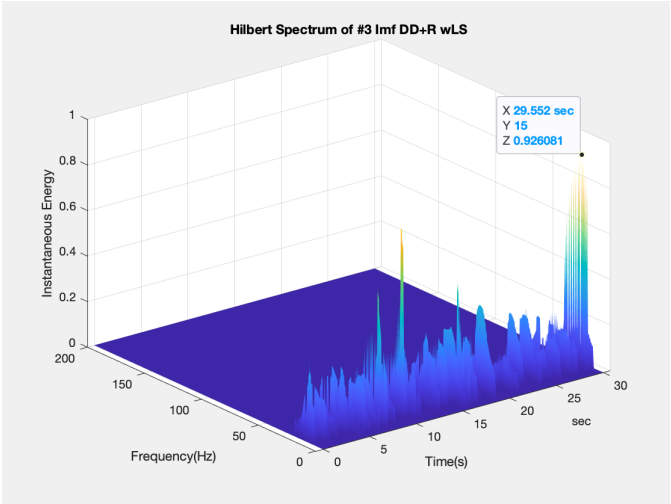

(b) DD+R wLS 30s: HHS 3

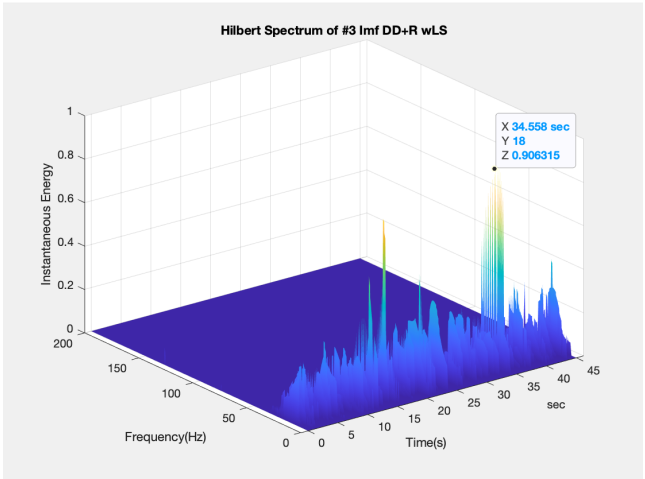

(c) DD+R wLS 45s: HHS 3

Figure 5.99: DD+R wLS: HHS 3

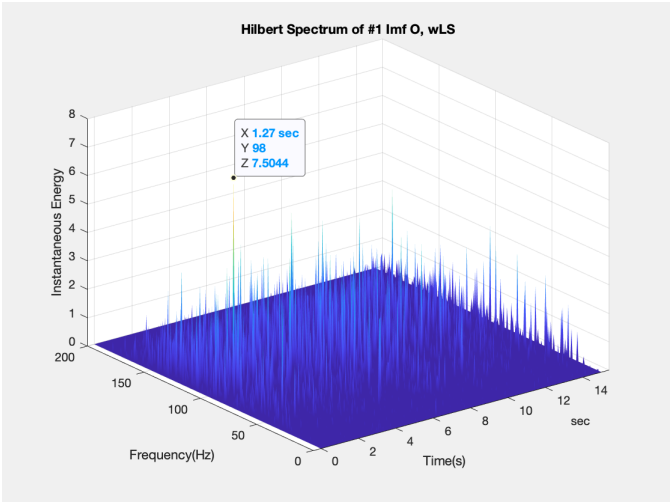

(a) O wLS 15s: HHS 1

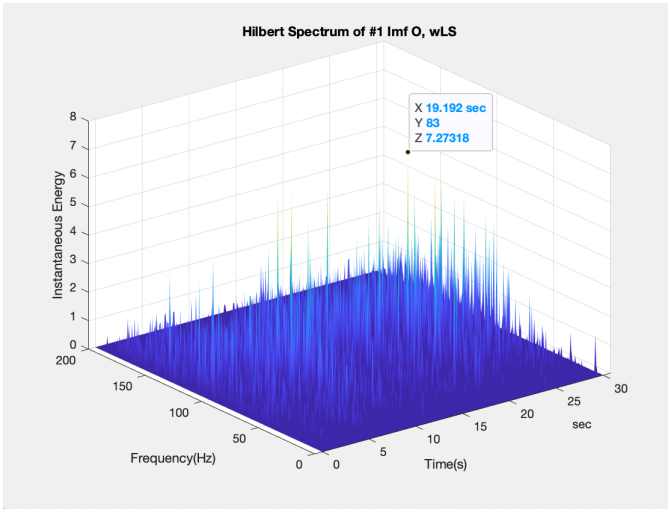

(b) O wLS 30s: HHS 1

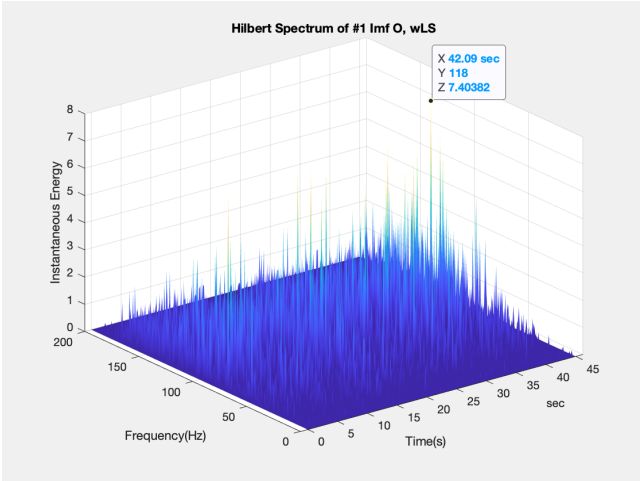

(c) O wLS 45s: HHS 1

Figure 5.100: O wLS: HHS1

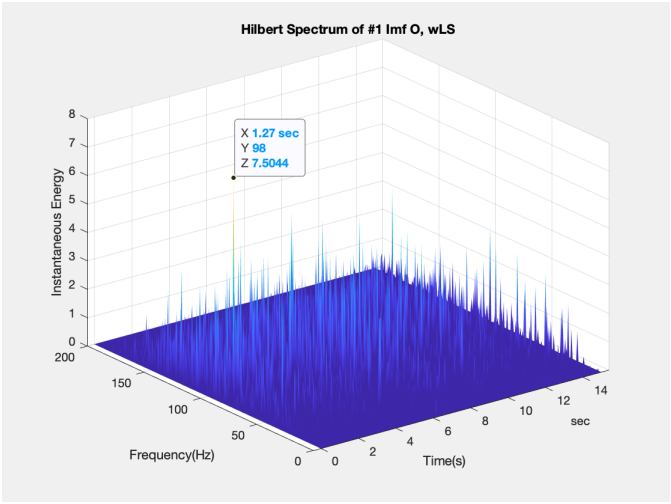

(a) O wLS 15s: HHS 3

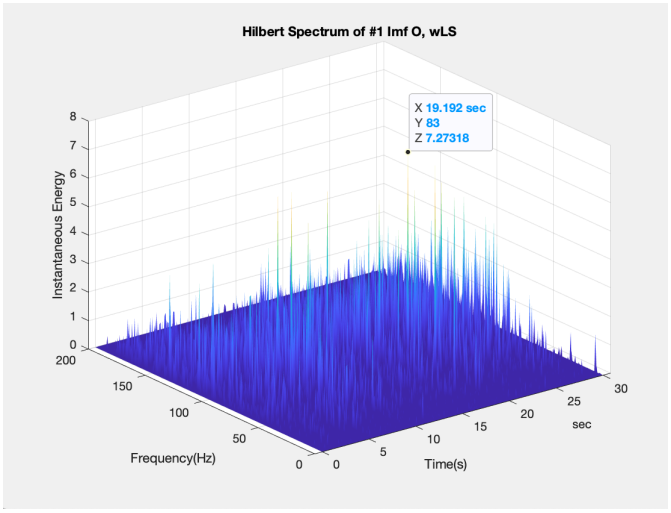

(b) O wLS 30s: HHS 3

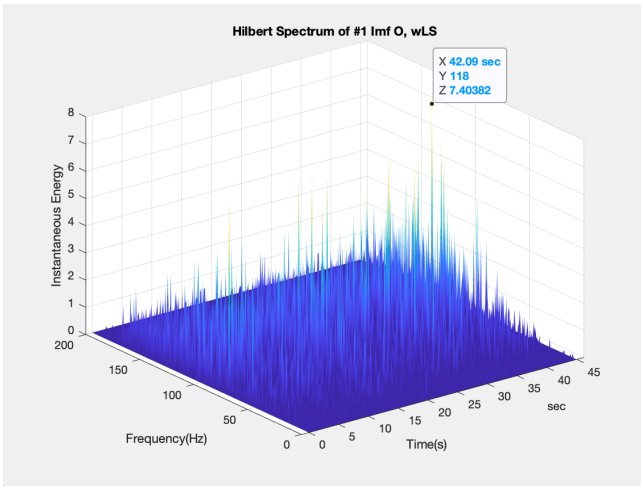

(c) O wLS 45s: HHS 3

Figure 5.101: O wLS: HHS 3

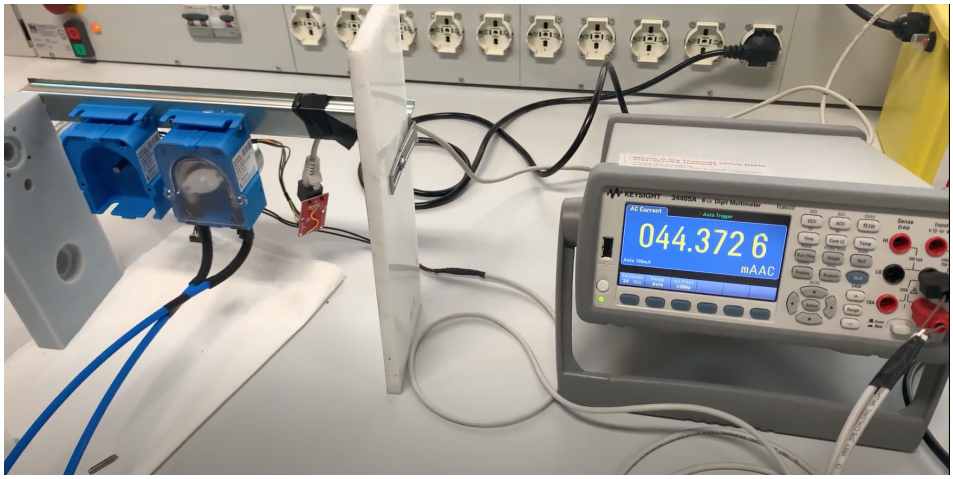

Figure 5.102: Digit Multimeter

5.3 Current Consumption

When monitoring a device, it is useful to combine different kind of measurements in order to provide a wide scenario of its health status. Current consumption would be useful to understand how a device is working: it is likely compare different situation.

A digit multimeter was connected to the plug of the pump as 5.102 shows. We can see whether the pump varies its sucking action with respect to the fluid that is flowing in the circuit, or if there are any differences that leads to identify a danger for the system. In the following graphs, values of A-AC vs N number of samples registered for 5 seconds shows peculiar differences: if the pump is working without any faulty occurrences processing different fluids (fig. 5.103a); depict a faulty case with respect to normal condition (figs.5.103b, 5.103c); understand how a damaged cases impact if processed with different fluids (figs.5.104a, 5.104b).

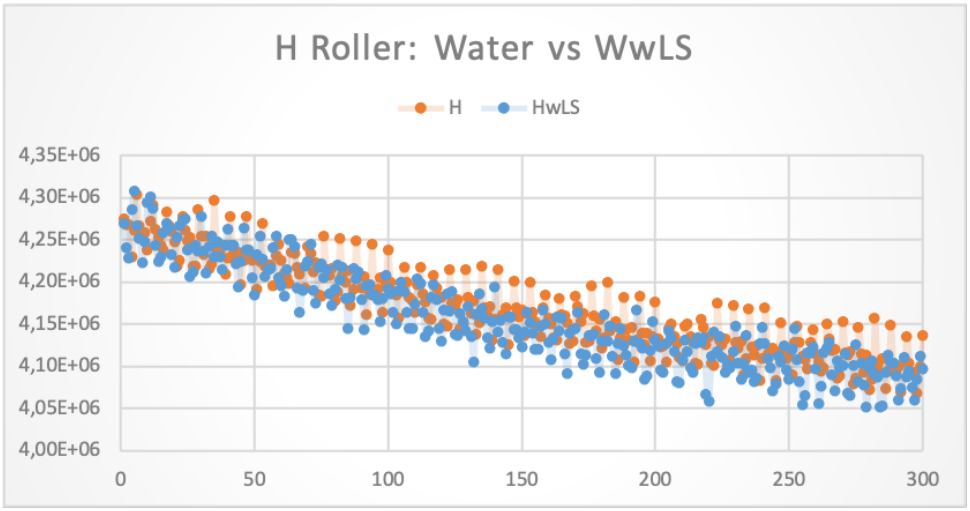

(a) H Roller: current consumption

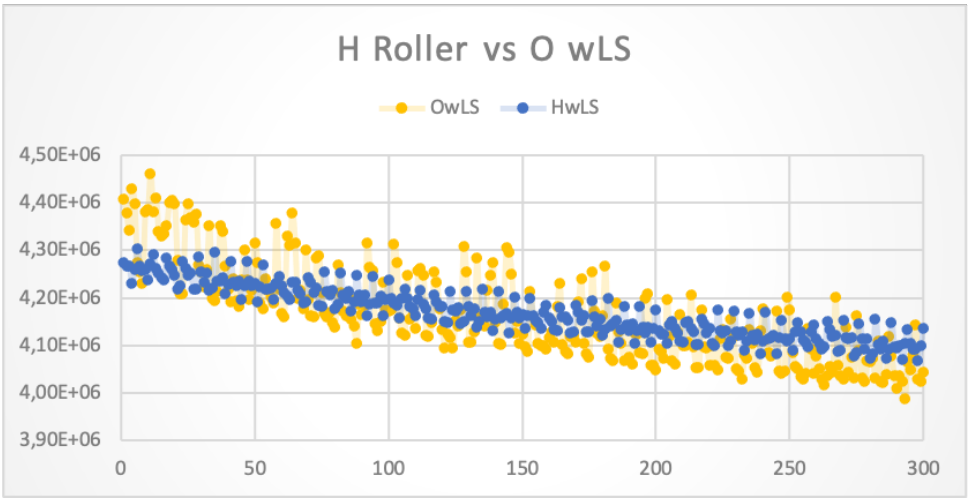

(b) H vs O Roller: current consumption

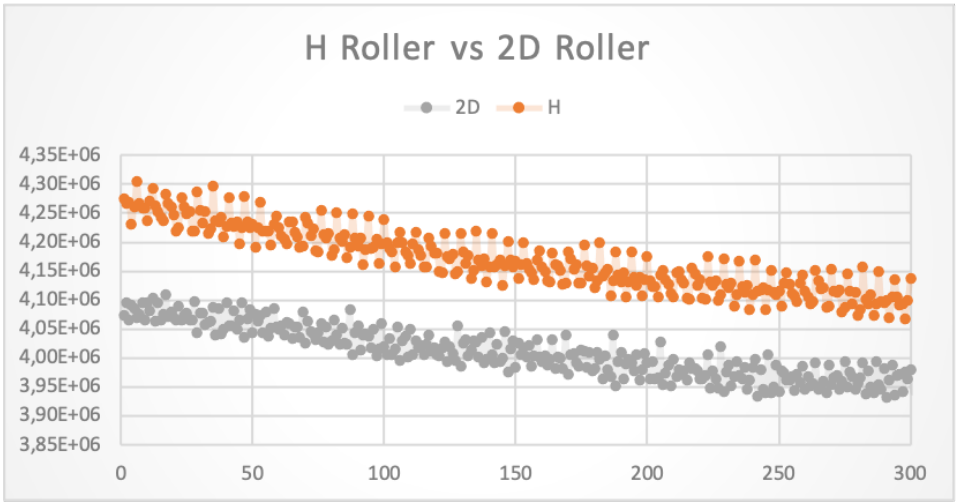

(c) H vs 2D Roller: current consumption

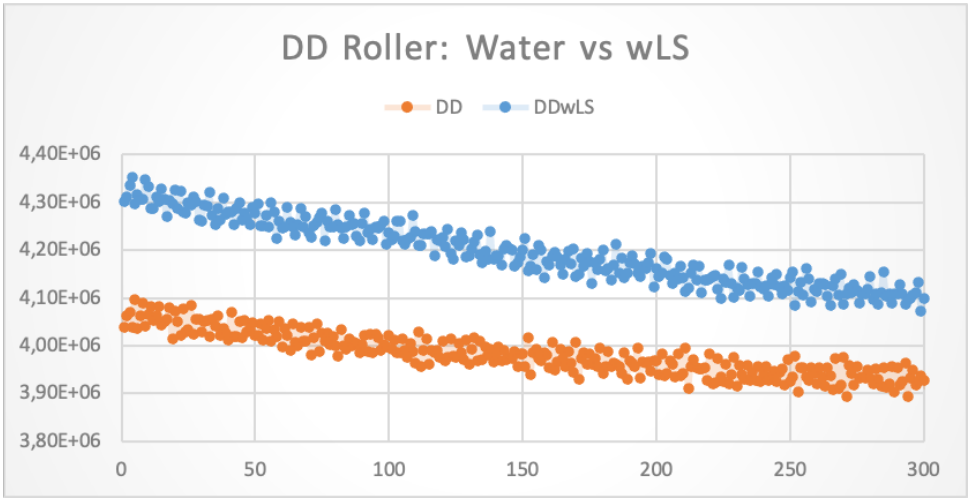

(a) DD Roller: current consumption

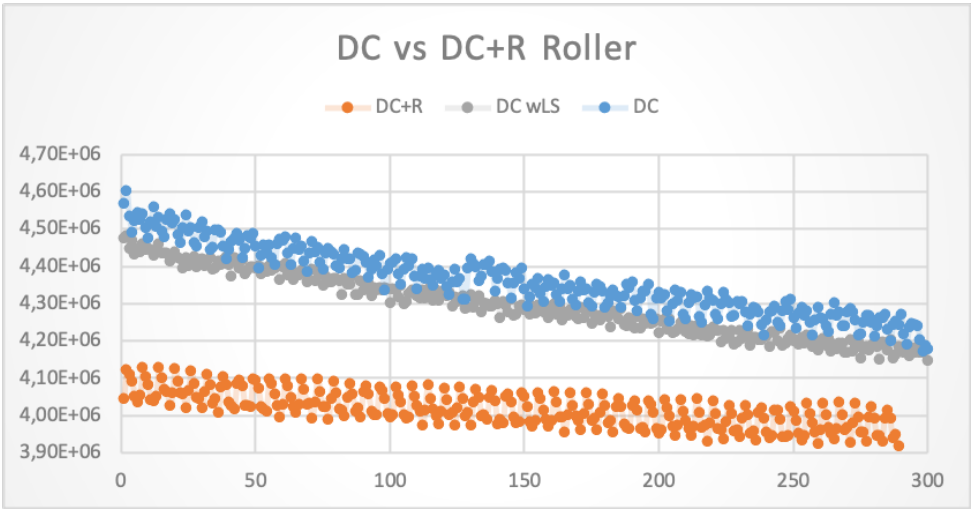

(b) DC vs Dc+R Roller: current consumption

6. Conclusions

In the framework of Predictive Maintenance, Condition monitoring is the process that continuously records the assessment of parameters on the current state of the machinery. Substituting a mechanical component such bearings is not expensive per se, but an accidental breakdown due to a failure in the system may lead to several problem, damages or injury to the surrounded environment, personnel included. Several techniques compete to prevent such consequences to happen, aiming to forecast the early detection of failures within a system, from the simplest component to complex mechanical parts. Unplanned stop translates in economic losses, higher maintenance costs and efforts.

PdM strategies are nowadays well-established in manufacturing and other facilities. In biomedical application and healthcare industry, conversely, maintenance is stuck to scheduled maintenance which is considered deprecated. PdM is not widely used, unless mentioned, despite huge amount and complexity of medical devices that everyday saves life (as it happens nowadays fighting against pandemic). This approach could bring benefit mainly in a more efficient resource utilization, in reducing the undesired human errors or the ones that normally occur by following another maintenance policy. If medical context is concerned, patient care could be precluded.

Reliability and availability of medical devices are the main aspect bioengineers need to take care of. Monitoring a device requires a good knowledge

of the physics of the device itself, its history along the time of utilization and its contextualization during its working condition. In support of these requests, collection of real-time data is needed: the use of a Raspberry eased the process. Thus the correct choice of a monitoring technique greatly relies on the sensor and the whole data acquisition.

Condition monitoring was then performed on two different mechanical objects focusing on their vibration: a roller bearing and a roller pump. In particular, three kind of signal processing techniques have been first validated on the roller bearing, for which theory is well-known, and then reflected on the roller pump.

Studying vibration, it has been proven that FFT and Envelope Spectrum are the most common tools to detect characteristics frequencies that result in a fault in the system in frequency domain. FFT shows all the frequency content adding harmonics that might hide the frequencies we are interested in, while a proper filter could remove noise from background leaving room for the most impulsive band where an impact is likely to be, as in Envelope Spectrum analysis happens. As a result, both BPFO and BPFI of the bearing case (Chapter 3) match with the theoretical values. Time-related information is lost, therefore Hilbert-Huang transform was introduced: this newest method enhances the detection of faults by decomposing the signal into intrinsic mode functions able to recognize the vibration modes that coexist in the system. The detection of specific pattern for the roller pump was possible specially due to the combination of both frequency domain and time-frequency related analysis (Chapter 5). In some cases it was not straightforward to discriminate singularly the listed damages (1D or +R conditions) from FFT or Envelope; with HHT, instead, importance is given to the probability energy density of the most stressed frequencies. Also the choice of the fluid influenced the results.

Current was monitored plugging the pump to a digit multimeter, which instantaneously detect the mAAC while pump was working. This information adds value to vibration signal.

With the combination of multiple parameters, the strategy will be preciser. Moreover, increasing the system's reliability implementing the PdM strategy will be a revolutionary breakthrough even in healthcare industry. Of course, PdM strategy not only detect possible faults but could guarantee equipment integrity over time.

6.1 Future Improvement

Thanks to this project, I challenged myself to build the acquisition system and the set up, from data acquisition to data analysis. However, the overall system can be improved with further specifics:

1 on data acquisition system implementing:

- low level kernel driver in order to avoid data loss due to delayed acknowledgement of the interrupt watermark signal
- software design pattern for multithreading in order to dequeue the data from driver memory and post process data real time. With this architecture it would also be possible to view and process data without having to transfer them to another computer;
- IoT-based infrastructure to collect and cloud-store data in order to implement dashboards and messaging for better managment of monitored devices.

2 using other advance signal processing tool such as wavelet decomposition;

3 constructing health indicators for prediction of remaining useful life of a device;

4 identifying other faults (e.g. on motor) or other sensor (e.g.to detect deterioration of tubes)

A. Codes

A.1 Python Codes

```
 LIS3DH Accelerometer Driver
# Based on the Arduino LIS3DH driver from:
#   https://github.com/adafruit/Adafruit_LIS3DH/
# Author: Alberto Sancandi

import time
import math
from collections import namedtuple
import struct
import smbus

#__repo__ = https://srv-git.rold.com/nadella/lis3dh_driver.git

# Register addresses:
# pylint: disable=bad-whitespace
_REG_OUTADC1_L = (0x08)
_REG_WHOAMI = (0x0F)
_REG_TEMPCFG = (0x1F)
_REG_CTRL1 = (0x20)
_REG_CTRL3 = (0x22)
```

```
_REG_CTRL4 = (0x23)
_REG_CTRL5 = (0x24)
_REG_OUT_X_L = (0x28)
_REG_INT1SRC = (0x31)
_REG_CLICKCFG = (0x38)
_REG_CLICKSRC = (0x39)
_REG_CLICKTHS = (0x3A)
_REG_TIMELIMIT = (0x3B)
_REG_TIMELATENCY = (0x3C)
_REG_TIMEWINDOW = (0x3D)
_REG_FIFO_CTRL = (0x2E)
_REG_FIFO_SRC = (0x2F)
_REG_STATUS = (0X27)

# Register value constants:
RANGE_16_G = (0b11) # +/- 16g
RANGE_8_G = (0b10) # +/- 8g
RANGE_4_G = (0b01) # +/- 4g
RANGE_2_G = (0b00) # +/- 2g (default value)
DATARATE_1344_HZ = (0b1001) # 1.344 KHz
DATARATE_400_HZ = (0b0111) # 400Hz
DATARATE_200_HZ = (0b0110) # 200Hz
DATARATE_100_HZ = (0b0101) # 100Hz
DATARATE_50_HZ = (0b0100) # 50Hz
DATARATE_25_HZ = (0b0011) # 25Hz
DATARATE_10_HZ = (0b0010) # 10 Hz
DATARATE_1_HZ = (0b0001) # 1 Hz
DATARATE_POWERDOWN = (0)
DATARATE_LOWPOWER_1K6HZ = (0b1000)
DATARATE_LOWPOWER_5KHZ = (0b1001)
```

```
# Other constants
STANDARD_GRAVITY = 9.806
# pylint: enable=bad-whitespace

# the named tuple returned by the class
AccelerationTuple = namedtuple("acceleration", ("x", "y", "z"))

class LIS3DH:
    """Driver base for the LIS3DH accelerometer."""
    def __init__(self, int1=None, int2=None):
        # Check device ID.
        device_id = self._read_register_byte(_REG_WHOAMI)
        if device_id != 0x33:
            raise RuntimeError("Failed to find LIS3DH!")
        # Reboot
        self._write_register_byte(_REG_CTRL5, 0x80)
        time.sleep(0.01) # takes 5ms
        # Enable all axes, normal mode.
        self._write_register_byte(_REG_CTRL1, 0b00000111)
        # Normal res & BDU enabled & 8g FSR.
        #self._write_register_byte(_REG_CTRL4, 0b10100000)
        # Enable ADCs.
        self._write_register_byte(_REG_TEMPCFG, 0x80)
        #CTR_REG5 for FIFO
        self._write_register_byte(_REG_CTRL5, 0b01000000)
        self._write_register_byte(_REG_FIFO_CTRL, 0b01010000) #FIFO
            mode
        #enable watermark interrupt on INT1
        self._write_register_byte(_REG_CTRL3, 0b00000100)
```

```
@property
def data_rate(self):
    """The data rate of the accelerometer. Can be
        DATA_RATE_400_HZ, DATA_RATE_200_HZ,
       DATA_RATE_100_HZ, DATA_RATE_50_HZ, DATA_RATE_25_HZ,
           DATA_RATE_10_HZ,
       DATA_RATE_1_HZ, DATA_RATE_POWERDOWN,
           DATA_RATE_LOWPOWER_1K6HZ, or
       DATA_RATE_LOWPOWER_5KHZ."""
    ctl1 = self._read_register_byte(_REG_CTRL1)
    return (ctl1 >> 4) & 0x0F

@data_rate.setter
def data_rate(self, rate):
    ctl1 = self._read_register_byte(_REG_CTRL1)
    ctl1 &= ~(0xF0)
    ctl1 |= rate << 4
    self._write_register_byte(_REG_CTRL1, ctl1)

@property
def range(self):
    """The range of the accelerometer. Can be RANGE_2_G,
        RANGE_4_G, RANGE_8_G, or
       RANGE_16_G."""
    ctl4 = self._read_register_byte(_REG_CTRL4)
    return (ctl4 >> 4) & 0x03

@range.setter
def range(self, range_value):
```

```
        ctl4 = self._read_register_byte(_REG_CTRL4)
        ctl4 &= ~0x30
        ctl4 |= range_value << 4
        self._write_register_byte(_REG_CTRL4, ctl4)

    @property
    def acceleration(self):
        """The x, y, z acceleration values returned in a 3-tuple
           and are in m / s ^ 2."""
        divider = 1
        accel_range = self.range
        if accel_range == RANGE_16_G:
            divider = 1365
        elif accel_range == RANGE_8_G:
            divider = 4096
        elif accel_range == RANGE_4_G:
            divider = 8190
        elif accel_range == RANGE_2_G:
            divider = 16380

        x, y, z = struct.unpack("<hhh",
            self._read_register(_REG_OUT_X_L | 0x80, 6))

        # convert from Gs to m / s ^ 2 and adjust for the range
        x = (x / divider) * STANDARD_GRAVITY
        y = (y / divider) * STANDARD_GRAVITY
        z = (z / divider) * STANDARD_GRAVITY

        return AccelerationTuple(x, y, z)
```

```
class LIS3DH_I2C(LIS3DH):
    """Driver for the LIS3DH accelerometer connected over I2C."""

    def __init__(self, i2cnum, *, address=0x18, int1=None,
        int2=None):
        import smbus # pylint: disable=import-outside-toplevel

        self.address = address
        self._i2cbus = smbus.SMBus(1)
        self._buffer = bytearray(6)
        super().__init__(int1=int1, int2=int2)

    def _read_register(self, register, length):
            self._buffer =
                bytearray(self._i2cbus.read_i2c_block_data(self.address,
                register & 0xFF, length))
            return self._buffer

    def _write_register_byte(self, register, value):
            self._i2cbus.write_byte_data(self.address, register &
                0xFF, value & 0xFF)
```

```
# x,y,z
import numpy as np
from collections import namedtuple
from collections import deque
import time
import threading
import signal
import math
```

```
import sys
import RPi.GPIO as GPIO
from LIS3DH import LIS3DH_I2C
from LIS3DH import *
global accl

def interrupt_gpio(channel):
    fifo_src = accl._read_register_byte(0x2F)
    for i in range(fifo_src & 0b00011111):
        dataQueue.append(accl.acceleration)
     accl._write_register_byte(0x2E, 0b00010000) # bypass mode
     accl._write_register_byte(0x2E, 0b01010000) # FIFO mode

def signal_handler(sig, frame):
    print('You pressed Ctrl+C!')
    sys.exit(0)

signal.signal(signal.SIGINT, signal_handler)
print('Press Ctrl+C for exit...')

AccelerationTuple = namedtuple("acceleration", ("x", "y", "z"))
dataQueue = deque([], maxlen=100)

GPIO.setwarnings(False)
GPIO.setmode(GPIO.BCM)
GPIO.setup(17, GPIO.IN, pull_up_down=GPIO.PUD_UP)
GPIO.setup(27, GPIO.OUT)
GPIO.add_event_detect(17, GPIO.RISING, callback=interrupt_gpio,
    bouncetime=1)
```

```
accl = LIS3DH_I2C(1, address=0x18)

accl._write_register_byte(0x2E, 0b00010000) #Continuous update,
    Full-scale selection = +/-2G
accl._write_register_byte(0x2E, 0b01010000) #FIFO

accl.data_rate = DATARATE_400_HZ

count=0
while True:
     non_empty = bool(dataQueue)
     if non_empty:
        xAccl, yAccl, zAccl =dataQueue.pop()
        r = math.sqrt(pow((xAccl),2)+pow((yAccl),2)+pow((zAccl),2))
        y.append(r)
        print("%d;%f;%f;%f;%f" % (count,(xAccl), (yAccl), (zAccl),
            r ))
        count=count+1
```

```
import scipy.fftpack
import scipy.signal
import pyhht
import emd
import matplotlib.scale
import matplotlib.pyplot as plt
import matplotlib.animation as animation
from matplotlib.lines import Line2D
from pyhht.visualization import plot_imfs
from pyhht import EMD
import numpy as np
```

```
from collections import namedtuple
from collections import deque
import time
import datetime as dt
import threading
import signal
import math
import RPi.GPIO as GPIO
import sys
#sys.path.append('./lis3dh_driver')
from LIS3DH import *

def interrupt_gpio(channel):
        fifo_src = accl._read_register_byte(0x2F)
        for i in range(fifo_src & 0b00011111):
                dataQueue.append(accl.acceleration)
        accl._write_register_byte(0x2E, 0b00010000) # bypass mode
        accl._write_register_byte(0x2E, 0b01010000) # FIFO mode

def signal_handler(sig, frame):
        print('You pressed Ctrl+C!')
        sys.exit(0)

signal.signal(signal.SIGINT, signal_handler)
print('Press Ctrl+C for exit...')
```

```
class Scope:
    def __init__(self, ax, ax1b, maxt, dt):
        self.line = Line2D(self.tdata, self.xaccdata, color='red',
            label='x')
```

```
        self.ax.add_line(self.line)
        self.ax.legend()
    def update(self, y):
        non_empty = bool(dataQueue)
        if non_empty:
            for i in range(len(dataQueue)):
                xacc, yacc, zacc = dataQueue.pop()
                y = math.sqrt(pow(xacc, 2)+pow(yacc, 2)+pow(zacc,
                    2)) - g
                y_fft.append(y)
                lastt = self.tdata[-1]
                if lastt > self.tdata[0] + self.maxt: # reset the
                    arrays
                        self.tdata = [self.tdata[-1]]
                        self.xaccdata = [self.xaccdata[-1]]
                        self.ax.set_xlim(self.tdata[0], self.tdata[0]
                            + self.maxt)
                        self.ax.figure.canvas.draw()
                t = self.tdata[-1] + self.dt
                self.tdata.append(t)
                self.xaccdata.append(xacc)
                self.ris.append(y)
                self.line.set_data(self.tdata, self.xaccdata)
                self.risult.set_data(self.tdata,self.ris)
            return self.line,
global accl
global dataQueue
global y_fft
global g
y_fft = list()
```

```
g = 9.806
N = 5000
fsample = 400
dt = 1.0 / fsample
maxf = fsample / 2
maxt = N / fsample
FSR = 2

fig, (sigPlot) = plt.subplots()
scope = Scope(sigPlot,sig2Plot,maxt,dt)
fig.canvas.set_window_title('Roller Acceleration')
ani =
    animation.FuncAnimation(fig,scope.update,interval=10,blit=True)
plt.show()
```

```
#FFT class
class FFT:
    def __init__ (self, ax2, N, fsample, dt, maxf):
        self.linefft = Line2D(self.xf, self.db)
        self.ax2.add_line(self.linefft)

    def updfft(self, q):
        self.xpeaks = []
        self.xf = np.linspace(0.0, 1.0/(2.0*dt), N//2)
        if(len(y_fft) >= N ):
                fft_cpy = np.array(y_fft[:(N-1)])
                self.yf = scipy.fftpack.fft(fft_cpy)
                self.yf2 = 2.0/N * np.abs(self.yf[:N//2])
                self.ax2.figure.canvas.draw()
                del y_fft[:(N-1)]
```

```
        self.linefft.set_data(self.xf, self.yf2)
        return self.linefft,
```

```
#HHT class
class HHT:
    def __init__ (self,ax3,ax4,N,maxt,fsample,maxf,dt):
        self.lineaimfs = Line2D(self.t, self.rr)
        self.ax3.add_line(self.lineaimfs)
        self.lineahilbspect= Line2D(self.xf, self.rr)
        self.ax4.add_line(self.lineahilbspect)

    def updimfs(self, q):
        if(len(y_fft) >= N and len(tt) >= N):
            self.t = np.array(tt[:(N-1)])
            self.acc_risultante = np.array(y_fft[:(N-1)])
            decomposer = EMD(self.acc_risultante)
            self.imfs = decomposer.decompose()
            print('Index of orthogonality: %.3f' % decomposer.io())
            self.nimfs = self.imfs.shape[0]
            self.xf = np.linspace(0.0, 1.0/(2.0*dt), N//2)
            for i in range(self.nimfs):
                self.r[i] = np.array(self.imfs[i,:])
                print('self.r[%d]' % i)
                self.h[i] = scipy.signal.hilbert(self.r[i])
                self.f[i] =
                    np.abs(scipy.fftpack.fft(self.h[i][:N//2]))
                self.a[i] =
                    np.sqrt(pow(self.r[i],2)+pow(self.h[i],2))

                self.lineaimfs=Line2D(self.t, self.r[i])
```

```
            self.list1.append(self.lineaimfs)
            self.lineaimfs.set_data(self.t, self.r[i])
            self.list1[-1].set_color("red")
            self.ax3 = plt.subplot(self.nimfs+1,1,i+2)
            self.ax3.set_ylabel('c%d' % i)
            #self.ax3.set_xlim(0,0)
            self.lineaimfs, = self.ax3.plot(self.t, self.r[i])
            self.ax3.figure.canvas.draw()
        plt.clf()

        for i in range(self.nimfs):
            self.lineahilbspect=Line2D(self.xf, self.f[i])
            self.list2.append(self.lineahilbspect)
            self.lineahilbspect.set_data(self.xf, self.f[i])
            self.ax4 = plt.subplot(self.nimfs+1,1,i+2)
            self.ax4.set_ylabel('h%d' % i)
            self.ax4.set_xlim(0,100)
            self.ax4.grid()
            self.lineahilbspect, = self.ax4.plot(self.xf,
                self.f[i])
            self.ax4.figure.canvas.draw()
        plt.clf()
        del y_fft[:(N-1)]
    return [self.lineaimfs, self.lineahilbspect]
```

A.2 MATLAB Codes

```
signal = xlsread('');
```

```
fsample = 400;
dt = 1/fsample;
N = length(signal);
maxt = N*dt;
xf = linspace(0.0, 1.0/(2.0*dt), N/2+1);
time = (0:N-1)*dt;

%FFT
fft_signal = fft(signal);
P2 = abs(fft_signal/N);
P1 = P2(1:N/2+1);
P1(2:end-1) = 2*P1(2:end-1);
plot(xf,P1)
xlim([0 fsample/2])
ylim([0 0.1])
xlabel('Frequency [Hz]')
ylabel('|P(f)|')
```

```
%Envelope Spectrum
level = 6;
figure
kurtogram(signal,fsample,level)
[~, ~, ~, fc, ~, BW] = kurtogram(signal,fsample, level);
a = (fc-BW/2);
b = (fc+BW/2);

bpf = designfilt('bandpassfir', 'FilterOrder', 2,
    'CutoffFrequency1',a,'CutoffFrequency2',b, 'SampleRate',
    fsample);
xBpf = filter(bpf,signal);
```

```
[pEnvBpf, fEnvBpf, xEnvBpf, tEnvBpf] = envspectrum(xBpf, fsample,
    ...
    'FilterOrder', 2, 'Band', [a b]);
xEnv=envelope(signal);
xEnvBpf=envelope(xBpf);

figure
plot(fEnvBpf, pEnvBpf);
xlim([0 fsample/2])
ylim([0 0.5])
xlabel('Frequency (Hz)')
ylabel('Peak Amplitude')
title('Envelope Spectrum of Bandpass Filtered Signal')
```

```
%HHT
[imfs,res,Info]=emd(signal);
[hs,f,t,imfinsf(:,1),imfinse(:,1)]=hht(imfs(:,1),fsample);
mesh(seconds(t),f,hs,'EdgeColor','none','FaceColor','interp')
xlabel('Time(s)')
ylabel('Frequency(Hz)')
zlabel('Instantaneous Energy')
title('Hilbert Spectrum')
```

B. Datasheet

LIS3DH Datasheet and Application Note

AN3308
Application note

LIS3DH: MEMS digital output motion sensor ultra-low-power high-performance 3-axis “nano” accelerometer

Introduction

This document describes the low-voltage 3-axis digital output linear MEMS accelerometer provided in an LGA package.

The LIS3DH is an ultra-low-power high-performance 3-axis linear accelerometer belonging to the “nano” family, with a digital I^2C/SPI serial interface standard output.

The device features ultra-low-power operational modes that allow advanced power saving and smart sleep-to-wake-up and return-to-sleep functions.

The LIS3DH has dynamic user-selectable full scales of ±2*g*/±4*g*/±8*g*/±16*g* and is capable of measuring accelerations with output data rates from 1 Hz to 5 kHz.

The device may be configured to generate interrupt signals using an independent inertial wake-up/free-fall event as well as by the position of the device itself. Thresholds and timing of the interrupt generator are programmable by the end user on the fly.

Automatic programmable sleep-to-wakeup and return-to-sleep functions are also available for enhanced power saving.

The LIS3DH has an integrated 32-level first-in first-out (FIFO) buffer allowing the user to store data in order to limit intervention by the host processor.

The LIS3DH is available in a small thin plastic land grid array package (LGA) and is guaranteed to operate over an extended temperature range from -40 °C to +85 °C.

The ultra-small size and weight of the SMD package make it an ideal choice for handheld portable applications such as smartphones, IoT connected devices, and wearables, or any other application where reduced package size and weight are required.

LIS3DH

MEMS digital output motion sensor: ultra-low-power high-performance 3-axis "nano" accelerometer

Datasheet - production data

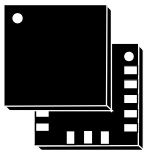

LGA-16 (3x3x1 mm)

Features

- Wide supply voltage, 1.71 V to 3.6 V
- Independent IO supply (1.8 V) and supply voltage compatible
- Ultra-low-power mode consumption down to 2 µA
- ±2*g*/±4*g*/±8*g*/±16*g* dynamically selectable full scale
- I^2C/SPI digital output interface
- 16-bit data output
- 2 independent programmable interrupt generators for free-fall and motion detection
- 6D/4D orientation detection
- Free-fall detection
- Motion detection
- Embedded temperature sensor
- Embedded self-test
- Embedded 32 levels of 16-bit data output FIFO
- 10000 *g* high shock survivability
- ECOPACK®, RoHS and "Green" compliant

Applications

- Motion activated functions
- Free-fall detection
- Click/double-click recognition
- Intelligent power saving for handheld devices
- Pedometers
- Display orientation
- Gaming and virtual reality input devices
- Impact recognition and logging
- Vibration monitoring and compensation

Description

The LIS3DH is an ultra-low-power high-performance three-axis linear accelerometer belonging to the "nano" family, with digital I^2C/SPI serial interface standard output. The device features ultra-low-power operational modes that allow advanced power saving and smart embedded functions.

The LIS3DH has dynamically user-selectable full scales of ±2*g*/±4*g*/±8*g*/±16*g* and is capable of measuring accelerations with output data rates from 1 Hz to 5.3 kHz. The self-test capability allows the user to check the functioning of the sensor in the final application. The device may be configured to generate interrupt signals using two independent inertial wake-up/free-fall events as well as by the position of the device itself. Thresholds and timing of interrupt generators are programmable by the end user on the fly. The LIS3DH has an integrated 32-level first-in, first-out (FIFO) buffer allowing the user to store data in order to limit intervention by the host processor. The LIS3DH is available in small thin plastic land grid array package (LGA) and is guaranteed to operate over an extended temperature range from -40 °C to +85 °C.

Table 1. Device summary

Order codes	Temp. range [°C]	Package	Packaging
LIS3DHTR	-40 to +85	LGA-16	Tape and reel

Bibliography

[1] 2020. URL: https://www.who.int/health-topics/.

[2] A. Shamayleh, M. Awad, and J. Farhat. "IoT Based Predictive Maintenance Management of Medical Equipment". In: *Journal of Medical System* (4 2020). DOI: 10.1007/s1091602015348. URL: https://doi.org/10.1007/s10916-020-1534-8.

[3] K. Ajaz. *The Importance of Equipment Efficiency for the Healthcare Sector*. 2018. URL: https://electronichealthreporter.com/.

[4] E. Iadanza et al. "Evidence-based medical equipment management: a convenient implementation". In: *Medical & Biological Engineering & Computing* 57 (Aug. 2019), pp. 2215–2230. DOI: 10.1007/s11517-019-02021-x. URL: https://doi.org/10.1007/s11517-019-02021-x.

[5] P. Derrico et al. "Clinical engineering". In: *Applied Biomedical Engineering* (2011), pp. 169–196.

[6] R. Stewart. *Getting the most of your mobile assets*. URL: http://healthcare.flexity.ca/healthcare-it-blog/2012/6/25/getting-the-most-of-your-mobile-assets.html.

[7] Mana Sezdi. "Two Different Maintenance Strategies in the Hospital Environment: Preventive Maintenance for Older Technology Devices and Predictive Maintenance for Newer High-Tech Devices". In: *Jour-*

nal of Healthcare Engineering (2016), p. 16. DOI: 10.1155/2016/7267983. URL: http://dx.doi.org/10.1155/2016/7267983.

[8] T.L. Rodziewicz, B. Houseman, and J.E. Hipskind. "Medical Error Prevention". In: (2020). URL: https://www.ncbi.nlm.nih.gov/books/NBK499956/.

[9] R. Miniatia, F. Dori, and G. Biffi Gentilic. "Design of a decision support system for preventive maintenance planning in health structures". In: *Technology and Health Care* 20 (2012), pp. 205–214. DOI: 10.3233/THC-2012-0670.

[10] J. Joseph and S. Madhukumar. "A novel approach to Data Driven Preventive Maintenance Scheduling of medical instruments". In: (2010), pp. 193–197. DOI: 10.1109/ICSMB.2010.5735370.

[11] D. Malombe Mutia, L. Mukhongo, and P. Chemweno. "Review in Maintenance Strategies for Haemodialysis Machine in Healthcare Facilities". In: *Industrial Engineering* 2 (1 2018), pp. 34–41. DOI: 10.11648/j.ie.20180201.15.

[12] C. Călin, A. Doru, and L. Cătălina. "A Modern Approach for Maintenance Prioritization of Medical Equipment". In: (June 2020). DOI: 10.5772/intechopen.92706. URL: https://www.intechopen.com/online-first/a-modern-approach-for-maintenance-prioritization-of-medical-equipment.

[13] H. Mahfoud, A. El Barkany, and A. El Biyaali. "Preventive Maintenance Optimization in Healthcare Domain: Status of Research and Perspective". In: *Journal of Quality and Reliability Engineering* 2016 (June 2016), p. 10. DOI: 10.1155/2016/5314312. URL: http://dx.doi.org/10.1155/2016/5314312.

[14] M. Ridgway, L. R. Atles, and A. Subhan. "Reducing equipment downtime: a new line of attack". In: *Journal of Clinical Engineering* 34 (4 2009), pp. 200–204.

[15] R.P. Santos and R.M Almeida. "Hospital medical equipment maintenance schedules using the mean time between failures". In: *Cadernos Saude Coletiva* 18 (2 2010), pp. 309–314.

[16] Taghipour and D. Banjevic. "Periodic inspection optimization models for a repairable system subject to hidden failures". In: *IEEE Transactions on Reliability* 60 (1 2011), 275–285.

[17] C.K.M Lee, Y. Cao, and Kam K.H.Ng. "Big Data Analytics for Predictive Maintenance Strategies". In: (2017). DOI: DOI:10.4018/978-1-5225-0956-1.ch004.

[18] G. Mummolo et al. "A fuzzy approach for medical equipment replacement planning". In: *Proceedings of the 3rd International Conference on Maintenance and Facility Management* (2007), pp. 229–235.

[19] J. Lee et al. "Industrial big data analytics and cyber-physical systems for future maintenance & service innovation". In: 38 (2015), pp. 3–7. DOI: doi:10.1016/j.procir.2015.08.026.

[20] S.Y. Chuang et al. "Predictive Maintenance with Sensor Data Analytics on a Raspberry Pi-Based Experimental Platform". In: *Sensors* (2019), pp. 205–214. DOI: doi:10.3390/s19183884.

[21] H. Li, Y. Zhang, and H. Zheng. "Hilbert-Huang transform and marginal spectrum for detection and diagnosis of localized defects in roller bearings". In: *Journal of Mechanical Science and Technology* 23 (2009), pp. 291–301. DOI: DOI10.1007/s12206-008-1110-5.

[22] K. Kamaras and I. Dimitrakopoulos. “Vibration Analysis of Rolling Element Bearings using Spectral Kurtosis and Envelope Analysis”. In: (2016). URL: https://fnt.com.cy/images/Advance_Bearing_Monitoring_FNT_Jan_2016.pdf.

[23] M. Al-Tubi et al. “Centrifugal Pump Condition Monitoring and Diagnosis Using Frequency Domain Analysis”. In: 15 (Feb. 2019), pp. 122–131. DOI: 10.1007/978-3-030-11220-2_13.

[24] Y. Zheng. “Predicting Remaining Useful Life Based on Hilbert–Huang Entropy with Degradation Model”. In: *Journal of Electrical and Computer Engineering* (2019), p. 11. DOI: doi.org/10.1155/2019/3203959. URL: https://doi.org/10.1155/2019/3203959.

[25] S. Orhan, N. Aktürk, and V. Çelik. “Vibration monitoring for defect diagnosis of rolling element bearings as a predictive maintenance tool: Comprehensive case studies”. In: *Ndt & E International - NDT E INT* 39 (Oct. 2005), pp. 293–298. DOI: 10.1016/j.ndteint.2005.08.008.

[26] *IoT Signal, SUMMARY OF RESEARCH LEARNINGS 2019*. 2019. URL: https://azure.microsoft.com/en-us/resources/iot-signals/.

[27] *Predictive Maintenance 4.0*. 2017. URL: https://www.pwc.nl/nl/assets/.

[28] *Accenture to Help Thames Water Prove the Benefits of Smart Monitoring Capabilities*. 2014. URL: http://newsroom.accenture.com/news/accenture-to-help-thames-water-prove-the-benefits-of-smart-monitoring-capabilities.html.

[29] 2020. URL: https://www.thyssenkrupp-elevator.com.

[30] 2015. URL: https://www.plantservices.com/articles/2015/smart-maintenance-on-the-rise.

[31] PD. McFadden and JD. Smith. "Model for the vibration produced by a single point defect in a rolling element bearing". In: *Journal of Sound and Vibration* 96 (1a 1984), pp. 69–82.

[32] B. Dolenc, P. Boškoski, and D. Đani Juričić. "Distributed bearing fault diagnosis based on vibration analysis". In: *Mechanical Systems and Signal Processing* 66-67 (2016), pp. 521 –532. ISSN: 0888-3270. DOI: https://doi.org/10.1016/j.ymssp.2015.06.007.

[33] A. Soualhi et al. "Early detection of bearing faults by the Hilbert-Huang transform". In: *2016 4th International Conference on Control Engineering & Information Technology (CEIT)* (2016), pp. 1–6. DOI: DOI:10.1109/CEIT.2016.7929064.

[34] R. Randall and J Antoni. "Rolling element bearing diagnostics—A tutorial". In: *Mechanical Systems and Signal Processing* 25 (2011), pp. 485–520.

[35] N.E. Huang. "Chapter 1: Introduction to the Hilbert-Huang transform and its related mathematical problems". In: 16 (2014), pp. 1–26. DOI: 10.1142/9789814508247_0001. URL: https://doi.org/10.1142/9789814508247_0001.

[36] N.E Huang, Z. Shen, and S.R. Long. "The empirical mode decomposition and the Hilbert spectrum for nonlinear and non-stationary time series analysis". In: *Proceedings of the Royal Society London* 454 (1998), pp. 903–995.

[37] E. Ranjbar et al. "Design of an IoT-Based System for Smart Maintenance of Medical Equipment". In: (2019), pp. 1–12. DOI: 10.1109/IICITA.2019.8808841.

[38] M. Karami and R. Madlener. “Smart Predictive Maintenance Strategy Based on Cyber-Physical Systems for Centrifugal Pumps: A Bearing Vibration Analysis”. In: *FCN Working Paper* (14/2019 Sept. 2019).

[39] C. He et al. “Medical rolling bearing fault prognostics based on improved extreme learning machine”. In: *Journal of Combinatorial Optimization* (2019). DOI: https://doi.org/10.1007/s10878-019-00494-y.

[40] C. Wahyu and T. Tegoeh. “A Review of Feature Extraction Methods in Vibration-Based Condition Monitoring and Its Application for Degradation Trend Estimation of Low-Speed Slew Bearing”. In: *Machines* (2017), pp. 1–28. DOI: doi:10.3390/machines5040021.